

RICE UNIVERSITY

**Deterministic and Stochastic Responses of Smart Variable Stiffness  
and Damping Systems and Smart Tuned Mass Dampers**

by

**Ertan Sonmez**

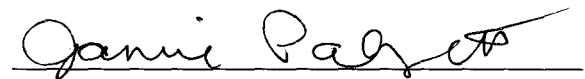
A THESIS SUBMITTED  
IN PARTIAL FULFILLMENT OF THE  
REQUIREMENTS FOR THE DEGREE

**Doctor of Philosophy**

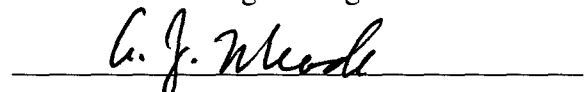
APPROVED, THESIS COMMITTEE:



Satish Nagarajaiah  
Professor of Civil and Environmental  
Engineering and Mechanical Engineering  
and Material Science



Jamie Padgett  
Assistant Professor of Civil and  
Environmental Engineering



Andrew J. Meade  
Professor of Mechanical Engineering and  
Material Science



Po D. Spanos  
Lewis B. Ryon Professor of Civil and  
Environmental Engineering and Mechanical  
Engineering and Material Science

HOUSTON, TEXAS  
NOVEMBER 2009

UMI Number: 3421186

All rights reserved

INFORMATION TO ALL USERS

The quality of this reproduction is dependent upon the quality of the copy submitted.

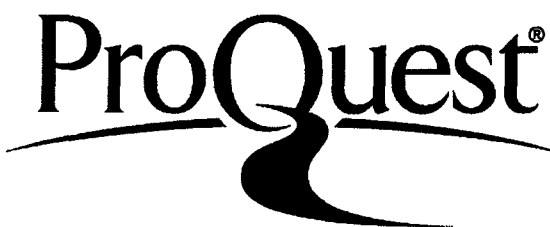
In the unlikely event that the author did not send a complete manuscript and there are missing pages, these will be noted. Also, if material had to be removed, a note will indicate the deletion.



UMI 3421186

Copyright 2010 by ProQuest LLC.

All rights reserved. This edition of the work is protected against unauthorized copying under Title 17, United States Code.



ProQuest LLC  
789 East Eisenhower Parkway  
P.O. Box 1346  
Ann Arbor, MI 48106-1346

## **ABSTRACT**

### **Deterministic and Stochastic Responses of Smart Variable Stiffness and Damping Systems and Smart Tuned Mass Dampers**

**by**

**Ertan Sonmez**

Semi-active control algorithms are developed and examined for a variety of civil engineering applications subjected to a wide range of excitations. Except two control algorithms based on continuous variable structure control and Lyapunov control, the semi-active controllers developed in this study are based on real-time estimation of instantaneous (dominant) frequency and the evolutionary power spectral density by time-frequency analysis of either the excitation or the response of the structure. Time-frequency analyses are performed by either short-time Fourier transform or wavelet transform.

The semi-active strategies are applied to three categories of structures: (1) smart single- and multi- degree-of-freedom (sSDOF/sMDOF) systems subjected to pulse-type and random ground excitations, (2) single/multiple smart tuned mass dampers (sTMD/sMTMD) subjected to random wind and ground excitations, and (3) smart tuned liquid column dampers (sTLCD) subjected to random wind and ground excitations.

For sSDOF/sMDOF systems, nonlinear control algorithms developed to independently vary stiffness (continuous variable structure control) and damping (Lyapunov control) are examined against near-fault earthquakes and pulse type of excitations fitted to them. Another semi-active (time-frequency) controller is developed based on minimizing the instan-

taneous  $H_2$  norm of the response of the structure.

Two time-frequency controllers (feedforward and feedback) are developed for single/multiple smart tuned mass dampers (sTMD/sMTMD) subjected to either force or base excitation. In the feedforward control, the smart tuned mass damper stiffness and damping are varied based on the instantaneous (dominant) frequency of the excitation, whereas in the feedback control the smart tuned mass damper stiffness is varied based on the instantaneous (dominant) frequency of the response. The developed algorithms are also extended to semi-active smart tuned liquid column dampers (sTLCD) subjected to either force or base excitation.

The performance of the control algorithms are evaluated by studying the deterministic and stochastic responses of the examined semi-active structures. Stochastic responses are computed from Monte Carlo simulations of various target evolutionary spectra. It is shown that smart variable stiffness and variable damping systems and smart tuned mass/liquid column dampers lead to significant response reduction over a broad frequency range and under a wide set of excitations.



## Acknowledgments

My PhD study was a long and difficult path that tested my endurance in many ways. Throughout this path, I was challenged with academic and non-academic problems that made me question at times regarding what I am doing and to where I am aiming to go, as most PhD students. Well, sometimes the only way to reach a goal is simply to persist till the end. And that's what I did. After an almost never ending period, I am closing this chapter of my life and about to open a new one. I am happy to see this day and I am grateful to all the people that helped me along this path.

I first of all wish to thank Dr. Satish Nagarajaiah who, as my advisor guided and encouraged me during the course of this study. I would like to express my sincere gratitude for his constant optimism and patience with me.

I would like to thank and express my gratitude to my committee members, Dr. Jamie Padgett, Dr. Andrew J. Meade and Dr. Pol D. Spanos, for their time to review my dissertation and their valuable comments.

I would like to extend my gratitude to Dr. Biswajit Basu, who provided significant help on the topics of wavelet transform and tuned liquid column dampers. His collaboration made a substantial impact on the progress of my research.

I have the honor of meeting many good friends during my time in Rice. I would like to start with Dr. Ashutosh Agrawal, to whom I am thankful for his continuous friendship since the early stages of our graduate studies. Some of the results of this study were obtained during our collaborative work on analytical and experimental studies of semiactive systems equipped with SAIVS device and MR dampers. I would also like to thank several alumni colleagues, Dr. Jale Tezcan, Dr. Prasad Dharap, Dr. Zhiling Li, Dr. Nadathur Varadarajan, Dr. Chen Bilei and Bayram Aygun for their friendship and support. I would also thank my

colleagues in our research group: Michael Contreras, Dharma Pasala, Srivishnu Vemuru and Chaojun Huang.

I would like to express my special thanks to my inner-circle anthropologist friends, Dr. Ebru Kayaalp and Dr. Erkan Saka. They definitely made my life in Rice more fun and interesting.

Lastly but most importantly, I would like to thank my late mother Leyla Sonmez, my father Ishak Sonmez, and my brother Tolga Sonmez for their continuous support to me, and making possible the completion of this dissertation.

I greatly appreciate the financial support of Department of Civil Engineering at Rice University. I would also like to express my sincere gratitude to Richard Newhouse, Structural Department Manager of J. Ray McDermott, for allowing me to take a leave of absence from my work to complete my dissertation.

# TABLE OF CONTENTS

Abstract	ii
Acknowledgments	iv
List of Tables	xii
List of Figures	xiii
<b>1 Introduction</b>	<b>1</b>
1.1 Objective and Scope of This Study . . . . .	1
1.2 Review of Previous Work . . . . .	3
1.2.1 Structural Control: Passive, Semiactive and Active Systems . . . . .	3
1.2.2 Semiactive Variable Damping and Stiffness Systems . . . . .	5
1.2.3 Base Isolation . . . . .	6
1.2.4 Tuned Mass Damper (TMD) . . . . .	7
1.2.5 Multiple Tuned Mass Dampers (MTMD) . . . . .	8
1.2.6 Semi-active Tuned Mass Damper (sTMD) . . . . .	9
1.2.7 Optimization of TMD parameters . . . . .	10
1.2.8 Tuned Liquid Column Dampers (TLCD) . . . . .	11
1.2.9 Random Vibration . . . . .	12
1.2.10 Evolutionary Spectra . . . . .	19
1.2.11 Digital Simulation of Random Processes . . . . .	26
1.2.12 Analytical Models of Power Spectral Density for Ground and Wind Excitations . . . . .	33

<b>2</b>	<b>Mathematical Formulation of Linear Time Varying (LTV) Systems</b>	<b>38</b>
2.1	Continuous-Time Linear Time Varying Systems . . . . .	38
2.1.1	State Model . . . . .	40
2.1.2	Stability . . . . .	44
2.1.3	Controllability and Observability . . . . .	45
2.2	Discrete-Time Linear Time-Varying Systems . . . . .	47
2.2.1	State Model . . . . .	49
2.2.2	Stability . . . . .	52
2.2.3	Controllability and Observability . . . . .	52
2.3	Mathematical Formulation of SDOF LTV System with sTMD . . . . .	55
2.4	Mathematical Formulation of MDOF LTV System with sTMD . . . . .	57
<b>3</b>	<b>Time-frequency Analysis</b>	<b>60</b>
3.1	Review of Time-Frequency Techniques . . . . .	60
3.2	Preliminary Definitions . . . . .	64
3.3	Uncertainty Principle . . . . .	67
3.4	Short Time Fourier Transform (STFT) . . . . .	68
3.5	Wavelet Transform (WT) . . . . .	70
<b>4</b>	<b>Frequency Tracking and Evolutionary Spectrum by STFT and WT</b>	<b>74</b>
4.1	Frequency Tracking and Evolutionary Spectrum Estimation by STFT . . . .	75
4.2	Frequency Tracking and Evolutionary Spectrum Estimation by WT . . . .	76
4.3	Numerical Examples . . . . .	82

4.3.1	Discrete Simple Sweep . . . . .	84
4.3.2	Narrow-band Stationary Process . . . . .	85
4.3.3	Wide-band Stationary Process . . . . .	86
4.3.4	Locally Stationary Process . . . . .	87
4.3.5	Non-stationary Process . . . . .	87
4.4	Concluding Remarks . . . . .	87
<b>5</b>	<b>Semi-active Single/Multiple-Degree-Of-Freedom Systems (sSDOF/sMDOF) under Deterministic Excitations</b>	<b>90</b>
5.1	SDOF Structural Model and Formulation . . . . .	90
5.2	MDOF Structural Model and Formulation . . . . .	91
5.3	Control Algorithms . . . . .	93
5.3.1	Variable stiffness based on continuous variable structure control . .	93
5.3.2	Variable damping based on Lyapunov control . . . . .	97
5.4	Pulse Type Excitations . . . . .	98
5.5	Nonlinear Least Squares Fitting of Single/Multiple Pulses to Near-Fault Earthquakes . . . . .	99
5.6	Results for Variable Stiffness Systems . . . . .	110
5.7	Results for Variable Damping Systems . . . . .	124
5.8	Results for Combined Variable Damping and Stiffness Systems . . . . .	138
5.9	Concluding Remarks . . . . .	141
<b>6</b>	<b>Semi-active Single/Multiple Tuned Mass Dampers (sTMD/sMTMD) under Deterministic Excitations</b>	<b>152</b>
6.1	Modelling of MDOF System with MTMD . . . . .	152

6.2	Modelling of MDOF System with SMTMD . . . . .	154
6.3	Formulation . . . . .	157
6.4	Results . . . . .	159
6.4.1	Excitation Frequency Tracking by STFT . . . . .	159
6.4.2	Parametric Study . . . . .	161
6.4.3	Time Histories . . . . .	165
6.5	Concluding Remarks . . . . .	168
<b>7</b>	<b>Semi-active Single/Multi-Degree-Of-Freedom Systems (sSDOF/sMDOF) under Stochastic Excitations</b>	<b>178</b>
7.1	SDOF Structural Model and Formulation . . . . .	179
7.2	MDOF Structural Model and Formulation . . . . .	181
7.3	Control Algorithm . . . . .	184
7.4	Results for sSDOF . . . . .	186
7.4.1	Wide-band Stationary Excitations . . . . .	188
7.4.2	Locally Stationary Excitations . . . . .	189
7.4.3	Non-stationary Excitations . . . . .	190
7.4.4	Recorded Earthquake . . . . .	190
7.5	Results for sMDOF . . . . .	191
7.5.1	Locally Stationary Excitations . . . . .	191
7.6	Approximate Response of sSDOF Systems through Time-Varying Complex Frequency Response Function . . . . .	192
7.7	Concluding Remarks . . . . .	195

<b>8</b>	<b>Semi-active Single/Multiple Tuned Mass Dampers (sTMD/sMTMD) under Stochastic Excitations</b>	<b>207</b>
8.1	Structural Model and Formulation . . . . .	208
8.2	Control Algorithm . . . . .	208
8.3	Results for sTMD/sMTMD Systems under Stochastic Excitations . . . . .	213
8.3.1	Narrow-band Stationary Excitations . . . . .	215
8.3.2	Locally Stationary Excitations . . . . .	216
8.3.3	Recorded Earthquake . . . . .	228
8.4	Concluding Remarks . . . . .	230
<b>9</b>	<b>Semi-active Tuned Liquid Column Dampers (sTLCD)</b>	<b>236</b>
9.1	Structural Model and Formulation . . . . .	237
9.2	Control Algorithm . . . . .	245
9.3	Results for sTLCD Systems . . . . .	247
9.3.1	Parametric Study . . . . .	247
9.3.2	Narrow-band Stationary Excitations . . . . .	251
9.3.3	Locally Stationary Excitations . . . . .	258
9.3.4	Recorded Earthquake . . . . .	265
9.4	Concluding Remarks . . . . .	273
<b>10</b>	<b>Conclusions and Future Work</b>	<b>274</b>
10.1	Conclusions . . . . .	274
10.2	Future Work . . . . .	282

**Bibliography****283**



## **List of Tables**

6.1	$H_\infty$ Optimized Parameters of Passive TMD and 5-TMD . . . . .	166
8.1	$H_2$ Optimized Parameters of Passive TMD and 5-TMD . . . . .	214
9.1	Comparison of pTLCD and sTLCD . . . . .	250

## List of Figures

2.1	Single Degree of Freedom System with TMD. . . . .	57
3.1	Short Time Fourier Transform (STFT) . . . . .	69
4.1	Frequency tracking and Evolutionary Spectrum Estimation by STFT . . . .	77
4.2	Frequency tracking and Evolutionary Spectrum Estimation by WT . . . . .	83
4.3	Discrete sine sweep: (a) Signal, (b) RMS history, (c) EPSD by STFT, (d) EPSD by WT, (e) Frequency tracking by STFT, and (f) Frequency tracking by WT . . . . .	84
4.4	Narrow-band stationary process: (a) Target EPSD, (b) Sample function, (c) EPSD by STFT, (d) EPSD by WT, (e) Frequency tracking, and (f) RMS history . . . . .	85
4.5	Wide-band stationary process: (a) Target EPSD, (b) Sample function, (c) EPSD by STFT, (d) EPSD by WT, (e) Frequency tracking, and (f) RMS history . . . . .	86
4.6	Locally stationary process: (a) Target EPSD, (b) Sample function, (c) EPSD by STFT, (d) EPSD by WT, (e) Frequency tracking, and (f) RMS history . .	88
4.7	Non-stationary process: (a) Target EPSD, (b) Sample function, (c) EPSD by STFT, (d) EPSD by WT, (e) Frequency tracking, and (f) RMS history . .	89
5.1	Analytical model of the SDOF system equipped with variable stiffness and variable damping device . . . . .	91
5.2	Analytical model of the MDOF system equipped with variable stiffness and variable damping device . . . . .	93
5.3	Pulse type of excitations . . . . .	100

5.4	1992 Landers: Lucerne-270 record and fitted pulse type A ( $v_p = 128.08 \text{ cm/s}$ , $T_p = 2.94 \text{ s}$ , $t_0 = 8.59 \text{ s}$ ): (a) ground acceleration, (b) ground velocity, (c) ground displacement, (d) SDOF spectral displacement, (e) SDOF spectral velocity, (f) SDOF spectral acceleration . . . . .	105
5.5	1979 Imperial Valley: El Centro #5-230-FN record and fitted pulse type B ( $v_p = 76.76 \text{ cm/s}$ , $T_p = 3.18 \text{ s}$ , $t_0 = 4.78 \text{ s}$ ): (a) ground acceleration, (b) ground velocity, (c) ground displacement, (d) SDOF spectral displacement, (e) SDOF spectral velocity, (f) SDOF spectral acceleration . . . . .	106
5.6	1992 Erzincan: NS record and fitted pulse type $C_1$ ( $v_p = -60.86 \text{ cm/s}$ , $T_p = 2.00 \text{ s}$ , $t_0 = 2.00 \text{ s}$ ): (a) ground acceleration, (b) ground velocity, (c) ground displacement, (d) SDOF spectral displacement, (e) SDOF spectral velocity, (f) SDOF spectral acceleration . . . . .	107
5.7	1994 Northridge: Sylmar-360-FN record and fitted pulse type $C_2$ ( $v_p = 35.85 \text{ cm/s}$ , $T_p = 2.25 \text{ s}$ , $t_0 = 2.24 \text{ s}$ ): (a) ground acceleration, (b) ground velocity, (c) ground displacement, (d) SDOF spectral displacement, (e) SDOF spectral velocity, (f) SDOF spectral acceleration . . . . .	108
5.8	1994 Northridge: Rinaldi-228-FN record and fitted pulse type $C_1+C_1+C_1$ ( $v_p = [-12.34 \quad -47.13 \quad 92.30] \text{ cm/s}$ , $T_p = [3.21 \quad 1.87 \quad 1.06] \text{ s}$ , $t_0 = [0.36 \quad 1.17 \quad 2.10] \text{ s}$ ): (a) ground acceleration, (b) ground velocity, (c) ground displacement, (d) SDOF spectral displacement, (e) SDOF spectral velocity, (f) SDOF spectral acceleration . . . . .	109
5.9	Response spectra of the SDOF system subjected to Lucerne-270 record and fitted pulse type A ( $T_p = 2.94 \text{ s}$ ) . . . . .	112
5.10	Response time histories, force-displacement loops, and variable stiffness history of the SDOF system subjected to Lucerne-270 record and fitted pulse type A ( $T_p = 2.94 \text{ s}$ ) . . . . .	113
5.11	Response spectra of the SDOF system subjected to El Centro #5-230-FN record and fitted pulse type B ( $T_p = 3.18 \text{ s}$ ) . . . . .	114
5.12	Response time histories, force-displacement loops, and variable stiffness history of the SDOF system subjected to El Centro #5-230-FN record and fitted pulse type B ( $T_p = 3.18 \text{ s}$ ) . . . . .	115

5.13	Response spectra of the SDOF system subjected to Erzincan-NS record and fitted pulse type $C_1$ ( $T_p = 2.00$ s) . . . . .	116
5.14	Response time histories, force-displacement loops, and variable stiffness history of the SDOF system subjected to Erzincan-NS record and fitted pulse type $C_1$ ( $T_p = 2.00$ s) . . . . .	117
5.15	Response spectra of the SDOF system subjected to Sylmar-360-FN record and fitted pulse type $C_2$ ( $T_p = 2.25$ s) . . . . .	118
5.16	Response time histories, force-displacement loops, and variable stiffness history of the SDOF system subjected to Sylmar-360-FN record and fitted pulse type $C_2$ ( $T_p = 2.25$ s) . . . . .	119
5.17	Response spectra of the SDOF system subjected to Rinaldi-228-FN record and fitted pulse type $C_1+C_1+C_1$ ( $T_p = [3.21 \ 1.87 \ 1.06]$ s) . . . . .	120
5.18	Response time histories, force-displacement loops, and variable stiffness history of the SDOF system subjected to Rinaldi-228-FN record and fitted pulse type $C_1+C_1+C_1$ ( $T_p = [3.21 \ 1.87 \ 1.06]$ s) . . . . .	121
5.19	Response time histories, force-displacement loops, and variable stiffness history of the 4-DOF system (base floor) subjected to Erzincan-NS record and fitted pulse type $C_1$ ( $T_p = 2.00$ s) . . . . .	122
5.20	Peak response profiles for 4-DOF system subjected to Erzincan-NS record and fitted pulse type $C_1$ ( $T_p = 2.00$ s) . . . . .	123
5.21	Response spectra of the SDOF system subjected to Lucerne-270 record and fitted pulse type A ( $T_p = 2.94$ s) . . . . .	126
5.22	Response time histories, force-displacement loops, and variable stiffness history of the SDOF system subjected to Lucerne-270 record and fitted pulse type A ( $T_p = 2.94$ s) . . . . .	127
5.23	Response spectra of the SDOF system subjected to El Centro #5-230-FN record and fitted pulse type B ( $T_p = 3.18$ s) . . . . .	128
5.24	Response time histories, force-displacement loops, and variable stiffness history of the SDOF system subjected to El Centro #5-230-FN record and fitted pulse type B ( $T_p = 3.18$ s) . . . . .	129

5.25	Response spectra of the SDOF system subjected to Erzincan-NS record and fitted pulse type $C_1$ ( $T_p = 2.00$ s) . . . . .	130
5.26	Response time histories, force-displacement loops, and variable stiffness history of the SDOF system subjected to Erzincan-NS record and fitted pulse type $C_1$ ( $T_p = 1.03$ s) . . . . .	131
5.27	Response spectra of the SDOF system subjected to Sylmar-360-FN record and fitted pulse type $C_2$ ( $T_p = 2.25$ s) . . . . .	132
5.28	Response time histories, force-displacement loops, and variable stiffness history of the SDOF system subjected to Sylmar-360-FN record and fitted pulse type $C_2$ ( $T_p = 2.25$ s) . . . . .	133
5.29	Response spectra of the SDOF system subjected to Rinaldi-228-FN record and fitted pulse type $C_1+C_1+C_1$ ( $T_p = [3.21 \ 1.87 \ 1.06]$ s) . . . . .	134
5.30	Response time histories, force-displacement loops, and variable stiffness history of the SDOF system subjected to Rinaldi-228-FN record and fitted pulse type $C_1+C_1+C_1$ ( $T_p = [3.21 \ 1.87 \ 1.06]$ s) . . . . .	135
5.31	Response time histories, force-displacement loops, and variable stiffness history of the 4-DOF system (base floor) subjected to Erzincan-NS record and fitted pulse type $C_1$ ( $T_p = 2.00$ s) . . . . .	136
5.32	Peak response profiles for 4-DOF system subjected to Erzincan-NS record and fitted pulse type $C_1$ ( $T_p = 2.00$ s) . . . . .	137
5.33	Response spectra of the SDOF system subjected to Lucerne-270 record and fitted pulse type A ( $T_p = 2.94$ s) . . . . .	140
5.34	Response time histories, force-displacement loops, and variable stiffness history of the SDOF system subjected to Lucerne-270 record and fitted pulse type A ( $T_p = 2.94$ s) . . . . .	141
5.35	Response spectra of the SDOF system subjected to El Centro #5-230-FN record and fitted pulse type B ( $T_p = 3.18$ s) . . . . .	142
5.36	Response time histories, force-displacement loops, and variable stiffness history of the SDOF system subjected to El Centro #5-230-FN record and fitted pulse type B ( $T_p = 3.18$ s) . . . . .	143

5.37	Response spectra of the SDOF system subjected to Erzincan-NS record and fitted pulse type $C_1$ ( $T_p = 2.00$ s) . . . . .	144
5.38	Response time histories, force-displacement loops, and variable stiffness history of the SDOF system subjected to Erzincan-NS record and fitted pulse type $C_1$ ( $T_p = 2.00$ s) . . . . .	145
5.39	Response spectra of the SDOF system subjected to Sylmar-360-FN record and fitted pulse type $C_2$ ( $T_p = 2.25$ s) . . . . .	146
5.40	Response time histories, force-displacement loops, and variable stiffness history of the SDOF system subjected to Sylmar-360-FN record and fitted pulse type $C_2$ ( $T_p = 2.25$ s) . . . . .	147
5.41	Response spectra of the SDOF system subjected to Rinaldi-228-FN record and fitted pulse type $C_1+C_1+C_1$ ( $T_p = [3.21 \ 1.87 \ 1.06]$ s) . . . . .	148
5.42	Response time histories, force-displacement loops, and variable stiffness history of the SDOF system subjected to Rinaldi-228-FN record and fitted pulse type $C_1+C_1+C_1$ ( $T_p = [3.21 \ 1.87 \ 1.06]$ s) . . . . .	149
5.43	Response time histories, force-displacement loops, and variable stiffness history of the 4-DOF system (base floor) subjected to Erzincan-NS record and fitted pulse type $C_1$ ( $T_p = 2.00$ s) . . . . .	150
5.44	Peak response profiles for 4-DOF system subjected to Erzincan-NS record and fitted pulse type $C_1$ ( $T_p = 2.00$ s) . . . . .	151
6.1	MDOF Structural Model with sMTMD (varying $k_1, \dots, k_n$ ) at the roof level: (a) Force Excited; (b) Base Excited . . . . .	155
6.2	Frequency Distribution of sMTMD . . . . .	156
6.3	Semiactive Independently Variable Stiffness (SAIVS) Device . . . . .	156
6.4	Control Algorithm . . . . .	161
6.5	Frequency Tracking by STFT and sTMD/sMTMD Tuning . . . . .	162
6.6	Frequency Tracking for (a) Harmonic Sinusoidal; (b) Discrete Sinusoidal Sweep; (c) Linear Chirp . . . . .	162

6.7	Frequency Response Functions of SDOF Main Structure ( $\zeta_n = 0.01$ ) for No TMD, TMD, MTMD, sTMD, and sMTMD ( $\mu = 0.01$ ): (a) Force Excitation; (b) Base Excitation . . . . .	164
6.8	Maximum Frequency Response versus MTMD Frequency Range for Force Excited SDOF with 5-TMD (- - -) / 5-sTMD (—) . . . . .	164
6.9	Maximum Frequency Response versus TMD Damping Ratio for Force Excited SDOF with TMD/sTMD and 5-TMD(- - -) / 5-sTMD (—) . . . . .	165
6.10	Dynamic Response of Force Excited SDOF Main Structure ( $f_n = 2 \text{ Hz}$ ) under Harmonic Sinusoidal Load ( $f = 2 \text{ Hz}$ ): (a) No TMD, TMD, sTMD; (b) No TMD, MTMD, sMTMD . . . . .	169
6.11	Maximum Steady-State Response of Force Excited 5-DOF Main Structure ( $f_{n1} = 2 \text{ Hz}$ ) under Harmonic Sinusoidal Loading ( $f = 2 \text{ Hz}$ ) for No TMD, TMD, MTMD, sTMD, sMTMD . . . . .	169
6.12	Dynamic Response of Force Excited SDOF Main Structure ( $f_n = 0.5 \text{ Hz}$ ) under Discrete Sinusoidal Sweep Load ( $1.6 \text{ Hz} < f < 2.4 \text{ Hz}$ ): (a) No TMD, TMD, sTMD; (b) No TMD, MTMD, sMTMD . . . . .	170
6.13	Maximum Transient Response of Force Excited 5-DOF Main Structure ( $f_{n1} = 2 \text{ Hz}$ ) under Discrete Sinusoidal Sweep Loading ( $1.6 \text{ Hz} < f < 2.4 \text{ Hz}$ ) for No TMD, TMD, MTMD, sTMD, sMTMD . . . . .	171
6.14	Dynamic Response of Force Excited SDOF Main Structure ( $f_n = 2 \text{ Hz}$ ) under Linear Chirp Load ( $1.6 \text{ Hz} < f < 2.4 \text{ Hz}$ ): (a) No TMD, TMD, sTMD; (b) No TMD, MTMD, sMTMD . . . . .	171
6.15	Maximum Transient Response of Force Excited 5-DOF Main Structure ( $f_{n1} = 2 \text{ Hz}$ ) under Linear Chirp Loading ( $1.6 \text{ Hz} < f < 2.4 \text{ Hz}$ ) for No TMD, TMD, MTMD, sTMD, sMTMD . . . . .	172
6.16	(a) Narrow Band Stationary Excitation; (b) Frequency Tracking; (c) STFT Spectrum . . . . .	172
6.17	Dynamic Response of Force Excited SDOF Main Structure ( $f_n = 0.5 \text{ Hz}$ ) under Stationary Excitation: (a) No TMD, TMD, sTMD; (b) No TMD, MTMD, sMTMD . . . . .	173

6.18	Maximum Transient Response of Force Excited 5-DOF Main Structure ( $f_{n1} = 0.5 \text{ Hz}$ ) under Stationary Excitation for No TMD, TMD, MTMD, sTMD, sMTMD . . . . .	173
6.19	(a) 1940 El Centro Earthquake ; (b) Frequency Tracking; (c) STFT Spectrum . . . . .	174
6.20	Dynamic Response of Base Excited SDOF Main Structure ( $f_n = 2 \text{ Hz}$ ) under 1940 El Centro Earthquake: (a) No TMD, TMD, sTMD; (b) No TMD, MTMD, sMTMD . . . . .	174
6.21	Maximum Transient Response of Base Excited 5-DOF Main Structure ( $f_{n1} = 2 \text{ Hz}$ ) under 1940 El Centro Earthquake for No TMD, TMD, MTMD, sTMD, sMTMD . . . . .	175
6.22	Top Floor Displacement of Force Excited 5-DOF Main Structure ( $f_{n1} = 0.5 \text{ Hz}$ ) under under Stationary Excitation: (a) Step Stiffness Change (b) No TMD, TMD, sTMD; (c) No TMD, MTMD, sMTMD . . . . .	175
6.23	Maximum Transient Response of Force Excited 5-DOF Main Structure ( $f_{n1} = 0.5 \text{ Hz}$ ) with a Step Stiffness Change under Stationary Excitation for No TMD, TMD, MTMD, sTMD, sMTMD . . . . .	176
6.24	Top Floor Displacement of Base Excited 5-DOF Main Structure ( $f_{n1} = 2 \text{ Hz}$ ) under under 1940 El Centro Earthquake: (a) Step Stiffness Change (b) No TMD, TMD, sTMD; (c) No TMD, MTMD, sMTMD . . . . .	176
6.25	Maximum Transient Response of Base Excited 5-DOF Main Structure ( $f_{n1} = 2 \text{ Hz}$ ) with a Step Stiffness Change under 1940 El Centro Earthquake for No TMD, TMD, MTMD, sTMD, sMTMD . . . . .	177
7.1	Analytical model of the SDOF system equipped with variable stiffness and variable damping device . . . . .	180
7.2	Analytical model of the MDOF system equipped with variable stiffness and variable damping device . . . . .	181
7.3	Control Algorithm . . . . .	187
7.4	Variable Stiffness and Damping Parameter Selection . . . . .	196



- 7.5 Wide-band stationary base excitation of SDOF: (a) EPSD for 500 sample, (b) Sample ground acceleration, (c) Displacement response spectra, (d) Acceleration response spectra, (e) RMS displacement response ( $f_n^{on} = 1.0$  - pass. on), (e) RMS acceleration response ( $f_n^{on} = 1.0$  - pass. on), (g) RMS displacement response ( $f_n^{on} = 2.0$  - pass. on), (h) RMS acceleration response ( $f_n^{on} = 2.0$  - pass. on) . . . . . 197
- 7.6 Wide-band stationary base excitation of SDOF: Sample ground acceleration, time history responses and variable stiffness: (1)  $f_n = 1.0Hz$  (pass. on); (2)  $f_n = 2.0Hz$  (pass. on) . . . . . 198
- 7.7 Locally stationary base excitation of SDOF: (a) EPSD for 500 sample, (b) Sample ground acceleration, (c) Displacement response spectra, (d) Acceleration response spectra, (e) RMS displacement response ( $f_n^{on} = 1.0$  - pass. on), (e) RMS acceleration response ( $f_n^{on} = 1.0$  - pass. on), (g) RMS displacement response ( $f_n^{on} = 2.0$  - pass. on), (h) RMS acceleration response ( $f_n^{on} = 2.0$  - pass. on) . . . . . 199
- 7.8 Locally stationary base excitation of SDOF: Sample ground acceleration, time history responses and variable stiffness: (1)  $f_n^{on} = 1.0Hz$  (pass. on); (2)  $f_n^{on} = 2.0Hz$  (pass. on) . . . . . 200
- 7.9 Non-stationary base excitation of SDOF: (a) EPSD for 500 sample, (b) Sample ground acceleration, (c) Displacement response spectra, (d) Acceleration response spectra, (e) RMS displacement response ( $f_n^{on} = 1.0$  - pass. on), (e) RMS acceleration response ( $f_n^{on} = 1.0$  - pass. on), (g) RMS displacement response ( $f_n^{on} = 3.0$  - pass. on), (h) RMS acceleration response ( $f_n^{on} = 3.0$  - pass. on) . . . . . 201
- 7.10 Non-stationary base excitation of SDOF: Sample ground acceleration, time history responses and variable stiffness: (1)  $f_n^{on} = 1.0Hz$  (pass. on); (2)  $f_n^{on} = 3.0Hz$  (pass. on) . . . . . 202
- 7.11 1940 El Centro Earthquake excitation of SDOF: (a) EPSD, (b) Ground acceleration, (c) Displacement response spectra, (d) Acceleration response spectra, (e) RMS displacement response ( $f_n^{on} = 1.0$  - pass. on), (e) RMS acceleration response ( $f_n^{on} = 1.0$  - pass. on), (g) RMS displacement response spectra ( $f_n^{on} = 3.0$  - pass. on), (h) RMS acceleration response ( $f_n^{on} = 3.0$  - pass. on) . . . . . 203

7.12	1940 El Centro Earthquake excitation of SDOF: Ground acceleration, time history responses and variable stiffness: (1) $f_n^{on} = 1.0Hz$ (pass. on); (2) $f_n^{on} = 3.0Hz$ (pass. on) . . . . .	204
7.13	Locally stationary base excitation of s4DOF ( $f_n^{on} = 1.53Hz$ - pass. on) (a) EPSD for 500 sample ( $0.5Hz < f_g < 2.5Hz$ ), (b) Sample ground acceleration, (c) RMS displacement response - top floor, (d) RMS acceleration response - top floor, (e) RMS displacement response - 1st floor, and (f) RMS acceleration response - 1st floor . . . . .	205
7.14	Peak RMS responses of s4DOF ( $f_n^{on} = 1.53Hz$ - pass. on, $0.5Hz < f_g < 2.5Hz$ ) (a) Displacements, (b) Drifts and (c) Accelerations . . . . .	206
7.15	Approximate solution via evolutionary complex frequency response function (a) EPSD for 500 sample ( $1Hz < f_g < 3Hz$ ), (b) Displacement response spectrum, (c) Mean stiffness variation ( $f_n^{on} = 1.5$ - pass. on), and (d) RMS displacement response ( $f_n^{on} = 1.5$ - pass. on) . . . . .	206
8.1	MDOF Structural Model with sMTMD (varying $k_1, \dots, k_n$ ) at the roof level: (a) Force Excited; (b) Base Excited . . . . .	209
8.2	Control Algorithm . . . . .	211
8.3	Variable Stiffness and Damping Parameter Selection . . . . .	212
8.4	Narrow-band stationary force excitation of SDOF (feedforward): (a) EPSD for 500 sample, (b) Sample acceleration, (c) Displacement response spectra, (d) RMS displacement response ( $f_n = 1.0 Hz$ ), (e) Displacement response spectra - damaged, (f) RMS displacement response - damaged ( $f_n = 1.5 \rightarrow 1.1 Hz$ for $t > 4.1 sec$ ) . . . . .	217
8.5	Narrow-band stationary force excitation of SDOF (feedforward): (a,b) Time history response, (c,d) variable stiffness and damping . . . . .	218
8.6	Narrow-band stationary force excitation of 5-DOF (feedforward): (a) Peak RMS displacements ( $f_n = 1.0 Hz$ ), (b) Peak RMS displacements - damaged ( $f_n = 1.2 \rightarrow 1.0 Hz$ for $t \geq 4.1 sec$ ) . . . . .	218
8.7	Narrow-band stationary force excitation of 5-DOF (feedforward): (a,b) Top floor displacement response history, (c,d) variable stiffness and damping . .	219

8.8	Narrow-band stationary wind excitation of SDOF (feedback): (a) EPSD for 500 sample, (b) Sample wind velocity, (c) Displacement response spectra, (d) RMS displacement response ( $f_n = 0.2 \text{ Hz}$ ), (e) Displacement response spectra - damaged, (f) RMS displacement response - damaged ( $f_n = 0.3 \rightarrow 0.21 \text{ Hz}$ for $t > 20 \text{ sec}$ ) . . . . .	220
8.9	Narrow-band stationary wind excitation of SDOF (feedback): (a,b) Time history response, (c,d) variable stiffness and damping . . . . .	221
8.10	Narrow-band stationary wind excitation of 5-DOF (feedback): (a) Peak RMS displacements ( $f_n = 0.2 \text{ Hz}$ ), (b) Peak RMS displacements - damaged ( $f_n = 0.25 \rightarrow 0.21 \text{ Hz}$ for $t \geq 20 \text{ sec}$ ) . . . . .	221
8.11	Narrow-band stationary wind excitation of 5-DOF (feedback): (a,b) Top floor displacement response history, (c,d) variable stiffness and damping . . . . .	222
8.12	Locally stationary base excitation of SDOF (feedforward): (a) EPSD for 500 sample, (b) Sample ground acceleration, (c) Displacement response spectra, (d) RMS displacement response ( $f_n = 1.0 \text{ Hz}$ ), (e) Displacement response spectra - damaged, (f) RMS displacement response - damaged ( $f_n = 1.5 \rightarrow 1.1 \text{ Hz}$ for $t > 4.1 \text{ sec}$ ) . . . . .	223
8.13	Locally stationary base excitation of SDOF (feedforward): (a,b) Time history response, (c,d) variable stiffness and damping . . . . .	224
8.14	Locally stationary base excitation of 5-DOF (feedforward): (a) Peak RMS displacements ( $f_n = 1.0 \text{ Hz}$ ), (b) Peak RMS displacements - damaged ( $f_n = 1.3 \rightarrow 1.1 \text{ Hz}$ for $t \geq 4.1 \text{ sec}$ ) . . . . .	224
8.15	Locally stationary base excitation of 5-DOF (feedforward): (a,b) Top floor displacement response history, (c,d) variable stiffness and damping . . . . .	225
8.16	Locally stationary base excitation of SDOF (feedback): (a) EPSD for 500 sample, (b) Sample ground acceleration, (c) Displacement response spectra, (d) RMS displacement response ( $f_n = 1.0 \text{ Hz}$ ), (e) Displacement response spectra - damaged, (f) RMS displacement response - damaged ( $f_n = 1.5 \rightarrow 1.1 \text{ Hz}$ for $t > 4.1 \text{ sec}$ ) . . . . .	226
8.17	Locally stationary base excitation of SDOF (feedback): (a,b) Time history response, (c,d) variable stiffness and damping . . . . .	227

8.18	Locally stationary base excitation of 5-DOF (feedback): (a) Peak RMS displacements ( $f_n = 1.0 \text{ Hz}$ ), (b) Peak RMS displacements - damaged ( $f_n = 1.2 \rightarrow 1.0 \text{ Hz}$ for $t \geq 4.1 \text{ sec}$ ) . . . . .	227
8.19	Locally stationary base excitation of 5-DOF (feedback): (a,b) Top floor displacement response history, (c,d) variable stiffness and damping . . . . .	228
8.20	1940 El Centro Earthquake excitation of SDOF (feedforward): (a) EPSD, (b) Ground acceleration, (c) Displacement response spectra, (d) RMS displacement response ( $f_n = 2.0 \text{ Hz}$ ), (e) Displacement response spectra - damaged, (f) RMS displacement response - damaged ( $f_n = 2.0 \rightarrow 1.4 \text{ Hz}$ for $t > 2.6 \text{ sec}$ ) . . . . .	230
8.21	1940 El Centro Earthquake excitation of SDOF (feedforward): (a,b) Time history response, (c,d) variable stiffness and damping . . . . .	231
8.22	1940 El Centro Earthquake excitation of 5-DOF (feedforward): (a) Peak RMS displacements ( $f_n = 1.7 \text{ Hz}$ ), (b) Peak RMS displacements - damaged ( $f_n = 1.7 \rightarrow 1.5 \text{ Hz}$ for $t \geq 2.6 \text{ sec}$ ) . . . . .	231
8.23	1940 El Centro Earthquake excitation of 5-DOF (feedforward): (a,b) Top floor displacement response history, (c,d) variable stiffness and damping . . . . .	232
8.24	1940 El Centro Earthquake excitation of SDOF (feedback): (a) EPSD, (b) Ground acceleration, (c) Displacement response spectra, (d) RMS displacement response ( $f_n = 1.5 \text{ Hz}$ ), (e) Displacement response spectra - damaged, (f) RMS displacement response - damaged ( $f_n = 3.0 \rightarrow 2.1 \text{ Hz}$ for $t > 2.6 \text{ sec}$ ) . . . . .	233
8.25	1940 El Centro Earthquake excitation of SDOF (feedback): (a,b) Time history response, (c,d) variable stiffness and damping . . . . .	234
8.26	1940 El Centro Earthquake excitation of 5-DOF (feedback): (a) Peak RMS displacements ( $f_n = 2.5 \text{ Hz}$ ), (b) Peak RMS displacements - damaged ( $f_n = 2.5 \rightarrow 2.0 \text{ Hz}$ for $t \geq 2.6 \text{ sec}$ ) . . . . .	234
8.27	1940 El Centro Earthquake excitation of 5-DOF (feedback): (a,b) Top floor displacement response history, (c,d) variable stiffness and damping . . . . .	235
9.1	MDOF Structural Model with sTLCD: (a) Force excited, (b) Base excited . . . . .	238

9.2	Control Algorithm . . . . .	246
9.3	Variable Stiffness Parameter Selection . . . . .	247
9.4	RMS value of SDOF system with sTLCD: (a) $f_n = 0.3 \text{ Hz}$ (force excited), (b) $f_n = 1.5 \text{ Hz}$ (base excited) . . . . .	250
9.5	Transfer functions for SDOF system with sTLCD: (a) $f_n = 0.3 \text{ Hz}$ (force excited), (b) $f_n = 1.5 \text{ Hz}$ (base excited) . . . . .	251
9.6	Narrow-band stationary force excitation of SDOF (feedforward): (a) EPSD for 500 sample, (b) Sample acceleration, (c) Displacement response spec- tra, (d) RMS displacement response ( $f_n = 1.0 \text{ Hz}$ ), (e) Displacement response spectra - damaged, (f) RMS displacement response - damaged ( $f_n = 1.5 \rightarrow 1.1 \text{ Hz}$ for $t > 4.1 \text{ sec}$ ) . . . . .	253
9.7	Narrow-band stationary force excitation of SDOF (feedforward): (a) Time history response, (b) Variable spring frequency . . . . .	254
9.8	Narrow-band stationary force excitation of 5-DOF (feedforward): (a) Peak RMS displacements ( $f_n = 1.0 \text{ Hz}$ ), (b) Peak RMS displacements - dam- aged ( $f_n = 1.2 \rightarrow 1.0 \text{ Hz}$ for $t \geq 4.1 \text{ sec}$ ) . . . . .	254
9.9	Narrow-band stationary force excitation of 5-DOF (feedforward): (a) Top floor displacement response history, (b) variable spring frequency . . . . .	255
9.10	Narrow-band stationary wind excitation of SDOF (feedback): (a) EPSD for 500 sample, (b) Sample wind velocity, (c) Displacement response spectra, (d) RMS displacement response ( $f_n = 0.2 \text{ Hz}$ ), (e) Displacement response spectra - damaged, (f) RMS displacement response - damaged ( $f_n = 0.2 \rightarrow$ $0.14 \text{ Hz}$ for $t > 20 \text{ sec}$ ) . . . . .	256
9.11	Narrow-band stationary wind excitation of SDOF (feedback): (a) Time his- tory response, (b) Variable spring frequency . . . . .	257
9.12	Narrow-band stationary wind excitation of 5-DOF (feedback): (a) Peak RMS displacements ( $f_n = 0.2 \text{ Hz}$ ), (b) Peak RMS displacements - dam- aged ( $f_n = 0.2 \rightarrow 0.17 \text{ Hz}$ for $t \geq 20 \text{ sec}$ ) . . . . .	257
9.13	Narrow-band stationary wind excitation of 5-DOF (feedback): (a) Top floor displacement response history, (b) Variable spring frequency . . . . .	258

9.14	Locally stationary base excitation of SDOF (feedforward): (a) EPSD for 500 sample, (b) Sample ground acceleration, (c) Displacement response spectra, (d) RMS displacement response ( $f_n = 1.0 \text{ Hz}$ ), (e) Displacement response spectra - damaged, (f) RMS displacement response - damaged ( $f_n = 1.5 \rightarrow 1.1 \text{ Hz}$ for $t > 4.1 \text{ sec}$ ) . . . . .	260
9.15	Locally stationary base excitation of SDOF (feedforward): (a) Time history response, (b) Variable spring frequency . . . . .	261
9.16	Locally stationary base excitation of 5-DOF (feedforward): (a) Peak RMS displacements ( $f_n = 1.0 \text{ Hz}$ ), (b) Peak RMS displacements - damaged ( $f_n = 1.3 \rightarrow 1.1 \text{ Hz}$ for $t \geq 4.1 \text{ sec}$ ) . . . . .	261
9.17	Locally stationary base excitation of 5-DOF (feedforward): (a) Top floor displacement response history, (b) Variable spring frequency . . . . .	262
9.18	Locally stationary base excitation of SDOF (feedback): (a) EPSD for 500 sample, (b) Sample ground acceleration, (c) Displacement response spectra, (d) RMS displacement response ( $f_n = 1.0 \text{ Hz}$ ), (e) Displacement response spectra - damaged, (f) RMS displacement response - damaged ( $f_n = 1.5 \rightarrow 1.1 \text{ Hz}$ for $t > 4.1 \text{ sec}$ ) . . . . .	263
9.19	Locally stationary base excitation of SDOF (feedback): (a) Time history response, (b) variable spring frequency . . . . .	264
9.20	Locally stationary base excitation of 5-DOF (feedback): (a) Peak RMS displacements ( $f_n = 1.0 \text{ Hz}$ ), (b) Peak RMS displacements - damaged ( $f_n = 1.2 \rightarrow 1.0 \text{ Hz}$ for $t \geq 4.1 \text{ sec}$ ) . . . . .	264
9.21	Locally stationary base excitation of 5-DOF (feedback): (a) Top floor displacement response history, (b) Variable spring frequency . . . . .	265
9.22	1940 El Centro Earthquake excitation of SDOF (feedforward): (a) EPSD, (b) Ground acceleration, (c) Displacement response spectra, (d) RMS displacement response ( $f_n = 1.5 \text{ Hz}$ ), (e) Displacement response spectra - damaged, (f) RMS displacement response - damaged ( $f_n = 2.0 \rightarrow 1.4 \text{ Hz}$ for $t > 2.6 \text{ sec}$ ) . . . . .	267
9.23	1940 El Centro Earthquake excitation of SDOF (feedforward): (a) Time history response, (b) Variable spring frequency . . . . .	268

9.24	1940 El Centro Earthquake excitation of 5-DOF (feedforward): (a) Peak RMS displacements ( $f_n = 1.6 \text{ Hz}$ ), (b) Peak RMS displacements - damaged ( $f_n = 1.6 \rightarrow 1.4 \text{ Hz}$ for $t \geq 2.6 \text{ sec}$ ) . . . . .	268
9.25	1940 El Centro Earthquake excitation of 5-DOF (feedforward): (a) Top floor displacement response history, (b) Variable spring frequency . . . . .	269
9.26	1940 El Centro Earthquake excitation of SDOF (feedback): (a) EPSD, (b) Ground acceleration, (c) Displacement response spectra, (d) RMS displacement response ( $f_n = 2.0 \text{ Hz}$ ), (e) Displacement response spectra - damaged, (f) RMS displacement response - damaged ( $f_n = 2.0 \rightarrow 1.4 \text{ Hz}$ for $t > 2.6 \text{ sec}$ ) . . . . .	270
9.27	1940 El Centro Earthquake excitation of SDOF (feedback): (a) Time history response, (b) Variable spring frequency . . . . .	271
9.28	1940 El Centro Earthquake excitation of 5-DOF (feedback): (a) Peak RMS displacements ( $f_n = 1.6 \text{ Hz}$ ), (b) Peak RMS displacements - damaged ( $f_n = 1.6 \rightarrow 1.4 \text{ Hz}$ for $t \geq 2.6 \text{ sec}$ ) . . . . .	271
9.29	1940 El Centro Earthquake excitation of 5-DOF (feedback): (a) Top floor displacement response history, (b) Variable spring frequency . . . . .	272

# Chapter 1

## Introduction

### 1.1 Objective and Scope of This Study

Many studies in the literature (Housner et al. 1997; Spencer and Nagarajaiah 2003) have shown that adaptive structures have major advantages over passive ones. With this motivation, many structural control devices and control algorithms have been developed and examined on wind and ground excited structures. Structures respond differently to different kind of excitations. Therefore, it is very important to be able to know the characteristics of the excitation signal fully and successfully incorporate it into the control algorithm. Although for stationary signals, classical spectral analysis based on Fourier transform describe the signal satisfactorily, it is not capable of describing time-varying, evolutionary spectra. In reality most signals in nature have non-stationary characteristics and have time-varying, evolutionary spectra. To be able to describe the evolutionary characteristics of a non-stationary signals, joint time-frequency methods such as short time Fourier transform (STFT) and wavelet transform (WT) need to be performed. In this study, the main objectives are (i) to employ time-frequency techniques such as STFT and WT to describe evolutionary spectra of the excitation and response signals, and to identify the instantaneous (dominant) frequency in real-time; and (ii) to develop novel control algorithms for smart semi-active systems using the real-time evolutionary spectra and the instantaneous (dominant) frequency.

In the remaining of this chapter, preliminary background and previous work in the literature have been presented. In Chapter 2, mathematical formulation of linear time varying (LTV) systems is summarized with a specific case study on the formulation of the semi-



active tuned mass damper (sTMD). Chapter 3 provides an introduction to time-frequency analysis with short time Fourier transform (STFT) and wavelet transform (WT).

Chapter 4 presents the algorithms used for frequency tracking and evolutionary spectrum estimation using STFT and WT. A discrete sine sweep and four different random processes are studied to compare the instantaneous frequency and evolutionary spectrum obtained by the two methods.

Chapter 5 - differing from other chapters - studies two nonlinear control algorithms which are not based on time-frequency analysis. The nonlinear control algorithms developed to independently vary stiffness and damping in structures are examined under near-fault earthquake records and pulse type of excitations fitted to them. Three cases of semi-active control are considered, which are (i) independently variable stiffness control, (ii) independently variable damping control, and (iii) combined variable stiffness and damping control.

Chapter 6 introduces feedforward semi-active single and multiple tuned mass dampers (sTMD/sMTMD), which are tuned to the instantaneous frequency of the excitation signal. Their deterministic responses are studied under several harmonic and random excitations.

Chapter 7 presents a novel control algorithm developed for semi-active single/multiple degree-of-freedom (sSDOF/sMDOF) systems based on adaptive  $H_2$  control. The algorithm involves obtaining the real-time time-frequency characteristics of the excitation and then applying instantaneous  $H_2$  control by an independently variable stiffness device. The proposed control basically keeps the fundamental frequency of the system away from the dominant frequencies of the excitation by minimizing the  $H_2$  norm of the instantaneous response spectrum. For MDOF systems, the scope is limited to the systems equipped with variable stiffness and variable damping devices between the base and first DOF. The performance of the control algorithm is evaluated for several random ground motion processes

and 1940 El Centro Earthquake.

Chapter 8 studies single and multiple semi-active variable stiffness tuned mass dampers (sTMD/ sMTMD) under a broader range of random excitations. Two different classes of sTMD are investigated: (i) feedforward sTMD/sMTMD which are tuned to instantaneous frequency of the excitation (similar to Chapter 6) and (ii) feedback sTMD/sMTMD which are tuned to the instantaneous frequency of the displacement response. SDOF and MDOF systems equipped with sTMD and sMTMD subjected to narrow-band stationary force excitations, wide-band locally stationary base excitations, and 1940 El Centro earthquake are investigated.

In chapter 9, feedforward and feedback control strategies of sTMD are extended to semi-active tuned liquid column dampers (sTLCD). SDOF and MDOF systems equipped with sTLCD subjected to narrow-band stationary force excitations, wide-band locally stationary base excitations, and 1940 El Centro earthquake are investigated.

The final chapter summarizes the main points of this study and presents the concluding remarks.

## **1.2 Review of Previous Work**

### **1.2.1 Structural Control: Passive, Semiactive and Active Systems**

The field of structural control has its roots back more than 100 years to John Milne, a professor of engineering in Japan, who built a small house of wood and placed it on ball bearings to demonstrate that a structure could be isolated from earthquake sliding (Housner et al. 1997). But it was after 1960 when the first applications of passive structural control had been seen. In the last few decades many structural control devices were developed and significant progress has been made in the field. Today, there are four types of structural

control: (1) passive, (2) active, (3) hybrid and (4) semi-active. In passive control, passive devices are employed to absorb and dissipate energy to reduce the response of the structure. No external energy is given to the system, so it is stable but not adaptive to varying structural and environmental conditions. Base isolation of low-rise and mid-rise buildings, and tuned mass dampers in tall buildings are such devices. Active control is the strategy to apply forces to the structure in a prescribed manner by an actuator powered by an external energy source. Active devices can both dissipate and add energy in the structure. Therefore, they may cause instability of the structure. Active mass damper is an example of active devices. A hybrid control system is defined as one which employs a combination of passive and active devices to exploit their potential to increase the overall reliability and efficiency (Spencer and Nagarajaiah 2003). The hybrid control system can be more reliable than a fully active system, but it is also often more complicated. An example of such device is hybrid mass damper where a tuned mass damper and an active control actuator are combined. Semiactive control is the strategy based on changing the structural properties (i.e. damping, stiffness) of the control device to minimize the response of the structure without applying any external force. Semiactive control strategies are particularly promising in addressing many of the challenges of structural control, offering the reliability of passive devices, yet maintaining the versatility and adaptability of fully active systems, without requiring the associated large power sources and can operate on battery power (Spencer and Nagarajaiah 2003). Unlike active control devices, semi-active control devices do not have the potential to destabilize the structural system. Semiactive systems perform significantly better than passive devices and have comparable performance to fully active systems with orders of magnitude less power consumption. Examples of such devices are variable-orifice fluid dampers, controllable friction devices, variable-stiffness devices, smart tuned mass dampers and tuned liquid dampers, and controllable fluid dampers. In the following

sections, some of these control devices are discussed in detail, further information can also be found in Housner et al. (1997) and Spencer and Nagarajaiah (2003).

### **1.2.2 Semiactive Variable Damping and Stiffness Systems**

Various semi-active devices that can change stiffness and damping and the corresponding control algorithms have been developed (Spencer and Nagarajaiah 2003). One such device, the semi-active independently variable stiffness device (SAIVS) that varies the stiffness of a system smoothly and continuously, has been developed by Nagarajaiah and Mate (1998). The effectiveness of the device in producing a non-resonant structure has been demonstrated by Nagarajaiah and Mate (1998) and was further studied by Nagarajaiah et al. (1999).

Kobori et al. (1993) developed the first active variable stiffness (AVS) system to control seismic response. In this system the input energy to the structure is reduced by changing its stiffness in real-time to avoid resonance phenomena. In addition, it can also provide additional damping by hysteretic energy dissipation. The effectiveness of the system has been demonstrated through several experiments and records obtained over a period of ten years after a three story steel building equipped with AVS was built in 1990 in Japan.

Use of resettable actuator in reducing vibration had been proposed in the literature. The effective stiffness of the structure is kept high so that it stores energy. At appropriate times, when the energy stored in the system has reached a peak value, the force is reduced for a short time and reset to a high value. As a result of this resetting, stored strain energy is dissipated. Yang et al. (2000) have proposed a control law based on the Lyapunov theory for resetting a semi-active stiffness damper.

Several researchers have investigated semi-active dampers (Karnopp et al. 1974; Ivers and Miller 1991; Spencer et al. 1997). The application of controllable MR fluid dampers

for seismic protection has been studied analytically and experimentally by Dyke et al. (1998).

More recently, Agrawal (2004) examined the response of semi-active variable stiffness and damping systems to pulse type excitations both analytically and experimentally. The experimental setup involved a sliding SDOF system equipped with an SAIVS spring and an MR damper. Three semi-active control strategies are investigated (i) independently variable stiffness control based on a variable structure control (ii) independently variable damping control based on a Lyapunov control and (iii) combined variable stiffness and damping control.

### **1.2.3 Base Isolation**

The basic concept of the base isolation is to uncouple the superstructure from ground to protect it from the damaging effects of earthquake excitations. There are two common types of base isolation system (Kelly 1993). Among those, the most widely adopted one is the system with elastomeric bearings. The system works by decoupling the superstructure from the horizontal components of the ground motion by creating a layer with low stiffness between the superstructure and the foundation (substructure). The horizontal flexibility leads to a much lower fundamental frequency of the structure than both its fixed base frequency and the dominant frequencies of the ground motion. The dynamic response is mostly controlled by the fundamental (first) mode and the deformation of the base level only, keeping the decoupled superstructure linear and rigid. The second type of the isolation is the system with sliding bearings. The system works by providing only a low level friction across the isolation interface that will limit the transfer of the shear. Despite the simplicity of this system, there are several drawbacks that needs to addressed in the design. To sustain wind loads and unnecessary slip under small earthquakes, a considerable amount

of friction is needed. Additionally, the slip phenomenon is intrinsically nonlinear requiring a non-linear dynamic analysis and sudden changes between slipping and sticking conditions can generate high frequency vibrations exciting the higher modes of the structure.

The application of controllable MR fluid dampers in smart base isolated buildings has been studied analytically and experimentally by Nagarajaiah and Varadarajan (2000), Sahasrabudhe et al. (2000), Mao (2002), and is shown to be effective in reducing seismic response. The application of controllable electrorheological dampers for response control of elastomeric base isolated buildings was originally studied by Makris (1997), followed by Gavin (2001) and is shown to be effective in reducing response. Response control of sliding isolated buildings using variable orifice dampers has been studied experimentally by Madden et al. (2002). Makris and Chang (2000b) have shown the effectiveness of viscous, viscoplastic, and friction damping in response of seismically isolated structures.

Narasimhan and Nagarajaiah (2005) developed an STFT semi-active controller for base isolated buildings with variable stiffness isolation systems. The controller varies the stiffness of the isolation system smoothly between minimum and maximum values when the energy of the excitation exceeds a predetermined threshold value. The algorithm is examined analytically on a five-story base isolated reinforced concrete building with linear elastomeric isolation bearings and a variable stiffness system located at the isolation level, under several near-fault earthquakes.

#### **1.2.4 Tuned Mass Damper (TMD)**

Tuned mass damper (TMD) is a widely used passive energy absorbing device consisting of a secondary mass, a spring and a viscous damper, which is attached to a primary or main vibratory system to reduce its dynamic motion. Its effectiveness depended on the closeness of absorber's natural frequency to the excitation frequency. TMD was first suggested by

Frahm in 1909 (Den Hartog 1956). First closed form expressions for optimum parameters of a TMD were derived by Den Hartog (1956) for an undamped single degree of freedom (SDOF) main structure subjected to harmonic force. Since then, optimum parameters of TMD have been studied extensively. TMD is usually designed by modelling the main structure as an equivalent SDOF structure. McNamara (1977) studied the effectiveness of TMD under wind and white noise excitations, including a 400 ton TMD for Citicorp Center (a 900 ft high office building). Warburton (1981) studied the optimum parameters of a TMD system with a 2-DOF main structure and reported that the parameters determined for 2-DOF main structure are in close agreement with the ones for SDOF approximation of the same structure if the ratio of two natural frequencies of the main system is reasonably large. Abe and Igusa (1995) showed that for multi degree of freedom (MDOF) primary structures with widely spaced natural frequencies, the SDOF approximation of the primary structure is the dominant term in the perturbation series and higher order terms can be eliminated by suitably placing several additional TMDs on the structure. Abe and Igusa (1995) also reported that for structures with  $p$  closely spaced natural frequencies at least  $p$  TMDs are necessary to control the response and derived an analytical condition on the TMD placement that decouples the response of the system onto  $p$  SDOF structure/TMD systems. It is well accepted that TMD is effective in reducing the response due to harmonic (Den Hartog 1956) or wind excitations (McNamara 1977). For the seismic effectiveness of TMD, there is no general agreement. Kaynia et al. (1981) and Sladek and Klingner (1983) reported that TMD is not effective in reducing response due to earthquake excitation.

### **1.2.5 Multiple Tuned Mass Dampers (MTMD)**

The effectiveness of a TMD is highly dependent to its optimum tuning frequency and optimum damping parameter. Mistuning due to error or change in the natural frequency

due to damage/deterioration of the primary structure or off-optimum damping will reduce the efficiency of a TMD significantly. In the past two decades, systems with multiple TMDs (MTMD) have been proposed to eliminate the disadvantages of single TMD systems. Several researchers (Xu and Igusa 1992; Igusa and Xu 1994; Yamaguchi and Harnpornchai 1993) studied the performance and optimum parameters of MTMD systems under harmonic and white noise excitations, and showed that optimally designed MTMD system is more effective than the single TMD system. Yamaguchi and Harnpornchai (1993) investigated the fundamental characteristics of MTMD with the parameters of the covering frequency range of MTMD, the damping ratio of each TMD and the total number of TMDs in comparison to a single TMD for harmonically forced primary structural vibration. Abe and Fujino (1994) reported that a properly designed MTMD can be much more robust than a conventional TMD. Kareem and Kline (1995) studied SDOF systems with MTMD under random loading.

### **1.2.6 Semi-active Tuned Mass Damper (sTMD)**

The conditions of a real primary structural system often change with time due to deterioration or damage and TMD can lose effectiveness due to mistuning. The need for adaptivity has led to development of semi-active and active TMDs. An extensive survey of passive, semi-active and active TMDs has been presented by Sun et al. (1995). The main advantage of semi-active TMD is the response reduction comparable to an active TMD, but with an order of magnitude less power consumption (Nagarajaiah and Varadarajan 2005). Semi-active TMDs have been investigated by Hrovat et al. (1983), Abe (1996), and Abe and Igusa (1996). Several variable damping devices, such as magnetorheological, variable orifice, and electrorheological dampers have been developed (Spencer and Nagarajaiah 2003). Variable stiffness systems, with either on or off states, have been developed by Ko-



bori et al. (1993) and Yang et al. (2000). Using the SAIVS device (described in Section 1.2.2) a new semi-active variable stiffness TMD (sTMD) has been developed by Nagarajaiah and Varadarajan (2000). The sTMD has the distinct advantage of continuously retuning its frequency in real time thus making it robust to changes in primary system stiffness and damping. Recently, the sTMD has been studied by developing online tuning using empirical mode decomposition-Hilbert transform and short time Fourier transform (STFT) algorithms by Varadarajan and Nagarajaiah (2004) and Nagarajaiah and Varadarajan (2005), which tune the frequency of sTMD and reduce the primary structural response; it has been shown that sTMD is effective in reducing wind induced response of buildings and is robust against the changes in building stiffness. Nagarajaiah (2009) introduced a new adaptive length pendulum sTMD along with the further development of the concepts of sTMD and adaptive passive TMD (APTMD).

### **1.2.7 Optimization of TMD parameters**

In some literature, the TMD can also be referred as a dynamic vibration absorber (DVA) - a passive vibration control device which is attached to a vibrating member (called the primary system) subjected to an exciting force or motion. As mentioned above, the first DVA (or TMD) was invented by Frahm, and it had no damping element, and it was useful only in a narrow range of frequencies close to the natural frequency of the DVA. In 1928, Ormondroyd and Den Hartog found that the DVAs with energy dissipation mechanisms are effective to an extended range of frequencies and the damped DVA systems proposed by them is now known as the Voigt type DVA in which a spring element and a dashpot are arranged in parallel, and it has been recognized as a standard model of the DVAs (Asami et al. 2002). Since then, many optimization criteria have been proposed. Two typical optimization criteria are given below.

$H_\infty$  Optimization: The objective of  $H_\infty$  optimization is to minimize the maximum amplitude magnification factor (called  $H_\infty$  norm) of the primary system. The method for deriving the optimum parameter is called the fixed-points theory, since two points of the response curves of the system are used for obtaining the optimum parameter and all curves pass through these points independent of the absorber damping. The most favorable curve is the one which passes with a horizontal tangent through the highest of the two fixed points. Past research on  $H_\infty$  optimization of the DVAs are given in detail by Asami et al. (2002).

$H_2$  Optimization: When the primary system is subjected to random excitation, the excitation contains infinitely many frequencies. Therefore, it is not necessary to stick to only the resonant frequencies of the system. The  $H_2$  optimization criterion in the design of the damped DVA was proposed by Crandall and Mark in 1963 (Asami et al. 2002). The objective is to reduce the total vibration energy of the system over all frequency by minimizing the area (called  $H_2$  norm) under the frequency response curve of the system. Past research on  $H_2$  optimization of the DVAs are given in detail by Asami et al. (2002).

### 1.2.8 Tuned Liquid Column Dampers (TLCD)

Modern civil engineering structures being built are much lighter and slender than before, especially for high rise building and long span bridges. For the advantages of low cost, easy installation and easy adjustment of damper frequency, liquid column mass dampers (LCDs) have been introduced as an alternative to TMDs as energy dissipation devices for suppression of structural vibrations. Tuned liquid dampers (TLD) are dampers whose damping effects depend on the liquid residing in the damper and which are specifically tuned to the natural frequency of the structure. TLCD is a U-shaped tube, which contains

liquid, usually water. The application of TLCD to civil engineering structures were studied by Sakai et al. (1991), Xu and Samali (1992) and Balendra et al. (1999). The tuning ratio, which is the ratio of the natural frequency of the TLCD to that of the structures, is optimized in order to ensure an efficient transfer of shear force from the TLCD to structure. Many improvement ideas for the TLCD system have been proposed such as the variable orifice system or so called pressure control mechanism (Kareem and Kline 1995) and the studies on the characteristics of variable cross section between the horizontal and vertical tube (Gao et al. 1997), (Kavand and Zahrai 2006), the optimal setting for TLCD (Yalla, Kareem, and Kantor 2001). Recently, Ghosh and Basu (2004) studied the application of a spring connected TLCD to short period stiff structures subjected to earthquake excitations.

### 1.2.9 Random Vibration

A random process is a family, or ensemble, of  $n$  random variables related to a similar phenomenon which may be functions of one or more independent variables, such as time or space or both. In such cases the outcome of each trial is called a realization or a sample function. A random process becomes a random variable when time is fixed at some particular value. The random variable will possess statistical properties, such as a mean value, moments, variance, etc. that are related to its probability density function (PDF). A random process is said to be stationary if its statistical properties do not change with time; otherwise it is called non-stationary.

For a particular time  $t_1$ , the cumulative distribution function (CDF) associated with random variable  $X_1 = X(t_1)$  is

$$F_X(x_1, t_1) = P(X_1 \leq x_1) \quad \text{for any real number } x_1 \quad (1.1)$$

For two random variables  $X_1 = X(t_1)$  and  $X_2 = X(t_2)$ , the second order joint distribution

function is

$$F_X(x_1, x_2; t_1, t_2) = P(X_1 \leq x_1, X_2 \leq x_2) \quad (1.2)$$

For  $N$  random variables  $X_i = X(t_i)$ ,  $i = 1, 2, \dots, N$  the  $N^{th}$  order joint distribution function is written as

$$F_X(x_1, \dots, x_N; t_1, \dots, t_N) = P(X_1 \leq x_1, \dots, X_N \leq x_N) \quad (1.3)$$

Joint density functions (PDF) for the above three cases can be derived as

$$f_X(x_1, t_1) = \frac{F_X(x_1, t_1)}{dx_1} \quad (1.4)$$

$$f_X(x_1, x_2; t_1, t_2) = \frac{F_X(x_1, x_2; t_1, t_2)}{\partial x_1 \partial x_2} \quad (1.5)$$

$$f_X(x_1, \dots, x_N; t_1, \dots, t_N) = \frac{F_X(x_1, \dots, x_N; t_1, \dots, t_N)}{\partial x_1 \dots \partial x_N} \quad (1.6)$$

The statistical properties of a single random variable  $X(t_a)$  at any time  $t_a$  of the random process are defined as below,

$$\text{Mean} = E[X(t_a)] = m \quad (1.7)$$

$$\text{Mean square} = E[X(t_a)^2] \quad (1.8)$$

$$\text{Variance} = \sigma^2 = E[(X(t_a) - m)^2] \quad (1.9)$$

A random process is called stationary to order one if its first order density function (PDF) does not change with a shift in time origin.  $f_X(x_1, t_1) = f_X(x_1, t_1 + \Delta)$  must be true for any  $t_1$  and any real number  $\Delta$ . It is called stationary to order two if its first order density function satisfies

$$f_X(x_1, x_2; t_1, t_2) = f_X(x_1, x_2; t_1 + \Delta, t_2 + \Delta) \quad (1.10)$$

By extending the above reasoning to  $N$  random variables,  $N^{th}$  order stationarity can be defined. The definition of stationary random processes imposes the mathematical requirements that the realizations of these processes must extend from  $-\infty$  to  $+\infty$ . Physically, stationarity implies a measure of temporal uniformity in the characteristics of the factors contributing to randomness. In practice, no random process can be truly stationary. However, long segments of random process realizations exhibiting uniform characteristics can be treated as stationary.

The autocorrelation function of a random process  $X(t)$  is the correlation  $E[X_1 X_2]$  of two random variables  $X_1 = X(t_1)$  and  $X_2 = X(t_2)$  defined by the process at time  $t_1$  and  $t_2$ .

$$R(t_1, t_2) = E[X(t_1)X(t_2)] \quad (1.11)$$

If the autocorrelation function of a stationary random process is dependent on only time differences, instead of absolute time, random process is said to be wide sense stationary. So for a wide sense stationary random process

$$E[X(t)] = m = \text{constant} \quad (1.12)$$

$$R(t_1, t_2) = E[X(t)X(t + \tau)] = R(\tau) \text{ where } \tau = t_2 - t_1 \text{ and } t = t_1 \quad (1.13)$$

A process stationary to order 2 is clearly wide sense stationary. However, the converse is not necessarily true. The most useful form is the wide sense stationary process, since problem solutions are greatly simplified in such cases.

In addition to ensemble averages it is possible to determine the average values by averaging the sample function with respect to time.  $A[.]$  is used to denote time average in a manner analogous to  $E$  for the statistical average. The time average of a sample function is

$$\overline{x(t)} = A[x(t)] = \lim_{T \rightarrow \infty} \frac{1}{T} \int_{-T/2}^{T/2} x(t) dt \quad (1.14)$$

Time average is taken over all time because, as applied to random processes, sample functions of processes are presumed to exist for all time. The time autocorrelation function is given by

$$R_t(\tau) = A[x(t)x(t + \tau)] = \lim_{T \rightarrow \infty} \frac{1}{T} \int_{-T/2}^{T/2} x(t)x(t + \tau)dt \quad (1.15)$$

For any one sample function of the process  $X(t)$ ,  $\overline{x(t)}$  and  $R_t(\tau)$  are two numbers. However, when all sample functions are considered,  $\overline{x(t)}$  and  $R_t(\tau)$  become actually random variables.

$$E[\overline{x(t)}] = E[X] \quad (1.16)$$

$$E[R_t(\tau)] = R(\tau) \quad (1.17)$$

A random process is said to be ergodic if the averages taken across the ensemble are the same as those taken along one representative outcome (sample function) history of the ensemble. Thus, ergodic random process means that all statistical family (ensemble) averages are equal to corresponding time averages for any specific family (ensemble) member.

$$\overline{x(t)} = E[X] \quad (1.18)$$

$$R_t(\tau) = R(\tau) \quad (1.19)$$

Ergodic property makes it possible to obtain the moment functions of a stationary random process from a single record. Physically, ergodicity implies that a sufficiently long record of a stationary random process contains all the statistical information about the random phenomenon. In practical applications, often only one or two records are available, so that ergodicity is commonly assumed; when more records become available, the ergodicity assumption can be verified.

The Fourier transform of the autocorrelation function and its inverse are given by

$$S_x(\omega) = \frac{1}{2\pi} \int_{-\infty}^{\infty} R_x(\tau)e^{-i\omega\tau} d\tau \quad (1.20)$$

and

$$R_x(\tau) = \int_{-\infty}^{\infty} S_x(\omega) e^{i\omega\tau} d\omega \quad (1.21)$$

where  $S_x(\omega)$  is called the spectral density of the process  $X(t)$  and  $\omega$  is the angular frequency. For a stationary process with zero mean the autocorrelation function at  $\tau = 0$  gives the mean square value of the process.

$$R_x(\tau = 0) = E[X^2] = \int_{-\infty}^{\infty} S_x(\omega) d\omega \quad (1.22)$$

If the spectral density  $S_x(\omega)$  of a stationary random process is known, then the spectral density of the derivative of the process can be obtained as follows.

$$\begin{aligned} \frac{dR_x(\tau)}{d\tau} &= \frac{d}{d\tau} E[X(t)X(t+\tau)] = E\left[X(t) \frac{d}{d\tau} X(t+\tau)\right] \\ &= E\left[X(t) \frac{d}{d(t+\tau)} X(t+\tau) \frac{d(t+\tau)}{d\tau}\right] \\ &= E[X(t)\dot{X}(t+\tau)] \end{aligned} \quad (1.23)$$

Thus,

$$\frac{d}{d\tau} (R_x(\tau)) = E[X(t)\dot{X}(t+\tau)] \quad (1.24)$$

For a stationary process,  $E[X(t)\dot{X}(t+\tau)] = E[X(t-\tau)\dot{X}(t)]$  leading to

$$\frac{d}{d\tau} (R_x(\tau)) = E[X(t-\tau)\dot{X}(t)] \quad (1.25)$$

Differentiating Equation (1.25) with respect to  $\tau$ , gives

$$\frac{d^2}{d\tau^2} (R_x(\tau)) = -E[\dot{X}(t-\tau)\dot{X}(t)] = -R_{\dot{x}}(\tau) \quad (1.26)$$

where  $R_{\dot{x}}(\tau)$  is the autocorrelation function for  $\dot{x}(t)$ .

Differentiating Equation (1.21) once and twice leads to

$$\frac{d}{d\tau} (R_x(\tau)) = \int_{-\infty}^{\infty} i\omega S_x(\omega) e^{i\omega\tau} d\omega \quad (1.27)$$

and

$$\frac{d^2}{d\tau^2} (R_x(\tau)) = - \int_{-\infty}^{\infty} \omega^2 S_x(\omega) e^{i\omega\tau} d\omega \quad (1.28)$$

Substituting Equation (1.26) into Equation (1.28) leads to

$$R_{\dot{x}}(\tau) = - \frac{d^2}{d\tau^2} (R_x(\tau)) = \int_{-\infty}^{\infty} \omega^2 S_x(\omega) e^{i\omega\tau} d\omega = \int_{-\infty}^{\infty} \omega^2 S_{\dot{x}}(\omega) e^{i\omega\tau} d\omega \quad (1.29)$$

From Equation (1.29), the following relation is obtained.

$$S_{\dot{x}}(\omega) = \omega^2 S_x(\omega) \quad (1.30)$$

Using this result, mean square values of first and second derivative of the process can be written as

$$E[\dot{X}^2] = \int_{-\infty}^{\infty} S_{\dot{x}}(\omega) e^{i\omega\tau} d\omega = \int_{-\infty}^{\infty} \omega^2 S_x(\omega) e^{i\omega\tau} d\omega \quad (1.31)$$

$$E[\ddot{X}^2] = \int_{-\infty}^{\infty} S_{\ddot{x}}(\omega) e^{i\omega\tau} d\omega = \int_{-\infty}^{\infty} \omega^4 S_x(\omega) e^{i\omega\tau} d\omega \quad (1.32)$$

Similar to spectral density function, cross-spectral density of a pair of random process is defined as the Fourier transform of the corresponding cross-correlation function for the two processes. The direct and inverse transforms are written as

$$S_{xy}(\omega) = \frac{1}{2\pi} \int_{-\infty}^{\infty} R_{xy}(\tau) e^{-i\omega\tau} d\tau \quad (1.33)$$

$$R_{xy}(\tau) = \int_{-\infty}^{\infty} S_{xy}(\omega) e^{i\omega\tau} d\omega \quad (1.34)$$

The response of a SDOF system ( $y(t)$ ) to an arbitrary input ( $x(t)$ ) can be computed by adding the separate responses to all the incremental impulses which make up the total time history of  $x(t)$ .

$$y(t) = \int_{-\infty}^t h(t - \tau) x(\tau) d\tau \quad (1.35)$$

or

$$y(t) = \int_{-\infty}^{\infty} h(\theta) x(t - \theta) d\theta \quad (1.36)$$



in which  $h(t - \tau)$  is the impulse response function giving the response at time  $t$  to a unit impulse at time  $\tau$  and  $\theta = t - \tau$ . The complex frequency response function is the Fourier transform of the impulse response function  $h(t)$  written as

$$H(\omega) = \int_{-\infty}^{\infty} h(t)e^{-i\omega t} dt \quad (1.37)$$

By applying the Fourier transform to both sides of Equation (1.35) the input-output relation can be obtained in frequency domain as

$$Y(\omega) = H(\omega)X(\omega) \quad (1.38)$$

The stochastic characteristics of the response of a SDOF system ( $y(t)$ ) to an arbitrary input ( $x(t)$ ) depend on the input process and input-output characteristics of the system. The autocorrelation function for the output process is

$$R_y(\tau) = E[y(t)y(t + \tau)] \quad (1.39)$$

Defining  $\theta = t - \tau$ ,  $\phi = t + \tau - \tau = t$  and substituting the solutions  $y(t) = \int_{-\infty}^t h(\theta)x(t - \theta)d\theta$  and  $y(t + \tau) = \int_{-\infty}^{t+\tau} h(\phi)x(t + \tau - \phi)d\phi$  into Equation (1.39) gives

$$\begin{aligned} R_y(\tau) &= E \left[ \int_{-\infty}^{\infty} h(\theta)x(t - \theta)d\theta \int_{-\infty}^{\infty} h(\phi)x(t + \tau - \phi)d\phi \right] \\ &= E \left[ \int_{-\infty}^{\infty} \int_{-\infty}^{\infty} h(\theta)h(\phi)x(t - \theta)x(t + \tau - \phi)d\theta d\phi \right] \\ &= \int_{-\infty}^{\infty} \int_{-\infty}^{\infty} h(\theta)h(\phi)E[x(t - \theta)x(t + \tau - \phi)]d\theta d\phi \\ &= \int_{-\infty}^{\infty} \int_{-\infty}^{\infty} h(\theta)h(\phi)R_x(\tau - \phi + \theta)d\theta d\phi \end{aligned} \quad (1.40)$$

The spectral density of the output process is

$$\begin{aligned} S_y(\omega) &= \frac{1}{2\pi} \int_{-\infty}^{\infty} R_y(\tau)e^{-i\omega\tau} d\tau \\ &= \frac{1}{2\pi} \int_{-\infty}^{\infty} h(\theta)d\theta \int_{-\infty}^{\infty} h(\phi)d\phi \int_{-\infty}^{\infty} R_x(\tau - \phi + \theta)e^{-i\omega\tau} d\tau \end{aligned} \quad (1.41)$$

Multiplying the right hand side by  $e^{\theta+\phi-\theta-\phi} = 1$  results in

$$\begin{aligned} S_y(\omega) &= \int_{-\infty}^{\infty} h(\theta) e^{-i\omega\phi} d\theta \int_{-\infty}^{\infty} h(\phi) e^{i\omega\theta} d\phi \frac{1}{2\pi} \int_{-\infty}^{\infty} R_x(\tau - \phi + \theta) e^{-i\omega(\tau - \phi + \theta)} d\tau \\ &= H^*(\omega) H(\omega) S_x(\omega) = |H(\omega)|^2 S_x(\omega) \end{aligned} \quad (1.42)$$

The mean square response of the SDOF system can be computed by

$$E[Y^2] = \int_{-\infty}^{\infty} S_y(\omega) d\omega = \int_{-\infty}^{\infty} |H(\omega)|^2 S_x(\omega) d\omega \quad (1.43)$$

The formulation above can be extended to MDOF systems with multiple inputs as

$$\mathbf{S}_y(\omega) = \mathbf{H}(\omega) \mathbf{S}_x(\omega) \mathbf{H}^T(\omega) \quad (1.44)$$

where  $\mathbf{H}(\omega)$  is the complex frequency response matrix and  $\mathbf{S}_x(\omega)$ ,  $\mathbf{S}_y(\omega)$  are the spectral density matrices for input and output processes, respectively.

### 1.2.10 Evolutionary Spectra

The theory of evolutionary spectra was developed by Priestley (1965) to provide a framework for interpreting the results of conventional spectral analysis applied to data from non-stationary processes. Using this approach a theory of linear prediction and filtering for non-stationary processes, which is similar to the classical Kolmogorov-Wiener theory for stationary process, was constructed (Priestley 1981; Priestley 1988). In this section, the theory is summarized with some of the important definitions and theorems from Priestley (1965,1981,1988).

Let  $X(t)$  be a stochastic process with zero mean and finite variance ( $E[X(t)] = 0$ ,  $E[|X(t)|^2] < \infty$ ) where  $t$  is a continuous parameter. The covariance function is defined by

$$R(s, t) = E[X^*(s)X(t)] \quad (1.45)$$

If  $X(t)$  is stationary, that  $R(s, t)$  is a function of  $|s - t|$  only, then from Wiener-Khintchine theorem  $R(s, t)$  can be written as

$$R(s, t) = \int_{-\infty}^{\infty} e^{i\omega(t-s)} dS(\omega) \quad (1.46)$$

where  $S(\omega)$  (the integrated spectrum of  $X(t)$ ) has the properties of a distribution function on the interval  $(-\infty, \infty)$ .

Using a Fourier-Stieltjes integral representation, stationary  $X(t)$  may be written in the form,

$$X(t) = \int_{-\infty}^{\infty} e^{i\omega t} dZ(\omega) \quad (1.47)$$

where  $Z(\omega)$  is an orthogonal-increment process with the following properties: (i)  $E[dZ(\omega)] = 0$ , (ii)  $E[|dZ(\omega)|^2] = dS(\omega)$ , where  $S(\omega)$  is the integrated spectrum of  $X(t)$ , (iii) for any two distinct frequencies,  $\omega, \omega'$ , ( $\omega \neq \omega'$ ),  $cov[dZ(\omega), dZ(\omega')] = E[dZ^*(\omega)dZ(\omega')] = 0$ .

When defining a time-dependent spectrum of a non-stationary signal which possesses a physical interpretation as a “local” power-frequency distribution, one must understand clearly what is it meant by “frequency”. When  $X(t)$  is stationary, the process has the form of Equation (1.47) which shows that any stationary process can be represented as the sum of sine and cosine waves with varying frequencies and (random) amplitudes and phases. But a non-stationary process cannot be represented as a sum of sine and cosine waves (with orthogonal coefficients) – instead it has to be represented as a sum of other kind of functions. For the term “frequency” to be meaningful, the function  $X(t)$  must have an “oscillatory form” which means that the Fourier transform of such a function will be concentrated around a particular frequency  $\omega_0$  (or around  $\pm\omega_0$  in the real case). Thus,  $\omega_0$  where Fourier transform has an absolute maximum is considered to be “the frequency” of the non-periodic function  $X(t)$ . In other words,  $X(t)$  behaves locally like a sine wave with frequency  $\omega_0$ , modulated by a smoothly varying amplitude function.

Consider a family  $\mathcal{F}$  of functions  $\{\phi(t, \omega)\}$  defined on a real line, and indexed by the suffix  $t$ , and a measure  $\mu(\omega)$  on the real line, such that for each  $s, t$  the covariance function is written as

$$R(s, t) = \int_{-\infty}^{\infty} \phi^*(s, \omega) \phi(t, \omega) d\mu(\omega) \quad (1.48)$$

In order for  $\text{var}[X(t)]$  to be finite for each  $t$ ,  $\phi(t, \omega)$  must be quadratically integrable with respect to measure  $\mu$ , for each  $t$ . Then, whenever  $R(s, t)$  has the representation Equation (1.48), the process  $X(t)$  can be written in the form,

$$X(t) = \int_{-\infty}^{\infty} \phi(t, \omega) dZ(\omega) \quad (1.49)$$

where  $Z(\omega)$  is an orthogonal process, with  $E[|dZ(\omega)|^2] = d\mu(\omega)$ ,

The measure  $\mu(\omega)$  is similar to the integrated spectrum  $S(\omega)$  in the case of stationary processes, so that the analogous situation to an absolutely continuous spectrum is obtained by assuming that the measure  $\mu(\omega)$  is absolutely continuous with respect to Lebesgue measure.

One family of functions  $\{\phi(t, \omega)\}$  which possess the required structure may be obtained as follows. Suppose that, for each fixed  $\omega$ ,  $\phi(t, \omega)$  (considered as a function of  $t$ ) possesses a (generalized) Fourier transform whose modulus has an absolute maximum at frequency  $\theta(\omega)$ . Then  $\phi(t, \omega)$  may be regarded as an amplitude modulated sine wave with frequency  $\theta(\omega)$  and written in the form

$$\phi(t, \omega) = A(t, \omega) e^{i\theta(\omega)t} \quad (1.50)$$

when the modulating function  $A(t, \omega)$  is such that the modulus of its (generalized) Fourier transform has an absolute maximum at the origin (i.e. zero frequency).

The function  $\phi(t, \omega)$  is called as an oscillatory function if, for some (necessarily unique)

$\theta(\omega)$  it may be written in the form of Equation (1.48) where  $A(t, \omega)$  is of the form

$$A(t, \omega) = \int_{-\infty}^{\infty} e^{it\theta} dK_{\omega}(\theta) \quad (1.51)$$

with  $|dK_{\omega}(\theta)|$  (the Fourier transform of  $A(t, \omega)$ ) having an absolute maximum at  $\theta = 0$ .

The function  $A(t, \omega)$  may be regarded as the envelope of  $\phi(t, \omega)$ . If, further, the family  $\{\phi(t, \omega)\}$  is such that  $\theta(\omega)$  is a single-valued function of  $\omega$ , then the variable  $\omega$  in Equation (1.48) can be changed to  $\theta(\omega)$  and redefining  $A(t, \omega)$ ,  $\mu(\omega)$  leads to

$$R(s, t) = \int_{-\infty}^{\infty} A^*(s, \omega) A(t, \omega) e^{i\omega(t-s)} d\mu(\omega) \quad (1.52)$$

and

$$X(t) = \int_{-\infty}^{\infty} A(t, \omega) e^{i\omega t} dZ(\omega) \quad (1.53)$$

where  $E[|dZ(\omega)|^2] = d\mu(\omega)$ .

If there exists a family of oscillatory functions  $\{\phi(t, \omega)\}$  in terms of which the process  $X(t)$  has a representation of the form Equation (1.49),  $X(t)$  is called an oscillatory process. Any family of oscillatory functions can be written in the form

$$\phi(t, \omega) = A(t, \omega) e^{i\omega t} \quad (1.54)$$

For an oscillatory process of the form Equation (1.53) with autocovariance function of the form Equation (1.52)

$$\text{var}[X(t)] = R(t, t) = \int_{-\infty}^{\infty} |A(t, \omega)|^2 d\mu(\omega) \quad (1.55)$$

$\text{var}[X(t)]$  may be interpreted as a measure of the total power of the process at time  $t$  giving a decomposition of total power in which the contribution from the frequency  $\omega$  is  $|A(t, \omega)|^2 d\mu(\omega)$ . The evolutionary power spectrum at time  $t$  with respect to the family  $\mathcal{F}$  of oscillatory functions,  $dS(t, \omega)$  is defined by

$$dS(t, \omega) = |A(t, \omega)|^2 d\mu(\omega) \quad (1.56)$$

When  $X(t)$  is stationary and  $\mathcal{F}$  is chosen to be the family of complex exponentials,  $dS(t, \omega)$  reduces to the standard definition of integrated spectrum. The evolutionary spectrum describes a distribution of power over frequency in the neighborhood of the time instant  $t$  unlike a stationary spectrum that describes the spectral content of the process over all time.

When the measure  $\mu(\omega)$  is absolutely continuous with respect to Lebesgue measure, evolutionary spectrum can be written as

$$dS(t, \omega) = S(t, \omega)d\omega \quad (1.57)$$

where  $S(t, \omega)$  is called the evolutionary spectral density function. The name is physically meaningful if  $S(t, \omega)$  is a slowly varying function of  $t$  within a time interval considerably longer than  $2\pi/\omega$  for any given  $\omega$ . Otherwise, the name was purely mathematical.

There is an interesting alternative interpretation of oscillatory processes in terms of time-varying filters. Let  $X(t)$  be defined by Equation (1.53). For each fixed  $t$ ,

$$A(t, \omega) = \int_{-\infty}^{\infty} e^{i\omega u} h_t(u) du \quad (1.58)$$

$$X(t) = \int_{-\infty}^{\infty} M(t - u) h_t(u) du \quad (1.59)$$

where

$$M(t) = \int_{-\infty}^{\infty} e^{i\omega t} dZ(\omega) \quad (1.60)$$

is a stationary stochastic process with spectrum  $d\mu(\omega) (= E|dZ(\omega)|^2)$ . Thus,  $X(t)$  may be interpreted as the result of passing a stationary process through a time-varying filter  $h_t(u)$ . Conversely, any process of the form Equation (1.59) (with  $h_t(u)$  chosen so that  $A(t, \omega)$  is of the required form) may be interpreted as the spectrum (in the classical sense) of the stationary process which would have been obtained if the filter  $h_t(u)$  was held fixed in the state which it attained at the time instant  $t$ .

A subclass within the class of evolutionary stochastic process is uniformly modulated process defined as

$$X(t) = A(t) \int_{-\infty}^{\infty} e^{i\omega t} dZ(\omega) \quad (1.61)$$

where  $A(t)$  is an envelope (or time-modulation) function.

One of the most useful features of stationary processes is that the effect of linear transformations (i.e. filters) can be described purely in terms of the effect on individual spectral components. A linear transformation of a stationary process  $X(t)$  is written as

$$Y(t) = \int_{-\infty}^{\infty} g(u) X(t-u) du \quad (1.62)$$

The spectra of  $X(t)$  and  $Y(t)$  are related by

$$dS_y(\omega) = |\Gamma(\omega)|^2 dS_x(\omega) \quad (1.63)$$

where

$$\Gamma(\omega) = \int_{-\infty}^{\infty} g(u) e^{-i\omega u} du \quad (1.64)$$

is the transfer function of the filter  $g(u)$ .  $dS_y(\omega_1)$  is determined purely by  $dS_x(\omega_1)$  and  $\Gamma(\omega_1)$ , and is not affected by  $dS_x(\omega)$  at other frequencies. It can be shown that this property holds (in an approximate sense) for evolutionary spectra in the case of linear transformations of non-stationary processes.

If  $X(t)$  satisfies a model of the form Equation (1.53), a more general form of the transformation Equation (1.62) can be written as

$$Y(t) = \int_{-\infty}^{\infty} g(u) X(t-u) e^{i\omega_0(t-u)} du \quad (1.65)$$

where  $\omega_0$  is any constant frequency.

$$Y(t) = \int_{-\infty}^{\infty} \Gamma_{t, \omega+\omega_0}(\omega) A(t, \omega+\omega_0) e^{i\omega t} dZ(\omega+\omega_0) \quad (1.66)$$

where for any  $t, \lambda, \theta$ ,

$$\Gamma_{t,\lambda}(\theta) = \int_{-\infty}^{\infty} g(u) \frac{A(t-u, \lambda)}{A(t, \lambda)} e^{-iu\theta} du \quad (1.67)$$

The function  $\Gamma_{t,\omega}(\omega)$  is the generalized transfer function of the filter  $g(u)$  with respect to the family  $\mathcal{F}$ .

The representation of  $Y(t)$  given by Equation (1.66) is not necessarily of the form Equation (1.53) since the modulus of (generalized) Fourier transform of  $\Gamma_{t,\omega+\omega_0}(\omega)A(t, \omega+\omega_0)$  may not have an absolute maximum at zero frequency. Even then, the function

$$\hat{\phi}(t, \omega)(\theta) = \Gamma_{t,\omega+\omega_0}(\omega)A(t, \omega+\omega_0)e^{i\omega t} \quad (1.68)$$

will still, in general, be oscillatory, but its dominant frequency will be slightly shifted from  $\omega$ .

For each  $t, \lambda$ , the function  $\Gamma_{t,\lambda}(\theta)$  reduces approximately to  $\Gamma(\theta)$  when  $A(t-u, \lambda)$  is, for each  $t, \lambda$ , slowly varying compared with the function  $g(u)$ . In other words, if it is assumed that  $g(u)$  decays rapidly to zero as  $|u| \rightarrow \infty$ , and that  $A(t-u, \lambda)$  is approximately constant over the range of  $u$  for which  $g(u)$  is non-negligible, then for heuristically, for each  $t, \lambda$

$$\Gamma_{t,\lambda}(\theta) \approx \Gamma(\theta), \text{ for all } \theta \quad (1.69)$$

Using Equation (1.65)

$$Y(t) \approx \int_{-\infty}^{\infty} A(t, \omega+\omega_0) e^{i\omega t} d\tilde{Z}(\omega) \quad (1.70)$$

where

$$E[|d\tilde{Z}(\omega)|^2] = |\Gamma(\omega)|^2 d\mu(\omega+\omega_0) \quad (1.71)$$

Thus,

$$dS_y(t, \omega) \approx |\Gamma(\omega)|^2 dS_x(t, \omega+\omega_0) \quad (1.72)$$



where the evolutionary spectra  $dS_y(t, \omega)$  and  $dS_x(t, \omega)$  are both defined with respect to the same family of oscillatory functions  $\mathcal{F} \equiv \{A(t, \omega)e^{i\omega t}\}$ .

If the input oscillatory process  $X(t)$  is locally (or semi) stationary such that the non-stationary characteristics are changing ‘slowly’ and the measure  $\mu^*(\omega)$  is absolutely continuous with respect to Lebesgue measure, then for each  $t$ ,

$$dS_x(t, \omega) = S_x(t, \omega)d\omega \quad (1.73)$$

where  $S_x(t, \omega)$ , the evolutionary spectral density function, exists for all  $\omega$  and time-varying mean square value of the non-stationary process is approximately given as

$$E[|Y(t)|^2] \approx \int_{-\infty}^{\infty} |\Gamma(\omega)|^2 |S_x(t, \omega + \omega_0)| d\omega \quad (1.74)$$

with the condition

$$B_g \ll B_{\mathcal{F}}$$

where  $B_{\mathcal{F}}$  and  $B_g$  are characteristic widths for the family of oscillatory functions  $\mathcal{F}$  and the filter  $g(u)$  given as

$$B_{\mathcal{F}}(\omega) = \left[ \sup_{\omega} \left\{ \int_{-\infty}^{\infty} |\theta| |dK_{\omega}(\theta)| \right\} \right]^{-1} \quad (1.75)$$

$$B_g = \int_{-\infty}^{\infty} |u| |g(u)| du \quad (1.76)$$

the condition  $B_g \ll B_{\mathcal{F}}$  implies that  $dS_x(t, \omega)$  is changing very slowly over the effective range of the filter  $g(u)$ . The accuracy depends on the ratio  $B_g/B_{\mathcal{F}}$ .

### 1.2.11 Digital Simulation of Random Processes

Digital simulation is a powerful technique to obtain a realization of a random process and the response statistics of linear/nonlinear systems subjected to random excitation. It

also provides a useful tool to evaluate the accuracy of approximate techniques for nonlinear random vibration analysis. Three methods for simulation of stationary and non-stationary processes are discussed in this section.

### Approximate Spectral Analysis:

A stationary random process can be simulated by the series (Shinozuka and Jan 1972)

$$X(t) = \sum_{k=1}^N \sqrt{2S(\omega)\Delta\omega} \cos(\omega_k t + \phi_k) \quad (1.77)$$

where  $S(\omega)$  is the power spectral density function of  $X(t)$  and  $\phi_k$  is the independent random phase uniformly distributed between 0 and  $2\pi$ .

$\phi_k$  = the independent random phase uniformly distributed between 0 and  $2\pi$ .

$$\omega_k = \omega_1 + \left(k - \frac{1}{2}\right) \Delta\omega \quad ; \quad k = 1, 2, \dots, N$$

A non-stationary random process can be simulated from its evolutionary power spectrum

$$X(t) = \sum_{k=1}^N \sqrt{2S(t, \omega)\Delta\omega} \cos(\omega_k t + \phi_k) \quad (1.78)$$

in which  $S(t, \omega)$  is the evolutionary power spectral density of the process.

### Time-Series Models:

An alternative approach is simulation based on time series models like moving-average (MA), autoregressive (AR) and autoregressive moving average (ARMA) models. They are computationally more efficient than simulation based on a discrete representation of the power spectral density of the process. An ARMA model of order (p,q) can be defined as

$$Y(n) = \sum_{k=0}^q b(k)X(n-k) - \sum_{i=1}^p a(i)y(n-i) \quad (1.79)$$

where  $a(k)$  and  $b(k)$  are the system coefficients. Two useful models are simplifications of the ARMA model. When  $a(i) = 0$  for  $i \geq 1$ , the model is reduced to the moving-average (MA) model of order  $q$ . When  $b(0) = 1$  and  $b(i) = 0$  for  $i \geq 1$ , the model is reduced to the autoregressive (AR) model of order  $p$ . Below, simulations of stationary and non-stationary processes using MA and AR models are described.

### **Moving-Average (MA) Method:**

A moving-average (MA) process can be written as

$$Y(n) = \sum_{k=0}^q b(k)X(n-k) \quad (1.80)$$

where  $X(t)$  is a normalized Gaussian white noise process whose autocorrelation function is represented by

$$R(n) = E[X(k)X(k+n)] = \delta_n = \begin{cases} 1, & n = 0 \\ 0, & n \neq 0 \end{cases} \quad (1.81)$$

where  $E[\ ]$  stands for the expectation value and  $\delta_n$  is the Dirac delta function.

For a MA process of order  $N$

$$Y(n) = b(1)X(n-1) + b(2)X(n-2) + \dots + b(N)X(n-N)$$

$$Y(n+1) = b(1)X(n) + b(2)X(n-1) + \dots + b(N)X(n+1-N)$$

and etc. Using the definitions above and Equation (1.81), the autocorrelation function of  $Y(t)$  can be written as

$$\begin{aligned} R(0) &= b(1)^2 + b(2)^2 + \dots + b(N)^2 \\ R(1) &= b(1)b(2) + b(2)b(3) + \dots + b(N-1)b(N) \\ &\vdots \\ R(0) &= b(1)b(N) \\ R(0) &= 0 \end{aligned} \quad (1.82)$$

For  $k = N$ ,  $Y(n)$  and  $Y(n + k)$  are uncorrelated. Equation (1.82) can be written in matrix form

$$\begin{bmatrix} R(0) \\ R(1) \\ \vdots \\ R(N-2) \\ R(N-1) \end{bmatrix} = \begin{bmatrix} b(1) & b(2) & \dots & b(N-1) & b(N) \\ b(2) & b(3) & \dots & b(N) & 0 \\ \vdots & \vdots & & \vdots & \vdots \\ b(N-1) & b(N) & \dots & 0 & 0 \\ b(N) & 0 & \dots & 0 & 0 \end{bmatrix} \begin{bmatrix} b(1) \\ b(2) \\ \vdots \\ b(N-1) \\ b(N) \end{bmatrix} \quad (1.83)$$

One way to obtain the coefficients  $b(k)$  is to solve Equation (1.83). Another way is to calculate  $b(k)$  as the Fourier coefficients of the power spectral density of the process in cosine series form.

$$b(k) = \frac{1}{\omega_c} \int_0^{\omega_c} \left[ \frac{\omega_c}{\pi} S(\omega) \right]^{1/2} \cos \frac{k\pi\omega}{\omega_c} d\omega \quad (1.84)$$

where  $\omega_c = \pi/\Delta t$ . The derivation can be found in Čačko et al. (1988). Using Equation (1.80),  $Y(t)$  is written as

$$Y(t) = \sum_{k=-p}^p \bar{b}(k) X(n-k) = \sum_{k=1}^N b(k) X(n-k) \quad (1.85)$$

in which  $N = 2p + 1$  and  $\bar{b}(k) = b(k - p + 1)$ . In practice,  $p$  may be chosen according to the inequality

$$\left| 1 - \frac{1}{\sigma^2} \sum_{-p}^p \bar{b}_k^2 \right| < \epsilon \quad (1.86)$$

where  $\sigma^2$  is the variance of the simulated process and  $\epsilon$  is a small positive number. This result can be obtained from the first equation in Equation (1.82) which states that the sum of the squares  $\bar{b}(k)$  is equal to variance.

$$\sum_{k=1}^N \bar{b}(k)^2 = R(0) = \sigma^2 \quad (1.87)$$

The procedure can easily be extended to non-stationary processes by replacing  $S(\omega)$  with evolutionary PSD,  $S(t, \omega)$ .

### **Autoregressive (AR) Method:**

Considering two discrete random processes  $Y_t = Y(t)$  and  $X_t = X(t)$ , the auto- and cross-correlation functions are defined as below.

$$C_{YY}(t, k) = E[Y_t Y_{t+k}] \quad (1.88)$$

$$C_{YX}(t, k) = E[Y_t X_{t+k}] \quad (1.89)$$

$$C_{XY}(t, k) = E[X_t Y_{t+k}] \quad (1.90)$$

The auto- and cross-correlation functions are functions not only of the lag  $k$ , but also of  $t$  with following properties

$$C_{YY}(t, k) = C_{YY}(t + k, -k) \quad (1.91)$$

$$C_{YX}(t, k) = C_{YX}(t + k, -k) \quad (1.92)$$

$$C_{XY}(t, 0) = C_{YX}(t, 0) \quad (1.93)$$

The general form of a non-stationary AR model with time-dependent coefficients  $a_i(t)$  and  $b_0(t)$  is written as

$$\sum_{i=0}^p a_i(t) Y_{t-i} = b_0(t) X_t \quad (1.94)$$

in which  $X_t$  is a normalized Gaussian white noise process satisfying

$$C_{XX}(t, k) = \begin{cases} 1 & \text{when } k = 0 \\ 0 & \text{when } k \neq 0 \end{cases} \quad (1.95)$$

From Equation (1.94)

$$C_{YX}(t, k) = 0 \quad \text{for } k > 0 \quad (1.96)$$

$$C_{XY}(t, k) = 0 \quad \text{for } k < 0 \quad (1.97)$$

$$C_{YX}(t, -k) = 0 \quad \text{for } k \geq t > 0 \quad (1.98)$$

It is also assumed that

$$a_0(t) = 1 \quad \forall t \quad (1.99)$$

The coefficients  $a_i(t)$  and  $b_0(t)$  can be calculated from some prescribed autocorrelation function  $C_{YY}(t, k)$  as follows (Deodatis and Shinozuka 1988). For  $t = t^*$ , Equation (1.94) can be written as

$$\sum_{i=0}^p a_i(t^*) Y_{t^*-i} = b_0(t^*) X_{t^*} \quad (1.100)$$

Post multiplying Equation (1.100) by  $Y_{t^*-j}$  and taking expectations for  $j = 1, 2, \dots, p$

$$\sum_{i=0}^p a_i(t^*) C_{YY}(t^* - i, i - j) = b_0(t^*) C_{XY}(t^*, -j) \quad (1.101)$$

Using Equation (1.97)

$$\sum_{i=0}^p a_i(t^*) C_{YY}(t^* - i, i - j) = 0 \quad (1.102)$$

and using Equation (1.99)

$$-C_{YY}(t^*, -j) = \sum_{i=1}^p a_i(t^*) C_{YY}(t^* - i, i - j) \quad j = 1, 2, \dots, p \quad (1.103)$$

Equation (1.103) can be written in matrix form

$$\begin{aligned}
 & \begin{bmatrix} C_{YY}(t^* - 1, 0) & C_{YY}(t^* - 2, 1) & \dots & C_{YY}(t^* - p, p - 1) \\ C_{YY}(t^* - 1, -1) & C_{YY}(t^* - 2, 0) & \dots & C_{YY}(t^* - p, p - 2) \\ \vdots & \vdots & & \vdots \\ C_{YY}(t^* - 1, 1 - p) & C_{YY}(t^* - 2, 2 - p) & \dots & C_{YY}(t^* - p, 0) \end{bmatrix} \begin{bmatrix} a_1(t^*) \\ a_1(t^*) \\ \vdots \\ a_p(t^*) \end{bmatrix} \\
 & = - \begin{bmatrix} C_{YY}(t^*, -1) \\ C_{YY}(t^*, -2) \\ \vdots \\ C_{YY}(t^*, -p) \end{bmatrix} \quad (1.104)
 \end{aligned}$$

The coefficients  $a_i(t^*)$ ;  $i = 1, 2, \dots, p$  can be calculated by solving this system of  $p$  equations with  $p$  unknowns. Post multiplying Equation (1.100) by  $Y_{t^*}$  and taking expectations

$$\sum_{i=0}^p a_i(t^*) C_{YY}(t^* - i, i) = b_0(t^*) C_{XY}(t^*, 0) \quad (1.105)$$

Post multiplying Equation (1.100) by  $X_{t^*}$  and taking expectations

$$\sum_{i=0}^p a_i(t^*) C_{YX}(t^* - i, i) = b_0(t^*) C_{XX}(t^*, 0) \quad (1.106)$$

Using Equations (1.95, 1.96, 1.99), Equation (1.106) leads to

$$C_{YX}(t^*, 0) = b_0(t^*) \quad (1.107)$$

Using Equation (1.107),  $b_0(t^*)$  can be obtained as

$$b_0(t^*) = \sqrt{\sum_{i=0}^p a_i(t^*) C_{YY}(t^* - i, i)} \quad (1.108)$$

Thus, the coefficients  $a_i(t^*)$  and  $b_0(t^*)$  can now be calculated from the prescribed autocorrelation function  $C_{YY}(t, k)$  and  $Y(t)$  can be generated recursively using Equation (1.90).

The derivations above are also valid for stationary processes if the coefficients  $a_i$  and  $b_0$  are modified to be time-independent.

If  $Y(t)$  is an oscillatory process of the form of Equation (1.53) and has an evolutionary spectrum  $dS(t, \omega) = S(t, \omega)d\omega = |A(t, \omega)|^2 S(\omega)d\omega$ , then the auto-correlation function can be calculated from the evolutionary power spectrum as

$$C_{YY}(s, t) = \int_{-\infty}^{\infty} A^*(s, \omega) A(t, \omega) e^{i\omega(t-s)} S(\omega) d\omega \quad (1.109)$$

### 1.2.12 Analytical Models of Power Spectral Density for Ground and Wind Excitations

Several analytical models of power spectral density are used to study the stochastic response of time-varying systems subjected to ground and wind excitations. They are summarized below.

#### Ground excitation

A shaping filter proposed by Narasimhan (2004) is used to simulate the random ground motion processes in this study. The shaping filter is obtained by least squares fit of the PSD of a set of near-fault earthquake records. The shaping filter for near-fault earthquakes is as follows:

$$S(\omega) = \frac{16\xi^2 \left(\frac{\omega}{\omega_g}\right)^2}{\left[ \left(1 - \left(\frac{\omega}{\omega_g}\right)^2\right)^2 + 4\xi^2 \left(\frac{\omega}{\omega_g}\right)^2 \right]} \quad (1.110)$$

$\omega_g$  and  $\xi_g$  in Equation (1.110) are the natural frequency and damping ratio corresponding to the soil condition.



## Wind excitation

The aerodynamic loads can be classified into four categories (Kareem 1987): (1) forces induced by incident turbulence, (2) forces induced by wake fluctuations, (3) forces due to interference of upstream and adjacent structures and (4) motion induced forces. Tall buildings subjected to aerodynamic loads oscillate in the alongwind, acrosswind, and torsional directions (Kareem 1992; Simiu and Scanlan 1986). The alongwind load is primarily induced by alongwind turbulence and can be calculated analytically from the gust spectrum with reasonable accuracy. The acrosswind load is principally introduced by vortex shedding in the wake region which is formed by separated shear layers due to sharp corners of the building. Torsional moments can be induced by either eccentricity between elastic center and mass center of the building and/or pressure fluctuations in the wake flow. Since both acrosswind forces and torsional moments result mainly from pressure fluctuations caused by vortex shedding in the wake flow through a complex mechanism, there is no generally accepted analytical method for calculating these loads. Thus, calculation acrosswind forces and torsional moments are generally relied on wind tunnel testing. It is reported that acrosswind response of tall buildings usually exceeds the alongwind response significantly (Liang et al. 2002; Yang et al. 2004) and torsion-induced response is comparable to the acrosswind response (Kareem 1985). Neglecting the interference of upstream and adjacent structures, coupled lateral-torsional motion and assuming aerodynamic damping due to motion induced forces is taken into account in the structural damping, alongwind, acrosswind and torsional responses can be calculated independently.

The longitudinal wind velocity at a given time can be defined as

$$U(z, t) = U(z) + u(x, y, z, t) \quad (1.111)$$

where  $U(z)$  is the mean wind velocity with respect to height  $z$  above ground and  $u(x, y, z, t)$

is the fluctuating turbulence component in the longitudinal direction.

The wind velocity is near zero at the surface due to the horizontal drag force exerted upon the moving air. It increases gradually from zero to a nearly constant value at the gradient height. This region varies from 300 to 500 m and is called earth's boundary layer (Nigam and Narayanan 1994). The mean velocity profile can be represented either by the power law

$$U(z) = U(z_{ref}) * \left( \frac{z}{z_{ref}} \right)^\alpha \quad (1.112)$$

or by the logarithmic law

$$U(z) = \frac{1}{k} u_* \ln \frac{z}{z_0} \quad (1.113)$$

where  $k$  is von Kármán's constant ( $k \simeq 0.4$ ),  $z$  is the height above the surface ground and  $z_0$  is the roughness length depending on the terrain type. The friction velocity  $u_*$  is defined by

$$u_* = \sqrt{\frac{\tau_0}{\rho}} \quad (1.114)$$

where  $\tau_0$  is the shear stress at the ground surface and  $\rho$  is the air density.

The friction velocity  $u_*$  is related to the root mean square (rms) value of  $u$ ,  $\sigma_u$  by

$$\sigma_u^2 = \beta u_*^2 \quad (1.115)$$

in which  $\beta$  value depends on  $z_0$ .

There are many spectra defining the longitudinal turbulence in the literature. A simple spectral density proposed by Davenport (1961) to simulate alongwind is given by

$$\frac{f S(z, f)}{u_*^2} = \frac{4.0 \bar{f}^2}{(1 + 50 \bar{f}^2)^{4/3}} \quad (1.116)$$

where  $\bar{f} = 1200f/U(10)$ ,  $f$  is the frequency in Hertz and  $U(10)$  is the mean wind speed in meters per second at  $z = 10$  m.

Another alongwind spectra is proposed by Kaimal and (1972) in the form of

$$\frac{f S(z, f)}{u_*^2} = \frac{200 \bar{f}}{(1 + 50 \bar{f})^{5/3}} \quad (1.117)$$

where  $f$  is the frequency in Hertz,  $\bar{f} = fz/U(z)$  is the non-dimensional frequency. Equation (1.113) implies  $\beta = 6$  leading to

$$\frac{f S(z, f)}{\sigma^2} = \frac{\frac{100}{3} \bar{f}}{(1 + 50 \bar{f})^{5/3}} \quad (1.118)$$

A simple power spectrum for the lateral turbulence component is approximately given in Simiu and Scanlan (1986) as

$$\frac{f S_v(z, f)}{u_*^2} = \frac{15 \bar{f}}{(1 + 9.5 \bar{f})^{5/3}} \quad (1.119)$$

There are also other acrosswind force spectra available in the literature for square buildings (Kareem 1984), chimneys (Vickery and Clark 1972) and square/rectangular buildings (Liang et al. 2002).

The wind drag force for a point-like structure can be written as

$$\begin{aligned} F_d(z, t) &= \frac{1}{2} \rho C A v_t^2(z, t) \\ &= [v_0(z) + v(z, t)]^2 \\ &= v_0^2(z) + v^2(z, t) + 2v_0(z)v(z, t) \end{aligned} \quad (1.120)$$

Assuming the fluctuating wind speed  $v(z, t)$  is small compared to the mean wind speed  $v_0$ , the along-wind force spectrum for a the fluctuating component can be approximately written as

$$\begin{aligned} S_F(f) &= \rho^2 C^2 v_0^2(z) A^2 S_v(z, f) \\ &= \rho^2 C^2 v_0^2(z_{ref}) A^2 \left( \frac{z}{z_{ref}} \right)^{2\alpha} S_v(z, f) \end{aligned} \quad (1.121)$$

The acceleration spectrum for a point mass  $m_0$  at height  $z$  can be written as

$$\begin{aligned} S_{F/m_0}(f) &= \frac{1}{m_0^2} S_F(f) \\ &= \left[ \frac{\rho C v_0^2(z_{ref}) A}{m_0} \right]^2 \frac{1}{v_0^2(z_{ref})} \left( \frac{z}{z_{ref}} \right)^{2\alpha} S_v(z, f) \end{aligned} \quad (1.122)$$

and the root-mean-square (RMS) acceleration can be written as

$$\sigma_{F/m_0} = \left[ \frac{\rho C v_0^2(z_{ref}) A}{m_0} \right] \frac{1}{v_0(z_{ref})} \left( \frac{z}{z_{ref}} \right)^\alpha \sqrt{\int_0^\infty S_v(z, f) df} \quad (1.123)$$

## Chapter 2

# Mathematical Formulation of Linear Time Varying (LTV) Systems

Fundamentals of linear time-varying (LTV) systems are presented in this chapter. Both continuous time and discrete time system are described (Kamen 1995). General formulation of a multi-degree of freedom building with SAIVS-TMD is presented.

### 2.1 Continuous-Time Linear Time Varying Systems

Consider a continuous-time system with single input  $u(t)$  and single output  $y(t)$ , where  $u(t)$  and  $y(t)$  are real-valued functions of the continuous-time variable  $t$ . It is assumed that there is no initial energy in the system prior to the application of the input  $u(t)$ , that is, the system is initially at rest before the application of the input. Then if the system is causal, it can be modelled by the input/output relationship

$$y(t) = F(u(\tau) : 0 < \tau \leq t, t) \quad (2.1)$$

where  $y(t)$  is the output response resulting from  $u(t)$  and  $F$  is a function that may be nonlinear. If the system is linear, then  $F$  is linear and Equation (2.1) becomes

$$y(t) = \int_0^t h(t, \tau) u(\tau) d\tau \quad (2.2)$$

where  $h(t, \tau)$  is the impulse response function, that is,  $h(t, \tau)$  is the response to the impulse  $\delta(t - \tau)$  applied at time  $\tau$  with no initial energy. It should be emphasized that  $y(t)$  given by Equation (2.2) is the output of the response assuming that the system is at rest prior to the application of the input  $u(t)$ . Also, it is assumed that there are conditions on  $h(t, \tau)$ , and/or  $u(t)$  which ensure that the integral in Equation (2.2) exists.

The linear system given by Equation (2.2) is time invariant (or constant) if and only if

$$h(t + \gamma, \tau + \gamma) = h(t, \tau) \quad \text{for all real numbers } t, \tau, \gamma \quad (2.3)$$

Time invariance means that if  $y(t)$  is the response to  $u(t)$ , then for any real number  $t_1$ , the shifted output  $y(t - t_1)$  is the response to the shifted input  $u(t - t_1)$ . Setting  $\gamma = -\tau$  in Equation (2.3) gives

$$h(t - \tau, 0) = h(t, \tau) \quad \text{for all real numbers } t, \tau \quad (2.4)$$

Hence, the system defined by Equation (2.2) is time invariant if and only if the impulse response function  $h(t, \tau)$  is a function only of the difference  $t - \tau$ . In the time-invariant case, Equation (2.2) reduces to the convolution relationship

$$y(t) = h(t) * u(t) = \int_0^t h(t - \tau)u(\tau)d\tau \quad (2.5)$$

where  $h(t) = h(t, 0)$  is the impulse response (i.e., the response to the impulse  $\delta(t)$  applied at time 0).

The linear system defined by Equation (2.2) is finite-dimensional or lumped if the input  $u(t)$  and the output  $y(t)$  are related by the  $n^{th}$ -order differential equation

$$y^{(n)}(t) + \sum_{i=0}^{n-1} a_i(t)y^{(i)}(t) = \sum_{i=0}^m b_i(t)u^{(i)}(t) \quad (2.6)$$

where  $y^{(i)}(t)$  is the  $i^{th}$  derivative of  $y(t)$ ,  $u^{(i)}(t)$  is the  $i^{th}$  derivative of  $u(t)$ , and  $a_i(t)$  and  $b_i(t)$  are real-valued functions of  $t$ . In Equation (2.6), it is assumed that  $m \leq n$ . The linear system given by Eq. (2.6) is time invariant if, and only if, all coefficients in Equation (2.6) are constants, that is,  $a_i(t) = a_i$  and  $b_i(t) = b_i$  for all  $i$ , where  $a_i$  and  $b_i$  are real constants.

### 2.1.1 State Model

A state model for the system given by Equation (2.6) can be constructed as follows.

First, suppose that  $m = 0$  so that Eq. (2.6) becomes

$$y^{(n)}(t) + \sum_{i=0}^{n-1} a_i(t)y^{(i)}(t) = b_0(t)u(t) \quad (2.7)$$

Then defining the state variables

$$x_i(t) = y^{i-1}(t), \quad i = 1, 2, \dots, n \quad (2.8)$$

the system defined by Equation (2.7) has the state model,

$$\dot{x}(t) = A(t)x(t) + B(t)u(t) \quad (2.9a)$$

$$y(t) = Cx(t) \quad (2.9b)$$

where the coefficient matrices  $A(t)$ ,  $B(t)$ ,  $C$  are given by

$$A(t) = \begin{bmatrix} 0 & 1 & 0 & \cdots & 0 & 0 \\ 0 & 0 & 1 & \cdots & 0 & 0 \\ 0 & 0 & 0 & \cdots & 0 & 0 \\ \vdots & \vdots & \vdots & \cdots & \vdots & \vdots \\ 0 & 0 & 0 & \cdots & 0 & 1 \\ -a_0(t) & -a_1(t) & -a_2(t) & \cdots & -a_{n-2}(t) & -a_{n-1}(t) \end{bmatrix}$$

$$B(t) = [0 \quad 0 \quad 0 \quad \cdots \quad b_0(t)]^T$$

$$C = [1 \quad 0 \quad 0 \quad \cdots \quad 0 \quad 0]$$

and  $x(t)$  is the  $n$ -dimensional state vector given by  $x(t) = [x_1(t) \quad x_2(t) \quad \cdots \quad x_{n-1}(t) \quad x_n(t)]^T$ .

For an  $m$ - input,  $p$ - output, linear  $n$ -dimensional, time-varying continuous-time system, the general form of the state model is

$$\dot{x}(t) = A(t)x(t) + B(t)u(t) \quad (2.10a)$$

$$y(t) = C(t)x(t) + D(t)u(t) \quad (2.10b)$$

where Equation (2.10a) is the state equation and Eq. (2.10b) is the output equation. In Equation (2.10),  $A(t)$  is the  $n \times n$  system matrix,  $B(t)$  is the  $n \times m$  input matrix,  $C(t)$  is the  $p \times n$  output matrix,  $D(t)$  is the  $p \times m$  direct feed matrix,  $u(t)$  is the  $m$ - dimensional input vector,  $x(t)$  is the  $n$ - dimensional state vector, and  $y(t)$  is the  $p$ - dimensional output vector. The term  $D(t)u(t)$  in Eq. (2.10b) is of little significance in the theory, and thus  $D(t)u(t)$  is usually omitted from Eq. (2.10b), which will be done here.

To solve Equation (2.10a), first consider the homogeneous equation

$$\dot{x}(t) = A(t)x(t), \quad t > t_0 \quad (2.11)$$

with the initial condition  $x(t_0)$  at initial time  $t_0$ . For any  $A(t)$  whose entries are piecewise continuous, it is known that, for any initial condition  $x(t_0)$ , there is a unique continuous solution of Equation (2.11) given by

$$x = \Phi(t_0, t)x(t_0), \quad t > t_0 \quad (2.12)$$

where  $\Phi(t, t_0)$  is a  $n \times n$  matrix function of  $t$  and  $t_0$ , called the state-transition matrix. The state-transition matrix has the following fundamental properties:

$$\Phi(t, t) = I = n \times n \text{ identity matrix, for all } t \quad (2.13a)$$

$$\Phi(t, \tau) = \Phi(t, t_1)\Phi(t_1, \tau), \text{ for all } t_1, t, \tau \quad (2.13b)$$

$$\Phi^{-1}(t, \tau) = \Phi(\tau, t), \text{ for all } t, \tau \quad (2.13c)$$



$$\frac{\partial}{\partial t}\Phi(t, \tau) = A(t)\Phi(t, \tau), \text{ for all } t, \tau \quad (2.13d)$$

$$\frac{\partial}{\partial \tau}\Phi^{-1}(t, \tau) = -\Phi^{-1}(t, \tau)A(\tau), \text{ for all } t, \tau \quad (2.13e)$$

$$\det \Phi(t, \tau) = \exp \left[ \int_{\tau}^t \text{trace}[A(\sigma)]d\sigma \right] \quad (2.13f)$$

Equation (2.13b) is called the composition property. It follows from this property  $\Phi(t, \tau)$  can be written in the factored form

$$\Phi(t, \tau) = \Phi(t, 0)\Phi(0, \tau), \text{ for all } t, \tau \quad (2.14)$$

It follows from Equation (2.13e) that the adjoint equation

$$\dot{\gamma}(t) = -A^T(t)\gamma(t) \quad (2.15)$$

has state-transition matrix equal to  $\Phi^T(\tau, t)$ , where again  $\Phi(t, \tau)$  is the state-transition matrix for Equation (2.12).

If the system  $A(t)$  is constant over the interval  $[t_1, t_2]$ , that is,  $A(t) = A$ , for all  $t \in [t_1, t_2]$ , then the state-transition matrix is equal to matrix exponential over  $[t_1, t_2]$ :

$$\Phi(t, \tau) = e^{A(t-\tau)} \text{ for all } t, \tau \in [t_1, t_2] \quad (2.16)$$

If  $A(t)$  is time varying and  $A(t)$  commutes with its integral over the interval  $[t_1, t_2]$ , that is,

$$A(t) \left[ \int_{\tau}^t A(\sigma)d\sigma \right] = \left[ \int_{\tau}^t A(\sigma)d\sigma \right] A(t), \text{ for all } t, \tau \in [t_1, t_2] \quad (2.17)$$

then  $\Phi(t, \tau)$  is given by

$$\Phi(t, \tau) = \exp \left[ \int_{\tau}^t A(\sigma)d\sigma \right], \text{ for all } t, \tau \in [t_1, t_2] \quad (2.18)$$

Note that the commutativity condition in Equation (2.17) is always satisfied in the time invariant case. It is also always satisfied in the one-dimensional case ( $n = 1$ ) because scalars

commute. Thus  $\Phi(t, \tau)$  is given by exponential form in Equation (2.18) when  $n = 1$ . Unfortunately, the exponential form for  $\Phi(t, \tau)$  does not hold for an arbitrary time-varying matrix  $A(t)$  when  $n > 1$ . However, approximations to  $\Phi(t, \tau)$  can be readily computed from  $A(t)$  by numerical techniques, such as the method of successive approximations. Approximations to  $\Phi(t, \tau)$  can also be determined by discretizing the time variable as shown below.

Given the state transition matrix  $\Phi(t, \tau)$ , for any given initial state  $x(t_0)$  and input  $u(t)$  applied for  $t \geq t_0$ , the complete solution to Equation (2.10a) is

$$x(t) = \Phi(t_0, t)x(t_0) + \int_{t_0}^t \Phi(t, \tau)B(\tau)u(\tau)d\tau, \quad t > t_0 \quad (2.19)$$

Then, when  $y(t) = C(t)x(t)$ , the output response  $y(t)$  is given by

$$y(t) = C(t)\Phi(t_0, t)x(t_0) + \int_{t_0}^t C(t)\Phi(t, \tau)B(\tau)u(\tau)d\tau, \quad t > t_0 \quad (2.20)$$

If the initial time  $t_0$  is taken to be 0 and there is no initial energy at  $t = 0$ , Equation (2.20) becomes

$$y(t) = \int_0^t C(t)\Phi(t, \tau)B(\tau)u(\tau)d\tau \quad (2.21)$$

Comparing Equation (2.21) with the  $m$ - input,  $p$ - output version of the input/output Equation (2.2) reveals that

$$H(t, \tau) = \begin{cases} C(t)\Phi(t, \tau)B(\tau) & \text{for } t \geq \tau \\ 0, & \text{for } t < \tau \end{cases} \quad (2.22)$$

where  $H(t, \tau)$  is the  $p \times m$  impulse response function matrix. Inserting Equation (2.14) into Equation (2.22) reveals that  $H(t, \tau)$  can be expressed in the factored form,

$$H(t, \tau) = H_1(t)H_2(\tau), \quad t \geq \tau \quad (2.23)$$

where  $H_1(t) = C(t)\Phi(t, 0)$  and  $H_2(\tau) = \Phi(0, \tau)B(\tau)$ . It turns out that a linear time-varying system with impulse response matrix  $H(t, \tau)$  has a state realization given by Equation (2.10) with  $D(t) = 0$  if, and only if,  $H(t, \tau)$  can be expressed in the factored form given in Equation (2.23).

### 2.1.2 Stability

Given a system with  $n$ - dimensional state model  $[A(t), B(t), C(t)]$ , again consider the homogeneous Equation

$$\dot{x}(t) = A(t)x(t), \quad t > t_0 \quad (2.24)$$

with solution

$$x(t) = \Phi(t_0, t)x(t_0), \quad t > t_0 \quad (2.25)$$

The system is said to be asymptotically stable if the solution  $x(t)$  satisfies the condition  $\|x(t)\| \rightarrow 0$  as  $t \rightarrow \infty$  for any initial state  $x(t_0)$  at initial time  $t_0$ . Here  $\|x(t)\|$  denotes the Euclidean norm of the state  $x(t)$  given by

$$\|x(t)\| = \sqrt{x_1^2(t) + x_2^2(t) + \dots + x_n^2(t)} \quad (2.26)$$

where  $x(t) = [x_1(t) \ x_2(t) \ \dots \ x_n(t)]^T$ . A system is asymptotically stable if, and only if,

$$\|\Phi(t_0, t)\| \rightarrow 0 \quad \text{as } t \rightarrow \infty \quad (2.27)$$

where  $\|\Phi(t_0, t)\|$  is the matrix norm equal to the square root of the largest eigenvalue of  $\Phi^T(t_0, t)\Phi(t_0, t)$ .

It should be noted that semi-active systems investigated in this study are inherently stable since there is no active control force input into the system, and dissipative condition is always satisfied and the variation of stiffness and damping is bounded.

### 2.1.3 Controllability and Observability

Given a system with  $n$ - dimensional state model  $[A(t), B(t), C(t)]$ , it is now assumed that the entries of  $A(t)$ ,  $B(t)$ , and  $C(t)$  are at least continuous functions of  $t$ . The system is said to be controllable on the interval  $[t_0, t_1]$ , where  $t_1 > t_0$ , if for any states  $x_0$  and  $x_1$ , a continuous input  $u(t)$  exists that drives the system to the state  $x(t_1) = x_1$  at time  $t = t_1$  starting from the state  $x(t_0) = x_0$  at time  $t = t_0$ .

Define the controllability Gramian which is the  $n \times n$  matrix given by

$$W(t_0, t_1) = \int_{t_0}^{t_1} \Phi(t_0, t) B(t) B^T(t) \Phi^T(t_0, t) dt \quad (2.28)$$

The controllability Gramian  $W(t_0, t_1)$  is symmetric positive semidefinite and is solution to the matrix differential equation

$$\frac{d}{dt} W(t, t_1) = A(t)W(t, t_1) + W(t, t_1)A^T(t) - B(t)B^T(t) \quad (2.29a)$$

$$W(t_1, t_1) = 0 \quad (2.29b)$$

Then the system is controllable on  $[t_0, t_1]$  if, and only if,  $W(t_0, t_1)$  is invertible, in which case a continuous input  $u(t)$  that drives the system from  $x(t_0) = x_0$  to  $x(t_1) = x_1$  is

$$u(t) = -B^T(t)\Phi^T(t_0, t)W^{-1}(t_0, t_1)[x_0 - \Phi(t_0, t_1)x_1], \quad t_0 \leq t \leq t_1 \quad (2.30)$$

When  $A(t)$  is  $n - 2$  times differentiable and  $B(t)$  is  $n - 1$  times differentiable, a sufficient condition for controllability is that the matrix  $K(t) = [K_0(t) \ K_1(t) \ \dots \ K_{n-1}(t)]$  with  $K_0(t) = B(t)$ ;  $K_i(t) = -A(t)K_{i-1}(t) + \dot{K}_{i-1}(t)$ ;  $i = 1, 2, \dots, n - 1$ ; and  $K(t)$  has rank  $n$  for at least one value of  $t \in [t_0, t_1]$ . The system is said to be uniformly controllable on  $[t_0, t_1]$  if the rank of  $K(t)$  is equal to  $n$  for all  $t \in [t_0, t_1]$ .

Now suppose that the system input  $u(t)$  is zero, so that the state model is given by

$$\dot{x}(t) = A(t)x(t) \quad (2.31a)$$

$$y(t) = C(t)x(t) \quad (2.31b)$$

From Equation (2.31), the output response  $y(t)$  resulting from initial state  $x(t_0)$  is

$$y(t) = C(t)\Phi(t_0, t)x(t_0), \quad t > t_0 \quad (2.32)$$

Then the system is said to be observable on the interval  $[t_0, t_1]$  if any initial state  $x(t_0) = x_0$  can be determined from the output response  $y(t)$  given by Equation (2.32) for  $t \in [t_0, t_1]$ .

Define the observability Gramian which is the  $n \times n$  matrix given by

$$M(t_0, t_1) = \int_{t_0}^{t_1} \Phi^T(t_0, t)C^T(t)C(t)\Phi(t_0, t)dt \quad (2.33)$$

The observability Gramian  $M(t_0, t_1)$  is symmetric positive semidefinite and is the solution to the matrix differential equation

$$\frac{d}{dt}M(t, t_1) = -A^T(t)M(t, t_1) - M(t, t_1)A(t) - C^T(t)C(t) \quad (2.34a)$$

$$M(t_1, t_1) = 0 \quad (2.34b)$$

Then the system is observable on  $[t_0, t_1]$  if, and only if,  $M(t_0, t_1)$  is invertible, in which case the initial state  $x(t_0)$  is given by

$$x_0 = M^{-1}(t_0, t_1) \int_{t_0}^{t_1} \Phi^T(t_0, t)C^T(t)y(t)dt \quad (2.35)$$

When  $A(t)$  is  $n - 2$  times differentiable and  $C(t)$  is  $n - 1$  differentiable, a sufficient condition for observability is that the matrix  $L(t) = [L_0(t) \quad L_1(t) \quad \dots \quad L_{n-1}(t)]^T$  with  $L_0(t) = C(t)$ ;  $L_i(t) = L_{i-1}(t)A(t) + \dot{L}_{i-1}(t)$ ;  $i = 1, 2, \dots, n - 1$ ; and  $L(t)$  has rank  $n$  for at least one value of  $t \in [t_0, t_1]$ . The system is said to be uniformly observable on  $[t_0, t_1]$  if the rank of  $L(t)$  is equal to  $n$  for all  $t \in [t_0, t_1]$ .

Again given a system with state model  $[A(t), B(t), C(t)]$ , the adjoint system is the system with the state model  $[-A^T(t), C^T(t), B^T(t)]$ . The system  $[A(t), B(t), C(t)]$  is controllable (resp., observable) on an interval  $[t_0, t_1]$  if, and only if, the adjoint system is observable (resp., controllable) on the interval  $[t_0, t_1]$ .

## 2.2 Discrete-Time Linear Time-Varying Systems

A discrete-time linear time-varying causal system with single input  $u(k)$  and single output  $y(k)$  can be modeled by the input/output relationship,

$$y(k) = \sum_{j=0}^k h(k, j)u(j) \quad (2.36)$$

where  $k$  is an integer-valued variable (the discrete-time index) and  $h(k, j)$  is the output response resulting from the unit pulse  $\delta(k - j)$  (where  $\delta(k - j) = 1$  for  $k = j$  and  $= 0$  for  $k \neq j$ ) applied at time  $j$  with no initial energy in the system. The output  $y(k)$  given by Equation (2.36) is the response resulting from the input  $u(k)$  assuming that the system is at rest prior to the application of  $u(k)$ . It is assumed that  $u(k)$  and/or  $h(k, j)$  is constrained so that the summation in Equation (2.36) is well defined. The system defined in Equation (2.36) is well defined if, and only if,  $h(k, j)$  is a function of only the difference  $k - j$ , in which case Equation (2.36) reduces to the convolution relationship,

$$y(k) = h(k) * u(k) = \sum_{j=0}^k h(k - j)u(j) \quad (2.37)$$

where  $h(k - j) = h(k - j, 0)$

The system defined by Equation (2.36) is finite dimensional if the input  $u(k)$  and the output  $y(k)$  are related by the  $n^{th}$  order difference equation,

$$y(k + n) + \sum_{i=0}^{n-1} a_i(k)y(k + i) = \sum_{i=0}^m b_i(k)u(k + i) \quad (2.38)$$

where  $m \leq n$  and the  $a_i(k)$  and the  $b_i(k)$  are real valued functions of the discrete time variable  $k$ . The system given by Equation (2.38) is time invariant if, and only if, all coefficients in Equation (2.38) are constants, that is  $a_i(k) = a_i$  and  $b_i(k) = b_i$  for all  $i$ , where  $a_i$  and  $b_i$  are constants.

When  $m < n$ , the system defined by Equation (2.38) has the  $n$ - dimensional state model

$$x(k+1) = A(k)x(k) + B(k)u(k) \quad (2.39a)$$

$$y(k) = Cx(k) \quad (2.39b)$$

where

$$A(k) = \begin{bmatrix} 0 & 0 & 0 & \cdots & 0 & -a_0(k) \\ 1 & 0 & 0 & \cdots & 0 & -a_1(k-1) \\ 0 & 1 & 0 & \cdots & 0 & -a_2(k-2) \\ \vdots & \vdots & \vdots & \cdots & \vdots & \vdots \\ 0 & 0 & 0 & \cdots & 0 & -a_{n-2}(k-n+2) \\ 0 & 0 & 0 & \cdots & 1 & -a_{n-1}(k-n+1) \end{bmatrix}$$

$$B(k) = [b_0(k) \quad b_1(k-1) \quad b_2(k-2) \quad \cdots \quad b_{n-2}(k-n+2) \quad b_{n-1}(k-n+1)]^T$$

$$C = [0 \quad 0 \quad 0 \quad \cdots \quad 0 \quad 1]$$

where  $b_i(k) = 0$  for  $i > m$ . This particular state model is referred to as the observer canonical form. There are other state realizations of Equation (2.38), but these will not be considered here. It is interesting to note that the entries of  $A(k)$  and  $B(k)$  in the observer canonical form are simply time shifts of the coefficients of the input/output differential Equation (2.38), whereas in the continuous-time case, this relationship is rather complicated.

### 2.2.1 State Model

For an  $m$ -input  $p$ -output linear  $n$ -dimensional time-varying discrete-time system, the general form of the state model is

$$x(k+1) = A(k)x(k) + B(k)u(k) \quad (2.40a)$$

$$y(k) = Cx(k) + D(k)u(k) \quad (2.40b)$$

where  $A(k)$  is  $n \times n$ ,  $B(k)$  is  $n \times m$ ,  $C(k)$  is  $p \times n$  and  $D(k)$  is  $p \times m$ . The state model given by Equation (2.40) may arise as a result of sampling a continuous-time system given by Equation (2.10). If the sampling interval is equal to  $T$ , then setting  $t = kT$  in Equation (2.10) yields an output equation of the form in Eq. (2.45) where  $C(k) = C(t)|_{t=kT}$  and  $D(k) = D(t)|_{t=kT}$ . To discretize, first recall that the solution to Equation (2.10) is Equation (2.19). Then setting  $t = kT + T$  and  $t_0 = kT$  in Equation (2.19) yields

$$x(kT + T) = \Phi(kT + T, kT)x(kT) + \int_{kT}^{kT+T} \Phi(kT + T, \tau)B(\tau)u(\tau)d\tau \quad (2.41)$$

The second term on the right hand side of the Equation (2.41) can be approximated by

$$\left[ \int_{kT}^{kT+T} \Phi(kT + T, \tau)B(\tau)d\tau \right] u(kT)$$

and thus Equation (2.41) is in the form of Equation (2.40) with

$$A(k) = \Phi(kT + T, kT) \quad (2.42a)$$

$$B(k) = \int_{kT}^{kT+T} \Phi(kT + T, \tau)B(\tau)d\tau \quad (2.42b)$$

Note that the matrix  $A(k)$  given by Equation (2.42) is always invertible since  $\Phi(kT+T, kT)$  is always invertible (see Equation (2.13c)). As discussed below, this implies that discretized or sampled data systems are "reversible".



From Equation (2.42) it is seen that the computation of  $A(k)$  and  $B(k)$  requires knowledge of the state-transition matrix  $\Phi(t, \tau)$  for  $\tau = kT + T$  and  $\tau \in [kT, kT + T]$ . If  $A(t)$  in Equation (2.10) is a continuous function of  $t$  over each interval  $[kT + T, kT]$  and the variation of  $A(t)$  over each interval  $[kT + T, kT]$  is sufficiently small, then  $\Phi(kT + T, \tau)$  can be approximated by

$$\Phi(kT + T, \tau) = e^{A(kT)(kT+T-\tau)} \quad \text{for } \tau \in [kT, kT + T] \quad (2.43)$$

and hence  $A(k)$  and  $B(k)$  can be determined using

$$A(k) = e^{A(kT)T} \quad (2.44a)$$

$$B(k) = \int_{kT}^{kT+T} e^{A(kT)(kT+T-\tau)} B(\tau) d\tau \quad (2.44b)$$

Given the discrete-time system defined by Equation (2.40), the solution to Equation (2.40a) is

$$x(k) = \Phi(k, k_0)x(k_0) + \sum_{j=k_0}^{k-1} \Phi(k, j+1)B(j)u(j), \quad k > k_0 \quad (2.45)$$

where the  $n \times n$  state transition matrix  $\Phi(k, j)$  is given by

$$\Phi(k, k_0) = \begin{cases} \text{not defined for } k < k_0 \\ I, & k = k_0 \\ A(k-1)A(k-2) \dots A(k_0), & k > k_0 \end{cases} \quad (2.46)$$

It follows directly from Equation (2.46) that  $\Phi(k, k_0)$  is invertible for  $k > k_0$  only if  $A(k)$  is invertible for  $k \geq k_0$ . Thus, in general, the initial state  $x(k_0)$  cannot be determined from the relationship  $x(k) = \Phi(k, k_0)x(k_0)$ . In other words, a discrete-time system is not necessarily reversible, although any continuous-time system given by Equation (2.10) is reversible since  $\Phi(t_0, t)$  is always invertible. However, as noted above, any sampled data system is reversible.

The state-transition matrix  $\Phi(k, k_0)$  satisfies the composition property:

$$\Phi(k, k_0) = \Phi(k, k_1)\Phi(k_1, k_0) \quad \text{where } k_0 \leq k_1 \leq k \quad (2.47)$$

and in addition,

$$\Phi(k+1, k_0) = A(k)\Phi(k, k_0), \quad k \geq k_0 \quad (2.48)$$

If  $A(k)$  is invertible for all  $k$ ,  $\Phi(k, k_0)$  can be written in the factored form

$$\Phi(k, k_0) = \Phi_1(k)\Phi_2(k_0), \quad k \geq k_0 \quad (2.49)$$

where

$$\Phi_1(k) = \begin{cases} A(k-1)A(k-2)\dots A(0), & k \geq 1 \\ I, & k = 0 \\ A^{-1}(k-2)A^{-1}(k-3)\dots A^{-1}(-1), & k < 0 \end{cases} \quad (2.50a)$$

$$\Phi_2(k_0) = \begin{cases} A^{-1}(0)A^{-1}(1)\dots A^{-1}(k_0-1), & k_0 > 0 \\ I, & k_0 = 0 \\ A(-1)A(-2)\dots A(k_0), & k_0 < 0 \end{cases} \quad (2.50b)$$

When  $y(k) = C(k)x(k)$ , the output response  $y(k)$  is given by

$$y(k) = C(k)\Phi(k, k_0)x(k_0) + \sum_{j=k_0}^{k-1} C(k)\Phi(k, j+1)B(j)u(j), \quad k > k_0 \quad (2.51)$$

If the initial time  $k_0$  is set equal to 0 and there is no initial energy at time  $k = 0$ , Equation (2.51) becomes

$$y(k) = \sum_{j=0}^{k-1} C(k)\Phi(k, j+1)B(j)u(j) \quad (2.52)$$

Comparing Equation (2.52) with  $m$ - input,  $p$ - output version of the input/output Equation (2.36) reveals that

$$H(k, j) = \begin{cases} C(k)\Phi(k, j+1)B(j), & k > j \\ 0, & k \leq j \end{cases} \quad (2.53)$$

where  $H(k, j)$  is the  $p \times m$  unit-pulse response function matrix. Note that if  $A(k)$  is invertible so that  $\Phi(k, k_0)$  has the factorization given in Equation (2.49), then  $H(k, j)$  can be expressed in the factored form

$$H(k, j) = [C(k)\Phi_1(k)][\Phi_2(j+1)B(j)] \quad \text{for } k > j \quad (2.54)$$

As in the continuous-time case, this factorization is a fundamental property of unit-pulse response matrices  $H(k, j)$  that are realizable by a state model (with invertible  $A(k)$ ).

### 2.2.2 Stability

Given a discrete-time with  $n$ - dimensional state model  $[A(k), B(k), C(k)]$ , consider the homogeneous equation

$$x(k+1) = A(k)x(k), \quad k \geq k_0 \quad (2.55)$$

The solution is

$$x(k) = \Phi(k, k_0)x(k_0), \quad k > k_0 \quad (2.56)$$

where  $\Phi(k, k_0)$  is the state-transition matrix defined by Equation (2.46).

The system is said to be asymptotically stable if the solution  $x(k)$  satisfies the condition  $\|x(k)\| \rightarrow 0$  as  $k \rightarrow \infty$  for any initial state  $x(k_0)$  at the initial time  $k_0$ . This is equivalent to requiring that

$$\|\Phi(k, k_0)\| \rightarrow 0 \quad \text{as } k \rightarrow \infty \quad (2.57)$$

### 2.2.3 Controllability and Observability

The system with state model  $[A(k), B(k), C(k)]$  is said to be controllable on the interval  $[k_0, k_1]$  with  $k_1 > k_0$  if, for any states  $x_0$  and  $x_1$ , an input  $u(k)$  exists that drives the system to the state  $x(k_1) = x_1$  at time  $k = k_1$  starting from the state  $x(k_0) = x_0$  at time  $k = k_0$ .

Define the  $n \times nm$  controllability (or reachability) matrix

$$R(k_0, k_1) = \begin{bmatrix} B(k_1 - 1) \\ \Phi(k_1, k_1 - 1)B(k_1 - 2) \\ \Phi(k_1, k_1 - 2)B(k_1 - 3) \\ \vdots \\ \Phi(k_1, k_0 + 1)B(k_0) \end{bmatrix} \quad (2.58)$$

Then from Equation (2.45), the state  $x(k_1)$  at time  $k = k_1$  resulting from state  $x(k_0)$  at time  $k = k_0$  and the input sequence  $u(k_0), u(k_0 + 1), \dots, u(k_1 - 1)$  is given by

$$x(k_1) = \Phi(k_1, k_0)x(k_0) + R(k_0, k_1)U(k_0, k_1) \quad (2.59)$$

where  $U(k_0, k_1)$  is the  $mn$ -element column vector of inputs given by

$$U(k_0, k_1) = [u^T(k_1 - 1) \ u^T(k_1 - 2) \ \dots \ u^T(k_0)]^T \quad (2.60)$$

Now for any states  $x(k_0) = x_0$  and  $x(k_1) = x_1$ , from Equation (2.59) there is a sequence of inputs given by  $U(k_0, k_1)$  that drives the system from  $x_0$  to  $x_1$  if, and only if, the matrix  $R(k_0, k_1)$  has rank  $n$ . If this is the case Equation (2.59) can be solved for  $U(k_0, k_1)$ , giving

$$U(k_0, k_1) = R^T(k_0, k_1)[R(k_0, k_1)R^T(k_0, k_1)]^{-1}[x_1 - \Phi(k_1, k_0)x_0] \quad (2.61)$$

Hence  $\text{rank } R(k_0, k_1) = n$  is a necessary and sufficient condition for controllability over the interval  $[k_0, k_1]$ .

Now set  $k_0 = k - n + 1$  and  $k_1 = k + 1$  in  $R(k_0, k_1)$ , which results in the matrix  $R(k - n + 1, k + 1)$  which will be denoted by  $R(k)$ . The system is said to be uniformly  $n$ -step controllable if  $\text{rank } R(k) = n$  for all  $k$ .

Suppose that system input  $u(k)$  is zero so that the state model is given by

$$x(k + 1) = A(k)x(k) \quad (2.62a)$$

$$y(k) = C(k)x(k) \quad (2.62b)$$

From Equation (2.62), the output response  $y(k)$  resulting from initial state  $x(k_0)$  is given by

$$y(k) = C(k)\Phi(k, k_0)x(k_0), \quad k \geq k_0 \quad (2.63)$$

Then the system is said to be observable on the interval  $[k_0, k_1]$  if any initial state  $x(k_0) = x_0$  can be determined from the output response  $y(k)$  given by Equation (2.63) for  $k = k_0, k_0 + 1, \dots, k_1 - 1$ . Using Equation (2.63),

$$\begin{bmatrix} y(k_0) \\ y(k_0 + 1) \\ \vdots \\ y(k_1 - 2) \\ y(k_1 - 1) \end{bmatrix} = \begin{bmatrix} C(k_0)x_0 \\ C(k_0 + 1)\Phi(k_0 + 1, k_0)x_0 \\ \vdots \\ C(k_1 - 2)\Phi(k_1 - 2, k_0)x_0 \\ C(k_1 - 1)\Phi(k_1 - 1, k_0)x_0 \end{bmatrix} \quad (2.64)$$

The right hand side of Equation (2.64) can be written in the form  $O(k_0, k_1)x_0$  where  $O(k_0, k_1)$  is the  $np \times n$  observability matrix defined by

$$O(k_0, k_1) = \begin{bmatrix} C(k_0) \\ C(k_0 + 1)\Phi(k_0 + 1, k_0) \\ \vdots \\ C(k_1 - 2)\Phi(k_1 - 2, k_0) \\ C(k_1 - 1)\Phi(k_1 - 1, k_0) \end{bmatrix} \quad (2.65)$$

Equation (2.64) can be always be solved for  $x_0$  if, and only if,  $\text{rank } O(k_0, k_1) = n$ , which is a necessary and sufficient condition for observability on  $[k_0, k_1]$ . If the rank condition holds, the solution for Equation (2.64) for  $x_0$  is

$$x_0 = [O^T(k_0, k_1)O(k_0, k_1)]^{-1}O^T(k_0, k_1)Y(k_0, k_1) \quad (2.66)$$

where

$$Y(k_0, k_1) = [y^T(k_0) \quad y^T(k_0 + 1) \quad \dots \quad y^T(k_1 - 1)]^T \quad (2.67)$$

Setting  $k_0 = k$  and  $k_1 = k + n$  in  $O(k_0, k_1)$  yields the matrix  $O(k, k + n)$  which will be denoted by  $O(k)$ . If  $\text{rank } O(k) = n$  for all  $k$ , the system is said to be uniformly  $n$ -step observable.

### 2.3 Mathematical Formulation of SDOF LTV System with sTMD

Figure 2.1 shows a single degree of freedom LTV system with sTMD. The primary structure is of mass,  $m_p$ , stiffness,  $k_p$ , and damping,  $c_p$  whereas the sTMD is composed of smaller secondary mass,  $m_s$ , a spring of stiffness,  $k_s + k_{sv}(t)$ , and a dashpot of viscous damping coefficient,  $c_s + c_{sv}(t)$ . The equation of motion for the primary mass is given by

$$m_p \ddot{u}_p + c_p \dot{u}_p + k_p u_p = (c_s + c_{sv}(t)) \dot{u}_r + (k_s + k_{sv}(t)) u_r + F_p \quad (2.68)$$

where

$$\ddot{u}_p = -\frac{c_p}{m_p} \dot{u}_p - \frac{k_p}{m_p} u_p + \frac{c_s}{m_p} \dot{u}_r + \frac{c_{sv}(t)}{m_p} \dot{u}_r + \frac{k_s}{m_p} u_r + \frac{k_{sv}(t)}{m_p} u_r + \frac{F_p}{m_p} \quad (2.69)$$

Substituting  $\omega_p^2 = \frac{k_p}{m_p}$ ,  $\xi_p = \frac{c_p}{2m_p\omega_p}$ ,  $\omega_s^2 = \frac{k_s}{m_s}$ ,  $\omega_{sv}^2(t) = \frac{k_{sv}(t)}{m_s}$ ,  $\xi_s = \frac{c_s}{2m_s\omega_s}$ ,  $\xi_{sv}(t) = \frac{c_{sv}(t)}{2m_s\omega_{sv}(t)}$  and  $\mu = \frac{m_s}{m_p}$ ,

$$\ddot{u}_p = -2\xi_p\omega_p\dot{u}_p - \omega_p^2 u_p + \mu 2\xi_s\omega_s\dot{u}_r + \mu 2\xi_{sv}(t)\omega_{sv}(t)\dot{u}_r + \mu\omega_s^2 u_r + \mu\omega_{sv}^2(t)u_r + \frac{F_p}{m_p} \frac{F_p}{m_p} \quad (2.70)$$

The equation of motion for the secondary mass is given by

$$m_s \ddot{u}_s + (c_s + c_{sv}(t)) \dot{u}_r + (k_s + k_{sv}(t)) u_r = F_s \quad (2.71)$$

where  $\ddot{u}_s = \ddot{u}_p + \ddot{u}_r$ , Equation (2.71) can be rewritten as,

$$\ddot{u}_r = -\frac{c_s}{m_s} \dot{u}_r - \frac{c_{sv}(t)}{m_s} \dot{u}_r - \frac{k_s}{m_s} u_r - \frac{k_{sv}(t)}{m_s} u_r + \frac{F_s}{m_s} - \ddot{u}_p \quad (2.72)$$

substituting for  $\ddot{u}_p$  from Equation (2.69)

$$\begin{aligned} \ddot{u}_r = & -2\xi_s\omega_s\dot{u}_r - 2\xi_{sv}(t)\omega_{sv}(t)\dot{u}_r - \omega_s^2u_r - \omega_{sv}^2(t)u_r + \frac{F_s}{m_s} + 2\xi_p\omega_p\dot{u}_p + \omega_p^2u_p \\ & - \mu 2\xi_s\omega_s\dot{u}_r - \mu 2\xi_{sv}(t)\omega_{sv}(t)\dot{u}_r - \mu\omega_s^2u_r - \mu\omega_{sv}^2(t)u_r - \frac{F_p}{m_p} \end{aligned} \quad (2.73)$$

### State Space Formulation

Equation (2.70) and Eq. (2.73) can be rewritten in state space form as

$$\dot{\mathbf{X}} = \mathbf{A}\mathbf{X} + \mathbf{A}_{sv}(t)\mathbf{X} + \mathbf{E}\mathbf{F} \quad (2.74)$$

where

$$\begin{aligned} \mathbf{A} = & \begin{bmatrix} 0 & 0 & 1 & 0 \\ 0 & 0 & 0 & 0 \\ -\omega_p^2 & \mu\omega_s^2 & -2\xi_p\omega_p & \mu 2\xi_s\omega_s \\ \omega_p^2 & -(1+\mu)\omega_s^2 & 2\xi_p\omega_p & -(1+\mu)2\xi_s\omega_s \end{bmatrix} \\ \mathbf{A}_{sv}(t) = & \begin{bmatrix} 0 & 0 & 0 & 0 \\ 0 & 0 & 0 & 0 \\ 0 & \mu\omega_{sv}^2(t) & 0 & \mu 2\xi_{sv}(t)\omega_{sv} \\ 0 & -(1+\mu)\omega_{sv}^2(t) & 0 & -(1+\mu)2\xi_{sv}(t)\omega_{sv}(t) \end{bmatrix} \\ \mathbf{E} = & \begin{bmatrix} 0 & 0 \\ 0 & 0 \\ \frac{1}{m_p} & 0 \\ -\frac{1}{m_p} & \frac{1}{\mu m_p} \end{bmatrix}; \mathbf{F} = \begin{bmatrix} F_p \\ F_s \end{bmatrix}; \mathbf{X} = \begin{bmatrix} u_p \\ u_r \\ \dot{u}_p \\ \dot{u}_r \end{bmatrix} \end{aligned}$$

using

$$\mathbf{B}\mathbf{F}_{sv}(t) = \mathbf{A}_{sv}(t)\mathbf{X} \quad (2.75)$$

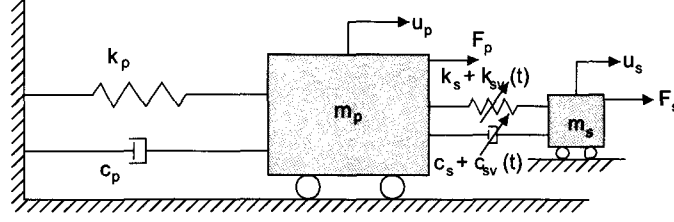


**Figure 2.1** Single Degree of Freedom System with TMD.

Equation (2.74) can be written as

$$\dot{\mathbf{X}} = \mathbf{A}\mathbf{X} + \mathbf{B}\mathbf{F}_{sv}(t) + \mathbf{E}\mathbf{F} \quad (2.76)$$

where

$$\mathbf{B} = \begin{bmatrix} 0 & 0 \\ 0 & 0 \\ \mu & 0 \\ 0 & -(1 + \mu) \end{bmatrix}$$

$$\mathbf{F}_{sv} = \begin{bmatrix} \omega_{sv}^2(t)u_r + 2\xi_s(t)\omega_s v(t)\dot{u}_r \\ \omega_{sv}^2(t)u_r + 2\xi_s(t)\omega_s v(t)\dot{u}_r \end{bmatrix}$$

## 2.4 Mathematical Formulation of MDOF LTV System with sTMD

In case of multi degree of freedom system with mass matrix  $\mathbf{M}_p$ , damping matrix,  $\mathbf{C}_p$ , stiffness matrix,  $\mathbf{K}_p$ , the equations of motion are as follows

$$\mathbf{M}_p \ddot{\mathbf{U}}_p + \mathbf{C}_p \dot{\mathbf{U}}_p + \mathbf{K}_p \mathbf{U}_p = -\mathbf{R}f_{sv}(t) + \mathbf{F}_p + \mathbf{R}(c_s \dot{u}_r + k_s u_r) \quad (2.77)$$

where  $f_{sv}(t) = c_{sv}(t)\dot{u}_r + k_{sv}(t)u_r$  and  $\mathbf{R} = [1 \ 0 \ \dots \ 0]^T$ .

$$\ddot{\mathbf{U}}_p = -\mathbf{M}_p^{-1} \mathbf{K}_p \mathbf{U}_p - \mathbf{M}_p^{-1} \mathbf{C}_p \dot{\mathbf{U}}_p - \mathbf{M}_p^{-1} \mathbf{R}f_{sv}(t) + \mathbf{M}_p^{-1} \mathbf{F}_p + \mathbf{M}_p^{-1} \mathbf{R}(c_s \dot{u}_r + k_s u_r) \quad (2.78)$$



$$m_s \ddot{u}_s = f_{sv}(t) + F_s \quad (2.79)$$

$$m_s(\ddot{u}_{pn} + \ddot{u}_r) = f_{sv}(t) + F_s \quad (2.80)$$

$$\ddot{u}_r = \frac{1}{m_s} f_{sv} + \frac{1}{m_s} F_s - \ddot{u}_{pn} \quad (2.81)$$

$$\begin{aligned} \ddot{u}_r = & \frac{1}{m_s} f_{sv} + \frac{1}{m_s} F_s + \mathbf{R}^T \mathbf{M}_p^{-1} \mathbf{K}_p \mathbf{u}_p + \mathbf{R}^T \mathbf{M}_p^{-1} \mathbf{C}_p \dot{\mathbf{u}}_p \\ & + \mathbf{R}^T \mathbf{M}_p^{-1} \mathbf{R} f_{sv} + \mathbf{R}^T \mathbf{M}_p^{-1} \mathbf{R} (c_s \dot{u}_r + k_s u_r) - \mathbf{R}^T \mathbf{M}_p^{-1} \mathbf{F}_p \end{aligned} \quad (2.82)$$

In state space form

$$\dot{\mathbf{X}} = \mathbf{A}\mathbf{X} + \mathbf{B}\mathbf{F}_{sv}(t) + \mathbf{E}\mathbf{F} \quad (2.83)$$

where

$$\begin{aligned} \mathbf{X} = & \begin{Bmatrix} \mathbf{u}_p \\ u_r \\ \dot{\mathbf{u}}_p \\ \dot{u}_r \end{Bmatrix}; \mathbf{A} = \begin{bmatrix} \mathbf{O}_{nn} & \mathbf{O}_{n1} & \mathbf{I}_{nn} & \mathbf{O}_{n1} \\ \mathbf{O}_{1n} & \mathbf{O}_{11} & \mathbf{O}_{1n} & \mathbf{I}_{11} \\ -\mathbf{M}_p^{-1} \mathbf{K}_p & -\mathbf{M}_p^{-1} \mathbf{R} k_s & -\mathbf{M}_p^{-1} \mathbf{C}_p & -\mathbf{M}_p^{-1} \mathbf{R} c_s \\ \mathbf{R}^T \mathbf{M}_p^{-1} \mathbf{K}_p & \mathbf{R}^T \mathbf{M}_p^{-1} \mathbf{R} k_s & \mathbf{R}^T \mathbf{M}_p^{-1} \mathbf{C}_p & \mathbf{R}^T \mathbf{M}_p^{-1} \mathbf{R} c_s \end{bmatrix} \\ \mathbf{B} = & \begin{bmatrix} \mathbf{O}_{nn} & \mathbf{O}_{n1} \\ \mathbf{O}_{1n} & \mathbf{O}_{11} \\ \mathbf{O}_{nn} & -\mathbf{M}_p^{-1} \mathbf{R} \\ -\mathbf{R}^T \mathbf{M}_p^{-1} & \mathbf{R}^T \mathbf{M}_p^{-1} \mathbf{R} + \frac{1}{m_s} \end{bmatrix}; \mathbf{F}_{sv} = \begin{bmatrix} \mathbf{O}_{n1} \\ f_{sv}(t) \end{bmatrix}; \mathbf{E} = \begin{bmatrix} \mathbf{O}_{nn} & \mathbf{O}_{n1} \\ \mathbf{O}_{1n} & \mathbf{O}_{11} \\ \mathbf{M}_p^{-1} & \mathbf{O}_{n1} \\ -\mathbf{R}^T \mathbf{M}_p^{-1} & \frac{1}{m_s} \end{bmatrix} \\ \mathbf{F} = & \begin{bmatrix} \mathbf{F}_p \\ F_s \end{bmatrix} \end{aligned}$$

If the semi-active stiffness is provided by a SAIVS device (Varadarajan 2005), the variable spring force is given by

$$f_{saivs}(t) = f_r(t) + f_f(t, \dot{u}) \quad (2.84)$$

where  $f_r(t) = k_e \cos^2 \theta(t) u(t)$  with  $k_e$  being the stiffness of one of the four springs,  $\theta(t)$  is a time-varying angle of the spring elements with the horizontal, and  $f_f$  being the frictional forces in the device.

## Chapter 3

### Time-frequency Analysis

This chapter presents a preliminary introduction to time-frequency analysis and the methods that will be employed in the following chapters. Classical time analysis and frequency analysis does not fully describe most signals in nature, where conditions change with time. Such individual approaches are adequate enough for signals that have the same spectral characteristics over time. For a signal whose frequency content changes with time, a time-varying spectrum needs to be defined to describe and analyze the non-stationary characteristics. Also, even if a signal is stationary, the response of a linear time varying system leads to time-varying spectrum, which can only be obtained by time-frequency analysis. The two methods studied in this chapter are (1) Short Time Fourier Transform (STFT), and (2) Wavelet Transform (WT).

#### 3.1 Review of Time-Frequency Techniques

The mathematics of the frequency representation was first derived by Fourier, whose main research was on heat flow. Fourier transform is simply an elegant tool to break down a signal to its harmonic components and re-synthesize it by adding these harmonic components. There are several versions of Fourier transform. The simplest one is Fourier series where a periodic arbitrary function with period  $T$  can be represented by an infinite trigonometric series of the form

$$f(t) = a_0 + \sum_{k=1}^{\infty} (a_k \cos \omega_k t + b_k \sin \omega_k t) \quad (3.1)$$

where  $\omega_k = 2\pi k/T$  and  $a_0$ ,  $a_k$  and  $b_k$  are constant Fourier coefficients given by

$$\begin{aligned} a_0 &= \frac{1}{T} \int_{-T/2}^{T/2} f(t) dt \\ a_k &= \frac{1}{T} \int_{-T/2}^{T/2} f(t) \cos \omega_k t dt \quad k \geq 1 \\ b_k &= \frac{1}{T} \int_{-T/2}^{T/2} f(t) \sin \omega_k t dt \quad k \geq 1 \end{aligned} \quad (3.2)$$

The Fourier series will converge to a periodically defined function in almost all practical situations. The function has to satisfy the following Dirichlet conditions:

1.  $f(t)$  must have a finite number of discontinuities over the period.
2.  $f(t)$  must have a finite number of maxima and minima over the period.
3.  $f(t)$  must be bounded or absolutely integrable,

$$\int_0^T |f(t)| dt < \infty$$

For non-periodic functions Fourier series can be extended to Fourier transform (or Fourier integral) by assuming the period  $T$  goes to infinity. As the period  $T$  becomes large, the frequency spacing  $\Delta\omega$  becomes small and in the limit the Fourier coefficients will merge together. Thus, Fourier series turns into a Fourier integral and the Fourier coefficients turn into continuous functions of frequency called Fourier transforms. The Fourier transform components are written as

$$\begin{aligned} A(\omega) &= \frac{1}{2\pi} \int_{-\infty}^{\infty} f(t) \cos \omega t dt \\ B(\omega) &= \frac{1}{2\pi} \int_{-\infty}^{\infty} f(t) \sin \omega t dt \end{aligned} \quad (3.3)$$

and the inverse Fourier transform is

$$f(t) = 2 \int_0^{\infty} A(\omega) \cos \omega t d\omega + 2 \int_0^{\infty} B(\omega) \sin \omega t d\omega \quad (3.4)$$

Using the Euler's formula of

$$e^{i\theta} = \cos \theta + i \sin \theta \quad (3.5)$$

Fourier series and Fourier transform can be written in exponential form as

$$z_m = \frac{1}{T} \int_0^T f(t) e^{-i\omega_m t} dt \quad -\infty \leq m \leq \infty$$

$$f(t) = \sum_{m=-\infty}^{\infty} z_m e^{i\omega_m t} \quad (3.6)$$

$$F(\omega) = \frac{1}{2\pi} \int_{-\infty}^{\infty} f(t) e^{-i\omega t} dt$$

$$f(t) = \int_{-\infty}^{\infty} F(\omega) e^{i\omega t} d\omega \quad (3.7)$$

There are also several forms of Fourier transform when both continuous and discrete time and frequency domains are considered. The Fourier series defines the relationship between continuous time and discrete frequency domains. The continuous time and frequency domains are related through the continuous time Fourier transform (CTFT). The transform and inverse transform pair in Equation (3.8) can also be written as

$$F_{CTFT}(f) = \int_{-\infty}^{\infty} f(t) e^{-i2\pi f t} dt$$

$$f(t) = \int_{-\infty}^{\infty} F_{CTFT}(f) e^{i2\pi f t} df \quad (3.8)$$

The discrete time and continuous frequency domains are related through the discrete time Fourier transform (DTFT). The transform and inverse transform pair are

$$F_{DTFT}(f) = \Delta t \sum_{-\infty}^{\infty} f(n\Delta t) e^{-i2\pi f n\Delta t}$$

$$f(n\Delta t) = \int_{-f_N}^{f_N} F_{DTFT}(f) e^{i2\pi f n\Delta t} df \quad (3.9)$$

where  $f_N = f_s/2 = 1/(2\Delta t)$ .  $f_N, f_s$  are the Nyquist and sampling frequency, respectively. For actual computer computation, both time and frequency domains must be discretized

leading to the discrete Fourier transform (DFT) pair

$$\begin{aligned} F_{DFT}(m\Delta f) &= \Delta t \sum_{n=-\infty}^{\infty} f(n\Delta t) e^{-i2\pi f n\Delta t} \\ f(n\Delta t) &= \frac{1}{n\Delta t} \sum_{m=0}^{n-1} F_{DFT}(m\Delta f) e^{i2\pi m n/N} \end{aligned} \quad (3.10)$$

The short-time Fourier transform (STFT) is one of the most popular methods for studying non-stationary signals. The basic idea of STFT is: to break up the signal into small time segments and Fourier analyze each time segment to identify the frequencies that existed in that segment. The totality of such spectra describes how the spectrum is varying in time (Cohen 1995). Mathematically, the short-time Fourier transform can be described by

$$STFT(t, \omega) = \frac{1}{2\pi} \int f(\tau) w(\tau - t) e^{-i\omega\tau} d\tau \quad (3.11)$$

where  $f(t)$  is the signal and  $w(\tau - t)$  is the window function which is chosen to leave the signal more or less unaltered around the time  $t$  but to suppress the signal for times distant from the time of interest. The short-time Fourier transform is best suited for signals with narrow instantaneous frequency bandwidth

The short-time Fourier transform compute correlations between the signal and a family of functions. In this transform, the time-frequency resolution is governed by the limits imposed by the uncertainty principle. Therefore, it may not work well in some problems. Another type of time-frequency representation is Wigner-Ville distribution which is computed by correlating the signal with a time and frequency translated version of itself.

$$WVD(t, \omega) = \int_{-\infty}^{\infty} f\left(t + \frac{\tau}{2}\right) f^*\left(t - \frac{\tau}{2}\right) e^{-i\omega\tau} d\tau \quad (3.12)$$

Unlike the short-time Fourier transform, there are no window functions causing to resolution limitations. Although Wigner-Ville distribution has superior properties, its applications are very limited due to cross-term interference.

Wavelet transform is a linear decomposition similar to the Fourier transform, but it breaks down the signal into its wavelet components instead of harmonic sinusoids (or exponentials). Wavelet is a small wave which has finite energy concentrated around a point in time. This time-frequency localization property makes wavelet transform best suited for highly non-stationary signals with sudden peaks or discontinuities. The continuous wavelet transform (CWT) can be defined by

$$CWT(a, b) = \frac{1}{\sqrt{|a|}} \int_{-\infty}^{\infty} f(t) \psi^* \left( \frac{t-b}{a} \right) dt \quad (3.13)$$

with an inverse transform of

$$f(t) = \frac{1}{C_\psi} \int_{-\infty}^{\infty} \int_{-\infty}^{\infty} \frac{1}{a^2} CWT(a, b) \psi \left( \frac{t-b}{a} \right) da db \quad (3.14)$$

## 3.2 Preliminary Definitions

A signal is a variation of a quantity in time, for example a seismic excitation characterized by sharp bursts of energy and gradual decay. It may also depend on position, but the time dependence is of primary interest and is given by,

$|s(t)|^2 =$  Instantaneous energy at time  $t$ , or

$|s(t)|^2 =$  Intensity per unit time at time  $t$ , or

$|s(t)|^2 \Delta t =$  the energy in  $\Delta t$  at time  $t$

The instantaneous energy defined above is the energy used to produce the signal at time  $t$ .

Total energy, normalized to one, is given by

$$E = \int |s(t)|^2 dt \quad (3.15)$$

The use of  $|s(t)|^2$  for the energy density comes from the fundamental laws. For example, if  $E(t)$  is the electric field then it is proven, from Maxwell's equations, that the energy density is given by  $|E(t)|^2$ ; or in case where the signal is the voltage then the energy density is proven to be  $|V(t)|^2$  per unit resistance. That is, in a small amount of time  $\Delta t$  it takes  $|s(t)|^2 \Delta t$  amount of energy to produce the signal at time  $t$ .

The averages are calculated in the standard way. The density function is multiplied with the function  $g(t)$  and integrated. Hence, the average of time function is

$$\overline{g(t)} = \int g(t) |s(t)|^2 dt \quad (3.16)$$

Mean or average time is

$$\bar{t} = \int t |s(t)|^2 dt \quad (3.17)$$

Duration is

$$T^2 = \sigma_t^2 = \int (t - \bar{t})^2 |s(t)|^2 dt = \bar{t^2} - \bar{t}^2 \quad (3.18)$$

It is often very advantageous to examine a signal in the frequency representation for the following reason: it simplifies our understanding of the wave form. A complicated signal in the time domain may often be simply understood in the frequency domain. For example if a signal is made up of a few sine waves then the signal will look very complicated in the time domain but will be simple in the frequency domain because a Fourier analysis will indeed reveal that it is just a few sine waves. Therefore a complicated signal in the time domain may, in some cases, be easily recognized and classified in the frequency domain.

For a signal  $s(t)$ , its Fourier transform is

$$S(\omega) = \frac{1}{2\pi} \int s(t) e^{-j\omega t} dt \quad (3.19)$$

where



$|S(\omega)|^2 = \text{Energy density spectrum } \omega, \text{ or}$

$|S(\omega)|^2 = \text{Intensity per unit frequency at frequency } \omega, \text{ or}$

$|S(\omega)|^2 \Delta\omega = \text{the energy in } \Delta\omega \text{ at frequency } \omega$

Total energy based on Parseval's theorem is:

$$E = \int |s(t)|^2 dt = \int |S(\omega)|^2 d\omega \quad (3.20)$$

Average of frequency function is

$$\overline{g(\omega)} = \int g(\omega) |S(\omega)|^2 d\omega \quad (3.21)$$

Mean frequency and bandwidth are

$$\bar{\omega} = \int \omega |S(\omega)|^2 d\omega \quad (3.22a)$$

$$B^2 = \sigma_\omega^2 = \overline{\omega^2} - \bar{\omega}^2 = \int (\omega - \bar{\omega})^2 |S(\omega)|^2 d\omega \quad (3.22b)$$

If the signal is written in terms of its amplitude and phase

$$s(t) = A(t)e^{j\varphi(t)} \quad (3.23)$$

where  $A(t)$  is the envelope or amplitude and  $\varphi(t)$  is the phase. If  $A(t)$  depends on time then amplitude modulation occurs; the mean frequency can then be written as

$$\begin{aligned} \bar{\omega} &= \int \omega |S(\omega)|^2 d\omega, \text{ or as,} \\ \bar{\omega} &= \int \varphi'(t) |s(t)|^2 dt \end{aligned} \quad (3.24)$$

where the derivative of the phase,  $\varphi'(t)$ , which is the instantaneous frequency. The term frequency modulation is used in the sense that the instantaneous frequency is itself changing.

This is an interesting and important result because it says that the average frequency may be calculated by integrating "something" with the density over all time. Therefore the "something" must be instantaneous value of the quantity for which the average is being calculated. Since the result is the average frequency; the derivative of the phase may then be appropriately called the frequency at each time or the instantaneous frequency  $\omega_i$

$$\omega_i(t) = \varphi'(t) \quad (3.25)$$

### 3.3 Uncertainty Principle

The duration of the signal is defined by  $\Delta t$  where

$$(\Delta t)^2 = \int (t - \bar{t})^2 |s(t)|^2 dt \quad (3.26)$$

and where the mean time is

$$\bar{t} = \int t |s(t)|^2 dt \quad (3.27)$$

The bandwidth is defined by  $\Delta \omega$  where

$$(\Delta \omega)^2 = \int (\omega - \bar{\omega})^2 |S(\omega)|^2 d\omega \quad (3.28)$$

with  $\bar{\omega}$  being the mean frequency,

$$\bar{\omega} = \int \omega |S(\omega)|^2 d\omega \quad (3.29)$$

Note that these definitions are identical to the definitions for variance, spread or root mean square deviation as defined for standard quantities such as weight - they are an indication of concentration around mean.

The time bandwidth relation or uncertainty principle is that for any signal

$$\Delta t \Delta \omega \geq \frac{1}{2} \quad (3.30)$$

The physical interpretation is that the duration and bandwidth cannot be both made narrow. Note that the uncertainty principle depends only on the time and frequency densities. The reason that the time-bandwidth relation holds is that indeed there is a relation between the two densities given by Equation (3.19); hence,  $|s(t)|^2$  and  $|S(\omega)|^2$  cannot be changed independently.

### 3.4 Short Time Fourier Transform (STFT)

The short-time Fourier transform (STFT) was the first tool devised for analyzing a signal in time and frequency. The basic idea is that if one wants to know what frequencies exist at a particular time, then take a small piece of the signal around that time and Fourier analyze it, neglecting the rest of the signal as shown in Figure 3.1. Since time interval is short compared to the whole signal this process is called taking the short-time Fourier transform.

$$STFT(t, \omega) = S(t, \omega) = \frac{1}{2\pi} \int s_w(\tau) e^{-i\omega\tau} d\tau \quad (3.31)$$

The energy per unit frequency at time  $t$  is  $|S(t, \omega)|^2$ . One wants to design a window function,  $w(\tau)$  which will emphasize the times around the time  $t$  as shown in Figure 3.1, such that, the weighted signal is centered around the time of interest  $\tau - t$

$$s_w(\tau) = s(\tau)w(\tau - t) \quad (3.32)$$

The running time is  $\tau$  and the fixed time is  $t$ . Considering this signal as a function of  $\tau$  one can ask for the spectrum of it. Since the window has been chosen to emphasize time  $t$  the spectrum will emphasize the frequencies at that time and hence give an indication of the

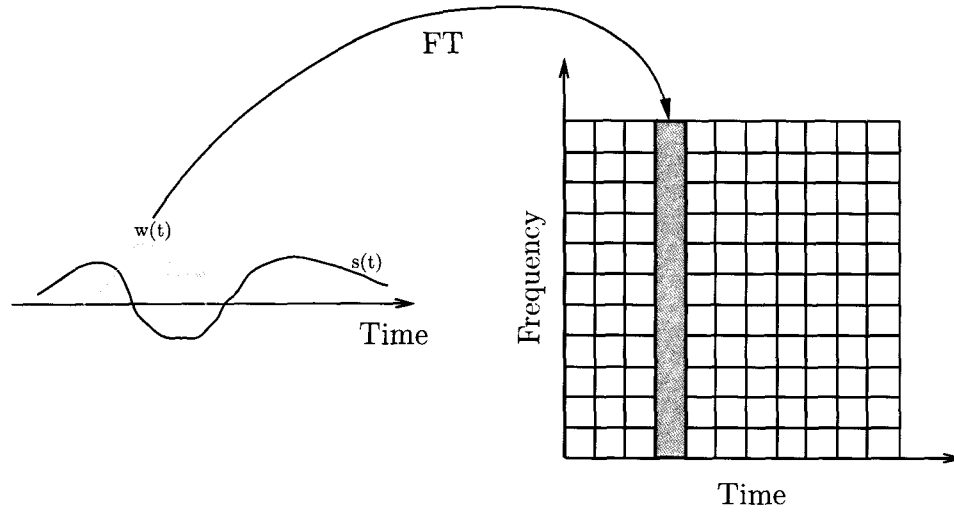


**Figure 3.1** Short Time Fourier Transform (STFT)

frequencies at that time. In particular the spectrum is

$$STFT(t, \omega) = \frac{1}{2\pi} \int e^{-i\omega\tau} s_w(\tau) d\tau \quad (3.33a)$$

$$= \frac{1}{2\pi} \int e^{-i\omega\tau} s(\tau) w(\tau - t) d\tau \quad (3.33b)$$

The energy density of the modified signal at fixed time  $t$  is

$$P_{SP}(t, \omega) = |STFT(t, \omega)|^2 \text{ or} \quad (3.34a)$$

$$P_{SP}(t, \omega) = \left| \frac{1}{2\pi} \int e^{-i\omega\tau} s(\tau) w(\tau - t) d\tau \right|^2 \quad (3.34b)$$

For each time one gets a different spectrum and the totality of these gives the time-frequency distribution called spectrogram, which is a member of a general class of distributions.

The STFT in terms of the Fourier transforms of the signal and window is

$$S(\omega) = \frac{1}{2\pi} \int s(t) e^{-i\omega t} dt \quad (3.35a)$$

$$H(\omega) = \frac{1}{2\pi} \int w(t) e^{-i\omega t} dt \quad (3.35b)$$

$$STFT(t, \omega) = \frac{1}{2\pi} \int s_w(\tau) e^{-i\omega \tau} d\tau \quad (3.35c)$$

$$= \frac{1}{2\pi} \int s(\tau) w(\tau - t) e^{-i\omega \tau} d\tau \quad (3.35d)$$

$$= \frac{1}{2\pi} \int S(\omega') H(\omega - \omega') e^{i\omega' t} d\omega' \quad (3.35e)$$

The spectrogram is then given by Equation (3.34) or by

$$P_{SP}(t, \omega) = \left| \frac{1}{2\pi} \int S(\omega') H(\omega - \omega') e^{i\omega' t} d\omega' \right|^2 \quad (3.36)$$

By analogy with the previous discussion it can be used to study the behavior of the signal around the frequency point  $\omega$ . This is done by choosing a time window function whose transform is weighted relatively higher at the frequency  $\omega$ .

The implementation procedure for the STFT in the discrete domain is carried out by extracting time windows of the original non-stationary signal  $s(t)$ . After zero padding and convolving the signal with the window function, the DFT is computed for each windowed signal to obtain STFT,  $s(\omega)$ , of signal  $s(t)$ . If the window width is  $n.\Delta t$  (where  $n$  is number of points in the window, and  $\Delta t$  is the sampling rate of the signal), the  $i$ -th element in  $s(\omega)$  is the Fourier coefficient that corresponds to the frequency,

$$\omega_i = i \frac{2\pi}{n.\Delta t} \quad (\text{for window width } n.\Delta t) \quad (3.37)$$

### 3.5 Wavelet Transform (WT)

Wavelets were introduced at the beginning of eighties by J. Morlet as a signal analysis tool to analyze seismic data. Although the original idea can be traced back to Haar, wavelets

gained popularity after eighties with contributions from many researchers who developed the mathematical foundation of wavelets. Wavelet transform is simply a linear transform which uses diluted (scaled) and translated (shifted) versions of a single prototype function  $\psi(t)$  namely mother wavelet to represent a signal. Wavelets constitute a family of functions derived from one single function and indexed by two parameters, one for position and one for scale.

$$\psi_{a,b}(t) = \frac{1}{\sqrt{|a|}} \psi\left(\frac{t-b}{a}\right) \quad (3.38)$$

where  $a, b \in \mathbb{R}$  (with the constraint  $a \neq 0$ ). The continuous wavelet transform can be defined by

$$CWT(a, b) = \frac{1}{\sqrt{|a|}} \int_{-\infty}^{\infty} f(t) \psi^*\left(\frac{t-b}{a}\right) dt = \int_{-\infty}^{\infty} f(t) \psi_{a,b}^*(t) dt \quad (3.39)$$

with an inverse transform of

$$f(t) = \frac{1}{C_\psi} \int_{-\infty}^{\infty} \int_{-\infty}^{\infty} \frac{1}{a^2} CWT(a, b) \psi\left(\frac{t-b}{a}\right) da db \quad (3.40)$$

The constant  $C_\psi$  is given by

$$C_\psi = \int_{-\infty}^{\infty} \frac{|\hat{\Psi}(\xi)|^2}{|\xi|} d\xi \quad (3.41)$$

where  $\hat{\Psi}(\xi)$  is the Fourier transform defined by

$$\hat{\Psi}(\xi) = \int_{-\infty}^{\infty} \psi(t) e^{-i\xi t} dt \quad (3.42)$$

In order the inverse continuous wavelet transform exists,  $C_\psi$  is required to be finite ( $< \infty$ ). Thus, the integrand defining  $C_\psi$  should be integrable at  $\xi = 0$  which implies that  $\psi(0) = 0$  leading to the result that the mean value of the wavelet  $\psi(t)$  should be zero.

Since the parameters  $a, b$  vary continuously over  $\mathbb{R}$ , the continuous wavelet transform has highly redundant information about the signal. A signal can still be decomposed and

synthesized using discretized values of  $a, b$ . The discrete wavelet transform can be classified into two groups: (1) Redundant discrete systems (frames) and (2) orthonormal (and other) bases of wavelets. In the redundant discrete wavelet transform (RDWT), the discretization can be done by choosing  $a = a_0^{-m}$  where  $a_0 > 1$  and  $b = nb_0a_0^{-m}$  where  $b_0 > 0$  is fixed and  $n \in \mathbb{Z}$ . The corresponding wavelets can be written as

$$\psi_{m,n}(t) = a_0^{-m/2} \psi\left(\frac{t - nb_0a_0^{-m}}{a_0^{-m}}\right) = a_0^{m/2} \psi(a_0^m t - nb_0) \quad (3.43)$$

$$DWT(m, n) = a_0^{m/2} \int_{-\infty}^{\infty} f(t) \psi^*(a_0^m x - nb_0) dt \quad (3.44)$$

In the redundant discrete wavelet transform, there does not exist, in general, a direct inverse transform like Equation (3.40). Nevertheless,  $f(t)$  can be covered from the sampled wavelet transform by

$$f(t) = \sum_{m=-\infty}^{\infty} \sum_{n=-\infty}^{\infty} DWT(m, n) \hat{\psi}_{m,n}(t) \quad (3.45)$$

where  $\{\hat{\psi}_{m,n}\}_{m,n \in \mathbb{Z}}$  denotes a dual frame of  $\{\psi_{m,n}\}_{m,n \in \mathbb{Z}}$ . A central issue of the wavelet transform is how to build dual frames  $\{\psi_{m,n}\}_{m,n \in \mathbb{Z}}$  and  $\{\hat{\psi}_{m,n}\}_{m,n \in \mathbb{Z}}$  with desired properties

The choice of wavelet  $\psi$  used in continuous wavelet transform and in frames is only restricted by the requirement  $C_\psi$  is finite in order to recover the original function from the transformations. If the objective is only to analyze the signal, then the mother wavelet can be any function. For practical reasons, one usually chooses  $\psi$  so that it is well concentrated in both time and frequency domain.

Most popular discretization is dyadic grid in which  $a_0 = 2$  and  $b_0 = 1$ . The dilated and translated mother wavelet is then defined by

$$\psi_{m,n}(t) = 2^{m/2} \psi(2^m x - n) \quad (3.46)$$

The continuous wavelet transform is shift-invariant whereas its sampled version is shift-variant. The quantity  $DWT(m, n)$  is subject to exactly where on the signal one starts processing.

For some very special choices of  $\psi$  and  $a_0, b_0$ , the  $\psi_{m,n}$  constitute an orthonormal basis for  $L^2(\mathbb{R})$ . Thus,  $f(t)$  can be recovered from the sampled wavelet transform by

$$f(t) = \sum_{m=-\infty}^{\infty} \sum_{n=-\infty}^{\infty} DWT(m, n) \psi_{m,n}(t) \quad (3.47)$$

Orthogonal basis functions allow simple calculation of wavelet coefficients and have Parseval's theorem that allows a partitioning of the signal energy in the wavelet transform domain.



## **Chapter 4**

# **Frequency Tracking and Evolutionary Spectrum by STFT and WT**

This chapter presents examples of real-time frequency tracking and evolutionary power spectral density (EPSD) estimation of several excitation signals, from simple harmonic signals to stationary and non-stationary processes. The results are obtained by both Short Time Fourier Transform (STFT) and Wavelet Transform (WT), and the two methods have been compared. The developed semi-active control algorithms throughout this study depend mainly on frequency tracking based on the evolutionary power spectral density of the excitation. The following sections present frequency tracking and evolutionary spectrum estimation on different types of excitation signals, which will be used in the subsequent chapters.

Simulations of random processes are generated from pre-defined target evolutionary spectra using the autoregressive (AR) method (described in Section 1.2.11). The target evolutionary spectra considered in this study are selected to demonstrate the benefits of the semi-active concepts. Earlier studies to describe the evolutionary power spectra of non-stationary ground motion processes from a set of observed accelerogram records and to synthesize artificial accelerograms are available in the literature (Conte and Peng 1997; Mukherjee and Gupta 2002; Giaralis and Spanos 2009). Spanos and Failla (2004) and Spanos et al. (2005) developed wavelet-based methods for evolutionary spectrum estimation. The aforementioned studies do not address real-time estimation of EPSD needed for instantaneous frequency tracking, which is the subject of this study.

## 4.1 Frequency Tracking and Evolutionary Spectrum Estimation by STFT

The short-time Fourier transform (STFT) is one of the most popular methods for studying time-frequency characteristics of non-stationary signals. A detailed introduction on short-time Fourier transform is given in Chapter 3. The instantaneous (dominant) frequency of a signal can be estimated from its spectrogram (magnitude squared of the STFT). Similarly, the power spectral density of a random signal can be estimated from the spectrogram of the signal. The developed semi-active control algorithms in the following chapters use frequency tracking and/or evolutionary power spectral density for adjusting the smart variable damping and stiffness systems.

The implementation of frequency tracking and evolutionary power spectral density estimation in real-time using STFT is shown in Figure 4.1. Since the estimation is to be used in semi-active control algorithms in real-time, for any given time only the portion of signal data up to that time is assumed to be known. The procedure starts by selecting an STFT window and a window length ( $WL$ ) of  $(n - 1)\Delta t$  (where  $n$  is the number of points in the window). A triangular window is employed for STFT throughout this study due to nature of real-time estimation where the information around the real-time  $t_i$  is most critical. Time lapse ( $TL$ ) of  $L\Delta t$  is the time period between successive windows. The window is multiplied by the portion of the signal,  $s(t)$  up to the real-time  $t_i$  and then zero padded for the desired frequency resolution. The instantaneous PSD (a time slice of the evolutionary PSD) is estimated by the FFT (fast Fourier transform) power spectrum of each windowed signal  $s(t)w(t_i)$  as given in Equation (4.1)

$$S(t_i, f) = \frac{1}{f_s N} |fft[s(t)w(t_i)]|^2 \quad (4.1)$$

where  $f$  is the cyclic frequency in  $Hz$ ,  $f_s = 1/\Delta t$  is the sampling frequency, and  $N$  is the

total number of the signal data.

The instantaneous (dominant) frequency is determined using Equation (4.2) by weighting the ridge frequency (corresponding to maximum PSD value) by its PSD value at the corresponding time.

$$f_{ins}(t_i) = \frac{\sum_{k=\max(1, i-m+1)}^i f_{max}(t_k) \max [ |S(t_i, f)|^2 ]}{\sum_{k=\max(1, i-m+1)}^i \max [ |S(t_i, f)|^2 ]} \quad (4.2)$$

in which the averaging length,  $AL = (m - 1)\Delta t$  is the time length considered in weighted averaging of dominant frequency and  $m$  is the number of points used for averaging.  $f_{max}$  is the ridge frequency corresponding to the frequency with maximum instantaneous PSD value.

## 4.2 Frequency Tracking and Evolutionary Spectrum Estimation by WT

Wavelet transform (WT) is a more accurate and efficient method of time-frequency analysis compared to STFT (Kaiser 1992). A detailed introduction on wavelet transform is given in Chapter 3. In STFT, performing Fourier transform on a sliding window of length  $T$  and a time series with a time step of  $\Delta t$ , and total length of  $N\Delta t$  results in a fixed frequency resolution of  $1/T$  between the frequency range of  $1/T$  to  $1/(2\Delta t)$ . The limited frequency range of the window causes inaccuracy by aliasing of low and high frequency components outside the frequency range. The fixed frequency resolution of STFT is also inefficient when the signal has a wide range of dominant frequencies. Wavelet transform overcomes the limitations of STFT by scaling the time-frequency localized wavelet basis functions, hence analyzing the signal with different window sizes (scales) simultaneously.

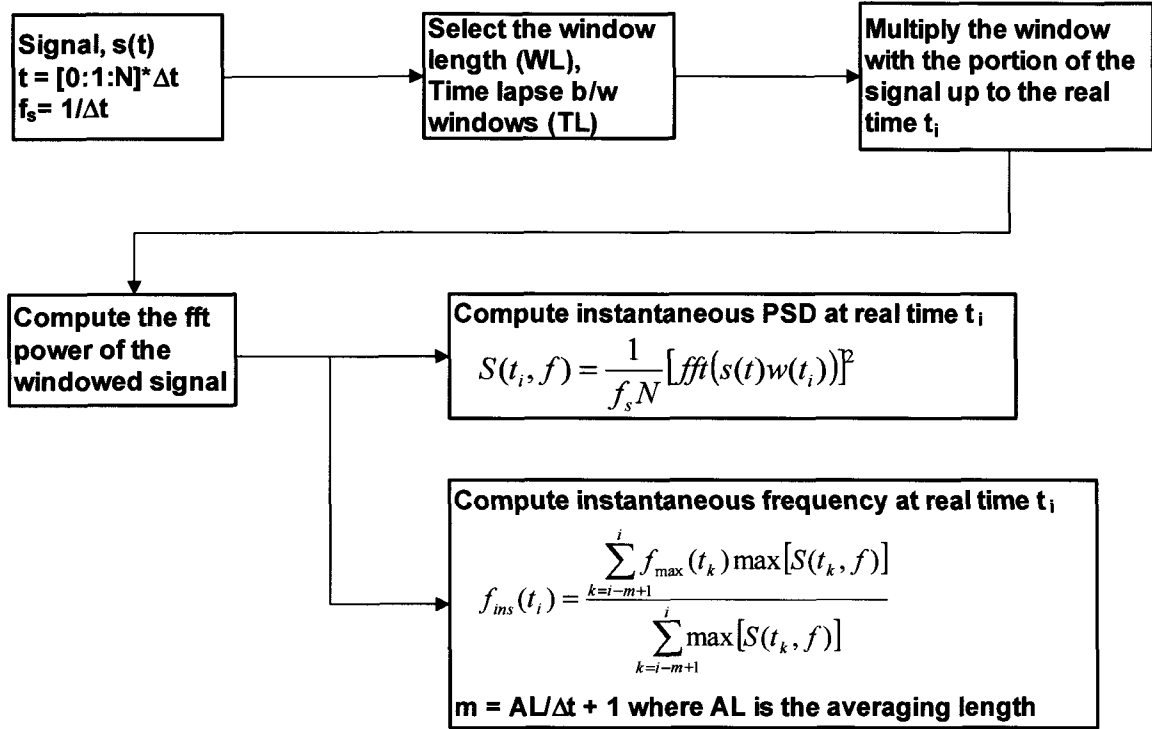


**Figure 4.1** Frequency tracking and Evolutionary Spectrum Estimation by STFT

This allows detecting the low frequencies in the signal by long windows (wavelets with larger scales) and the high frequencies by short windows (wavelets with smaller scales).

There are many possible wavelet functions (continuous or discrete, orthogonal or non-orthogonal, complex or real) to analyze any given signal. In this study, complex Morlet wavelet is employed for its good localization properties in both time and frequency domains. A complex wavelet is specifically selected to separate the phase and amplitude components within the signal. This provides consistent ridges at the dominant frequencies of the wavelet transform rather than large undulations due to moving of wavelet (at scale corresponding the dominant frequency) in and out of phase with the signal (Addison 2002). The wavelet transform algorithm used in this study is summarized below following the approach outlined in Torrence and Compo (1998).

The continuous wavelet transform of a discrete sequence  $x_n$  is defined as the convolution of  $x_n$  with a scaled and translated version of mother wavelet,  $\psi_0(n)$

$$W(n, a) = \sum_{n'=0}^{N-1} x_n \psi^* \left[ \frac{(n' - n)\Delta t}{a} \right] \quad (4.3)$$

where the  $*$  indicates the complex conjugate,  $a$  is the wavelet scale  $a$  and  $n$  is the localized time index  $n$ .

The wavelet transform in Equation (4.3) can be calculated considerably faster in Fourier space. The DFT of  $x_n$  is

$$X_k = \frac{1}{N} \sum_{n=0}^{N-1} x_n e^{-2\pi i k n / N} \quad (4.4)$$

where  $k = 0, 1, \dots, N - 1$  is the frequency index. In the continuous limit, the Fourier transform of the scaled wavelet  $\psi(t/s)$  is given by  $\Psi(a\omega)$ . By the convolution theorem, the wavelet transform is the inverse Fourier transform of the product  $X_k \Psi(a\omega)^*$ :

$$W(n, a) = \sum_{k=0}^{N-1} X_k \Psi^*(a\omega_k) e^{i\omega_k n \Delta t} \quad (4.5)$$

where the angular frequency is defined as

$$\omega_k = \begin{cases} \frac{2\pi k}{N\Delta t} & : k \leq \frac{N}{2} \\ -\frac{2\pi k}{N\Delta t} & : k > \frac{N}{2} \end{cases} \quad (4.6)$$

In order to ensure the wavelet transforms in Equation (4.5) at each scale  $a$  are directly comparable to each other and to the transforms of other time series, the wavelet function at each scale  $a$  is normalized to have unit energy (Torrence and Compo 1998):

$$\Psi(a\omega_k) = \left( \frac{2\pi a}{\Delta t} \right)^{1/2} \Psi_0(a\omega_k) = (a\omega N)^{1/2} \Psi_0(a\omega_k) \quad (4.7)$$

with also Fourier transform of the mother wavelet defined to have unit energy.

$$\int_{-\infty}^{+\infty} |\Psi(\omega')|^2 d\omega' = 1 \quad (4.8)$$

Using these normalizations, at each scale

$$\sum_{k=0}^{N-1} |\Psi(a\omega_k)|^2 = N \sum_{k=0}^{N-1} |\Psi_0(a\omega_k)|^2 (a\Delta\omega) = N \quad (4.9)$$

where  $N$  is the number of points. Thus, the wavelet transform is weighted only by the amplitude of the Fourier coefficients  $X_k$  and not by the wavelet function. The normalization in time domain is

$$\psi \left[ \frac{(n' - n)\Delta t}{a} \right] = \left( \frac{\Delta t}{a} \right)^{1/2} \psi_0 \left[ \frac{(n' - n)\Delta t}{a} \right] \quad (4.10)$$

where  $\psi_0(n)$  is normalized to have unit energy.

The normalized Morlet mother wavelet and its Fourier transform can be written as

$$\psi_0(t) = \pi^{-1/4} \left( \frac{f_b}{2} \right)^{-1/4} e^{i\omega_0 t} e^{-t^2/f_b} \quad (4.11)$$

$$\Psi_0(a\omega) = \begin{cases} \pi^{-1/4} \left( \frac{f_b}{2} \right)^{1/4} e^{-f_b(a\omega - \omega_0)^2/4} & \text{for } \omega > 0 \\ 0 & \text{for } \omega \leq 0 \end{cases} \quad (4.12)$$

where  $\omega_0$  is the frequency parameter of the mother wavelet. In some literature, a correction term  $(-\pi^{-1/4}(f_b/2)^{-1/4}e^{-\omega^2/2}e^{-t^2/f_b})$  is included in Equation (4.11) to correct for non-zero mean of Equation (4.11) (i.e. the zero frequency term of its corresponding energy spectrum is non-zero) to satisfy the wavelet admissibility condition. In practice, the error becomes negligible for  $\omega_0 \geq 6$ ) and can be ignored. The  $\pi^{-1/4}(f_b/2)^{-1/4}$  is the normalization factor which ensures that the wavelet has unit energy.

The wavelet scale can be related to an equivalent Fourier frequency by taking wavelet transform of a cosine wave of a known frequency and computing the scale  $a$  at which the wavelet power spectrum reaches its maximum (Meyers et al. 1993). The relationship between the Morlet wavelet scale and the equivalent Fourier period is given by

$$T_j = \lambda a_j = \left( \frac{4\pi}{\omega_0 + \sqrt{4/f_b + \omega_0^2}} \right) a_j \quad (4.13)$$

For the Morlet wavelet with  $\omega_0 = 6$  and  $f_b = 2$ , Equation (4.13) gives a value of  $\lambda = 1.03$ , indicating that the wavelet scale is almost equal to Fourier period.

The wavelet power spectrum (scalogram) can be defined as  $|W(n, a)|^2$ . Using the normalization in Equation (4.7), the expectation value for  $|W(n, a)|^2$  is equal to  $N$  times the expectation value of  $|X_k|^2$ . For a white noise time series, this expectation value is  $\sigma^2/N$ , where  $\sigma^2$  is the variance. Thus, for a white noise process, the expectation value for the wavelet transform is  $|W(n, a)|^2 = \sigma^2$  at all  $n$  and  $a$ .

For non-orthogonal wavelet analysis, an arbitrary set of scales can be used to obtain a more complete time-frequency picture. It is convenient to define the scales as fractional powers of two:

$$a_j = a_0 2^{j\Delta_j} \quad , \quad j = 0, 1, \dots, J \quad (4.14)$$

$$J = \Delta_j^{-1} \log_2 \left( \frac{N\Delta t}{a_0} \right) \quad (4.15)$$

where  $a_0$  is the smallest resolvable scale and  $J$  is the largest scale. The  $a_0$  is chosen so that the equivalent Fourier period is approximately  $2\Delta t$ . The choice of a sufficiently small  $\Delta_j$  depends on the width in spectral-space of the wavelet function.  $\Delta_j^{-1}$  gives the number of voices per octave, in other words, the number of fractionally dilated versions of the wavelet in each scale.

The redundancy of continuous wavelet transform makes it possible to reconstruct the time series using a completely different wavelet function, the easiest of which is a delta ( $\delta$ ) function (Farge 1992). In this method, the reconstructed time series is just the sum of the real part of the wavelet transform over all scales.

$$x_n = \frac{\Delta_j \Delta t^{1/2}}{C_\delta \Psi_0(0)} \sum_{j=0}^J \frac{\Re [W(n, a_j)]}{a_j^{1/2}} \quad (4.16)$$

The factor  $\Psi_0(0)$  removes the energy scaling, while  $a_j^{1/2}$  converts the wavelet transform to an energy density. The factor  $C_\delta$  comes from the reconstruction of a  $\delta$  function from its

wavelet transform using the function  $\psi_0(t)$ . The  $C_\delta$  is a constant for each wavelet function and is equal to 0.776 for complex Morlet wavelet with  $\omega_0 = 6$  and  $f_b = 2$ . Note that if original time series were complex, then the sum of the complex  $W(n, a)$  would be used in Equation (4.16).

To derive  $C_\delta$  for a new wavelet function, first assume a time series with a  $\delta$  function at time  $n = 0$ , given by  $x_n = \delta_{n0}$ . This time series has a Fourier transform  $X_k = N^{-1}$ , constant for all  $k$ . Substituting  $X_k$  into Equation (4.5), at time  $n = 0$  (the peak), the wavelet transform becomes

$$W_\delta(n = 0, a) = \frac{1}{N} \sum_{k=0}^{N-1} \Psi^*(a\omega_k) \quad (4.17)$$

The reconstruction in Equation (4.16) then gives

$$C_\delta = \frac{\Delta j \Delta t^{1/2}}{\Psi_0(0)} \sum_{j=0}^J \frac{\Re[W_\delta(n = 0, a_j)]}{a_j^{1/2}} \quad (4.18)$$

The total energy is conserved under the wavelet transform, and the equivalent of Parseval's theorem for wavelet analysis is

$$\sigma^2 = \frac{\Delta j \Delta t}{C_\delta N} \sum_{n=0}^{N-1} \sum_{j=0}^J \frac{|W(n, a_j)|^2}{a_j} \quad (4.19)$$

where  $\sigma^2$  is the variance and a  $\delta$  function has been assumed for reconstruction.

The implementation of frequency tracking and evolutionary power spectral density estimation in real-time using WT is shown in Figure 4.2. Since the estimation is to be used in semi-active control algorithms in real-time, for any given time only the portion of signal data up to that time is assumed to be known. The procedure starts by selecting a window and a window length ( $WL$ ) of  $(n - 1)\Delta t$  (where  $n$  is the number of points in the window). Time lapse ( $TL$ ) of  $L\Delta t$  is the time period between successive windows. The window is multiplied by the portion of the signal,  $s(t)$  up to the real-time  $t_i$  and zero padded for



the desired frequency resolution. Then the Fourier transform of the windowed signal is multiplied by the Fourier transform of the wavelet and the inverse Fourier transform of the product gives the wavelet transform in real-time. The instantaneous PSD (a time slice of the evolutionary PSD) is estimated by the wavelet power spectrum of each windowed signal,  $s(t)w(t_i)$  as given in Equation (4.21)

$$S(t_i, f_j = \frac{f_0}{a_j}) = \frac{\Delta j \Delta t}{C_\delta} \sum_{j=0}^J \frac{|W(t_i, a_j)|^2}{a_j^2 \Delta \omega} \quad (4.20)$$

where  $f_0 = \omega_0/(2\pi)$ .

The instantaneous (dominant) frequency is determined using Equation (4.22) by weighting the ridge frequency (corresponding to maximum PSD value) by its PSD value at the corresponding time.

$$f_{ins}(t_i) = \frac{\sum_{k=\max(1, i-m+1)}^i f_{\max}(t_k) \max [ |S(t_i, f)|^2 ]}{\sum_{k=\max(1, i-m+1)}^i \max [ |S(t_i, f)|^2 ]} \quad (4.21)$$

in which the averaging length,  $AL = (m - 1)\Delta t$  is the time length considered in weighted averaging of dominant frequency and  $m$  is the number of points used for averaging.  $f_{\max}$  is the ridge frequency corresponding to the frequency with maximum instantaneous PSD value.

### 4.3 Numerical Examples

Several excitation signals, from simple harmonic signals to stationary and non-stationary processes are analyzed in real-time by STFT and WT, as explained in the previous sections. The instantaneous (dominant) frequency of the excitation and evolutionary power spectral density estimated by two methods are compared. Although wavelet transform in general

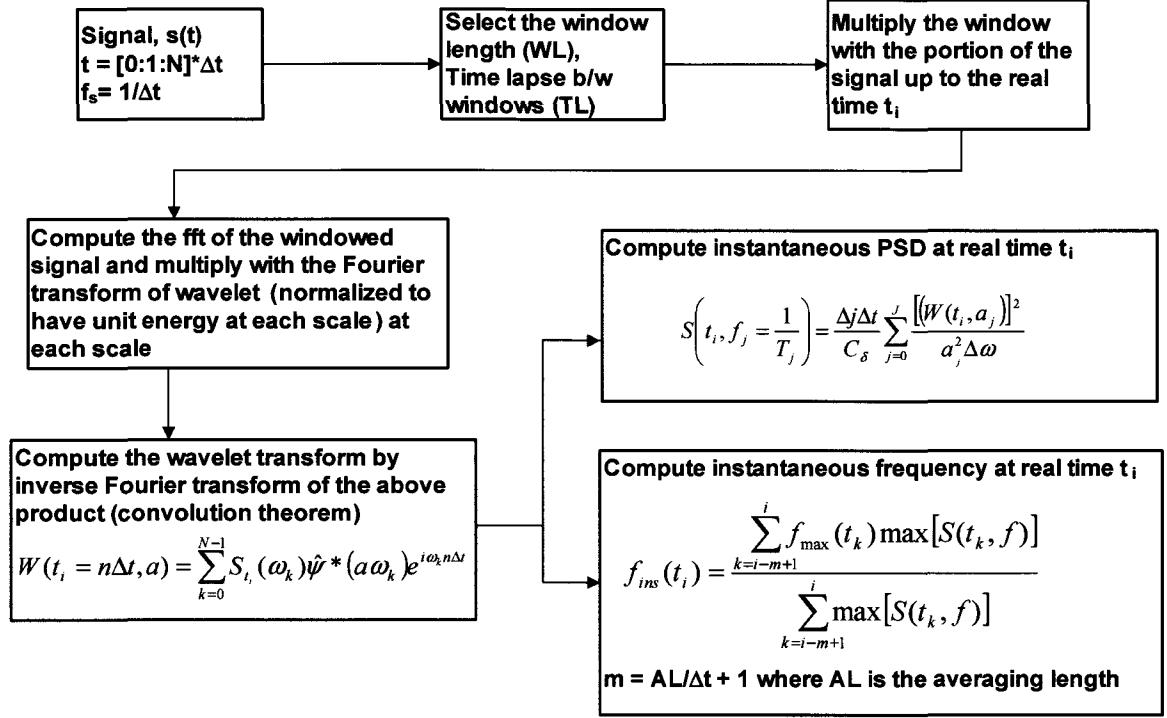


**Figure 4.2** Frequency tracking and Evolutionary Spectrum Estimation by WT

suits better for highly non-stationary signals, use of a window to analyze the signal in real-time imposes the inherent limitation of STFT to the wavelet transform in terms of aliasing low and high frequencies outside the frequency range of the window. Nevertheless, both methods give similar qualitative results and provide adequate time-frequency information for the signals considered. A triangular window is used for STFT whereas a rectangular window is used for WT in the examples of the following sections. The sample simulations for the random processes are generated using auto-regressive (AR) method defined in Section 1.2.10 with  $p = 40$ .

### 4.3.1 Discrete Simple Sweep

A discrete sine sweep consisting of four different frequencies (1.6 Hz, 1.8 Hz, 2.0 Hz and 2.2 Hz) and amplitudes (0.5, 1.0, 2.0, and 1.0) is tracked in real-time by STFT and WT, and the results are compared in Figure 4.3. Both STFT and WT were able to track the dominant frequency quite accurately.

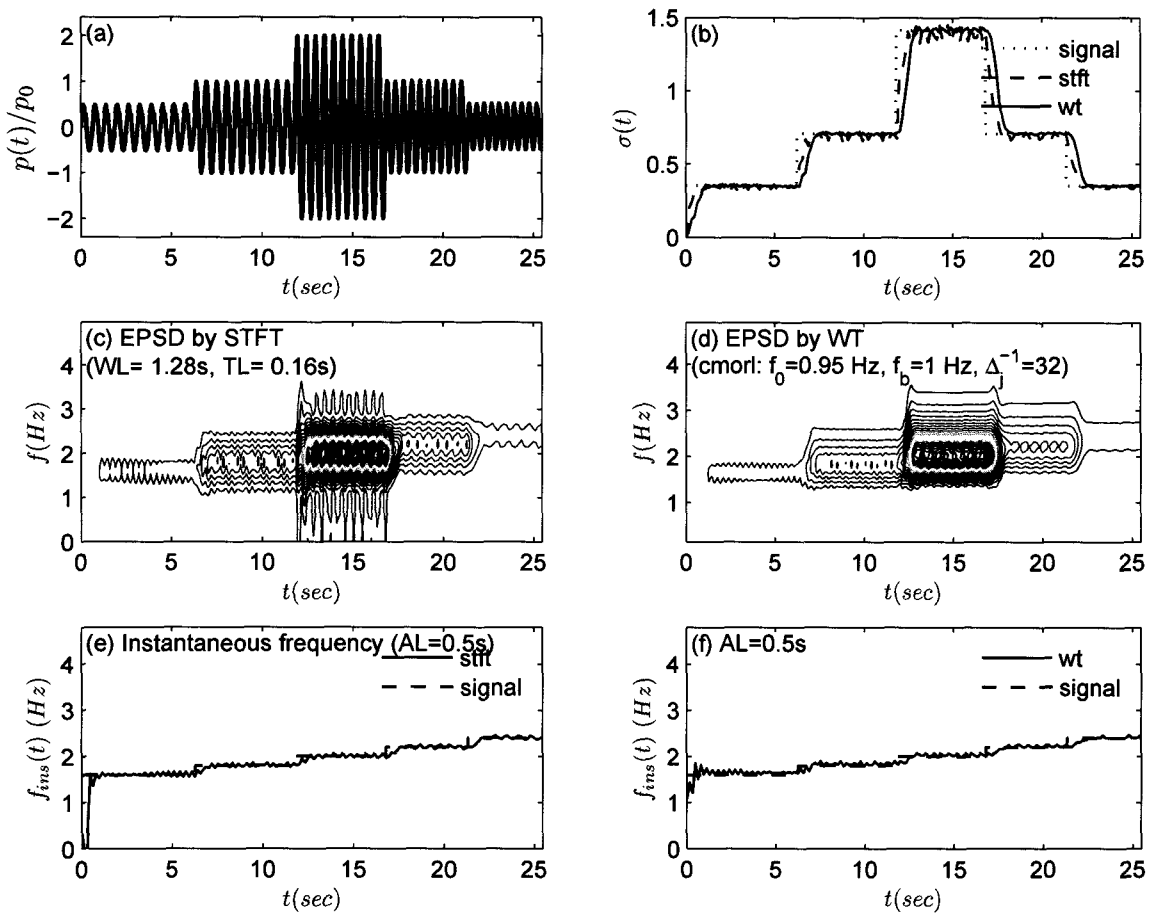


**Figure 4.3** Discrete sine sweep: (a) Signal, (b) RMS history, (c) EPSD by STFT, (d) EPSD by WT, (e) Frequency tracking by STFT, and (f) Frequency tracking by WT

### 4.3.2 Narrow-band Stationary Process

500 narrow-band stationary force excitations are simulated using the same filter for the near-fault earthquake spectrum (defined in Section 1.2.10) with parameters  $f_g = 1 \text{ Hz}$  and  $\xi_g = 0.05$ . Each sample is analyzed in real-time by STFT and WT, and the ensemble results are compared in Figure 4.4. The results indicate that both STFT and WT were able to track the dominant frequencies and estimate the EPSD quite accurately.

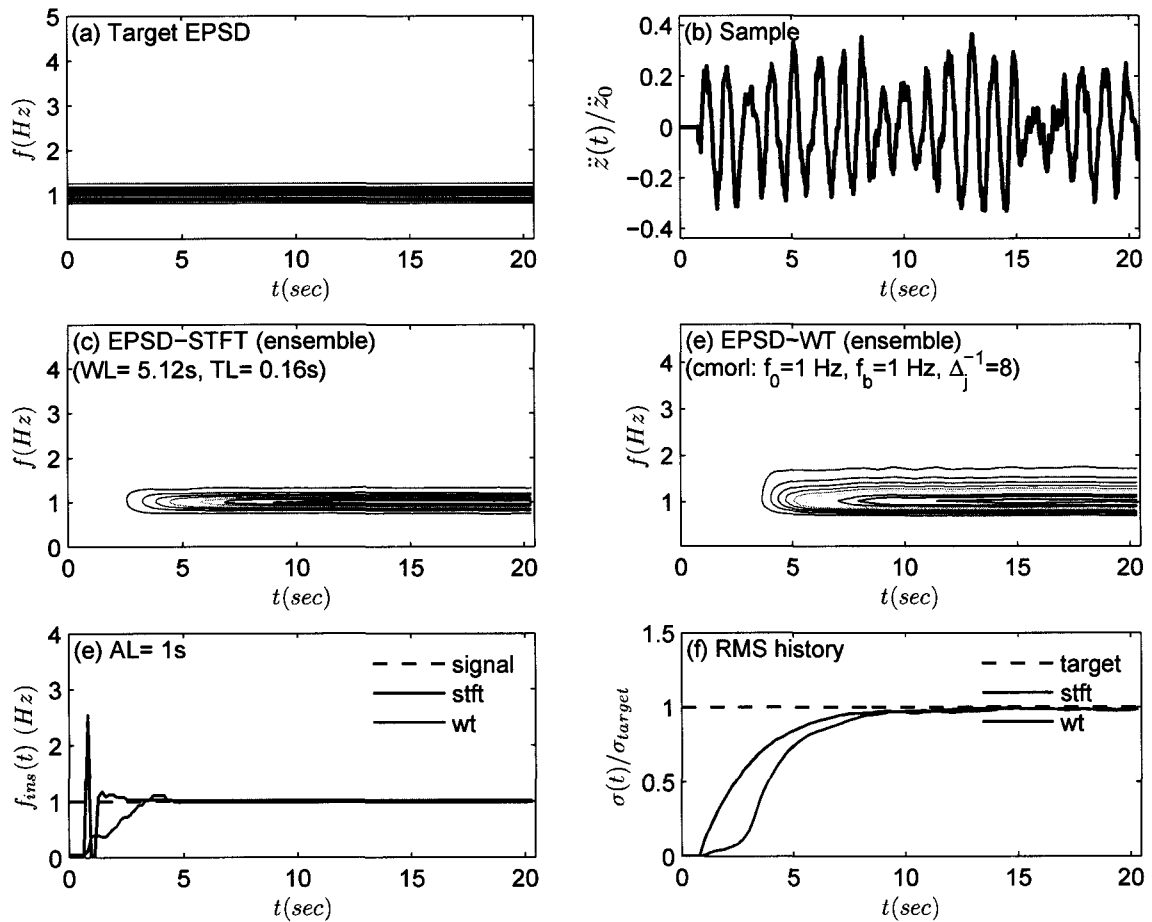


**Figure 4.4** Narrow-band stationary process: (a) Target EPD, (b) Sample function, (c) EPD by STFT, (d) EPD by WT, (e) Frequency tracking, and (f) RMS history

### 4.3.3 Wide-band Stationary Process

500 samples are generated from a wide-band stationary process defined by the near-fault earthquake spectrum (Narasimhan 2004) given in Section 1.2.10. Each sample is analyzed in real-time by STFT and WT, and the ensemble results are compared in Figure 4.5. The results indicate that both STFT and WT were able to track the dominant frequencies and estimate the EPSD quite accurately.

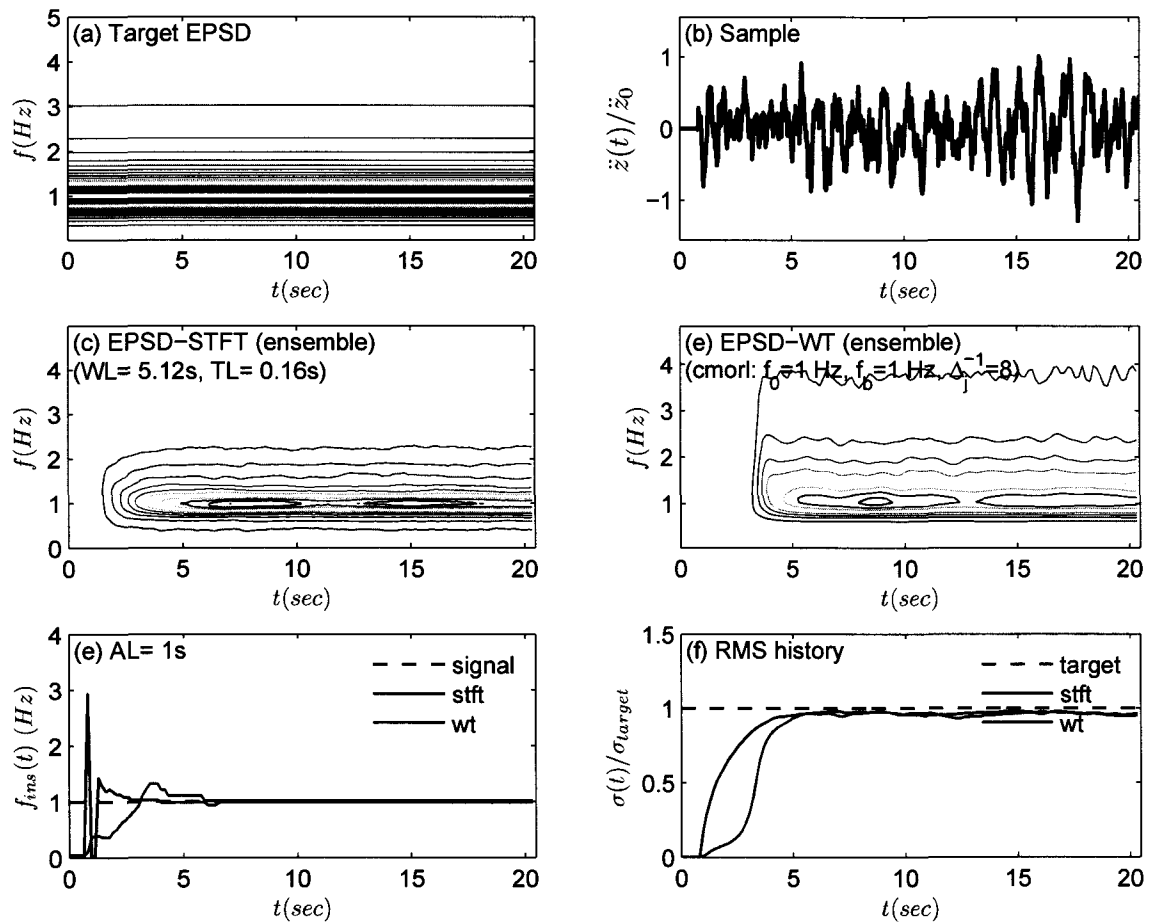


**Figure 4.5** Wide-band stationary process: (a) Target EPD, (b) Sample function, (c) EPD by STFT, (d) EPD by WT, (e) Frequency tracking, and (f) RMS history

#### 4.3.4 Locally Stationary Process

500 samples are generated from a locally stationary process defined by the near-fault earthquake spectrum. Each sample is analyzed in real-time by STFT and WT, and the ensemble results are compared in Figure 4.6. The results indicate that both STFT and WT were able to track the dominant frequencies and estimate the EPSD quite accurately. The target evolutionary spectrum has the following time envelope applied to the near-fault earthquake spectrum.

$$A(t) = \frac{e^{-at} - e^{-bt}}{\max(e^{-at} - e^{-bt})} \quad (4.22)$$

where  $a$  and  $b$  are selected as 0.2 and 0.25, respectively.

#### 4.3.5 Non-stationary Process

500 samples are generated from a non-stationary process defined by the near-fault earthquake spectrum. The target evolutionary spectrum has the time envelope given in Equation (4.22) and a dominant frequency shift from 0.5 Hz to 2.5 Hz. Each sample is analyzed in real-time by STFT and WT, and the ensemble results are compared in Figure 4.7. The results indicate that both STFT and WT were able to track the dominant frequencies and estimate the EPSD quite accurately.

### 4.4 Concluding Remarks

Wavelet transform (WT) has two major advantages over short-time Fourier transform (STFT): (i) it is more accurate due to variable window lengths (scales) instead of fixed window length (as in STFT), which causes inaccuracy by aliasing of low and high frequency components outside the frequency range of the window; and (ii) it is more efficient due to variable frequency (or scale) resolution with high resolution in high frequency (small

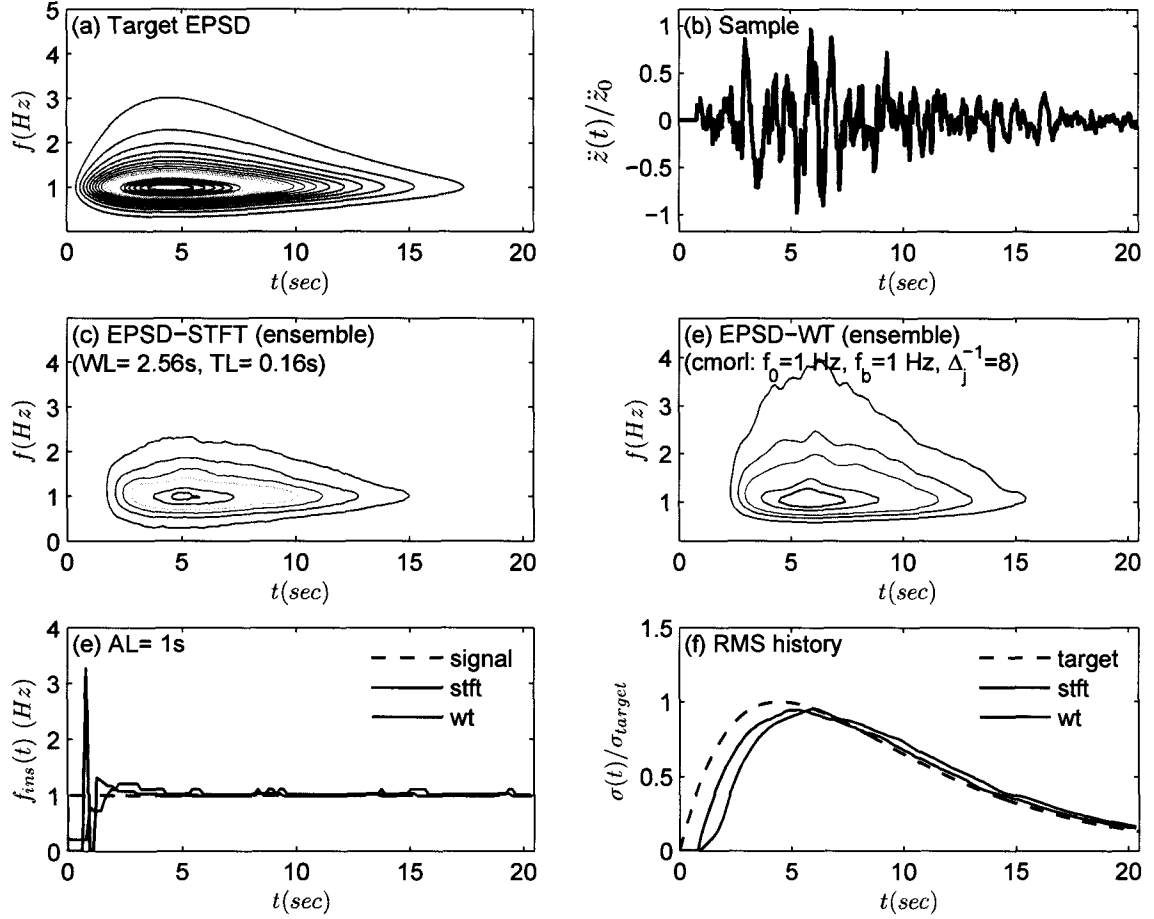


**Figure 4.6** Locally stationary process: (a) Target EPD, (b) Sample function, (c) EPD by STFT, (d) EPD by WT, (e) Frequency tracking, and (f) RMS history

scales) region and low resolution in low frequency (large scales) region, which allows identifying low and high frequency components of the signal efficiently. These advantages favor wavelet transform in time-frequency analysis of non-stationary signals, where sudden changes occur.

Real-time estimation of instantaneous frequency and evolutionary power spectrum requires use of a window with only priori data at any given time instant. This imposes the same limitation of STFT to wavelet transform limiting its accuracy.

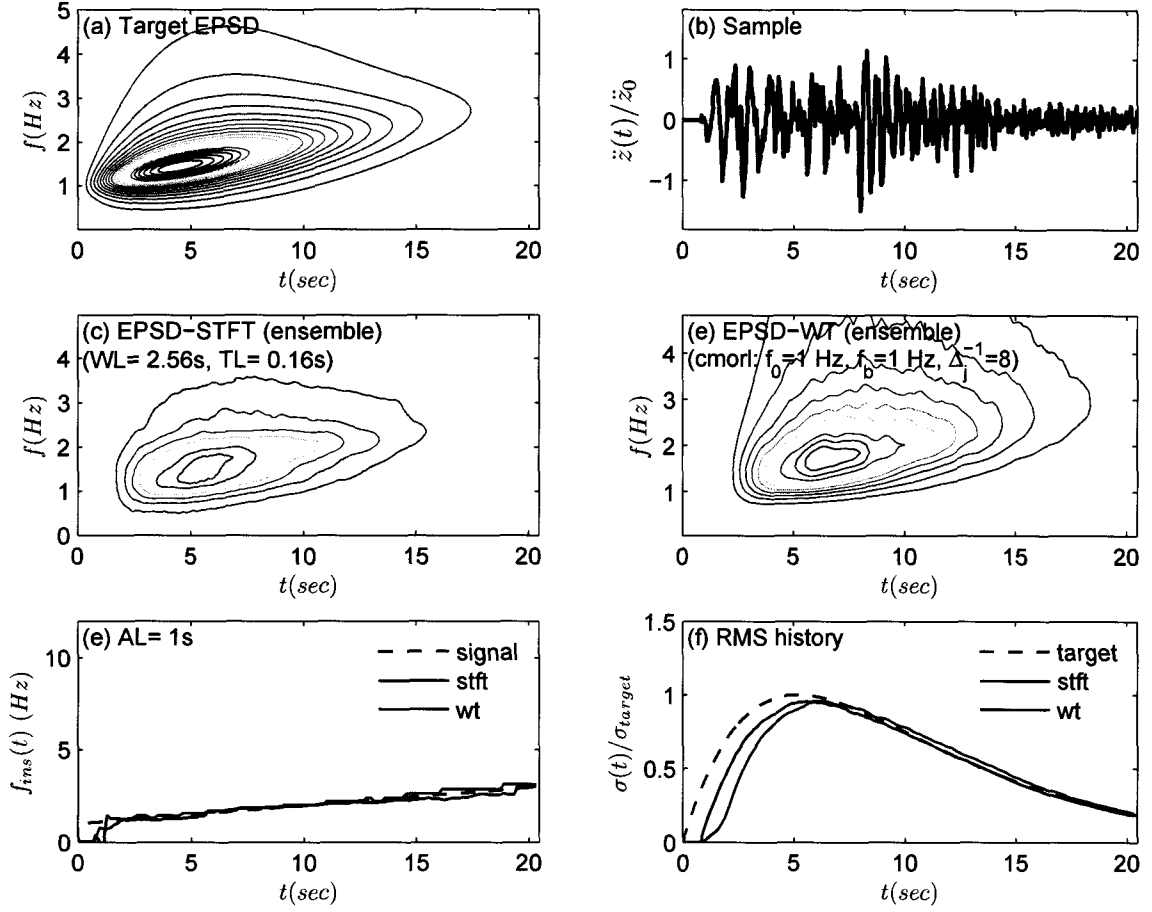


**Figure 4.7** Non-stationary process: (a) Target EPSD, (b) Sample function, (c) EPSD by STFT, (d) EPD by WT, (e) Frequency tracking, and (f) RMS history

Both STFT and WT accurately track the instantaneous frequency of harmonic and sine sweep signals.

For the target evolutionary spectra of random processes studied, the real-time instantaneous frequency and root mean square (RMS) values obtained from Monte Carlo simulations indicate similar performances by STFT and WT. However, this is also partly due to averaging of the sample simulations. For individual sample simulations, it is likely that WT would detect the non-stationarity characteristics more accurately.



## Chapter 5

### Semi-active Single/Multiple-Degree-Of-Freedom Systems (sSDOF/sMDOF) under Deterministic Excitations

Two nonlinear control algorithms developed to independently vary stiffness and damping in structures are studied under near-fault earthquake records and pulse type of excitations fitted to them. Three cases of semi-active control are considered, which are (i) independently variable stiffness control, (ii) independently variable damping control, and (iii) combined variable stiffness and damping control. The nonlinear control law for variable stiffness systems is designed to produce a variable structure without sliding mode. Semi-active damping control algorithm has been derived based on Lyapunov method, such that the derivative of a Lyapunov function (representing total energy) is always negative. Results for single-degree-of-freedom and multi-degree-of-freedom systems equipped with semi-active stiffness and damping devices on the base floor are presented. The control algorithms can be successfully implemented in base-isolated buildings.

#### 5.1 SDOF Structural Model and Formulation

The semi-active single-degree-of-freedom structural model (sSDOF) equipped with both variable damping and stiffness devices is shown in Figure 5.1. The equation of motion is given by

$$m\ddot{u}(t) + (c_{min} + c_s f(u_a, \dot{u}_a, \dot{u}_r)) \dot{u}(t) + (k_{max} - k_s f(u_r, \dot{u}_r)) u(t) = P(t) \quad (5.1)$$

where  $m$  is the mass,  $c_{min}$  is the damping coefficient corresponding to conventional damping mechanisms within the structures itself,  $c_s$  is the maximum additional damping due to variable damping device (i.e.  $c_{max} = c_{min} + c_s$ ),  $k_{max}$  is the maximum stiffness,  $k_s$  is the maximum reduction in stiffness (i.e.  $k_{max} = k_{min} + k_s$ ).  $u$ ,  $\dot{u}$ ,  $\ddot{u}$  are the relative displacement, velocity and acceleration with respect to ground.  $f(u_a, \dot{u}_a, \dot{u}_r)$  and  $f(u_r, \dot{u}_r)$  are the appropriate functions for varying stiffness and damping.  $P(t)$  is the external force which is equal to  $-m\ddot{u}_g(t)$  for base excited systems where  $\ddot{u}_g(t)$  is the ground acceleration.

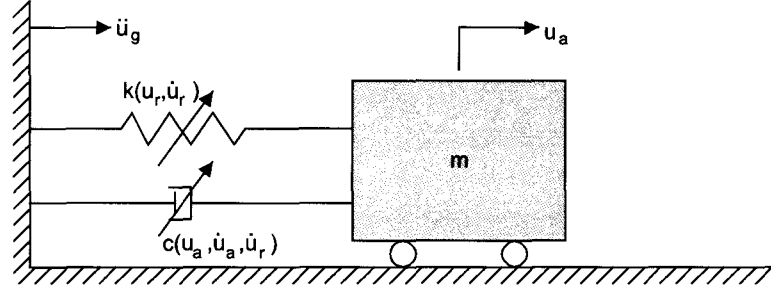


**Figure 5.1** Analytical model of the SDOF system equipped with variable stiffness and variable damping device

## 5.2 MDOF Structural Model and Formulation

The semi-active multi-degree-of-freedom structural model (sMDOF) equipped with both variable damping and stiffness devices between the base and the first DOF is shown in Figure 5.2. The equations of motion are given by

$$\mathbf{M}\ddot{\mathbf{U}}(t) + \mathbf{C}(t)\dot{\mathbf{U}}(t) + \mathbf{K}(t)\mathbf{U}(t) = \mathbf{P}(t) \quad (5.2)$$

where  $\mathbf{M}$  is the mass matrix,  $\mathbf{C}(t)$  is the time-varying damping matrix, and  $\mathbf{K}(t)$  is the time-varying stiffness matrix.  $\mathbf{P}(t)$  is the external force that is equal to  $-\mathbf{M}\mathbf{1}\ddot{u}_g(t)$  for base excited systems, where  $\ddot{u}_g(t)$  is the ground acceleration.

Limiting the MDOF system to have uniform structural properties, the system matrices can be written as

$$\mathbf{M} = \begin{bmatrix} m_1 & 0 & \cdots \\ 0 & m_2 & 0 & \cdots \\ \vdots & 0 & \ddots & \ddots \\ & \vdots & \ddots & m_N \end{bmatrix} = m_0 \mathbf{I} \quad (5.3)$$

$$\mathbf{C}(t) = \begin{bmatrix} c_1(t) + c_2 & -c_2 & 0 & \cdots \\ -c_2 & c_2 + c_3 & \ddots & \ddots \\ 0 & \ddots & \ddots & -c_{N-1} \\ \vdots & \ddots & -c_{N-1} & c_N \end{bmatrix} = c_0 \bar{\mathbf{C}}(t) \quad (5.4)$$

$$\mathbf{K}(t) = \begin{bmatrix} k_1(t) + k_2 & -k_2 & 0 & \cdots \\ -k_2 & k_2 + k_3 & \ddots & \ddots \\ 0 & \ddots & \ddots & -k_{N-1} \\ \vdots & \ddots & -k_{N-1} & k_N \end{bmatrix} = k_0 \bar{\mathbf{K}}(t) \quad (5.5)$$

in which  $c_1(t) = c_{min} + c_s f(u_a, \dot{u}_a, \dot{u}_r)$  and  $k_1(t) = k_{max} - k_s f(u_r, \dot{u}_r)$ . Similar to SDOF system,  $c_{min}$  is the damping coefficient corresponding to conventional damping mechanisms between the base and the first DOF,  $c_s$  is the maximum additional damping due to variable damping device (i.e.  $c_{max} = c_{min} + c_s$ ),  $k_{max}$  is the maximum stiffness,  $k_s$  is the maximum reduction in stiffness (i.e.  $k_{max} = k_{min} + k_s$ ).  $f(u_a, \dot{u}_a, \dot{u}_r)$  and  $f(u_r, \dot{u}_r)$  are the functions for varying stiffness and damping.

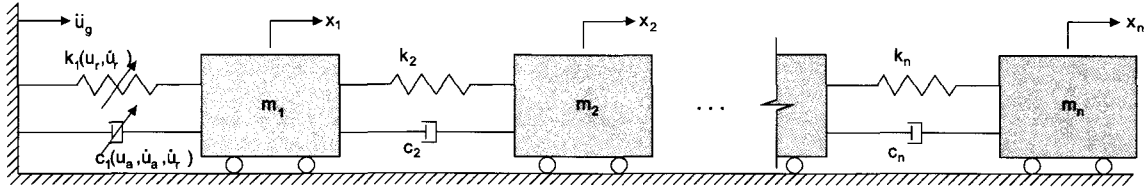


**Figure 5.2** Analytical model of the MDOF system equipped with variable stiffness and variable damping device

## 5.3 Control Algorithms

### 5.3.1 Variable stiffness based on continuous variable structure control

Variable structure control is a discontinuous nonlinear control method where a system switches frequently between two different structures based on the current position of the state trajectory. Consider two different undamped SDOF structures A and B, described as follows.

$$\ddot{x} + \frac{k}{m}x = 0 \quad \text{or} \quad \begin{cases} \dot{x}_1 = x_2 \\ \dot{x}_2 = -\frac{k}{m}x_1 \end{cases} \quad (A) \quad (5.6)$$

$$\ddot{x} - \frac{k}{m}x = 0 \quad \text{or} \quad \begin{cases} \dot{x}_1 = x_2 \\ \dot{x}_2 = \frac{k}{m}x_1 \end{cases} \quad (B) \quad (5.7)$$

The controller is implemented using a switching function (line). The instant position of a representative point (RP) is measured and the system is switched between from structure A to structure B or vice versa when RP goes through the switching line. The switching line is given by

$$x_2 + s_1 x_1 = 0 \quad (5.8)$$

Two types of trajectories exist: one is the sliding mode switch and the other is variable structure switch. The types of the trajectory are determined by relative position of the switching line with respect to the asymptote line ( $s_1 = \sqrt{k/m}$ ). The sliding regime exists within the range of  $0 < s_1 < \sqrt{k/m}$ .

Consider a first order dynamical system

$$\frac{dx_i}{dt} = f_i(x_1, \dots, x_n, t) \quad (i = 1, \dots, n) \quad (5.9)$$

Selecting a certain hypersurface (switching surface) described by  $\sigma = \sigma(x_1, \dots, x_n) = 0$  and defining a Lyapunov function as

$$V(\sigma(\mathbf{x})) = \frac{1}{2} \sigma^T(\mathbf{x}) \sigma(\mathbf{x}) \quad (5.10)$$

a sufficient condition for the existence of the sliding regime can be written as

$$\lim_{\sigma \rightarrow 0} \frac{dV}{dt} = \lim_{\sigma \rightarrow 0} \frac{\partial V}{\partial \sigma} \frac{d\sigma}{dt} = \lim_{\sigma \rightarrow 0} \sigma^T \frac{d\sigma}{dt} \leq 0 \quad (5.11)$$

Assuming the system has always a control that can move the trajectory to the sliding mode, the system will stay on the sliding surface after it enters the sliding regime. Since along the sliding mode trajectories  $\sigma((x)) = \text{constant}$ , the following equations will hold.

$$\frac{d\sigma}{dt} = \sum_{i=1}^n \frac{\partial \sigma}{\partial x_i} f_i = 0 \quad (5.12)$$

$$\sigma(x_1, x_2, \dots, x_n) = 0 \quad (5.13)$$

Equations (5.12) and (5.13) represent the motion of the system in a sliding regime, where RP always move on  $\sigma = 0$ .

The behavior of the variable structure is described by:

$$\ddot{u} + \frac{c}{m} \dot{u} + \frac{k + \Psi}{m} u = 0 \quad \text{or} \quad \begin{cases} \dot{x}_1 = \dot{u} = x_2 \\ \dot{x}_2 = -\frac{c}{m} x_2 - \frac{k + \Psi}{m} x_1 \end{cases} \quad (5.14)$$

The control law is given by

$$\Psi = \begin{cases} k\alpha, & x_1 \sigma \geq 0 \\ k\beta, & x_1 \sigma < 0 \end{cases} \quad (5.15)$$

where  $\alpha > 0$ ,  $\beta < 0$  and  $\sigma = x_2 + s_1 x_1$ .  $\sigma = 0$  is the switching plane (hyperplane).  $m$ ,  $c$ ,  $k$ ,  $s_1$  are the known variables and  $k\alpha$ ,  $k\beta$  are the unknown variables. The objective is to obtain the values of  $k\alpha$  and  $k\beta$  such that the sliding regime and the occurrence of the hitting of RP against the switching line exists.

For the sliding regime to exist, Equations (5.11) and (5.12) should be satisfied. Substituting  $\sigma = x_2 + s_1 x_1$  and Equation (5.14) into Equation (5.12)

$$\begin{aligned}\frac{d\sigma}{dt} &= \dot{x}_2 + s_1 \dot{x}_1 \\ &= -\frac{c}{m}x_2 - \frac{k + \Psi}{m}x_1 + s_1 x_2 \\ &= \left(s_1 - \frac{c}{m}\right)x_2 - \frac{k + \Psi}{m}x_1\end{aligned}\tag{5.16}$$

The control law can be expressed as

$$\lim_{\sigma \rightarrow 0} \frac{d\sigma}{dt} = -\frac{1}{m}(\Psi - cs_1 + ms_1^2 + k)x_1\tag{5.17}$$

Thus, Equation (5.11) becomes

$$\begin{aligned}\lim_{\sigma \rightarrow 0} \sigma \frac{d\sigma}{dt} &= -\frac{1}{m}(\Psi - cs_1 + ms_1^2 + k)x_1\sigma \\ &= \begin{cases} -\frac{1}{m}(k\alpha - cs_1 + ms_1^2 + k)x_1\sigma & x_1\sigma \geq 0 \\ -\frac{1}{m}(k\beta - cs_1 + ms_1^2 + k)x_1\sigma & x_1\sigma < 0 \end{cases}\end{aligned}\tag{5.18}$$

The sufficient condition for this to be satisfied is

$$\begin{aligned}k\alpha &\geq cs_1 - ms_1^2 - k \\ k\beta &\leq cs_1 - ms_1^2 - k\end{aligned}\tag{5.19}$$

which can be re-written as

$$\begin{aligned}\frac{k\alpha}{m} &\geq 2\xi\omega_n s_1 - s_1^2 - \omega_n^2 \\ \frac{k\beta}{m} &\leq 2\xi\omega_n s_1 - s_1^2 - \omega_n^2\end{aligned}\tag{5.20}$$

where  $\xi$  and  $\omega_n$  are the damping ratio and natural frequency of the system, respectively.  $k\alpha + k$  and  $k\beta + k$  are the two switching states. From practical considerations minimum stiffness should be greater than zero. This condition is met when  $s_1 < 2\xi\omega_n$ .

In the sliding regime

$$\begin{aligned} x_2 + s_1 x_1 &= 0 \\ \dot{x}_1 &= x_2 \end{aligned} \quad (5.21)$$

which has the following solution for the displacement

$$u = x_1 = x_1(0)e^{-s_1(t-t_0)} \quad (5.22)$$

Equation (5.22) indicates that the displacement is independent of the structural parameters. RP takes a trajectory depending on the initial state of switching, characterized by the slope of the switching line ( $s_1$ ) which has the dimension of circular frequency.

The necessary and sufficient condition for the RP to hit the switching line is that the characteristic equation of the system with  $\Psi = k\alpha$  should have negative real roots. Thus, for the characteristic equation

$$y^2 + \frac{c}{m}y + \frac{k + k\alpha}{m} = 0 \quad (5.23)$$

one sufficient condition is

$$\Delta = \frac{1}{m} \left( \frac{c^2}{m} - 4(k + k\alpha) \right) < 0 \quad (5.24)$$

which can be written as

$$\begin{aligned} k\alpha &> \frac{c^2}{4m} - k \text{ or} \\ \frac{k\alpha}{m} &> \xi^2\omega_n^2 - \omega_n^2 \end{aligned} \quad (5.25)$$

Setting  $s_1 = 0$  and the switching line  $\sigma = x_2 = \dot{u} = 0$ , a discontinuous variable structure control law can be written as

$$k(t) = k(u_r, \dot{u}_r) = \begin{cases} k_{max} & u_r \dot{u}_r \geq 0 \\ k_{min} & u_r \dot{u}_r < 0 \end{cases} \quad (5.26)$$

The discontinuous variable structure control law in Equation (5.26) can be replaced by the following continuous smooth control law for variable structures.

$$k(t) = k(u_r, \dot{u}_r) = k_{max} - \frac{k_s}{1 + e^{-(u_r \dot{u}_r \rho)}} \quad (5.27)$$

where  $\rho$  is the smoothness constant with appropriate dimensions,  $u_r$  is the relative displacement, and  $\dot{u}_r$  is the relative velocity. The continuous controller in Equation (5.27) is designed to produce only a variable structure system and controller.

### 5.3.2 Variable damping based on Lyapunov control

Semi-active damping control algorithm developed by Nagarajaiah et al. (2000), is derived based on Lyapunov method, such that the derivative of a Lyapunov function (representing total energy) is always negative. Consider the state space formulation of SDOF system given by

$$\dot{X} = AX - Bc(t)\dot{u}_r + Bku_g \quad (5.28)$$

where

$$A = \begin{bmatrix} 0 & 1 \\ \frac{-k}{m} & 0 \end{bmatrix} \quad (5.29)$$

$$B = \begin{bmatrix} 0 \\ \frac{1}{m} \end{bmatrix} \quad (5.30)$$

$$X = \begin{bmatrix} u_a \\ \dot{u}_a \end{bmatrix} = \begin{bmatrix} u_a \\ v_a \end{bmatrix} \quad (5.31)$$

Defining a Lyapunav function ( $V$ ) as

$$V = \frac{1}{2} \sigma^T(X) \sigma(X) \quad (5.32)$$



where

$$\sigma(X) = P^T X = \begin{bmatrix} \sqrt{k} & \sqrt{m} \end{bmatrix} \begin{Bmatrix} u_a \\ \dot{u}_a \end{Bmatrix} \quad (5.33)$$

in which  $P$  is a constant vector.

Substituting Equation (5.33) into Equation (5.32), Lyapunov function  $V$  can be written as

$$V = \frac{1}{2}ku_a^2 + \sqrt{k}\sqrt{m}u_a\dot{u}_a + \frac{1}{2}m\dot{u}_a^2 \quad (5.34)$$

where the first term represents the total strain energy in the spring, the second term represents the dissipated energy, and the third term represents the total kinetic energy.

Taking the first derivative of Equation (5.34)

$$\dot{V} = \sigma(X)P^T B\dot{u}_r \left( -c(t) + \frac{1}{\dot{u}_r} \left( \sqrt{k}\sqrt{m}\dot{u}_a - ku_r \right) \right) \quad (5.35)$$

For  $\dot{V}$  to be negative, the time-varying damping coefficient should satisfy

$$c(t) = \begin{cases} c_{max} & (\sqrt{k}u_a + \sqrt{m}\dot{u}_a)\dot{u}_r > 0 \\ c_{min} & (\sqrt{k}u_a + \sqrt{m}\dot{u}_a)\dot{u}_r < 0 \end{cases} \quad (5.36)$$

The variable damping control function in Equation (5.1) can be written as

$$f(u_a, \dot{u}_a, \dot{u}_r) = \begin{cases} 1 & (\sqrt{k}u_a + \sqrt{m}\dot{u}_a)\dot{u}_r > 0 \\ 0 & (\sqrt{k}u_a + \sqrt{m}\dot{u}_a)\dot{u}_r < 0 \end{cases} \quad (5.37)$$

## 5.4 Pulse Type Excitations

Studies of the near-source ground motion records have shown that such motions often resemble to long period pulses (especially in ground displacement and velocity) and the response of flexible structures subjected to near-source earthquakes also resemble to the response due to cycloidal pulses (Makris and Chang 2000b; Makris and Chang 2000a). Although such simple cycloidal pulses can capture many of the kinematic characteristics of

near-fault ground displacement and velocity, they do not capture the high-frequency components of the acceleration record and sometimes local, distinguishable acceleration pulses can override the long period velocity (and displacement) pulses. Despite their limitations, these cycloidal pulses are very useful for interpreting the kinematics of the earthquakes and the associated responses. They are particularly beneficial for longer period structures, such as base isolated buildings. The displacement, velocity and acceleration histories of some of these pulse type of excitations, shown in Figure 5.3, are summarized below:

Type *A* pulse:

$$u_g(t) = \frac{v_p t}{2} - \frac{v_p}{2\omega_p} \sin(\omega_p t), \quad 0 \leq t \leq T_p \quad (5.38)$$

Type *B* pulse:

$$u_g(t) = \frac{v_p}{\omega_p} - \frac{v_p}{\omega_p} \cos(\omega_p t), \quad 0 \leq t \leq T_p \quad (5.39)$$

Type *C<sub>n</sub>* pulse:

$$u_g(t) = -\frac{v_p}{\omega_p} \cos(\omega_p t + \theta) - v_p t \sin(\theta) + \frac{v_p}{\omega_p} \cos(\theta), \quad 0 \leq t \leq \left(n + \frac{1}{2} - \frac{\theta}{\pi}\right) T_p \quad (5.40)$$

where  $v_p$  is the maximum ground velocity,  $T_p$  is the time period of the excitation defined as the duration of a full-cycle acceleration pulse and  $\omega_p = 2\pi/T_p$  is the pulse frequency. The value of the phase angle  $\theta$  can be obtained from the following transcendental equation:

$$\cos[(2n+1)\pi - \theta] + [(2n+1)\pi - 2\theta] \sin(\theta) - \cos(\theta) = 0 \quad (5.41)$$

For Type-*C<sub>1</sub>* pulse ( $n = 1$ ),  $\theta = 0.0697\pi$ , and for Type-*C<sub>2</sub>* pulse ( $n = 2$ ),  $\theta = 0.0410\pi$ .

## 5.5 Nonlinear Least Squares Fitting of Single/Multiple Pulses to Near-Fault Earthquakes

Single pulses can lead to similar responses (especially in displacement and velocity) when compared to the response to the actual records near the region of the pulse period;

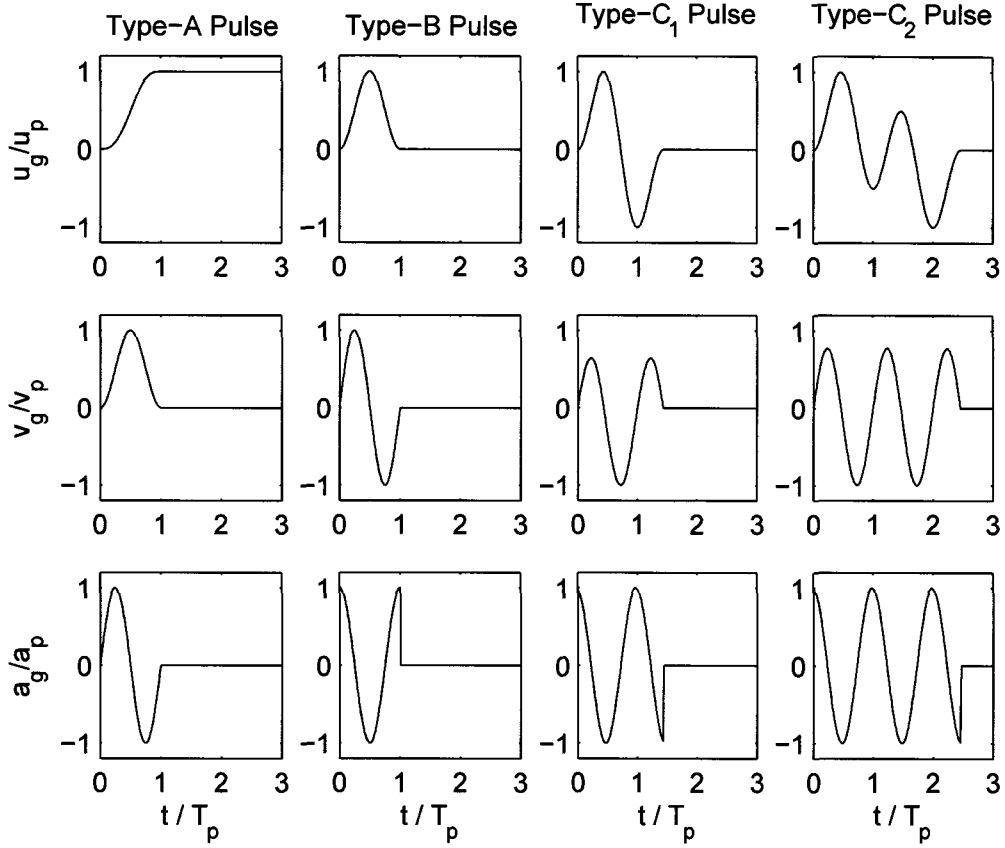


**Figure 5.3** Pulse type of excitations

their similarity decreases beyond that region in the spectra. However, acceleration response is not represented well by single pulse models. Hence, there is a need to fit the actual record with multiple pulses or even combinations using nonlinear least squares method. A new method is developed in this study.

Nonlinear least squares fitting is based on determining the values of the parameters of nonlinear models (equations) by minimizing the sum of the squares of the residuals. One main difference from linear least squares is, the solution is obtained iteratively.

The Gauss-Newton method is one algorithm for minimizing the sum of the squares of the residuals between data and nonlinear equations (Chapra and Canale 2002). The key

concept of the technique is expressing the original nonlinear equation in an approximate, linear form by a Taylor series expansion. Then, least squares theory can be used to obtain new estimates of the parameters that move in the direction of minimizing the residual.

Given a function  $f(x)$  of a variable  $x$  and  $m$  parameters

$$y_i = f(x_i; a_1, a_2, \dots, a_m) + e_i \quad (5.42)$$

where  $y_i$  = a measured value of the dependent variable,  $f(x_i; a_1, a_2, \dots, a_m)$  = nonlinear function of independent variable  $x_i$  and the parameters  $a_1, a_2, \dots, a_m$ , and  $e_i$  = a random error. Expanding the nonlinear model in a Taylor series around the parameter values up to the first derivative

$$f(x_i)_{j+1} = f(x_i)_j + \sum_{k=1}^m \frac{\partial f(x_i)_j}{\partial a_k} da_k \quad (5.43)$$

where  $j$  = the initial guess,  $j + 1$  = the prediction,  $da_k = a_{k,j+1} - a_{k,j}$ .

Substituting Equation (5.43) into Equation (5.42),

$$y_i - f(x_i)_j = \sum_{k=1}^m \frac{\partial f(x_i)_j}{\partial a_k} da_k + e_i \quad (5.44)$$

or in a matrix form

$$\mathbf{D} = \mathbf{Z}_j \mathbf{dA} + \mathbf{E} \quad (5.45)$$

where  $\mathbf{Z}_j$  is the matrix of partial derivatives of the function evaluated at the initial guess  $j$ .

$$\mathbf{Z}_j = \begin{bmatrix} \frac{\partial f_1}{\partial a_1} & \dots & \frac{\partial f_1}{\partial a_m} \\ \frac{\partial f_2}{\partial a_1} & \dots & \frac{\partial f_2}{\partial a_m} \\ \vdots & \vdots & \vdots \\ \frac{\partial f_n}{\partial a_1} & \dots & \frac{\partial f_n}{\partial a_m} \end{bmatrix} \quad (5.46)$$

where  $n$  = the number of data points and  $\partial f_i / \partial a_k$  = the partial derivative of the function with respect to the  $k^{th}$  parameter evaluated at the  $i^{th}$  data point. The vector  $\mathbf{D}$  contains the

differences between the measurements and the function values,

$$\mathbf{D} = \begin{bmatrix} y_1 - f(x_1) \\ y_2 - f(x_2) \\ \vdots \\ y_n - f(x_n) \end{bmatrix} \quad (5.47)$$

and the vector  $d\mathbf{A}$  contains the changes in the parameter values

$$d\mathbf{A} = \begin{bmatrix} da_1 \\ da_2 \\ \vdots \\ da_m \end{bmatrix} \quad (5.48)$$

Applying linear least squares theory to Equation (5.45) results in

$$\mathbf{Z}_j^T \mathbf{Z}_j d\mathbf{A} = \mathbf{Z}_j^T \mathbf{D} \quad (5.49)$$

Solving Equation (5.48) for  $d\mathbf{A}$  gives improved values for the parameters

$$a_{k,j+1} = a_{k,j} + \Delta a_k \quad k = 1, \dots, m \quad (5.50)$$

The above procedure is repeated until the solution converges such that

$$\epsilon = \left| \frac{a_{k,j+1} - a_{k,j}}{a_{k,j+1}} \right| \times 100\% < tolerance \quad k = 1, \dots, m \quad (5.51)$$

Using nonlinear least squares technique, five different types of cycloidal pulses ( $A$ ,  $B$ ,  $C_1$ ,  $C_2$ ,  $C_1 + C_1 + C_1$ ) are fitted to several near-fault ground motion records to be used to evaluate the performance of the nonlinear control algorithms and to compare the responses of fitted pulses to that of the near-fault earthquakes.

A Type- $A$  pulse is fitted to 1992 Landers: Lucerne-270 record and is shown in Figure 5.4. The pulse parameters are computed as  $v_p = 128.08 \text{ m/s}$ ,  $T_p = 2.94 \text{ s}$ ,  $t_0 = 8.59 \text{ s}$ .

As seen in Figure 5.4(a,b,c), the fitted pulse captures the velocity and the displacement kinematics of the ground motion despite the poor fit in acceleration. The spectral responses (displacement, velocity, acceleration) of a SDOF (5% damped) are also computed and compared for both the pulse and the record in Figure 5.4(d,e,f). Similar trends are observed in the spectral responses with good approximation in displacement and velocity while there are differences in acceleration.

A Type-*B* pulse is fitted to 1979 Imperial Valley: El Centro #5-230-FN record and is shown in Figure 5.5. The pulse parameters are computed as  $v_p = 76.76 \text{ m/s}$ ,  $T_p = 3.18 \text{ s}$ ,  $t_0 = 4.78 \text{ s}$ . As seen in Figure 5.5(a,b,c), the fitted pulse captures the velocity and the displacement kinematics of the ground motion despite the poor fit in acceleration. The spectral responses (displacement, velocity, acceleration) of a SDOF (5% damped) are also computed and compared for both the pulse and the record in Figure 5.5(d,e,f). Similar trends are observed in the spectral responses with good approximation in displacement and velocity while there are differences in acceleration.

A Type-*C*<sub>1</sub> pulse is fitted to 1992 Erzincan-NS record and is shown in Figure 5.6. The pulse parameters are computed as  $v_p = -60.86 \text{ m/s}$ ,  $T_p = 2.00 \text{ s}$ ,  $t_0 = 2.00 \text{ s}$ . As seen in Figure 5.6(a,b,c), the fitted pulse captures the velocity and the displacement kinematics of the ground motion despite the poor fit in acceleration. The spectral responses (displacement, velocity, acceleration) of a SDOF (5% damped) are also computed and compared for both the pulse and the record in Figure 5.6(d,e,f). Similar trends are observed in the spectral responses with good approximation in displacement and velocity while there are differences in acceleration.

A Type-*C*<sub>2</sub> pulse is fitted to 1994 Northridge: Sylmar-360-FN record and is shown in Figure 5.7. The pulse parameters are computed as  $v_p = 35.85 \text{ m/s}$ ,  $T_p = 2.25 \text{ s}$ ,  $t_0 = 2.24 \text{ s}$ . As seen in Figure 5.7(a,b,c), the fitted pulse captures the velocity and the

displacement kinematics of the ground motion despite the poor fit in acceleration. The spectral responses (displacement, velocity, acceleration) of a SDOF (5% damped) are also computed and compared for both the pulse and the record in Figure 5.7(d,e,f). Similar trends are observed in the spectral responses with good approximation in displacement and velocity while there are differences in acceleration.

Observations on Figures 5.4 to 5.7 indicate that although single pulses can lead to similar responses (especially in displacement and velocity) when compared to the response to the actual records near the region of the pulse period; their similarity decreases beyond that region in the spectra. In order to improve the fitting, multiple  $C_1$  pulses (Type- $C_1 + C_1 + C_1$ ) are fitted to 1994 Northridge: Rinaldi-228-FN record and are shown in Figure 5.8. The pulse parameters are computed as  $v_p = [-12.34 \quad -47.13 \quad 92.30] \text{ m/s}$ ,  $T_p = [3.21 \quad 1.87 \quad 1.06] \text{ s}$ ,  $t_0 = [0.36 \quad 1.17 \quad 2.10] \text{ s}$ . As seen in Figure 5.8(a,b,c), the fitted multiple pulses capture the kinematics of the ground motion better than the single pulse. The spectral responses (displacement, velocity, acceleration) of a SDOF (5% damped) are also computed and compared for both the pulse and the record in Figure 5.8(d,e,f). Similar trends are observed in the spectral responses with better approximation in all responses.

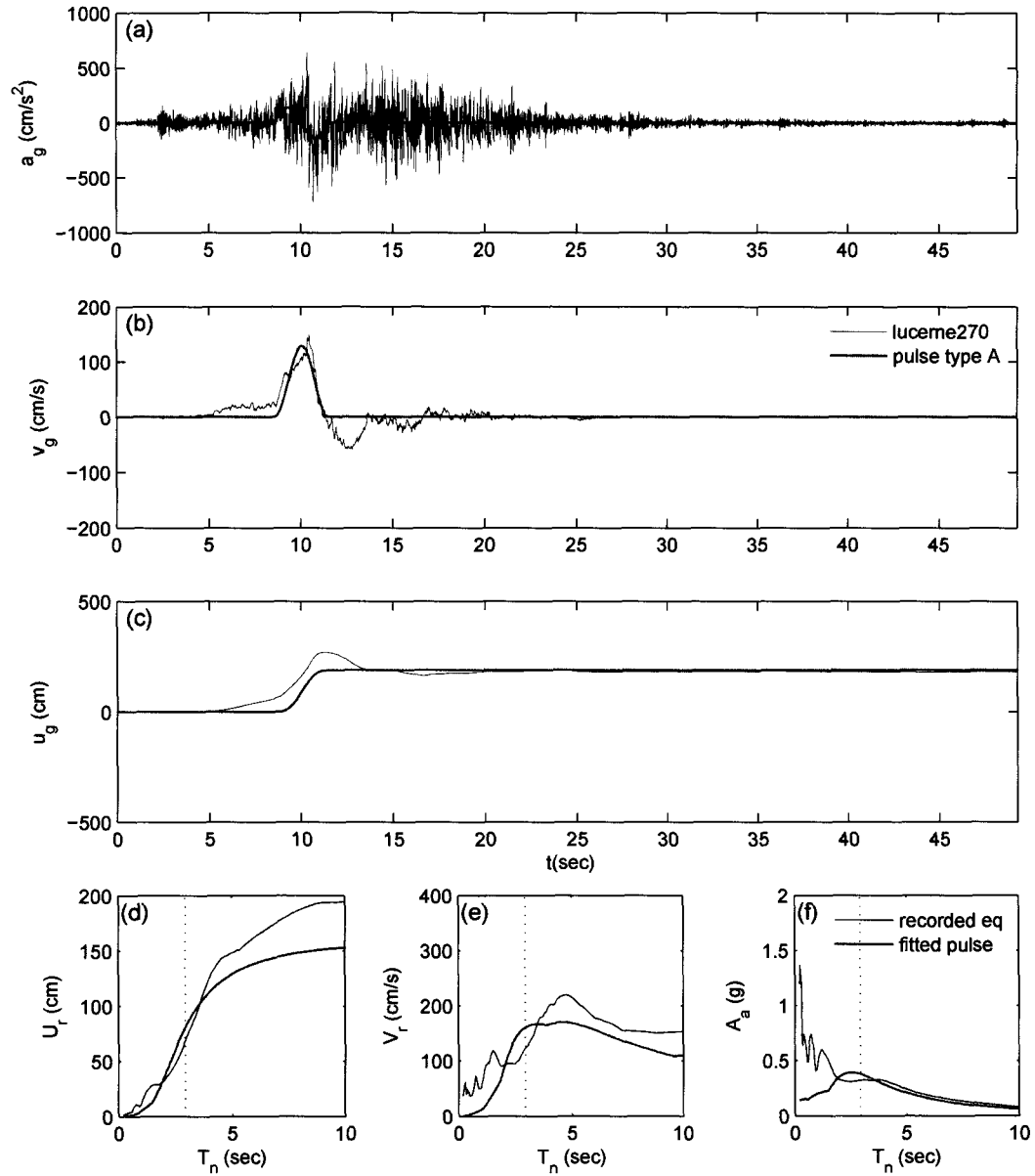


**Figure 5.4** 1992 Landers: Lucerne-270 record and fitted pulse type A ( $v_p = 128.08$  cm/s,  $T_p = 2.94$  s,  $t_0 = 8.59$  s): (a) ground acceleration, (b) ground velocity, (c) ground displacement, (d) SDOF spectral displacement, (e) SDOF spectral velocity, (f) SDOF spectral acceleration



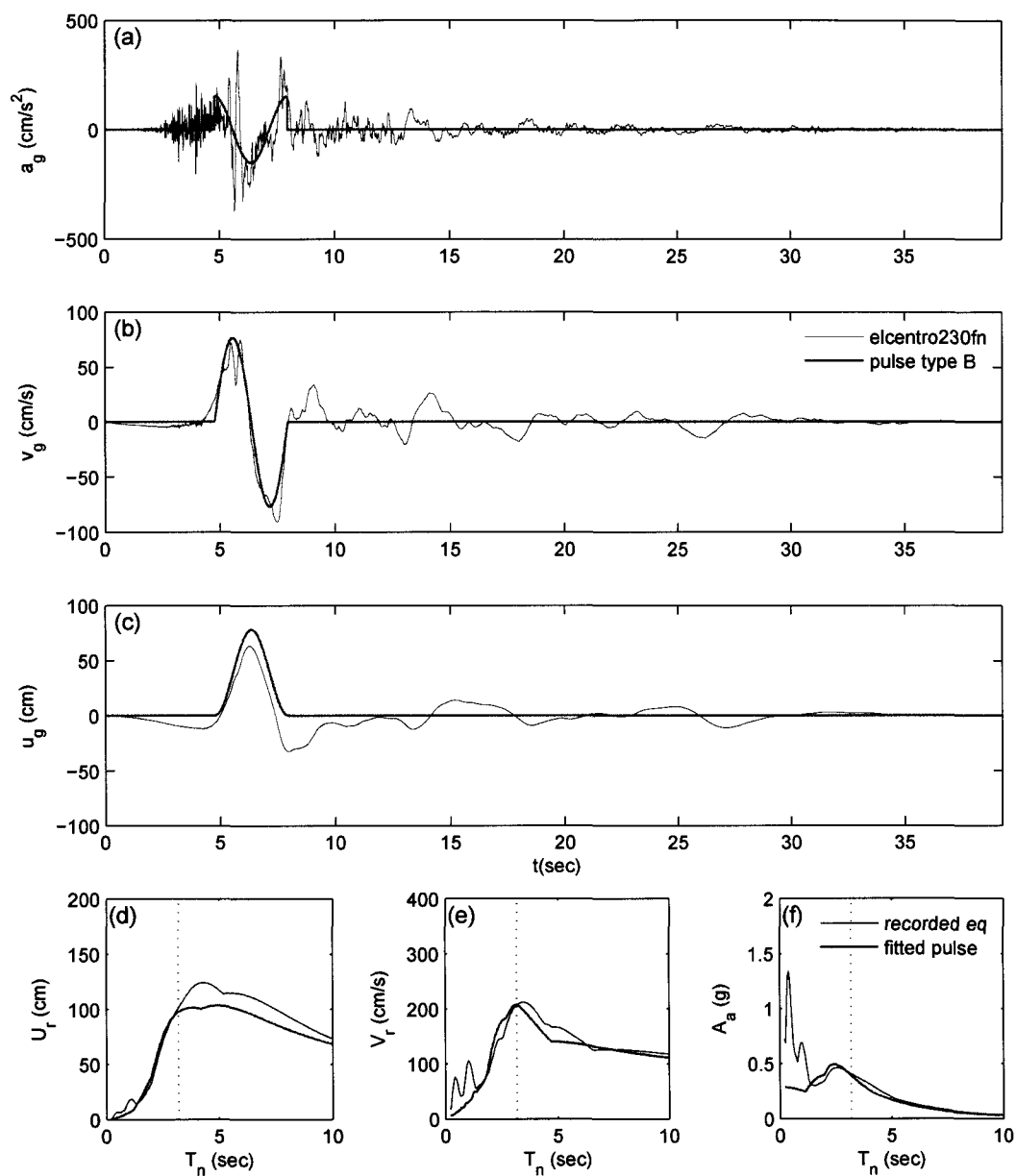


**Figure 5.5** 1979 Imperial Valley: El Centro #5-230-FN record and fitted pulse type B ( $v_p = 76.76$  cm/s,  $T_p = 3.18$  s,  $t_0 = 4.78$  s): (a) ground acceleration, (b) ground velocity, (c) ground displacement, (d) SDOF spectral displacement, (e) SDOF spectral velocity, (f) SDOF spectral acceleration

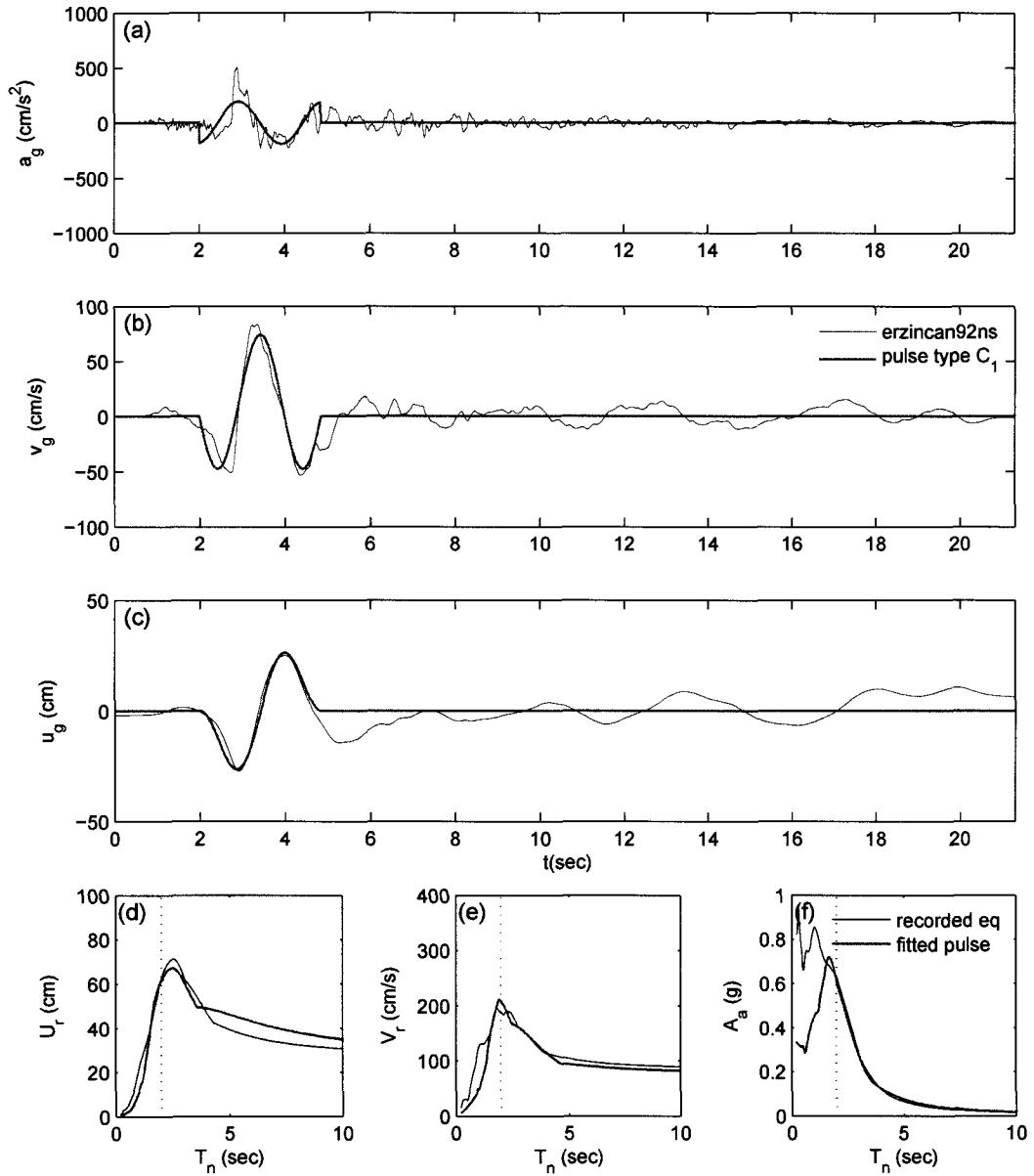


**Figure 5.6** 1992 Erzincan: NS record and fitted pulse type  $C_1$  ( $v_p = -60.86$  cm/s,  $T_p = 2.00$  s,  $t_0 = 2.00$  s): (a) ground acceleration, (b) ground velocity, (c) ground displacement, (d) SDOF spectral displacement, (e) SDOF spectral velocity, (f) SDOF spectral acceleration

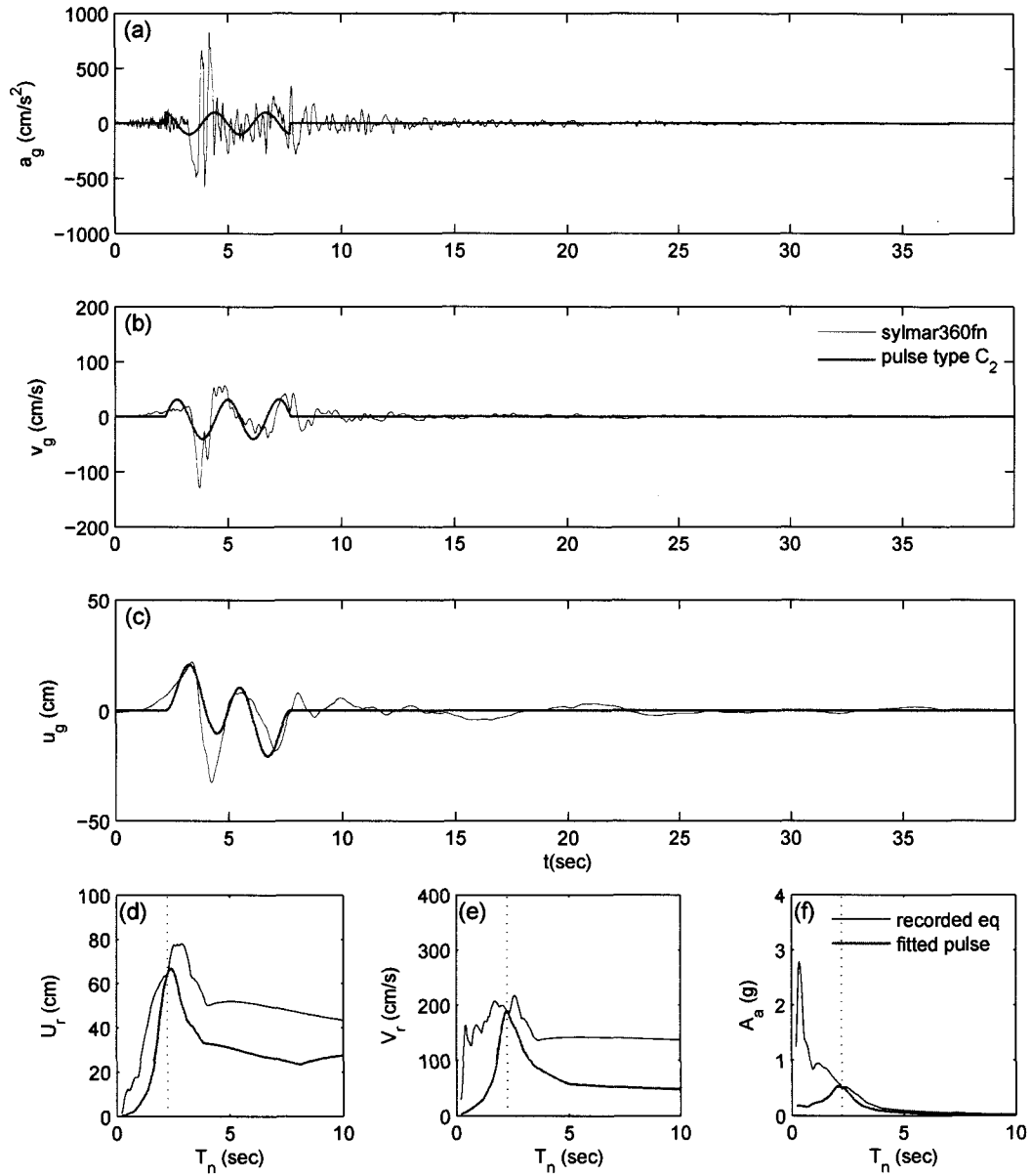


**Figure 5.7** 1994 Northridge: Sylmar-360-FN record and fitted pulse type  $C_2$  ( $v_p = 35.85$  cm/s,  $T_p = 2.25$  s,  $t_0 = 2.24$  s): (a) ground acceleration, (b) ground velocity, (c) ground displacement, (d) SDOF spectral displacement, (e) SDOF spectral velocity, (f) SDOF spectral acceleration

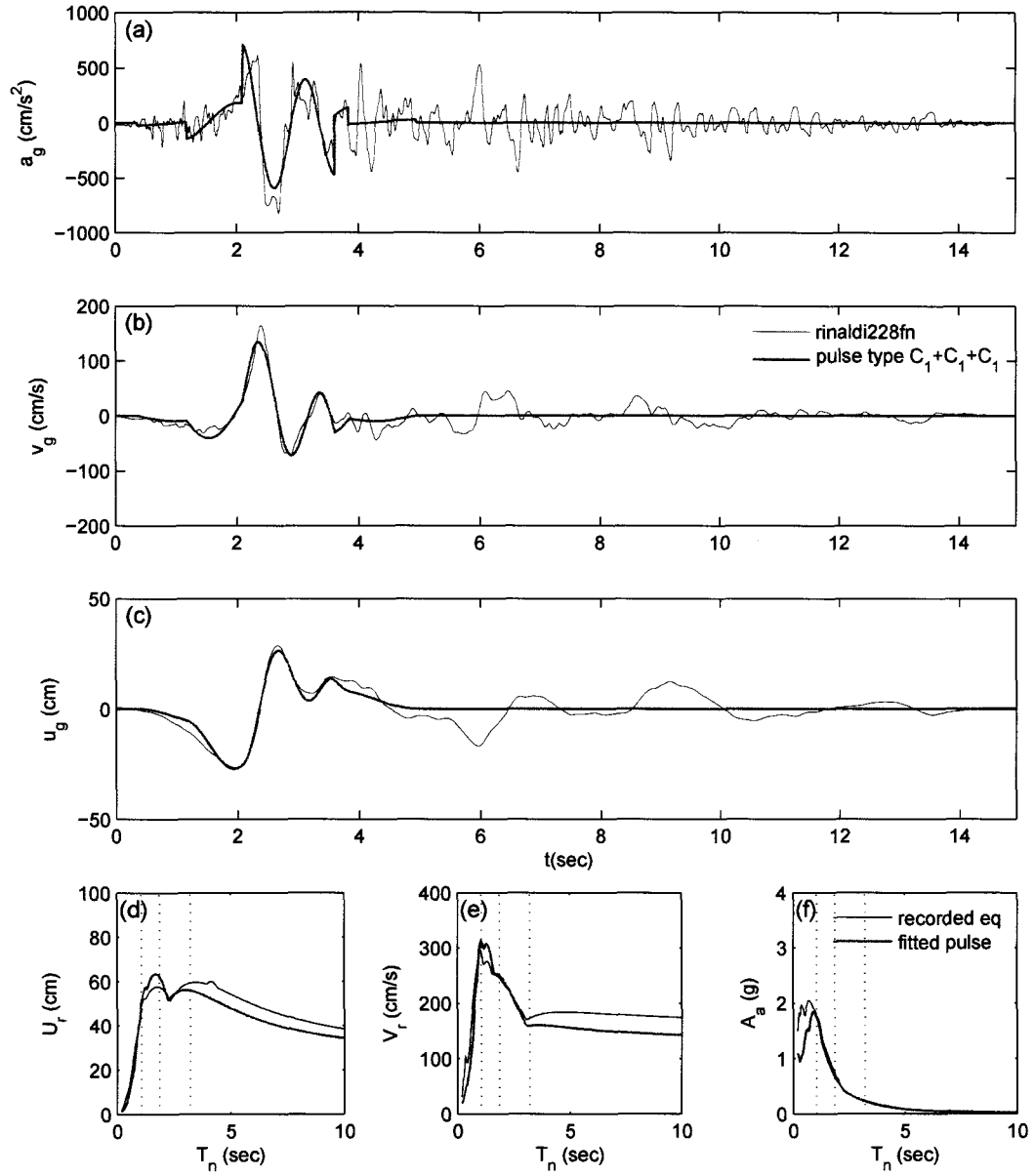


**Figure 5.8** 1994 Northridge: Rinaldi-228-FN record and fitted pulse type  $C_1+C_1+C_1$  ( $v_p = [-12.34 \ -47.13 \ 92.30] \text{ cm/s}$ ,  $T_p = [3.21 \ 1.87 \ 1.06] \text{ s}$ ,  $t_0 = [0.36 \ 1.17 \ 2.10] \text{ s}$ ): (a) ground acceleration, (b) ground velocity, (c) ground displacement, (d) SDOF spectral displacement, (e) SDOF spectral velocity, (f) SDOF spectral acceleration

## 5.6 Results for Variable Stiffness Systems

The five different type of pulses studied in Section 5.5 and the near-fault ground motions that they were fitted to are used to evaluate the performance of the continuous variable structure control (VSC) given in Section 5.3.1. The spectral responses shown are maximum relative displacement  $U_r$ , maximum relative velocity  $V_r$ , and maximum absolute acceleration  $A_a$ , normalized appropriately.  $T_n$  is the period in seconds. ‘pass. on’ corresponds to the passive system with maximum stiffness ( $k_{max}$ ), ‘pass. off’ corresponds to the passive system with minimum stiffness ( $k_{min}$ ), and ‘controlled’ corresponds to the semi-active system with variable stiffness. The ratio  $k_{max}/k_{min}$  is set as 2.

Figures 5.9 and 5.10 show the response spectra and time histories of the SDOF system subjected to Lucerne-270 record and fitted pulse type A ( $T_p = 2.94$  s). The VSC system provides response reduction in long period range ( $> T_p$ ). The time history shown in Figure 5.10 shows this response reduction due to VSC system. During VSC switching, stiffness from  $k_{max}$  to  $k_{min}$  the acceleration response is reduced also.

Figures 5.11 and 5.12 show the response spectra and time histories of the SDOF system subjected to El Centro #5-230-FN record and fitted pulse type B ( $T_p = 3.18$  s). The VSC system provides response reduction in long period range ( $> T_p$ ). The time history shown in Figure 5.12 shows this response reduction due to VSC system. During VSC switching, stiffness from  $k_{max}$  to  $k_{min}$  the acceleration response is reduced also.

Figures 5.13 and 5.14 show the response spectra and time histories of the SDOF system subjected to Erzincan-NS record and fitted pulse type C<sub>1</sub> ( $T_p = 2.00$  s). The VSC system provides response reduction in medium period range ( $T_p < T < 4$  sec). The time history shown in Figure 5.14 shows this response reduction due to VSC system. During VSC switching, stiffness from  $k_{max}$  to  $k_{min}$  the acceleration response is reduced also.

Figures 5.15 and 5.16 show the response spectra and time histories of the SDOF system subjected to Sylmar-360-FN record and fitted pulse type  $C_2$  ( $T_p = 2.25$  s). The VSC system provides response reduction in medium period range ( $T_p < T < 4$  sec). The time history shown in Figure 5.16 shows this response reduction due to VSC system. During VSC switching, stiffness from  $k_{max}$  to  $k_{min}$  the acceleration response is reduced also.

Figures 5.17 and 5.18 show the response spectra and time histories of the SDOF system subjected to Rinaldi-228-FN record and fitted pulse type  $C_1+C_1+C_1$  ( $T_p = [3.21 \ 1.87 \ 1.06]$  s). The VSC system provides response reduction in medium period range ( $1 \text{ sec} < T < 3 \text{ sec}$ ). The time history shown in Figure 5.18 shows this response reduction due to VSC system. During VSC switching, stiffness from  $k_{max}$  to  $k_{min}$  the acceleration response is reduced also.

Figures 5.19 and 5.20 show the base floor time histories and the peak floor profiles of 4-DOF base isolated system subjected to Erzincan-NS record and fitted pulse type  $C_1$  ( $T_p = 2.00$  s). The peak floor profiles in Figure 5.19 indicate that VSC system has the least displacement response compared to passive systems and has improved floor drifts and acceleration with respect to 'pass. on' system.

In summary, VSC system provides reductions in medium period ranges from  $T_p < T < 4$  sec. The response spectra of fitted pulses provide good approximation for the response spectra of the actual earthquake records, especially in the neighborhood of the pulse period.

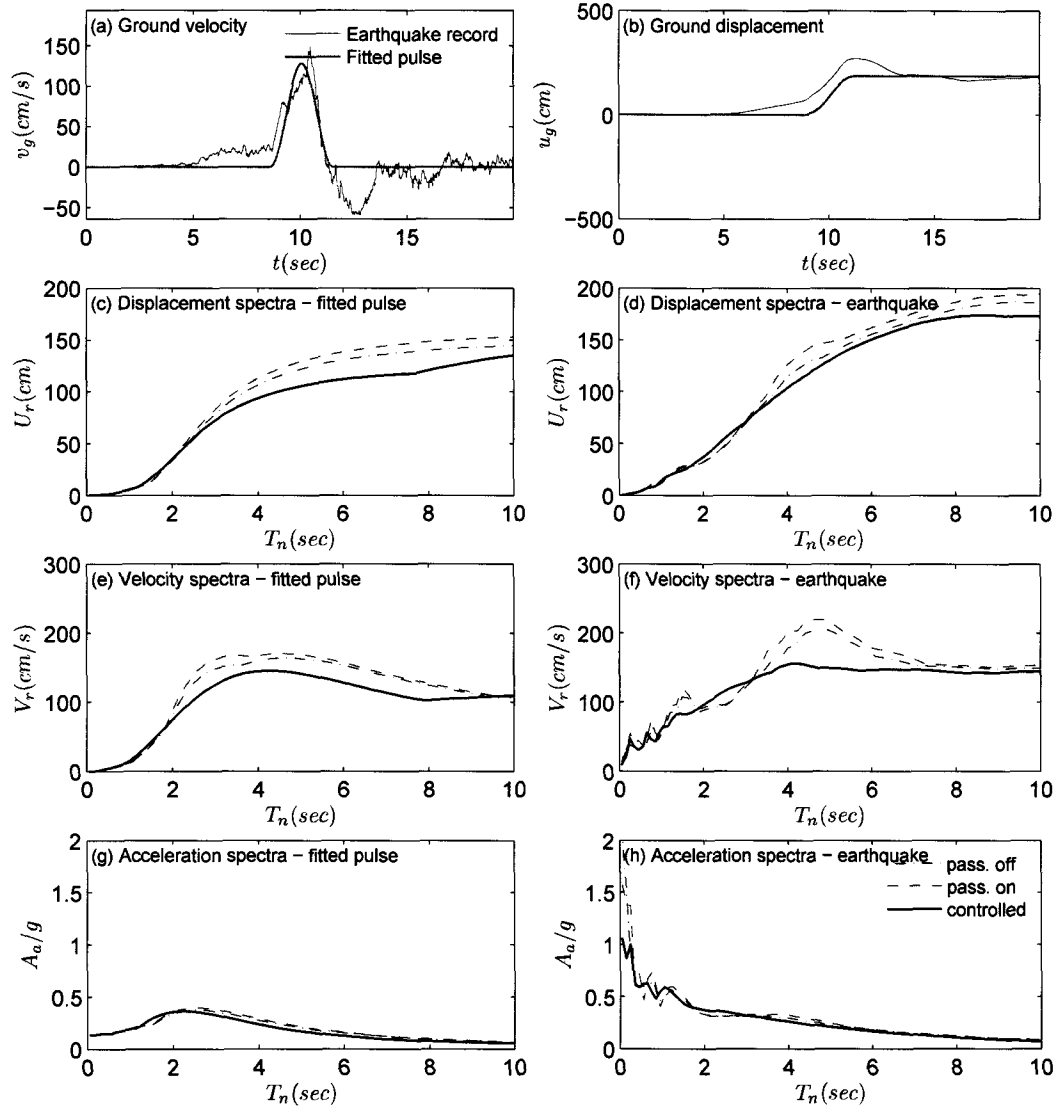


**Figure 5.9** Response spectra of the SDOF system subjected to Lucerne-270 record and fitted pulse type A ( $T_p = 2.94$  s)

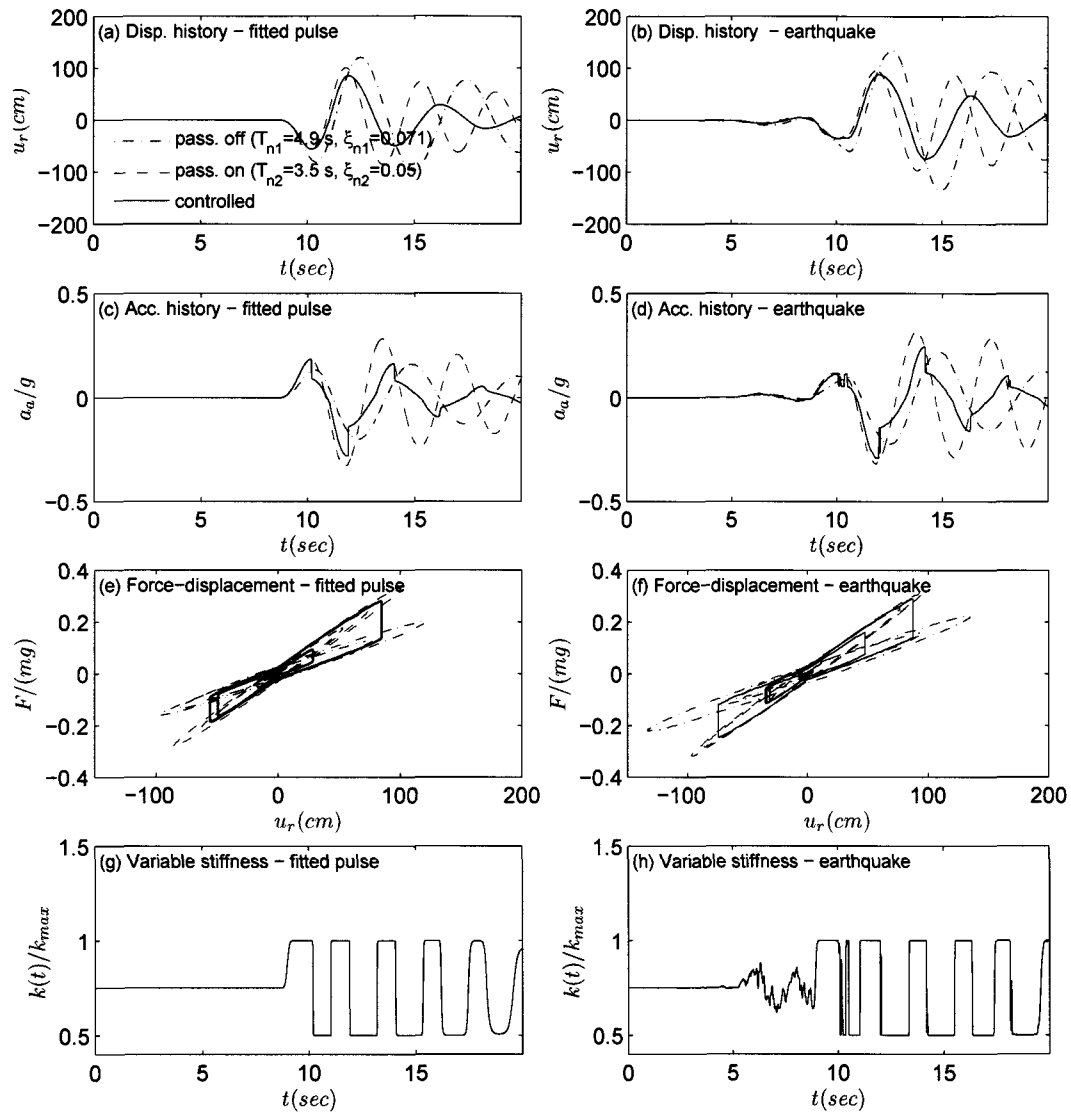


**Figure 5.10** Response time histories, force-displacement loops, and variable stiffness history of the SDOF system subjected to Lucerne-270 record and fitted pulse type A ( $T_p = 2.94$  s)



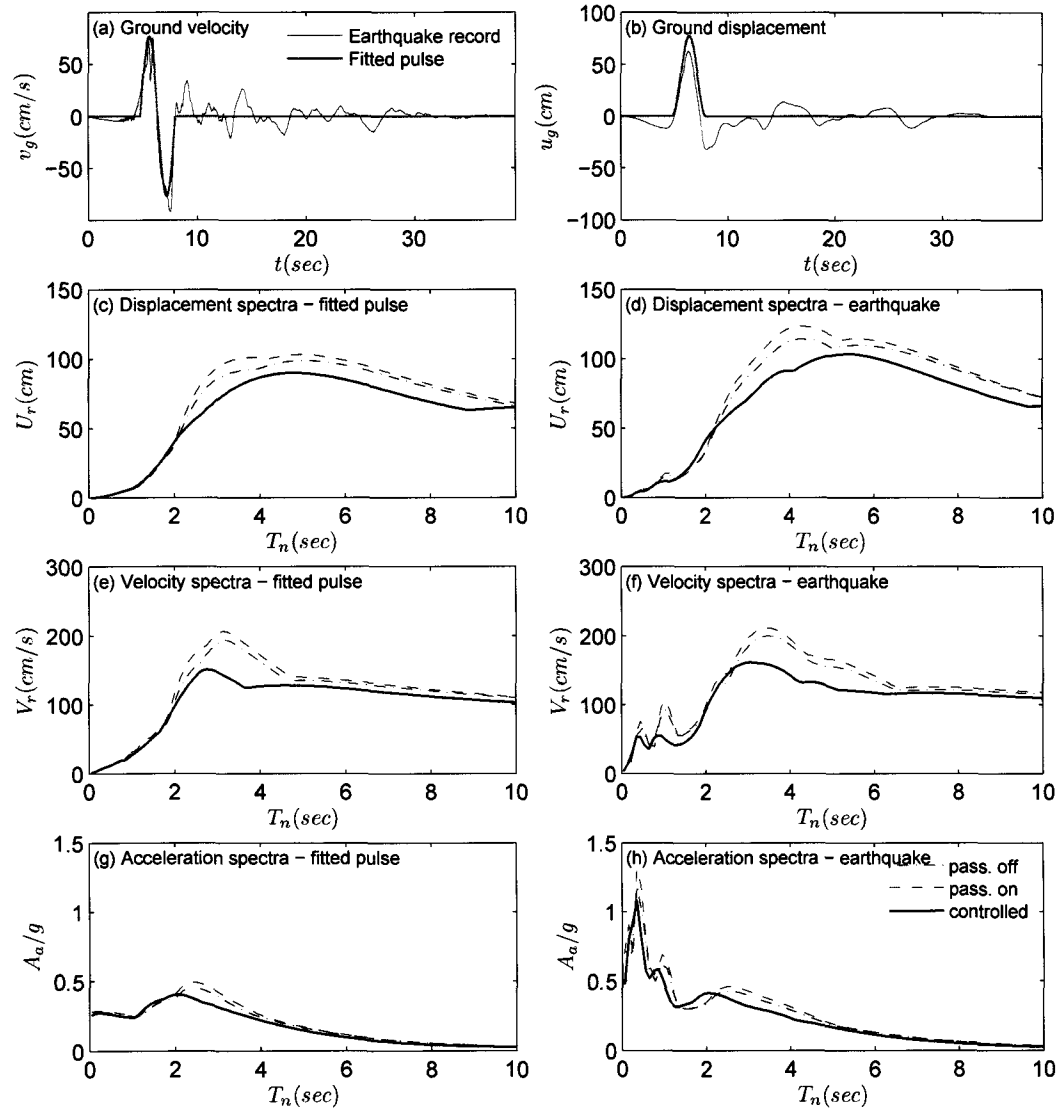


**Figure 5.11** Response spectra of the SDOF system subjected to El Centro #5-230-FN record and fitted pulse type B ( $T_p = 3.18$  s)

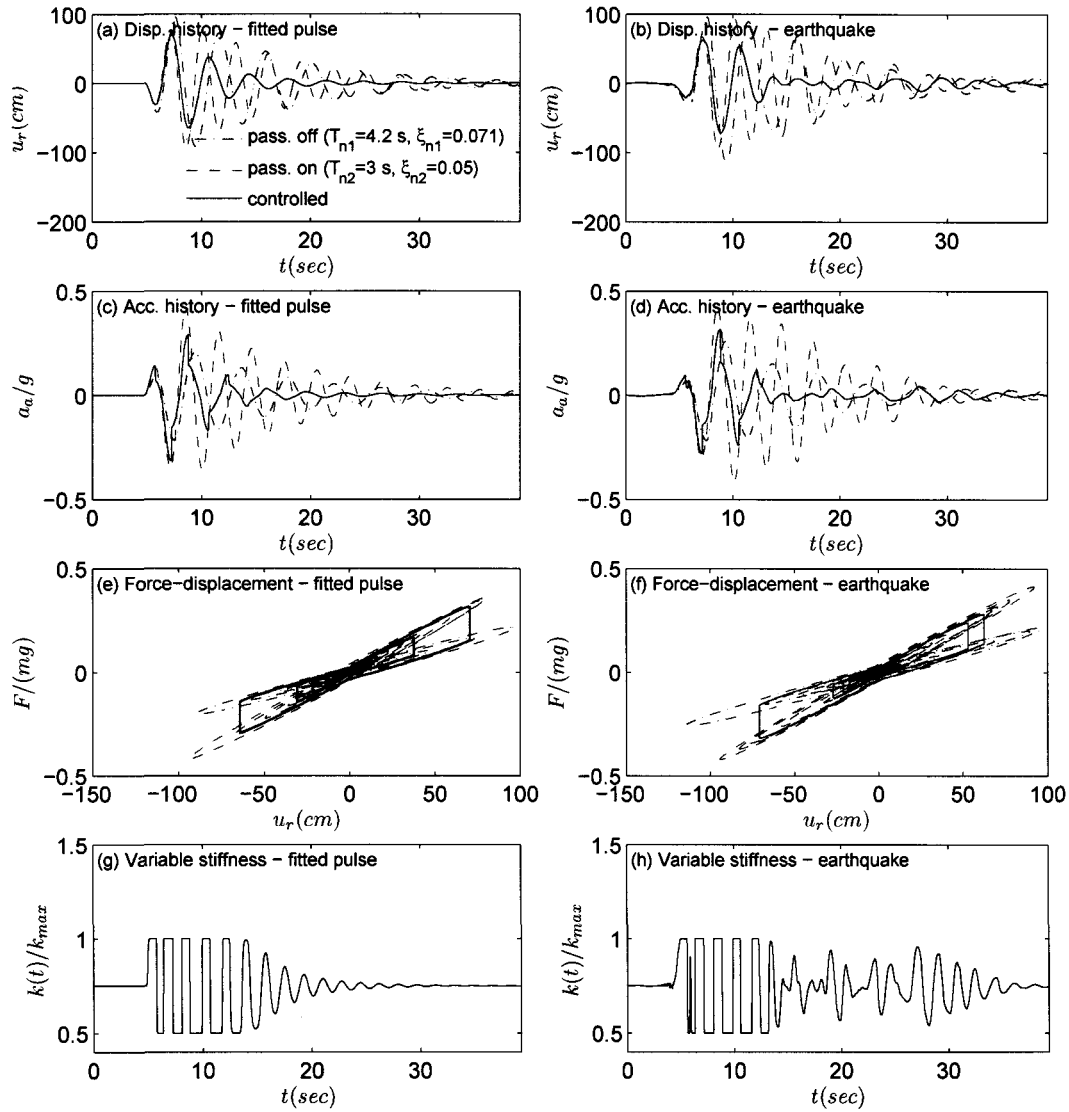


**Figure 5.12** Response time histories, force-displacement loops, and variable stiffness history of the SDOF system subjected to El Centro #5-230-FN record and fitted pulse type B ( $T_p = 3.18$  s)

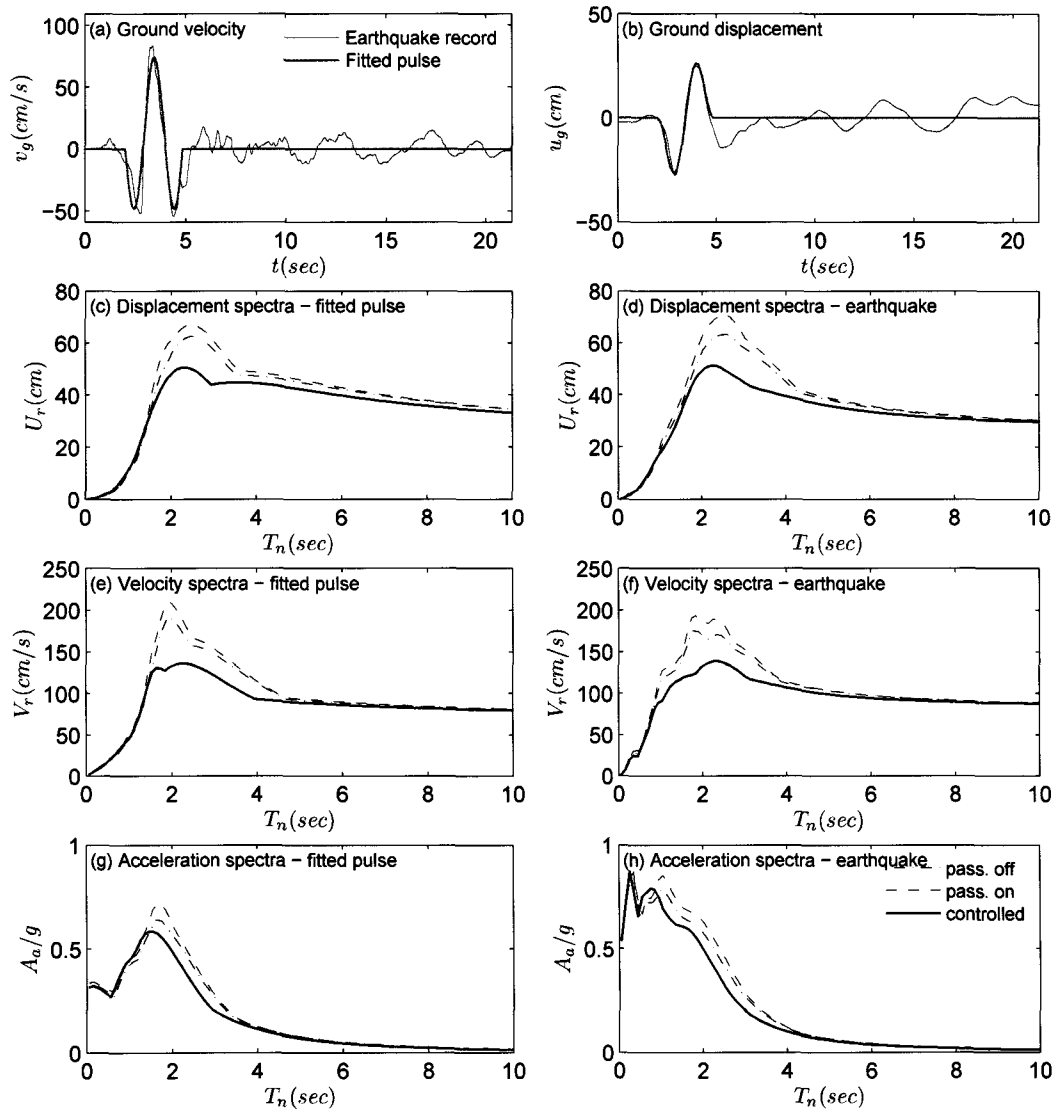


**Figure 5.13** Response spectra of the SDOF system subjected to Erzincan-NS record and fitted pulse type  $C_1$  ( $T_p = 2.00$  s)

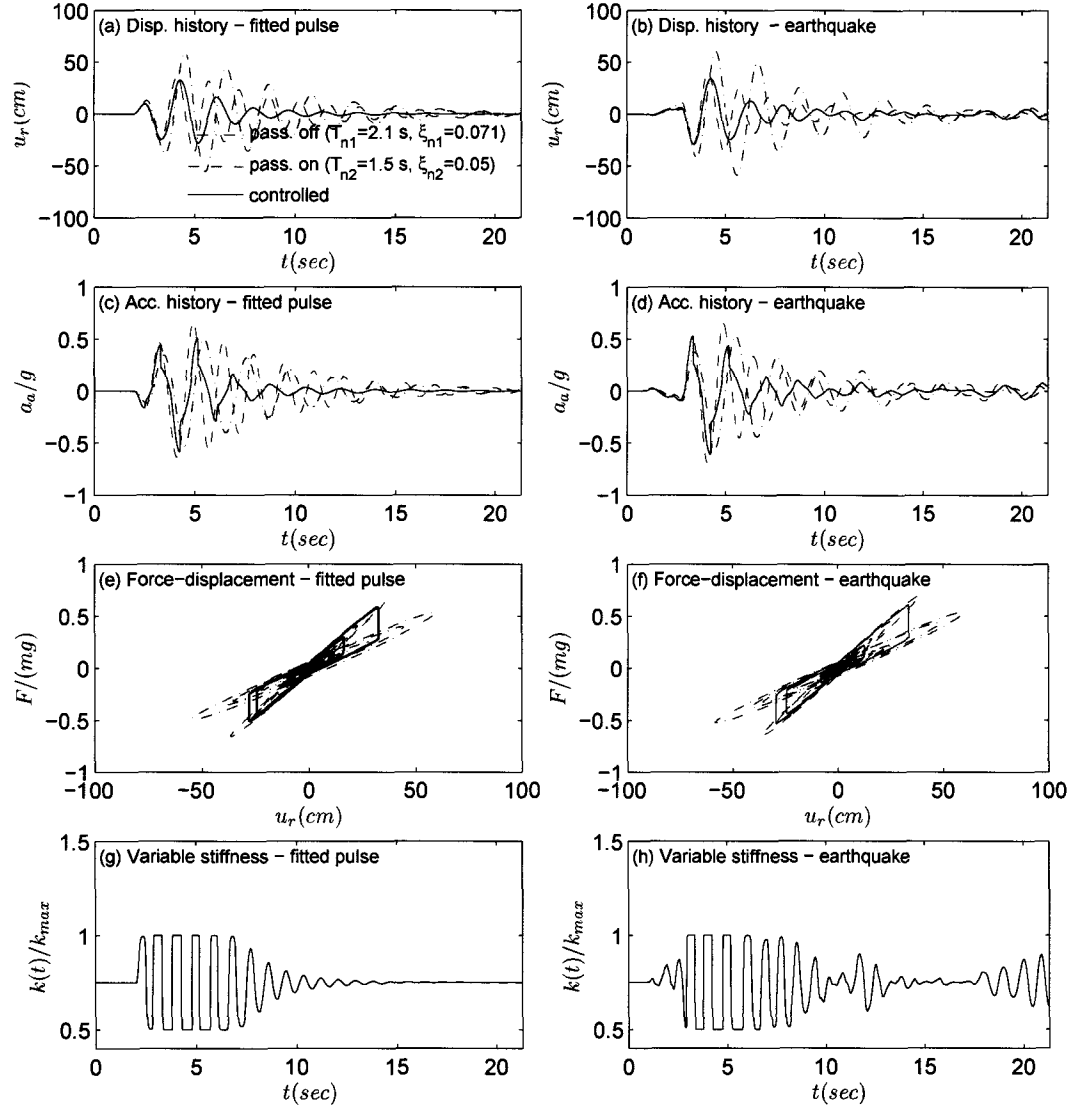


**Figure 5.14** Response time histories, force-displacement loops, and variable stiffness history of the SDOF system subjected to Erzincan-NS record and fitted pulse type  $C_1$  ( $T_p = 2.00$  s)

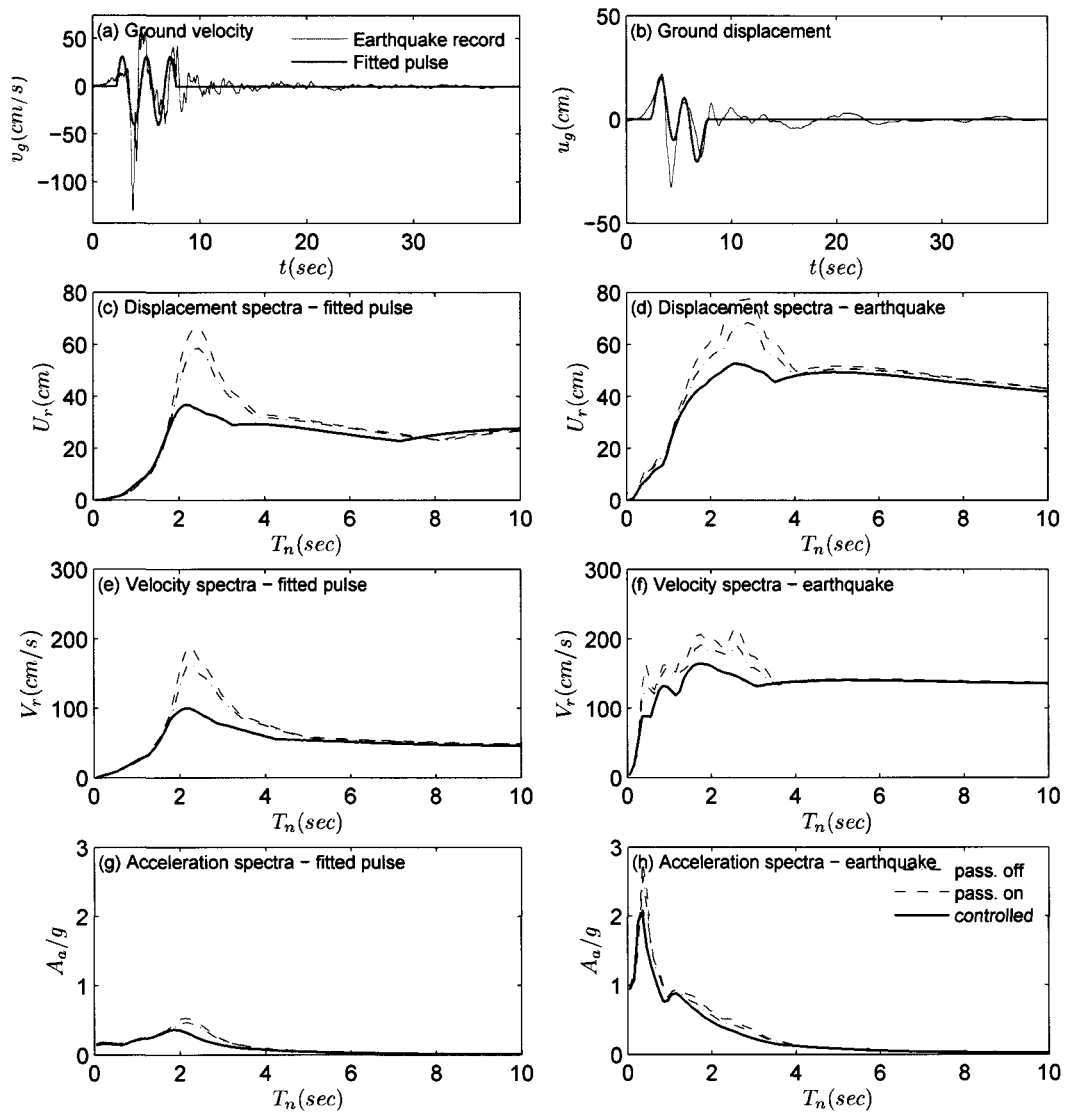


**Figure 5.15** Response spectra of the SDOF system subjected to Sylmar-360-FN record and fitted pulse type  $C_2$  ( $T_p = 2.25$  s)

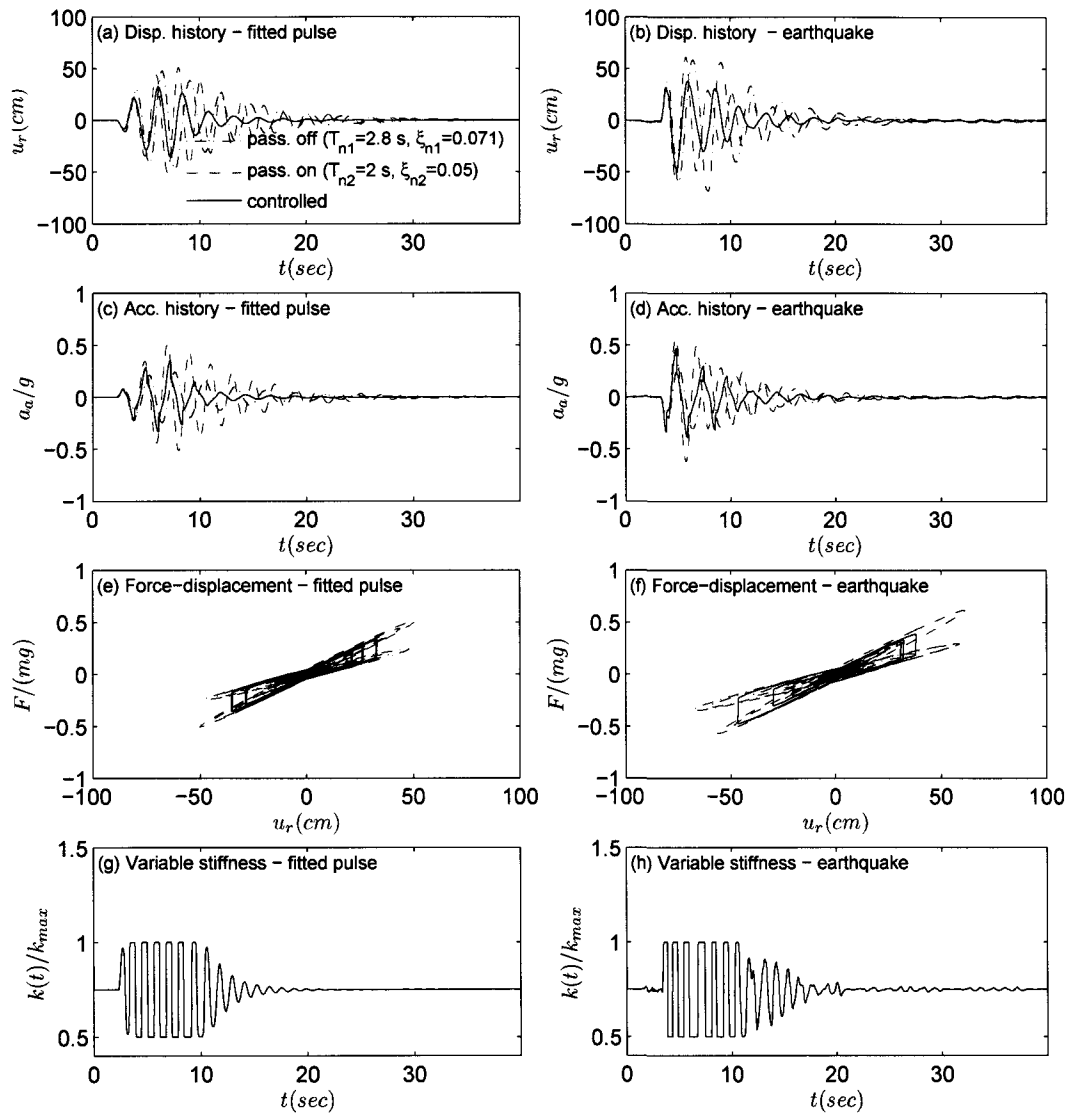


**Figure 5.16** Response time histories, force-displacement loops, and variable stiffness history of the SDOF system subjected to Sylmar-360-FN record and fitted pulse type  $C_2$  ( $T_p = 2.25$  s)

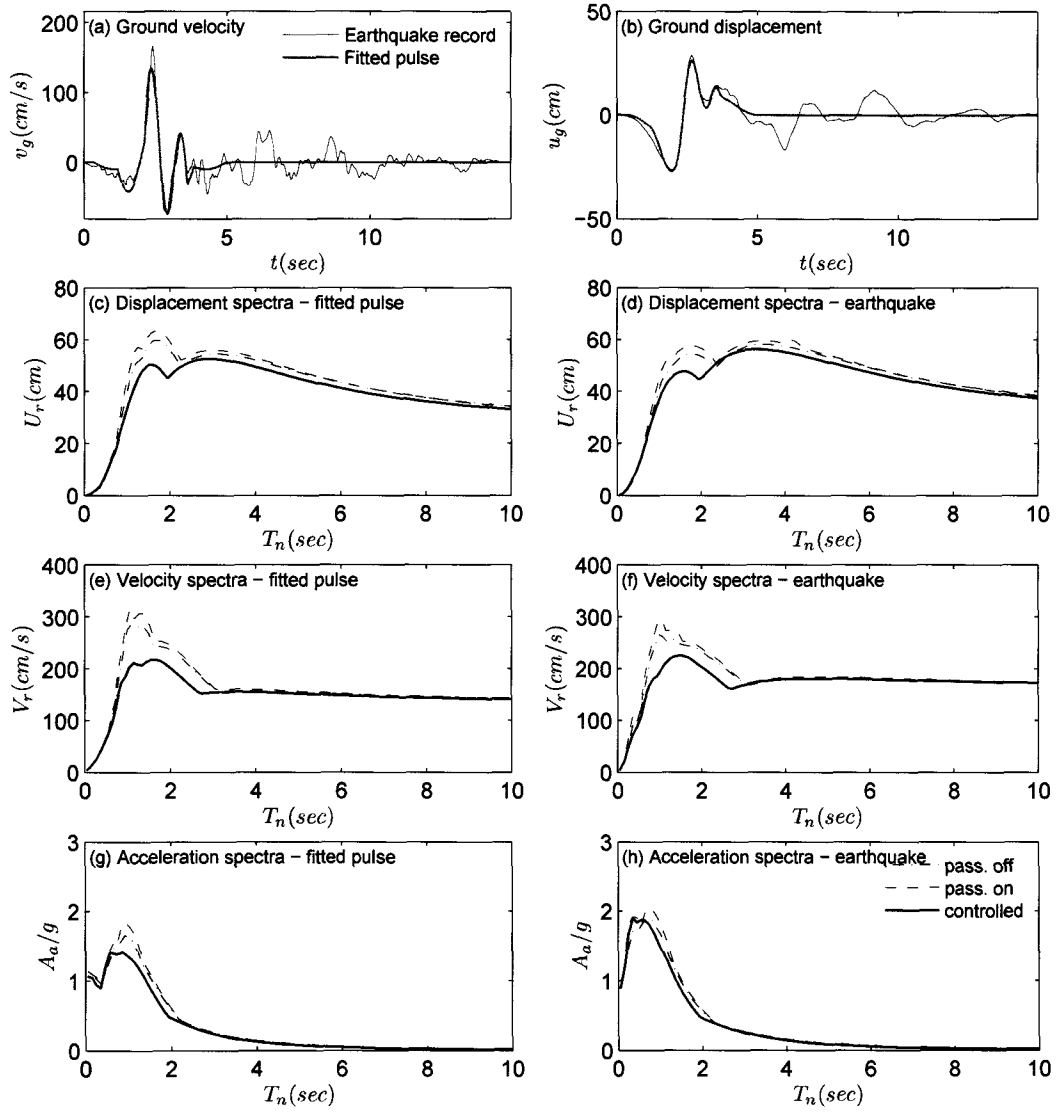


**Figure 5.17** Response spectra of the SDOF system subjected to Rinaldi-228-FN record and fitted pulse type  $C_1+C_1+C_1$  ( $T_p = [3.21 \ 1.87 \ 1.06] \text{ s}$ )

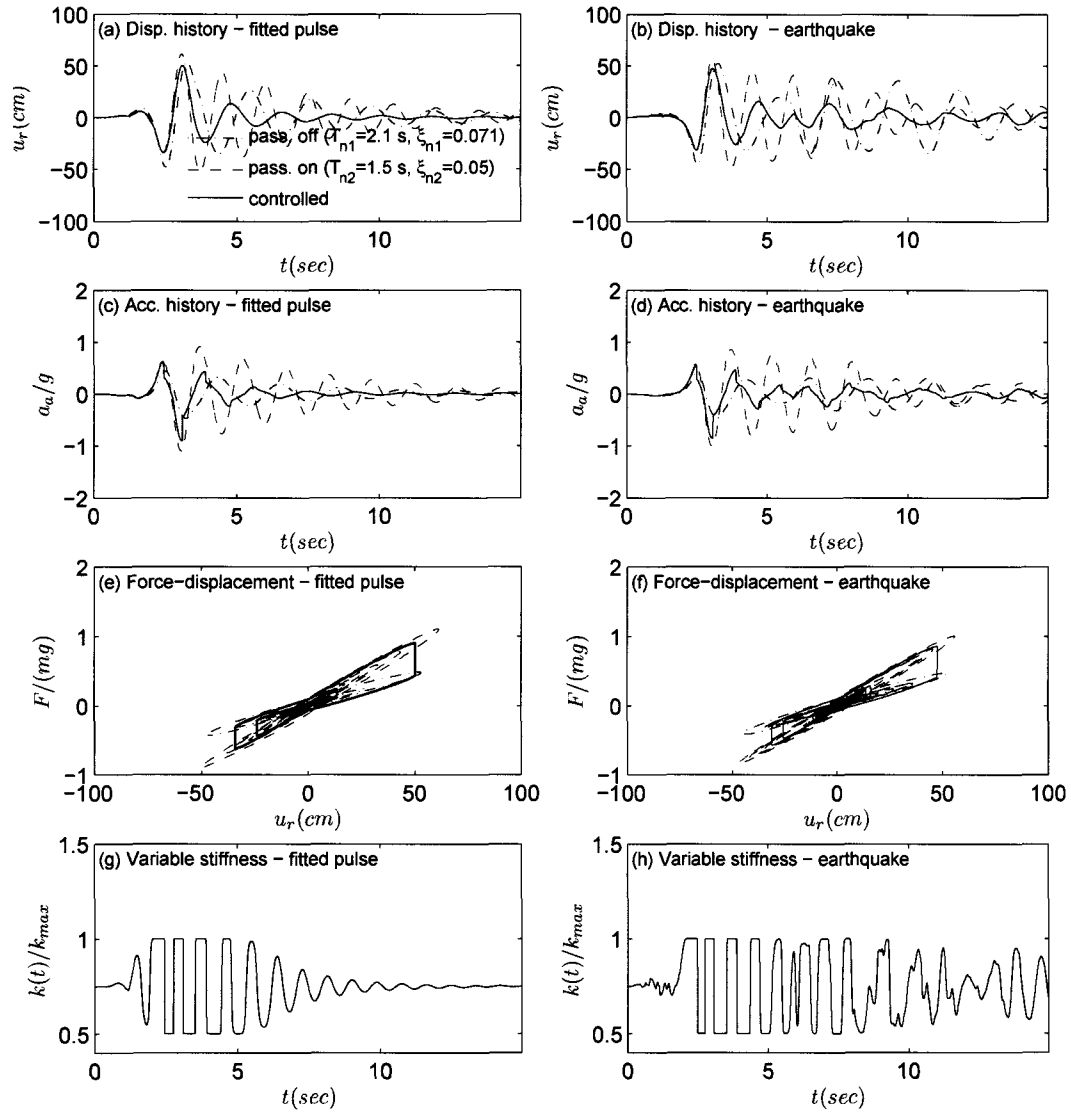


**Figure 5.18** Response time histories, force-displacement loops, and variable stiffness history of the SDOF system subjected to Rinaldi-228-FN record and fitted pulse type  $C_1+C_1+C_1$  ( $T_p = [3.21 \ 1.87 \ 1.06] \text{ s}$ )



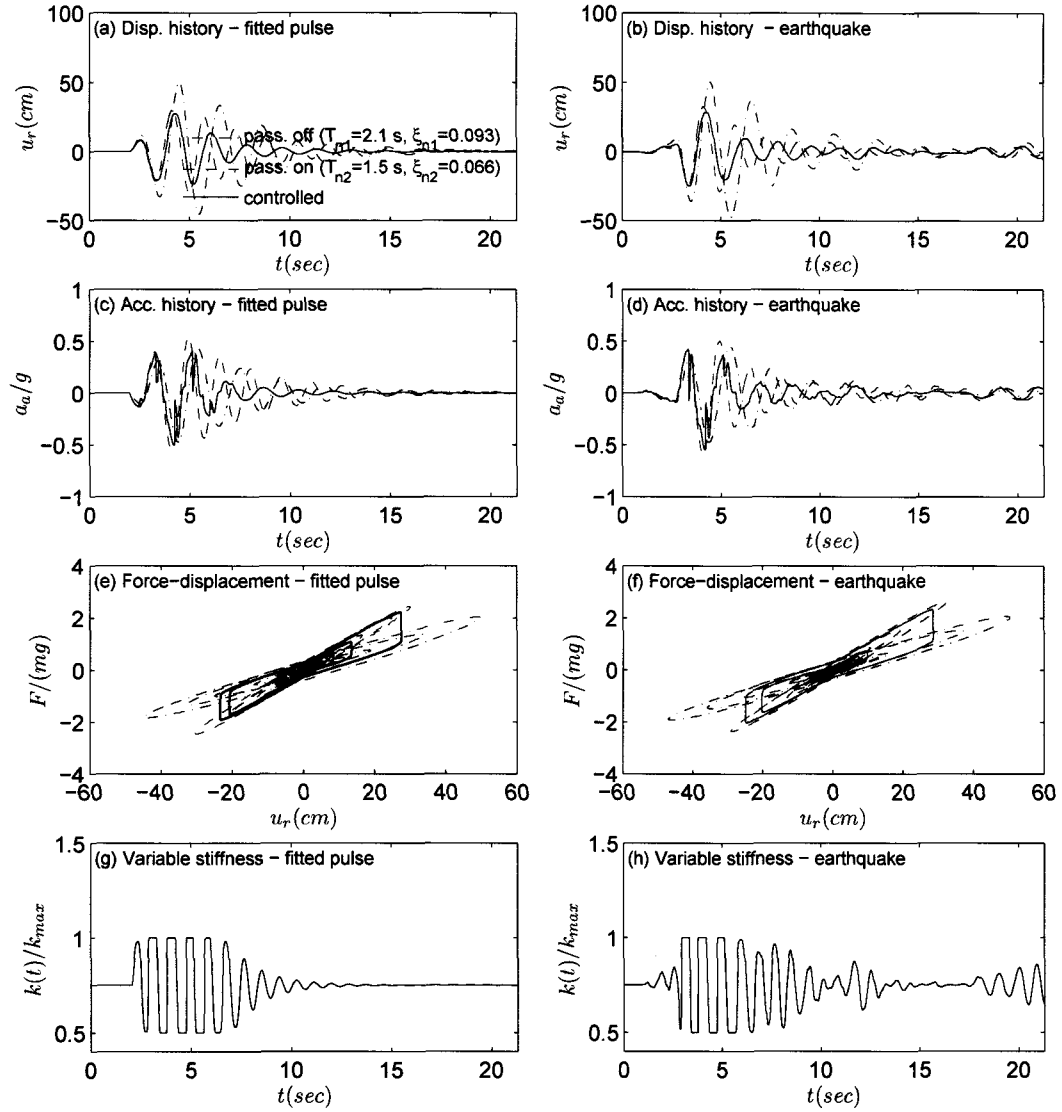


**Figure 5.19** Response time histories, force-displacement loops, and variable stiffness history of the 4-DOF system (base floor) subjected to Erzincan-NS record and fitted pulse type  $C_1$  ( $T_p = 2.00$  s)

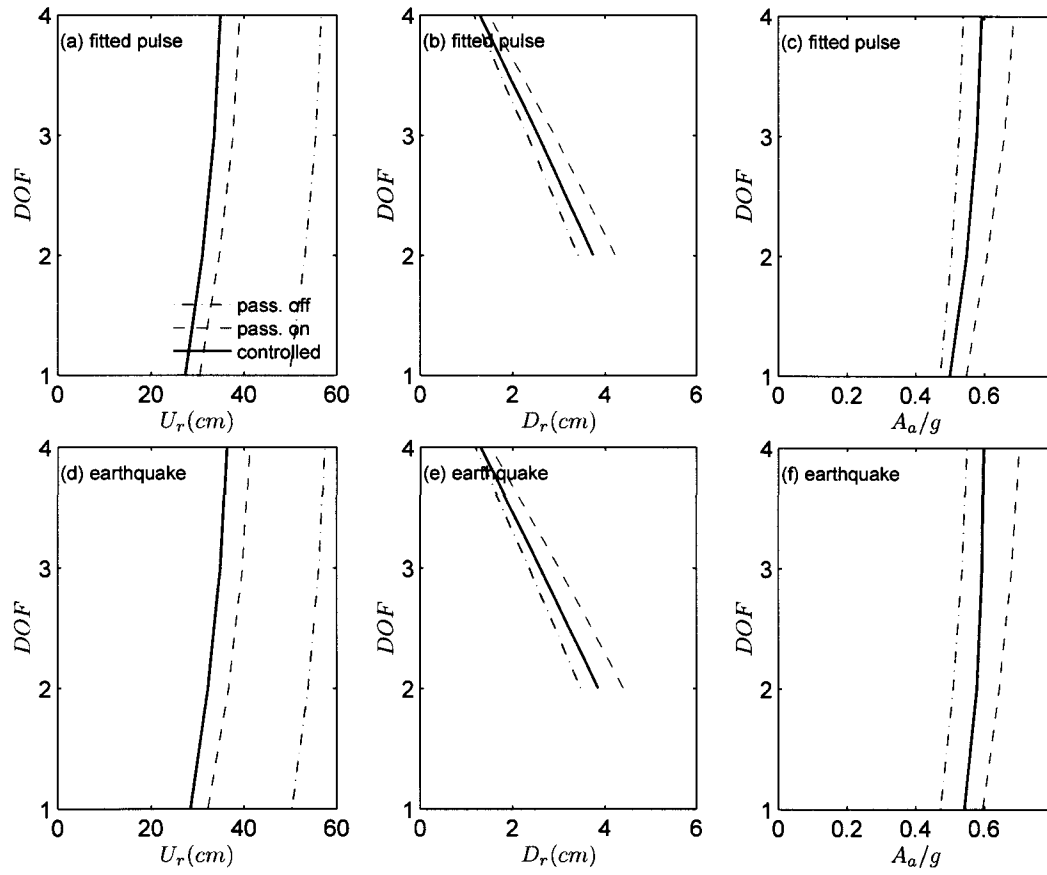


**Figure 5.20** Peak response profiles for 4-DOF system subjected to Erzincan-NS record and fitted pulse type  $C_1$  ( $T_p = 2.00$  s)

## 5.7 Results for Variable Damping Systems

The five different type of pulses studied in Section 5.5 and the near-fault ground motions that they were fitted to are used to evaluate the performance of the variable damping (Lyapunov) control given in Section 5.3.2. The spectral responses shown are maximum relative displacement  $U_r$ , maximum relative velocity  $V_r$ , and maximum absolute acceleration  $A_a$ , normalized appropriately.  $T_n$  is the period in seconds. ‘pass. on’ corresponds to the passive system with maximum damping ( $c_{max}$ ), ‘pass. off’ corresponds to the passive system with minimum damping ( $c_{min}$ ), and ‘controlled’ corresponds to the semi-active system with variable damping. The ratio  $c_{max}/c_{min}$  is set as 3.

Figures 5.21 and 5.22 show the response spectra and time histories of the SDOF system subjected to Lucerne-270 record and fitted pulse type A ( $T_p = 2.94$  s). The Lyapunov control provides similar or slightly higher response than ‘pass. on’ system in higher period range ( $> T_p$ ).

Figures 5.23 and 5.24 show the response spectra and time histories of the SDOF system subjected to El Centro #5-230-FN record and fitted pulse type B ( $T_p = 3.18$  s). The Lyapunov control provides similar response reduction with ‘pass. on’ system over the entire period range.

Figures 5.25 and 5.26 show the response spectra and time histories of the SDOF system subjected to Erzincan-NS record and fitted pulse type C<sub>1</sub> ( $T_p = 2.00$  s). The Lyapunov control provides response reduction in long period range ( $T > 3$  sec).

Figures 5.27 and 5.28 show the response spectra and time histories of the SDOF system subjected to Sylmar-360-FN record and fitted pulse type C<sub>2</sub> ( $T_p = 2.25$  s). The Lyapunov control provides response reduction in long period range ( $T > 4$  sec).

Figures 5.29 and 5.30 show the response spectra and time histories of the SDOF system

subjected to Rinaldi-228-FN record and fitted pulse type  $C_1+C_1+C_1$  ( $T_p = [3.21 \ 1.87 \ 1.06] \text{ s}$ ). The Lyapunov control provides response reduction in long period range ( $T > 3 \text{ sec}$ ).

Figures 5.31 and 5.32 show the base floor time histories and the peak floor profiles of 4-DOF base isolated system subjected to Erzincan-NS record and fitted pulse type  $C_1$  ( $T_p = 2.00 \text{ s}$ ). The peak floor profiles in Figure 5.32 indicate that Lyapunov control has similar response compared to passive-on system.

From the spectra shown in Figures 5.21 to 5.32, it is evident that the variable damping provides reductions in response, primarily at long periods ( $> 3 \text{ sec}$ ), when compared to the passive-on case. The responses in the two cases are similar in most other period ranges. The response spectra of fitted pulses provide good approximation for the response spectra of the actual earthquake records, especially in the long period range and the neighborhood of the pulse period.

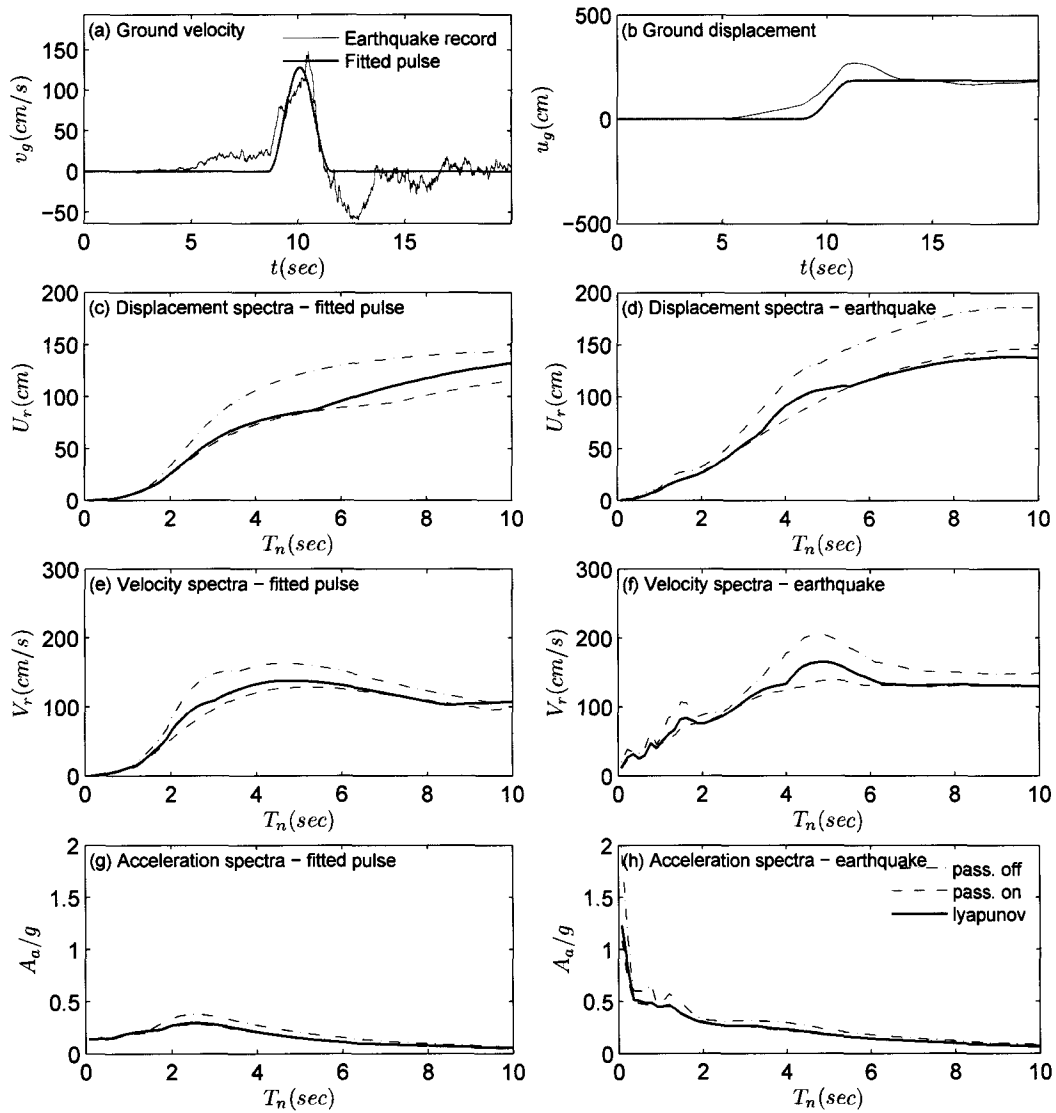


**Figure 5.21** Response spectra of the SDOF system subjected to Lucerne-270 record and fitted pulse type A ( $T_p = 2.94$  s)

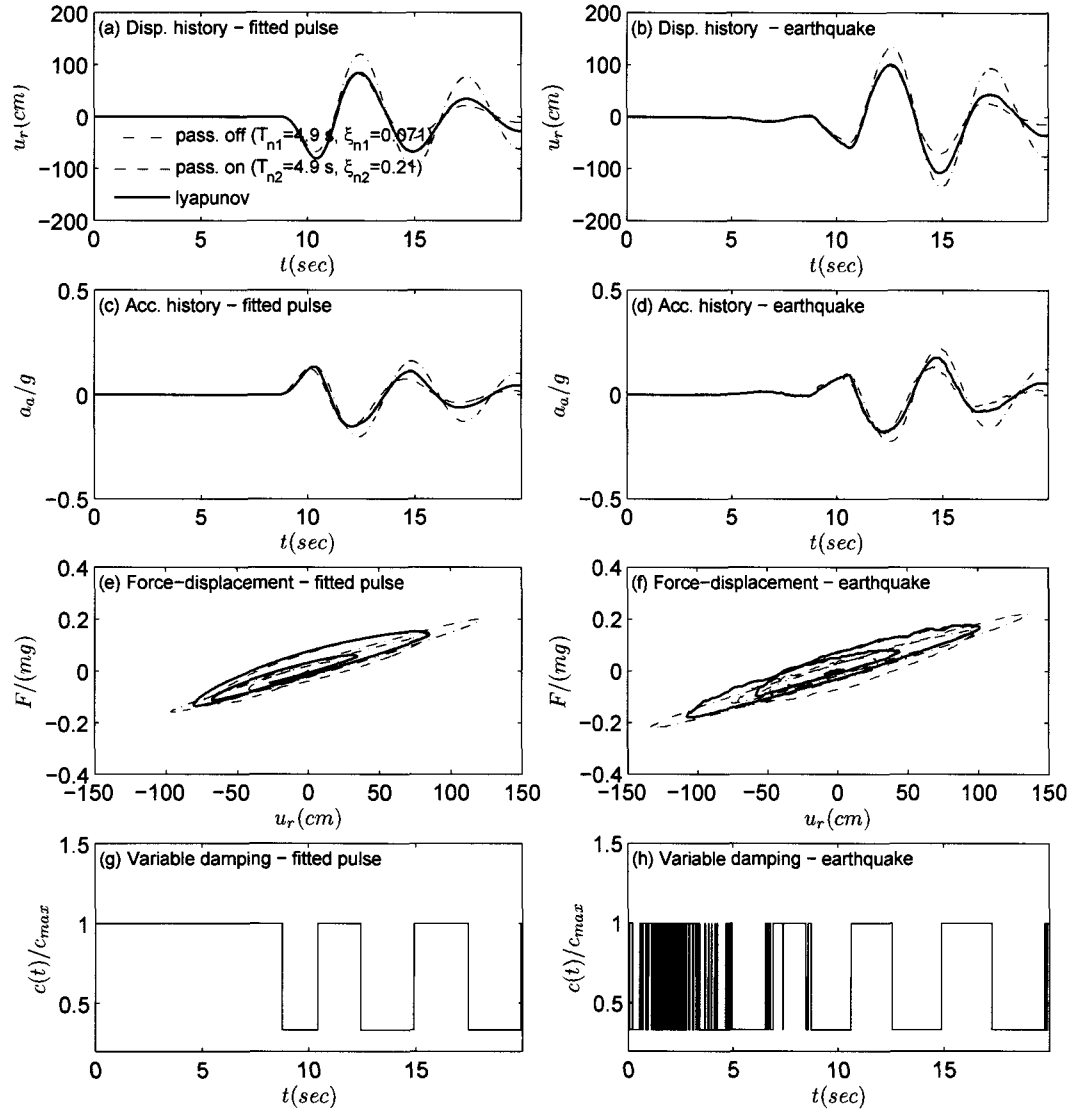


**Figure 5.22** Response time histories, force-displacement loops, and variable stiffness history of the SDOF system subjected to Lucerne-270 record and fitted pulse type A ( $T_p = 2.94$  s)

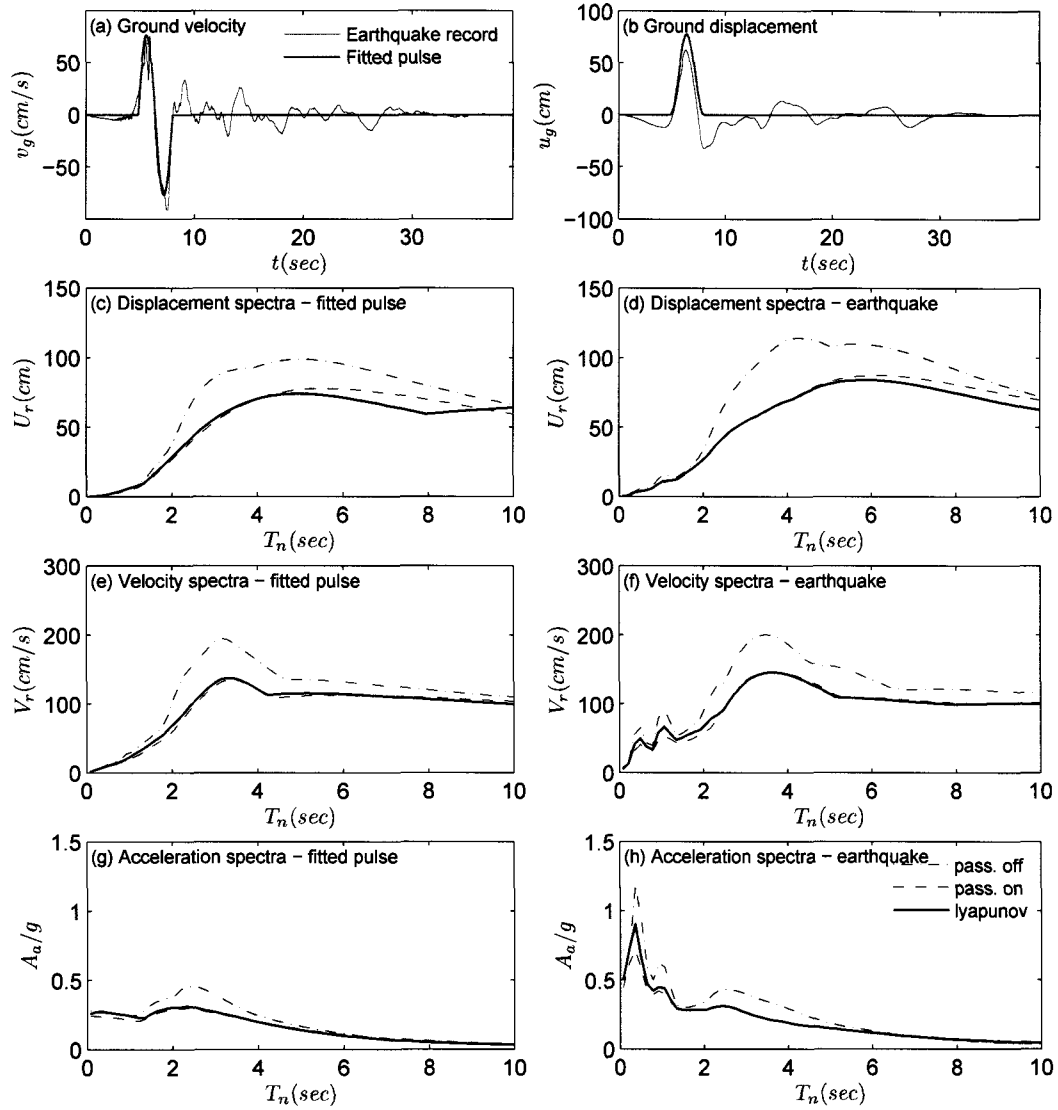


**Figure 5.23** Response spectra of the SDOF system subjected to El Centro #5-230-FN record and fitted pulse type B ( $T_p = 3.18$  s)

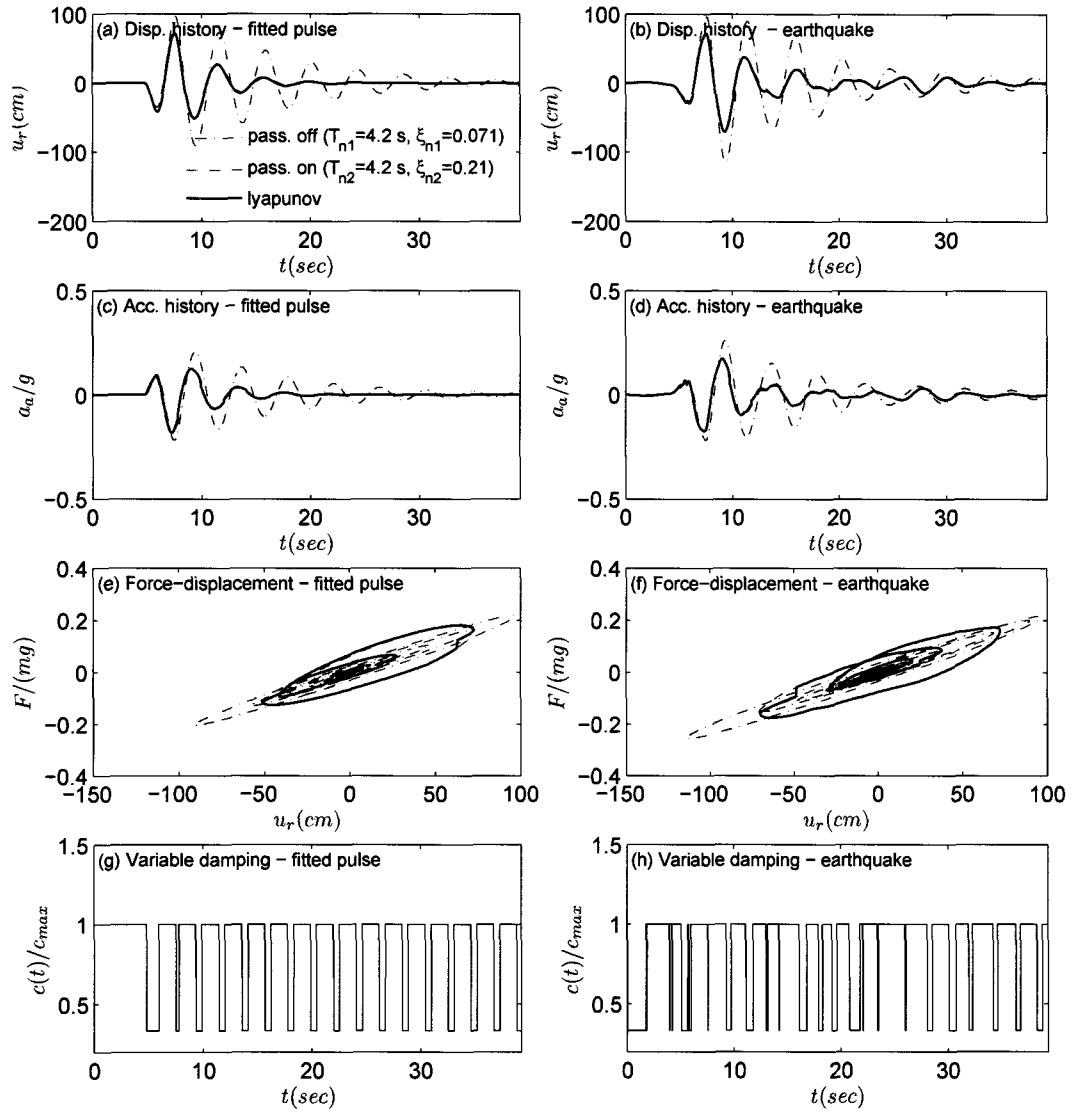


**Figure 5.24** Response time histories, force-displacement loops, and variable stiffness history of the SDOF system subjected to El Centro #5-230-FN record and fitted pulse type B ( $T_p = 3.18$  s)



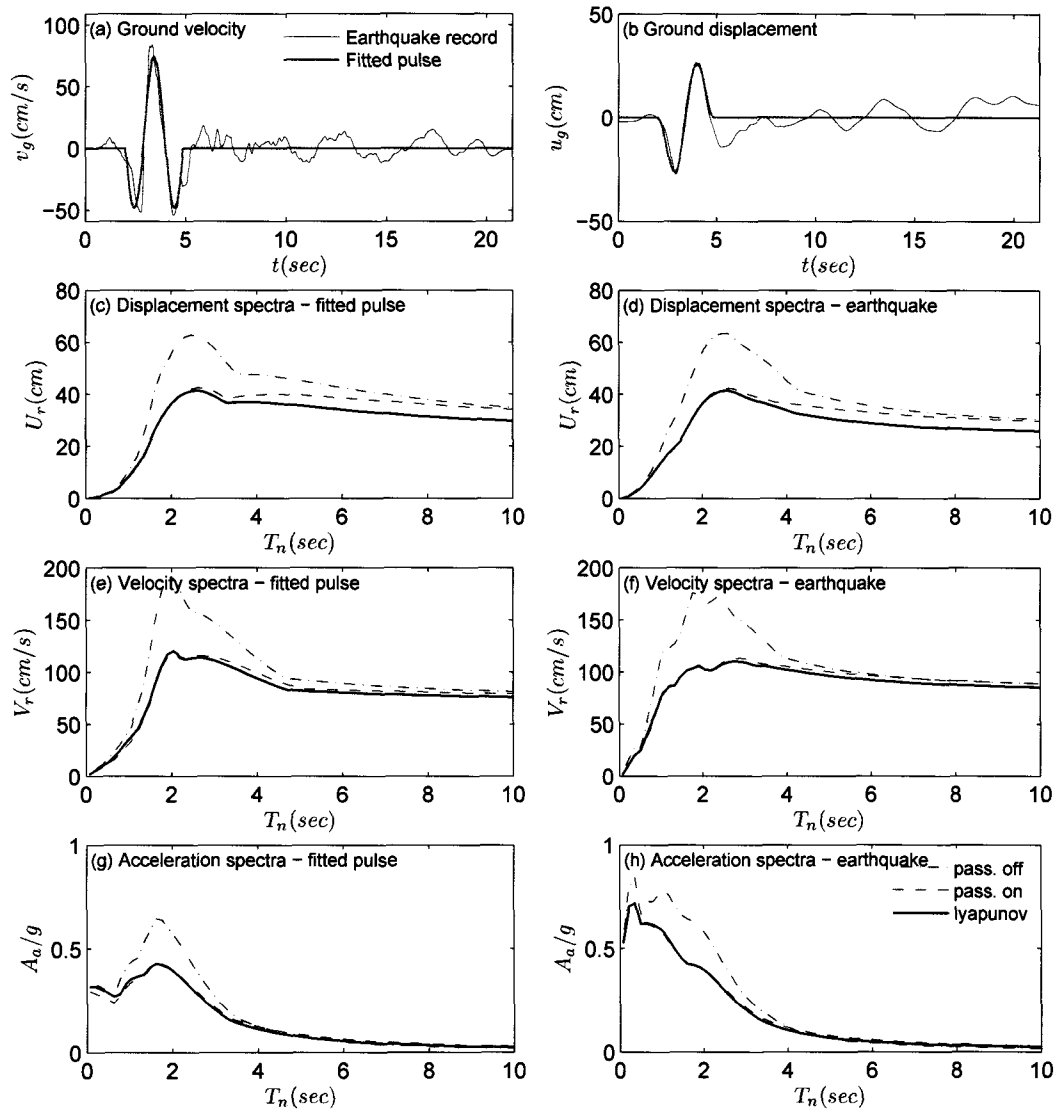


**Figure 5.25** Response spectra of the SDOF system subjected to Erzincan-NS record and fitted pulse type  $C_1$  ( $T_p = 2.00$  s)

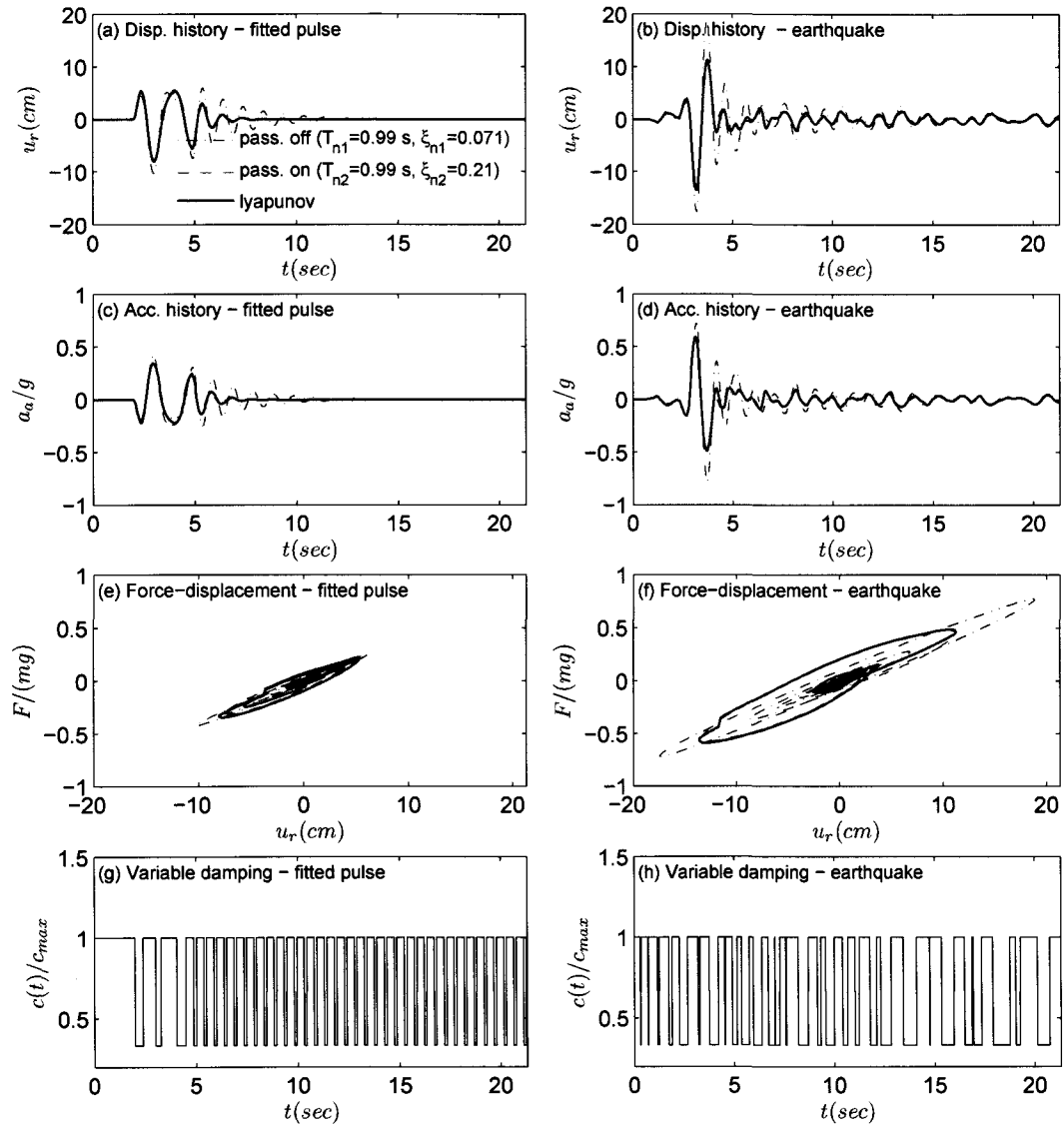


**Figure 5.26** Response time histories, force-displacement loops, and variable stiffness history of the SDOF system subjected to Erzincan-NS record and fitted pulse type  $C_1$  ( $T_p = 1.03$  s)

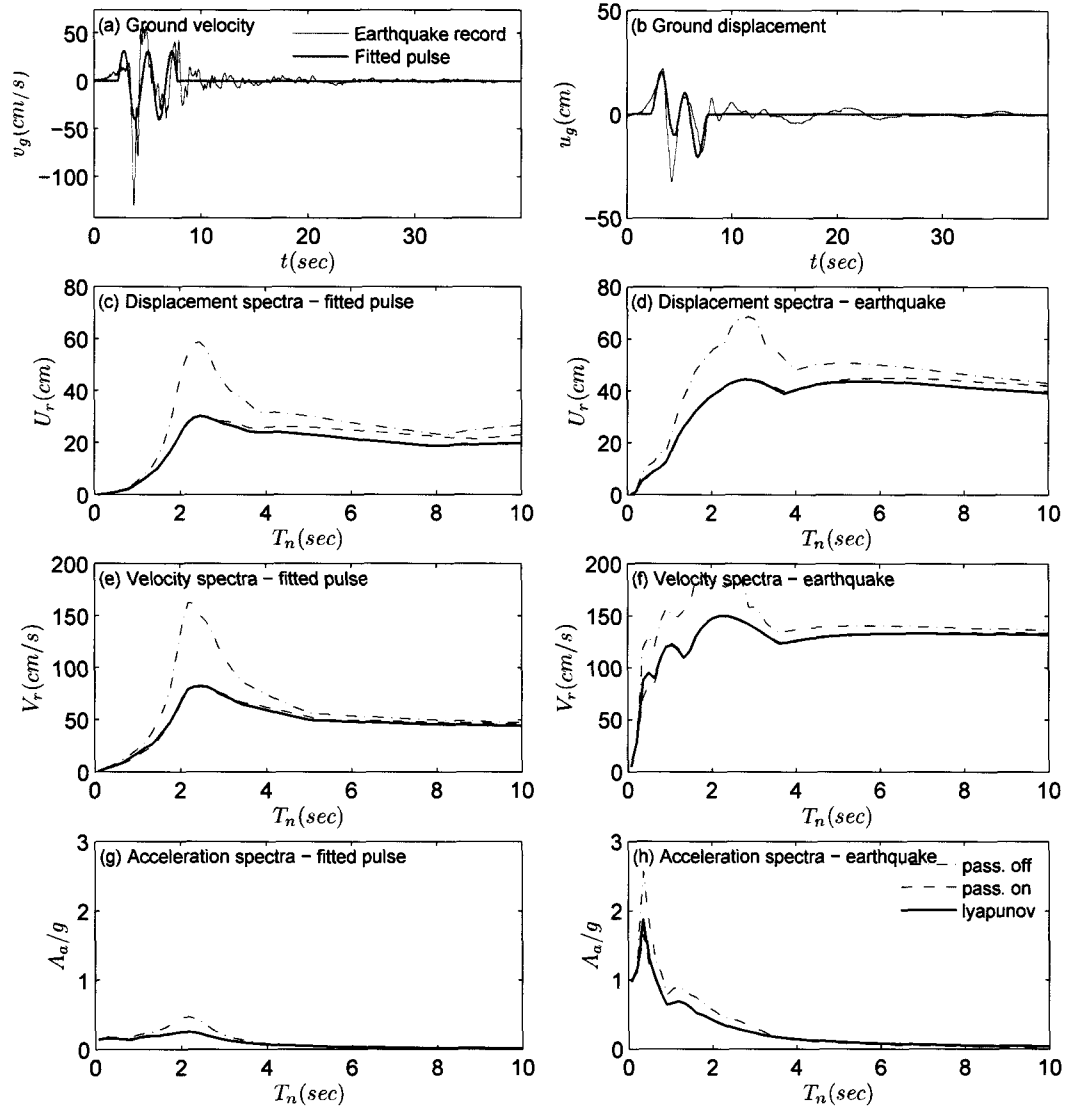


**Figure 5.27** Response spectra of the SDOF system subjected to Sylmar-360-FN record and fitted pulse type  $C_2$  ( $T_p = 2.25$  s)

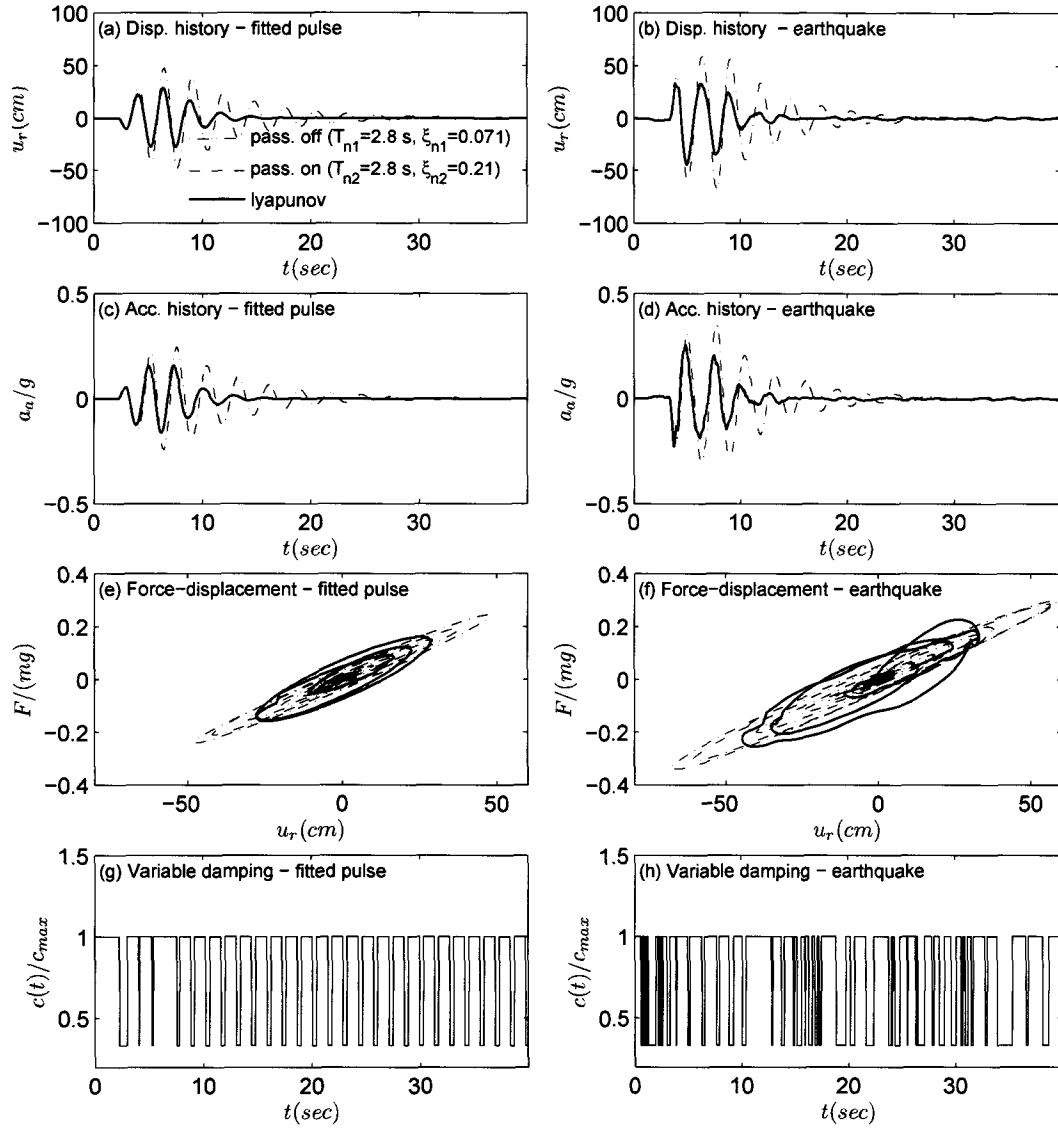


**Figure 5.28** Response time histories, force-displacement loops, and variable stiffness history of the SDOF system subjected to Sylmar-360-FN record and fitted pulse type  $C_2$  ( $T_p = 2.25$  s)

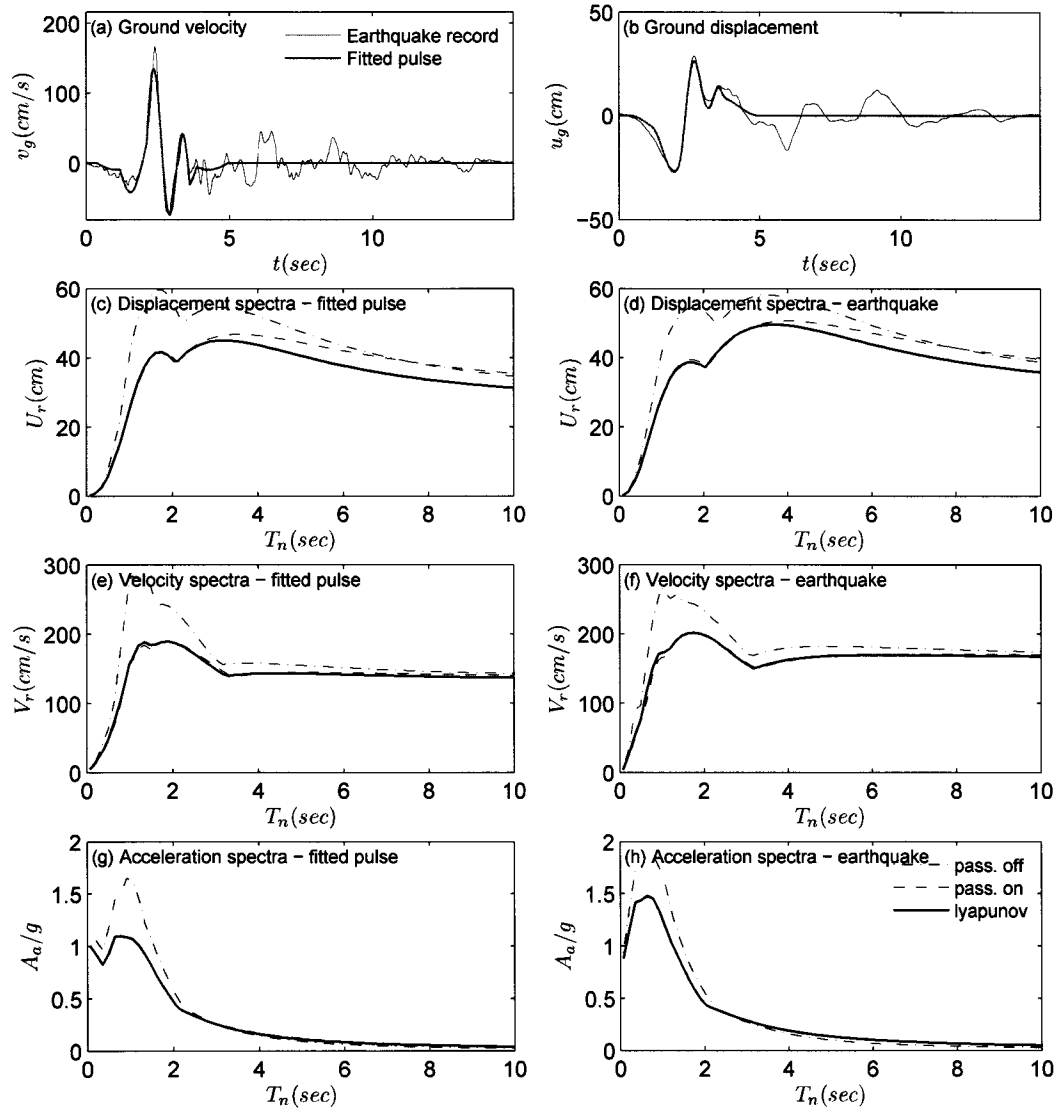


**Figure 5.29** Response spectra of the SDOF system subjected to Rinaldi-228-FN record and fitted pulse type  $C_1+C_1+C_1$  ( $T_p = [3.21 \ 1.87 \ 1.06] \text{ s}$ )

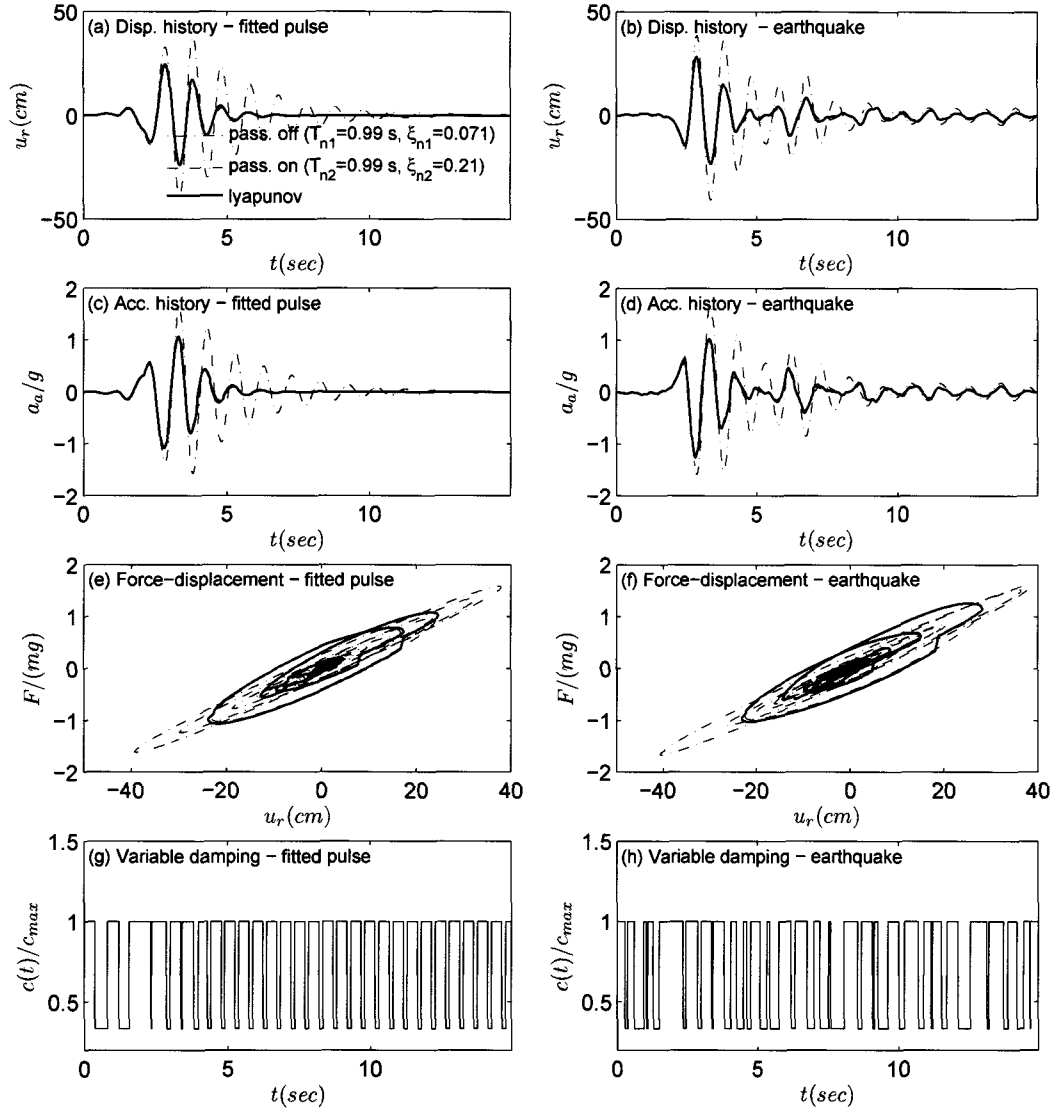


**Figure 5.30** Response time histories, force-displacement loops, and variable stiffness history of the SDOF system subjected to Rinaldi-228-FN record and fitted pulse type  $C_1+C_1+C_1$  ( $T_p = [3.21 \ 1.87 \ 1.06] \text{ s}$ )

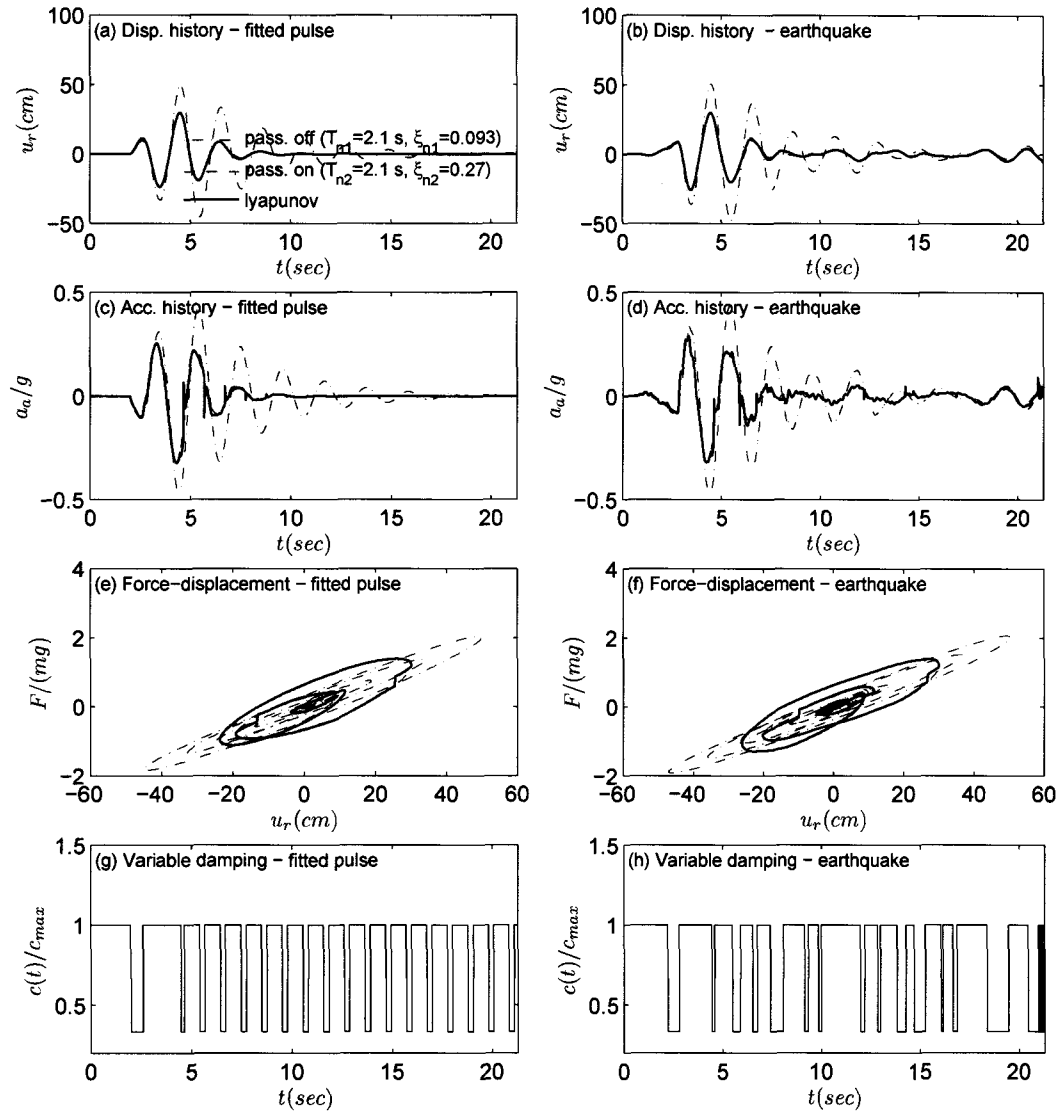


**Figure 5.31** Response time histories, force-displacement loops, and variable stiffness history of the 4-DOF system (base floor) subjected to Erzincan-NS record and fitted pulse type  $C_1$  ( $T_p = 2.00$  s)

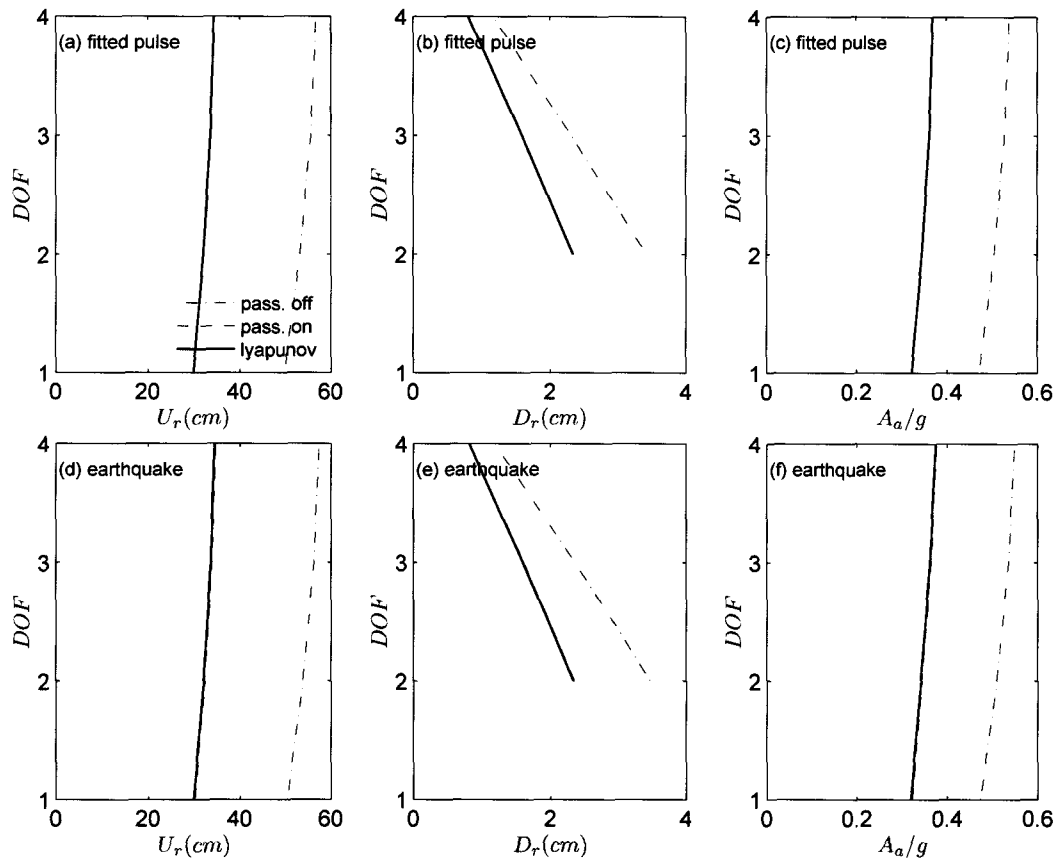


**Figure 5.32** Peak response profiles for 4-DOF system subjected to Erzincan-NS record and fitted pulse type  $C_1$  ( $T_p = 2.00$  s)



## 5.8 Results for Combined Variable Damping and Stiffness Systems

The five different type of pulses studied in Section 5.5 and the near-fault ground motions that they were fitted to are used to evaluate the performance of the combined variable stiffness (Section 5.3.1) and variable damping (Lyapunov) control (Section 5.3.2). The spectral responses shown are maximum relative displacement  $U_r$ , maximum relative velocity  $V_r$ , and maximum absolute acceleration  $A_a$ , normalized appropriately.  $T_n$  is the period in seconds. ‘S-on’ corresponds to the maximum stiffness ( $k_{max}$ ), ‘S-off’ corresponds to the minimum stiffness ( $k_{min}$ ), and ‘S-contr’ corresponds to the variable stiffness. Similarly, ‘D-on’ corresponds to the maximum damping ( $c_{max}$ ), ‘D-off’ corresponds to the minimum damping ( $c_{min}$ ), and ‘D-contr’ corresponds to the variable damping. The ratio  $k_{max}/k_{min}$  is set as 2 and the ratio  $c_{max}/c_{min}$  is set as 3.

Figures 5.33 and 5.34 show the response spectra and time histories of the SDOF system subjected to Lucerne-270 record and fitted pulse type A ( $T_p = 2.94$  s). The combined VSC-VD system reduces the response in a broader period range ( $T > T_p$ ). The acceleration response  $A_a$  is reduced significantly over the entire period range, in particular in the range 0 to  $T_p$ . The time history shown in Figure 5.33 clearly shows the reduction in displacement response, as well as acceleration response.

Figures 5.35 and 5.36 show the response spectra and time histories of the SDOF system subjected to El Centro #5-230-FN record and fitted pulse type B ( $T_p = 3.18$  s). The combined VSC-VD system reduces the response in a broader period range ( $T > T_p$ ). The acceleration response  $A_a$  is reduced significantly over the entire period range, in particular in the range 0 to  $T_p$ . The time history shown in Figure 5.36 clearly shows the reduction in displacement response, as well as acceleration response.

Figures 5.37 and 5.38 show the response spectra and time histories of the SDOF system

subjected to Erzincan-NS record and fitted pulse type  $C_1$  ( $T_p = 2.00$  s). The combined VSC-VD system reduces the response in a broader period range ( $T > T_p$ ). The time history shown in Figure 5.38 clearly shows the reduction in displacement response, as well as acceleration response.

Figures 5.39 and 5.40 show the response spectra and time histories of the SDOF system subjected to Sylmar-360-FN record and fitted pulse type  $C_2$  ( $T_p = 2.25$  s). The combined VSC-VD system reduces the response in a broader period range ( $T > T_p$ ). The acceleration response  $A_a$  is reduced significantly over the entire period range, in particular in the range 0 to  $T_p$ . The time history shown in Figure 5.40 clearly shows the reduction in displacement response, as well as acceleration response.

Figures 5.41 and 5.42 show the response spectra and time histories of the SDOF system subjected to Rinaldi-228-FN record and fitted pulse type  $C_1+C_1+C_1$  ( $T_p = [3.21 \ 1.87 \ 1.06]$  s). The combined VSC-VD system reduces the response in a broader period range ( $T > T_p$ ). The time history shown in Figure 5.42 clearly shows the reduction in displacement response, as well as acceleration response.

Figures 5.43 and 5.44 show the base floor time histories and the peak floor profiles of 4-DOF base isolated system subjected to Erzincan-NS record and fitted pulse type  $C_1$  ( $T_p = 2.00$  s). The peak floor profiles in Figure 5.44 indicate that combined VSC-VD system effectively reduces the displacement, acceleration and drift responses.

In summary, the combined VSC-VD system reduces the response in a broader period range. The VSC reduces response in the range  $T_p < T < 3$  sec and VD reduces response in the long period range; thus VSD & VD provide complimentary response reductions. The system with combined VSC and VD is effective and has significant potential. The response spectra of fitted pulses provide good approximation for the response spectra of the actual earthquake records, especially in the long period range and the neighborhood of the pulse

period.

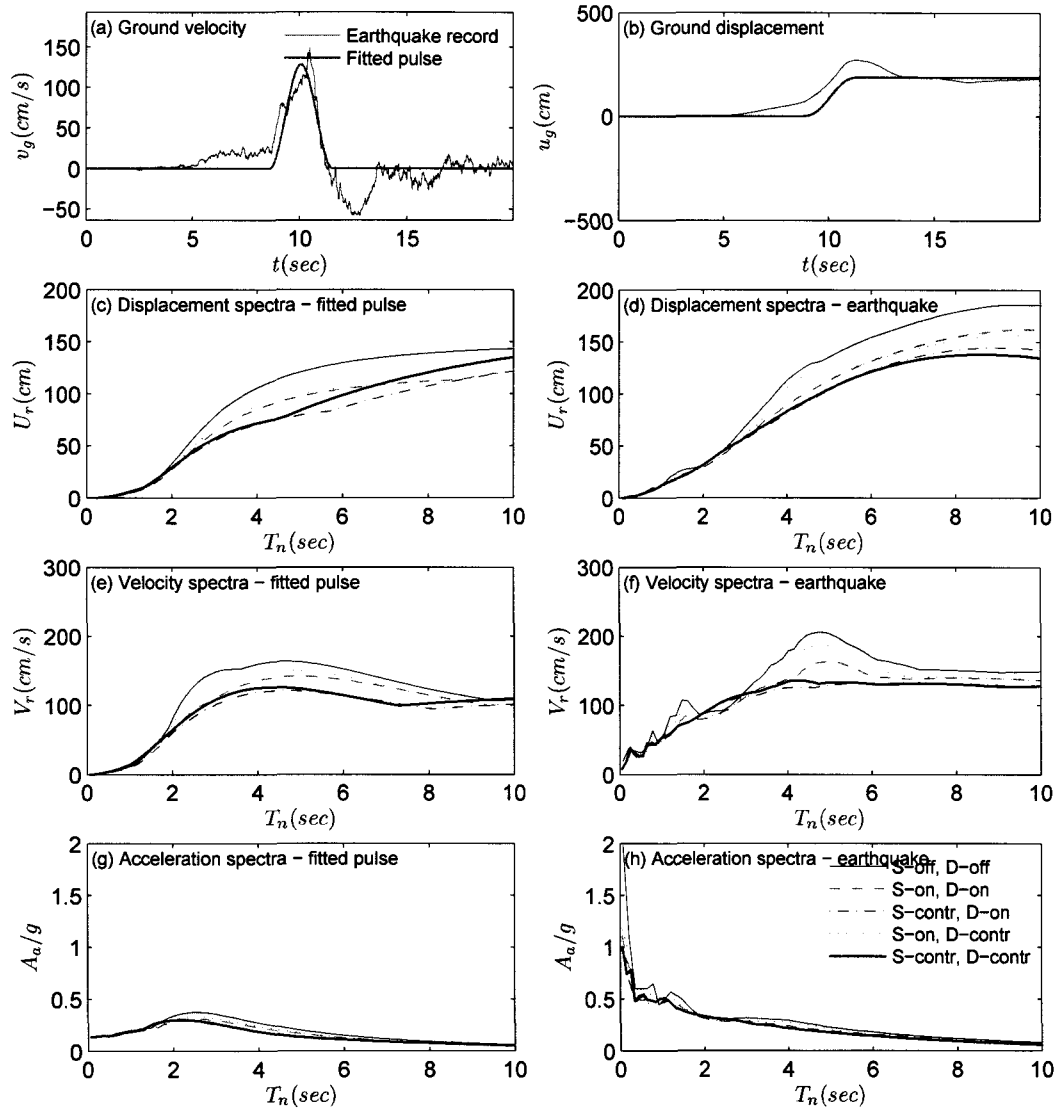


**Figure 5.33** Response spectra of the SDOF system subjected to Lucerne-270 record and fitted pulse type A ( $T_p = 2.94$  s)

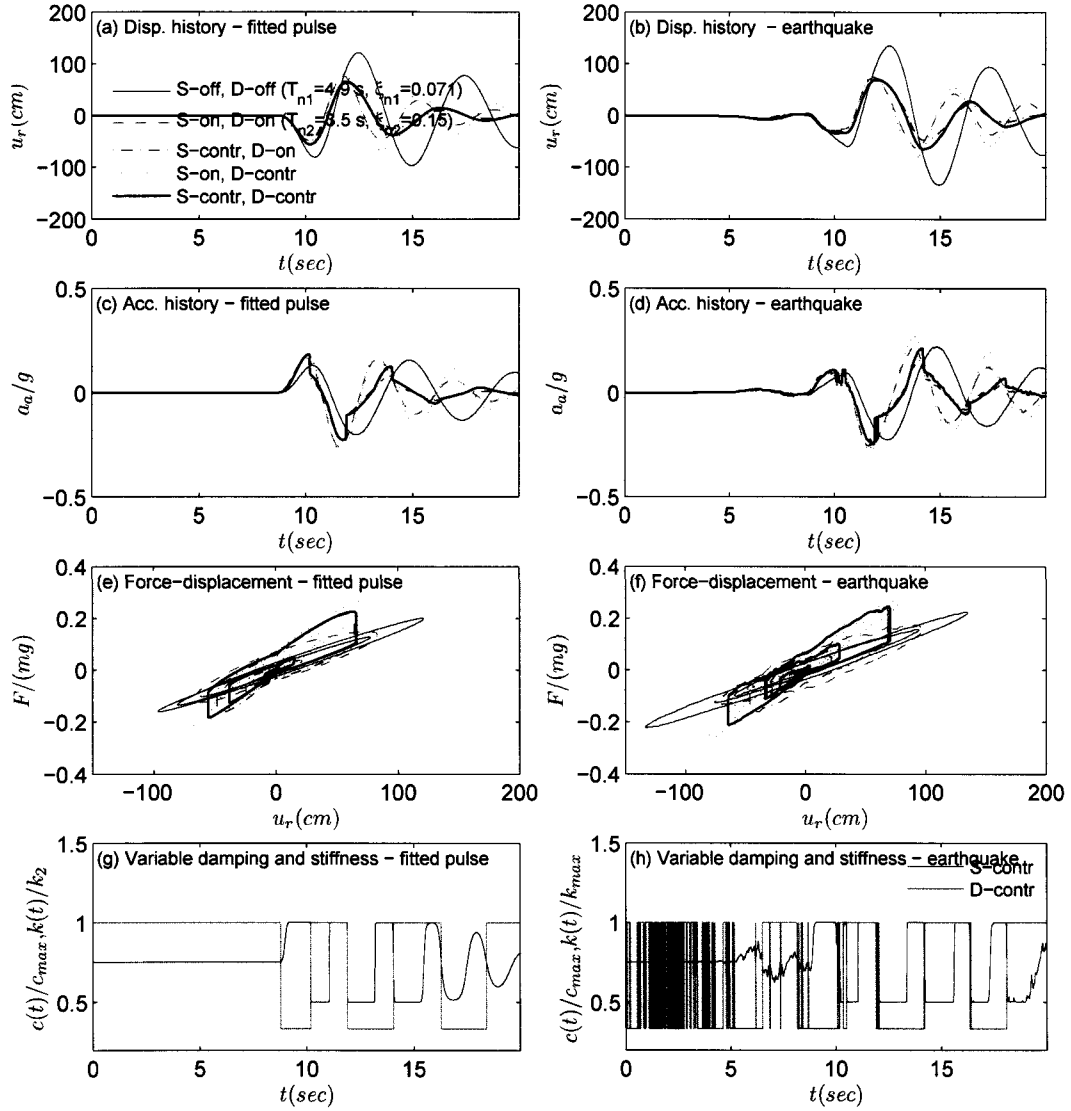


**Figure 5.34** Response time histories, force-displacement loops, and variable stiffness history of the SDOF system subjected to Lucerne-270 record and fitted pulse type A ( $T_p = 2.94$  s)

## 5.9 Concluding Remarks

Similar to passive systems, responses of sSDOF/sMDOF subjected to fitted cycloidal pulses provide good approximation to those of the actual records. The approximation is especially good for the higher period systems as commented above.

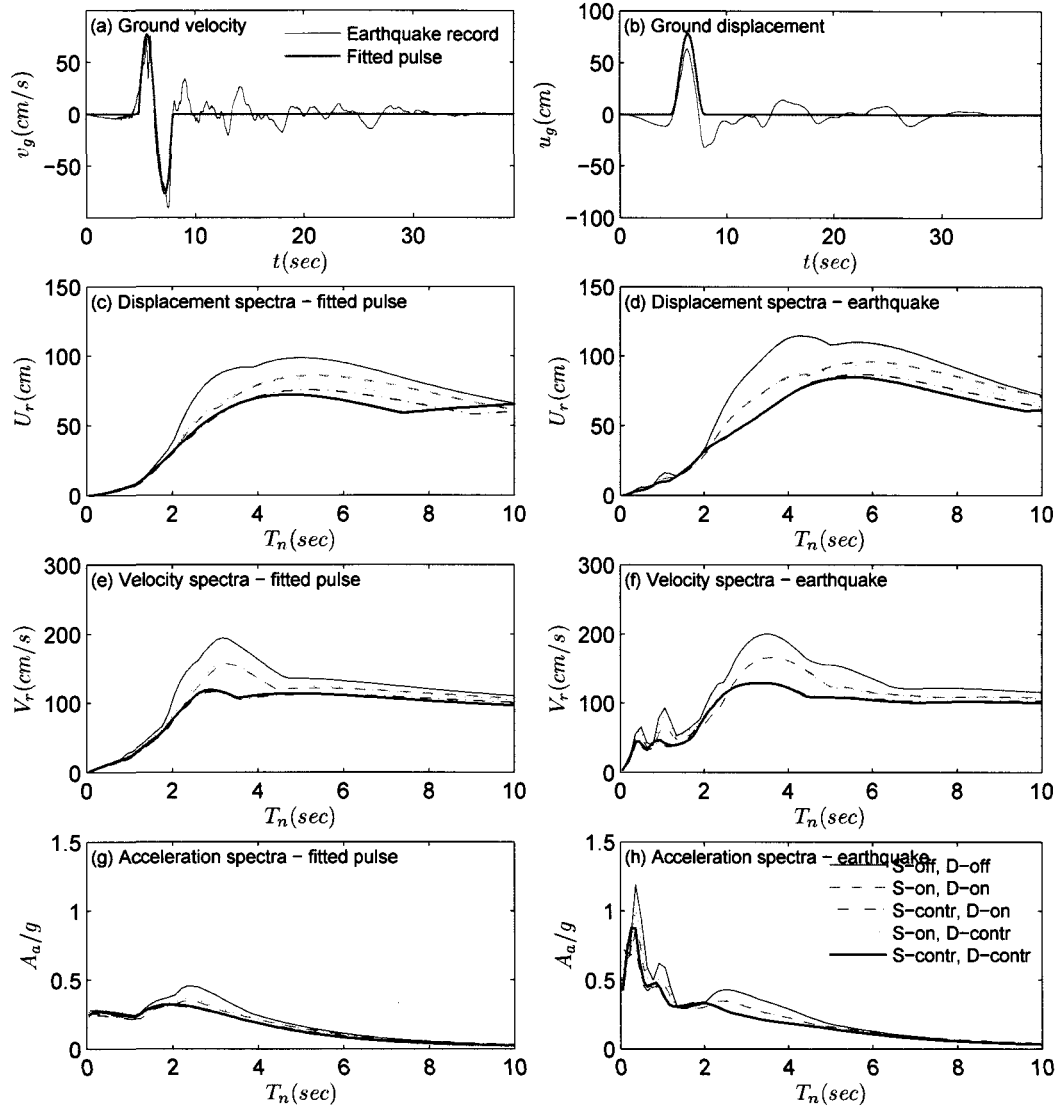


**Figure 5.35** Response spectra of the SDOF system subjected to El Centro #5-230-FN record and fitted pulse type B ( $T_p = 3.18$  s)

The variable structure control is very effective in reducing the response in the neighborhood of the resonant peaks of the passive systems for all types of pulses.

The Lyapunov control for semi-active damping is effective in reducing the response for pulse type excitations, however its performance is about same as 'pass. on' system (with

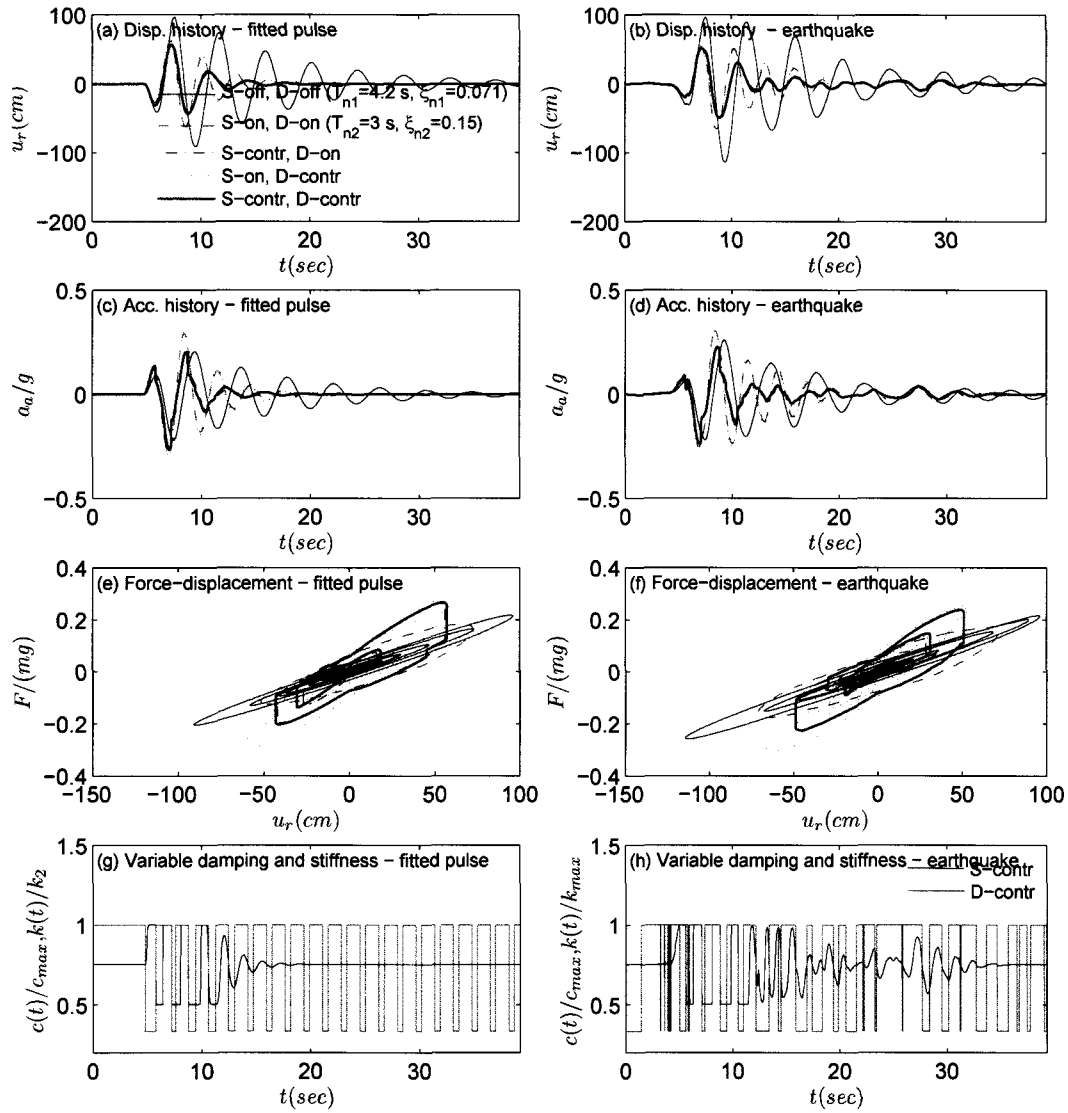


**Figure 5.36** Response time histories, force-displacement loops, and variable stiffness history of the SDOF system subjected to El Centro #5-230-FN record and fitted pulse type B ( $T_p = 3.18$  s)

higher damping). For Type-A pulse, the control leads to higher response in the high period region (higher  $T/T_p$  range, typically greater than  $T/T_p = 1.5 - 2.0$ ) of the response spectra. For other pulses (B,  $C_1$ ,  $C_2$ ), Lyapunov control leads to slightly lower response than 'pass. on' system and its performance improves for higher damped systems.

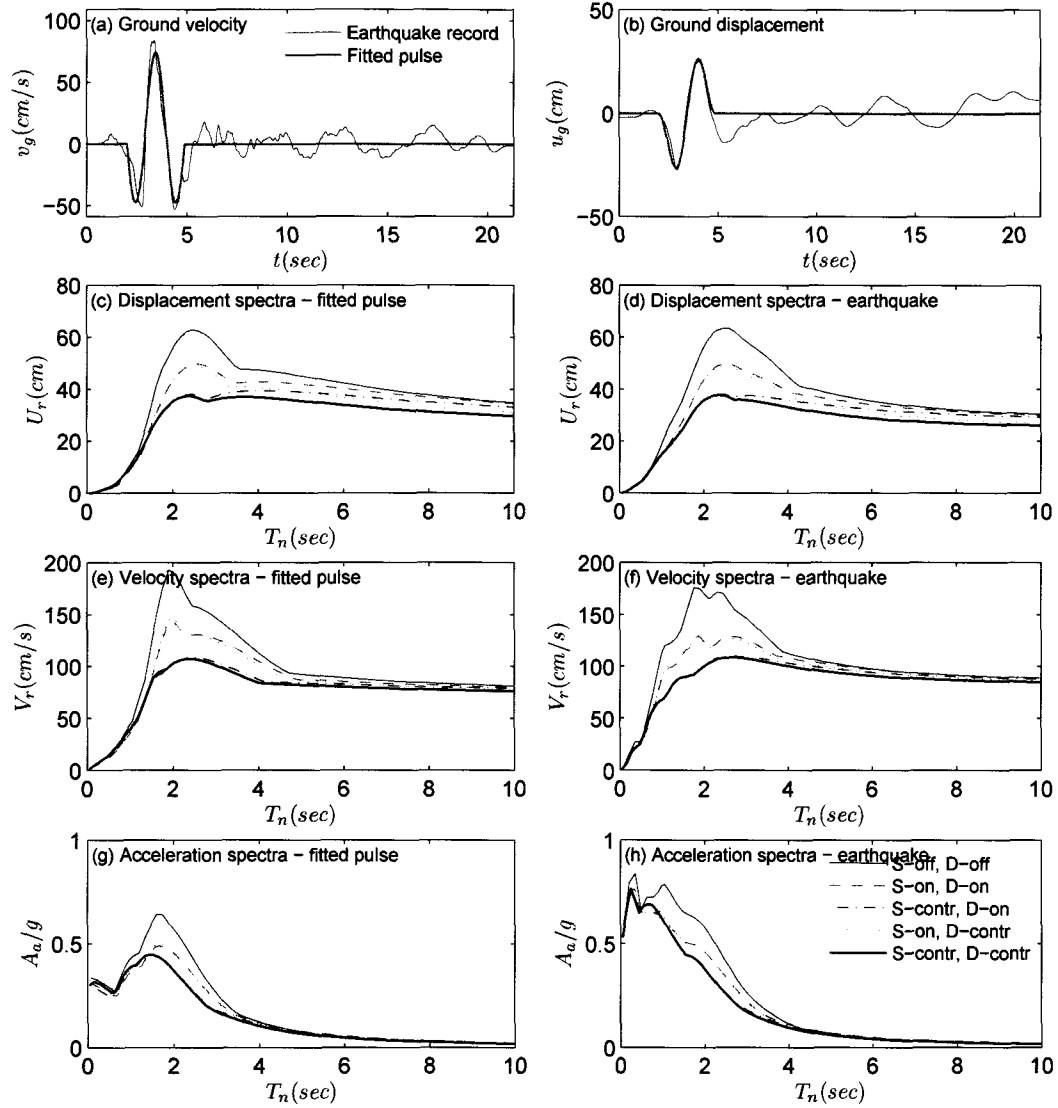


**Figure 5.37** Response spectra of the SDOF system subjected to Erzincan-NS record and fitted pulse type  $C_1$  ( $T_p = 2.00$  s)

When the two controls are executed simultaneously the benefits of both the controls are superimposed. Significant reduction in all the response quantities is observed for a wider range of  $T/T_p$  from spectra. This is because of the fact that the two control algorithms are effective in almost complementary  $T = T_p$  ranges.

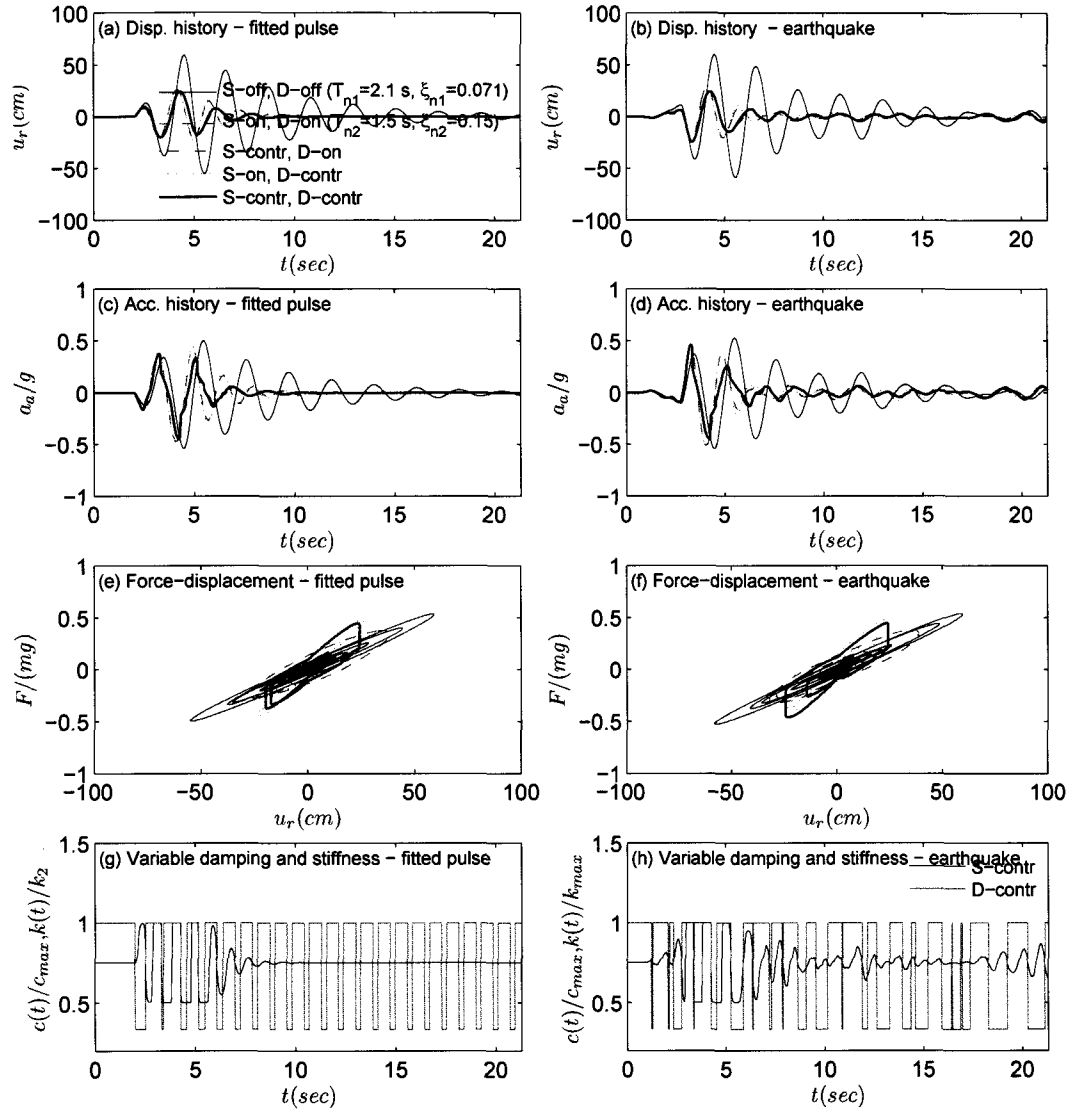


**Figure 5.38** Response time histories, force-displacement loops, and variable stiffness history of the SDOF system subjected to Erzincan-NS record and fitted pulse type  $C_1$  ( $T_p = 2.00$  s)

The control strategies - variable structure control for stiffness and Lyapunov control for damping - can be effectively implemented in long period structures such as base-isolated structures either separately or together to reduce vibrations.



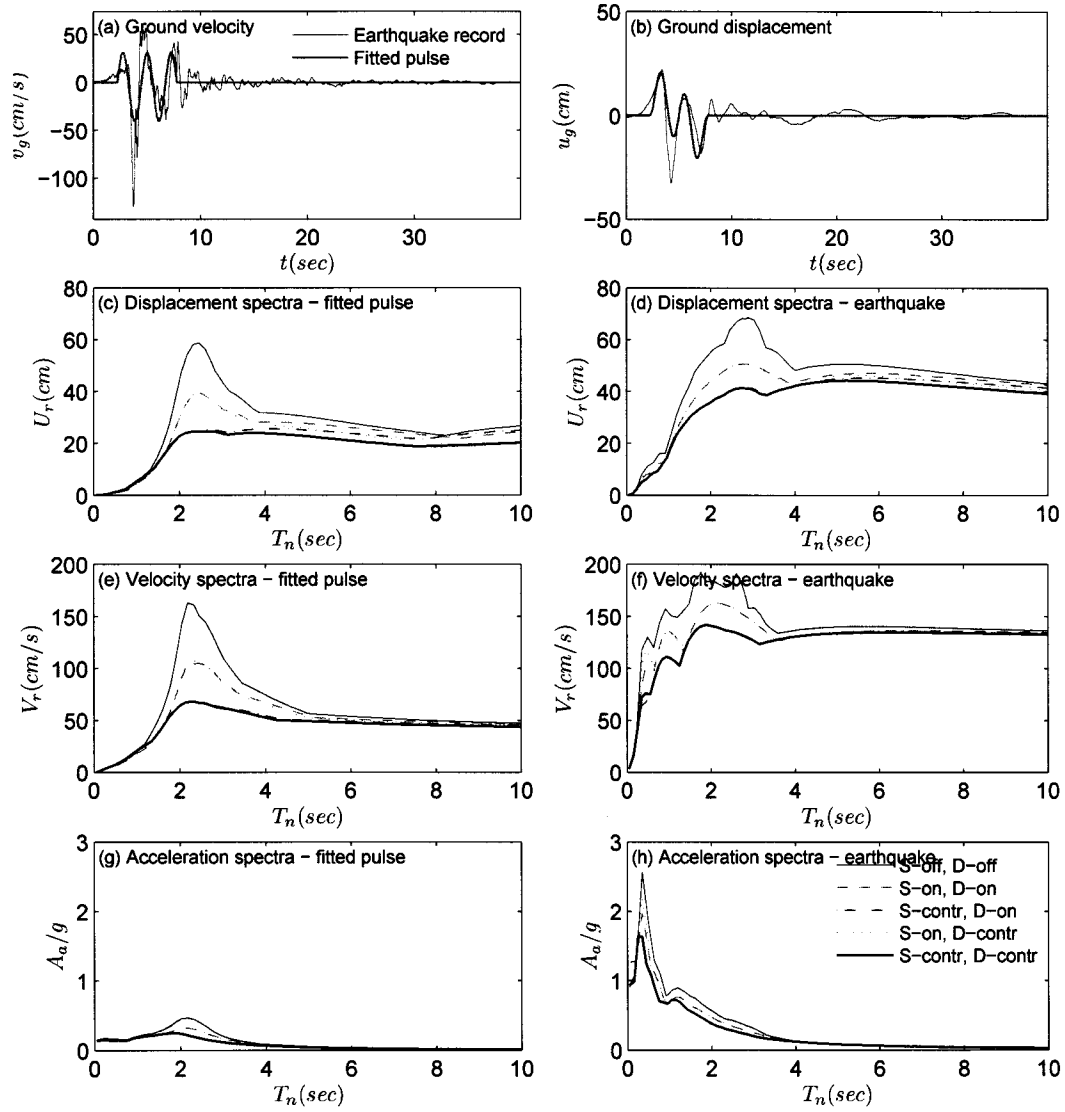


**Figure 5.39** Response spectra of the SDOF system subjected to Sylmar-360-FN record and fitted pulse type  $C_2$  ( $T_p = 2.25$  s)

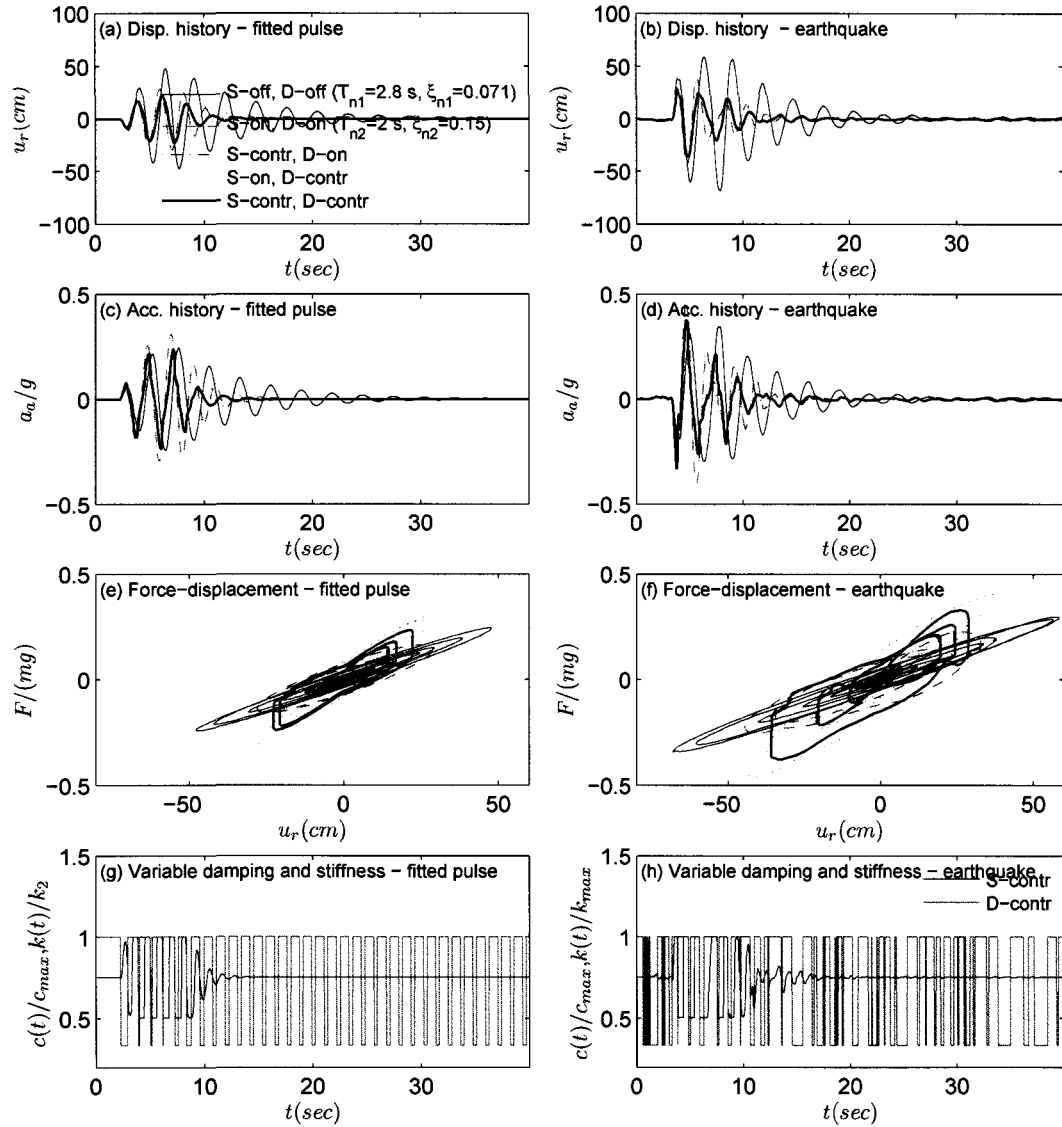


**Figure 5.40** Response time histories, force-displacement loops, and variable stiffness history of the SDOF system subjected to Sylmar-360-FN record and fitted pulse type  $C_2$  ( $T_p = 2.25$  s)

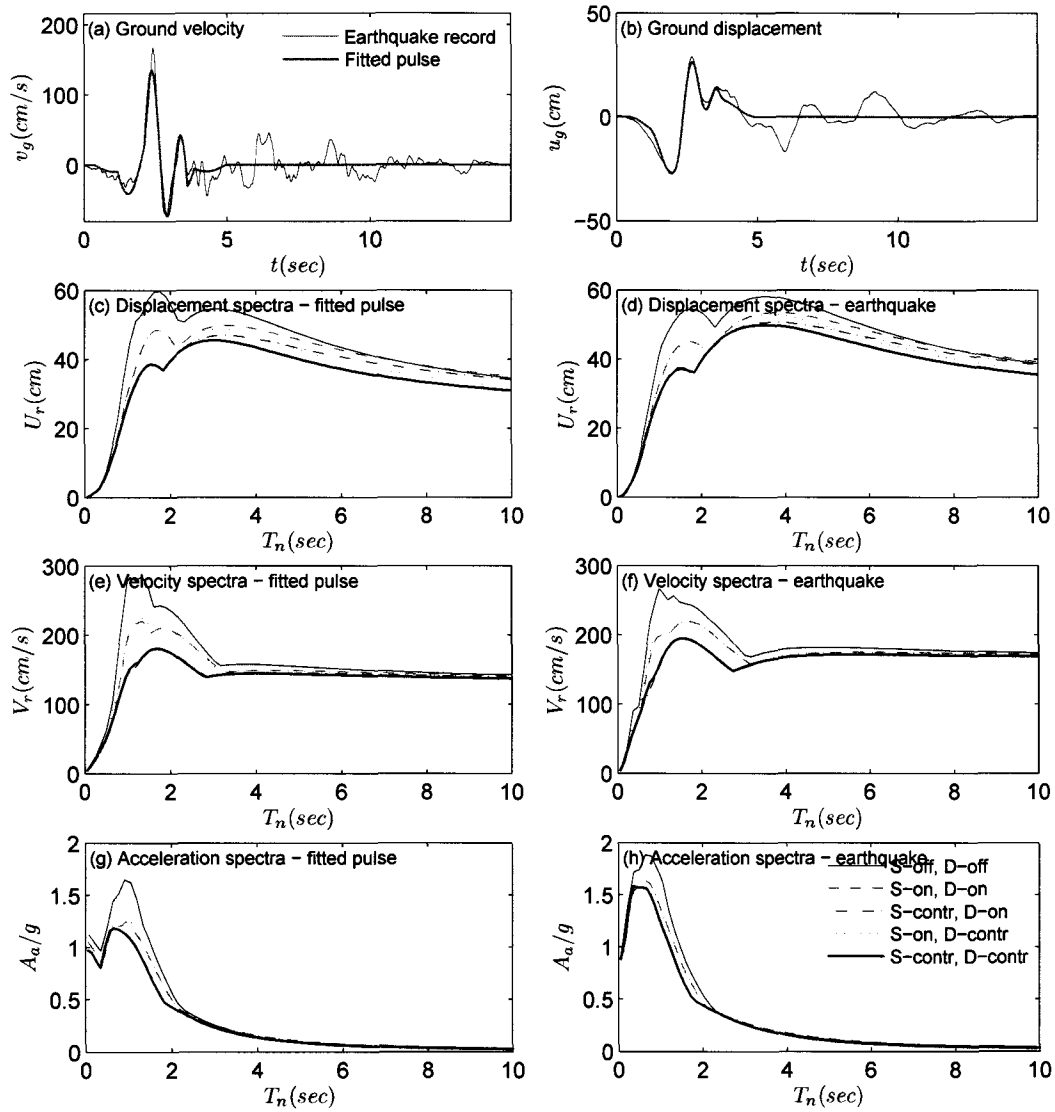


**Figure 5.41** Response spectra of the SDOF system subjected to Rinaldi-228-FN record and fitted pulse type  $C_1+C_1+C_1$  ( $T_p = [3.21 \ 1.87 \ 1.06] \text{ s}$ )

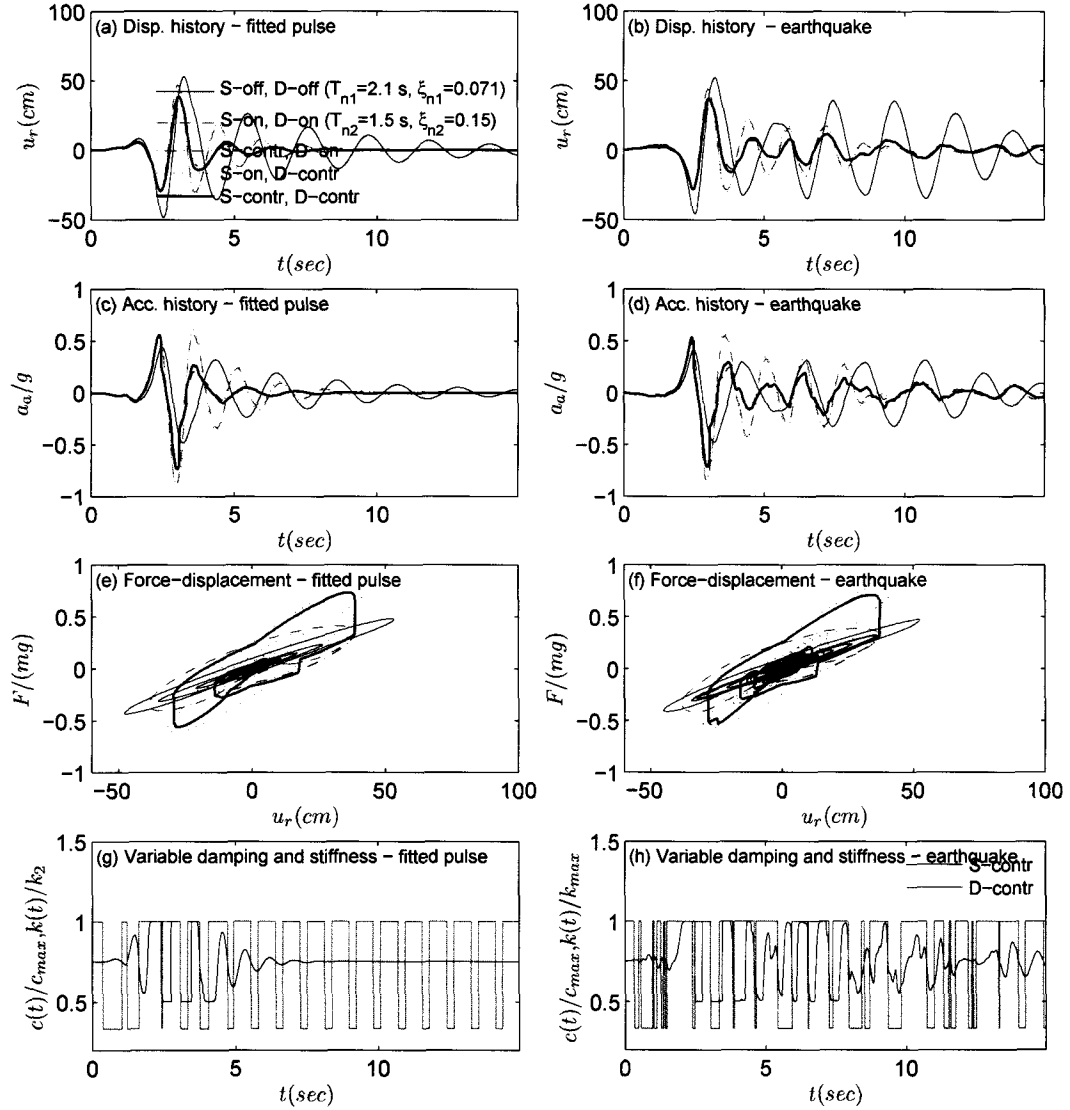


**Figure 5.42** Response time histories, force-displacement loops, and variable stiffness history of the SDOF system subjected to Rinaldi-228-FN record and fitted pulse type  $C_1+C_1+C_1$  ( $T_p = [3.21 \ 1.87 \ 1.06] \text{ s}$ )

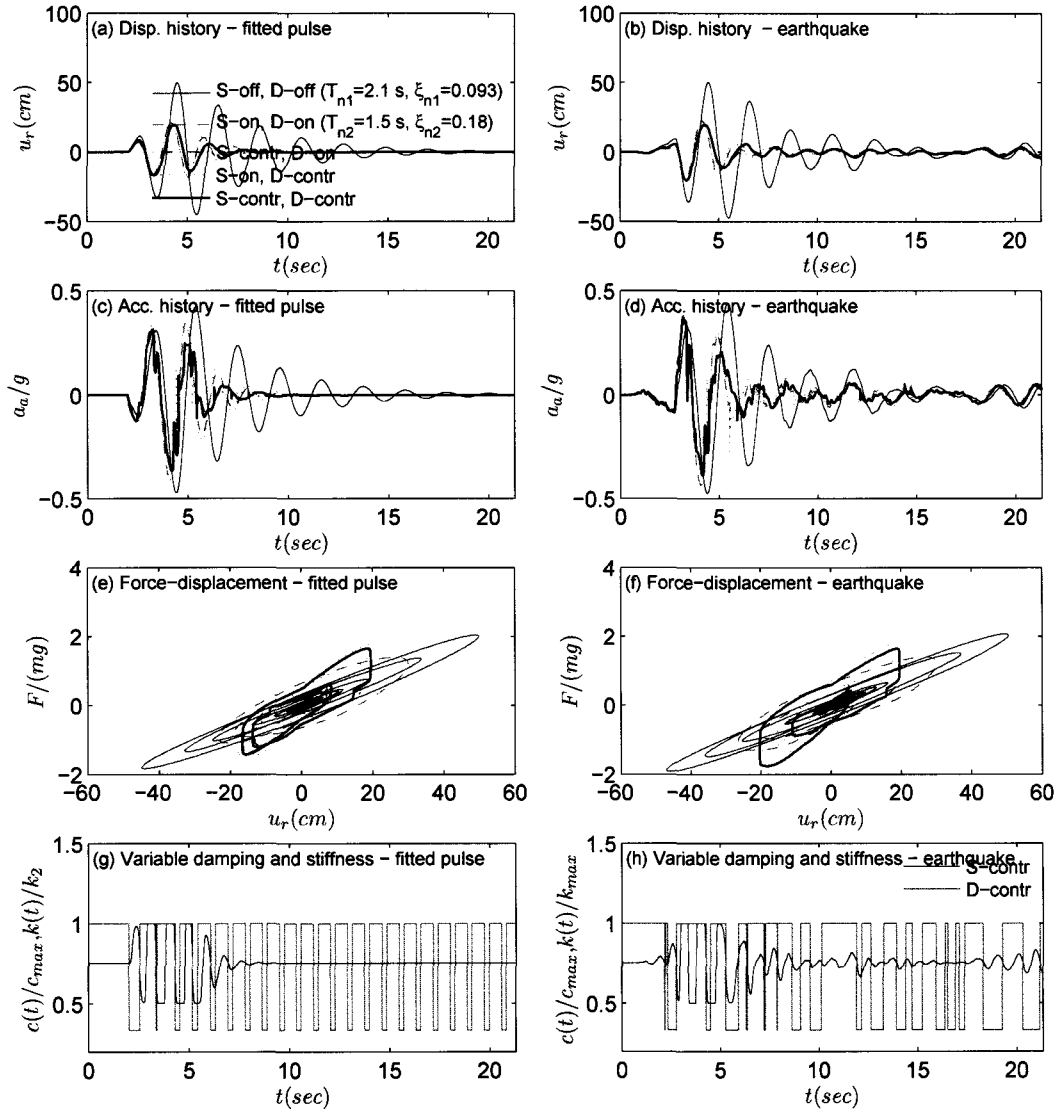


**Figure 5.43** Response time histories, force-displacement loops, and variable stiffness history of the 4-DOF system (base floor) subjected to Erzincan-NS record and fitted pulse type C1 ( $T_p = 2.00$  s)

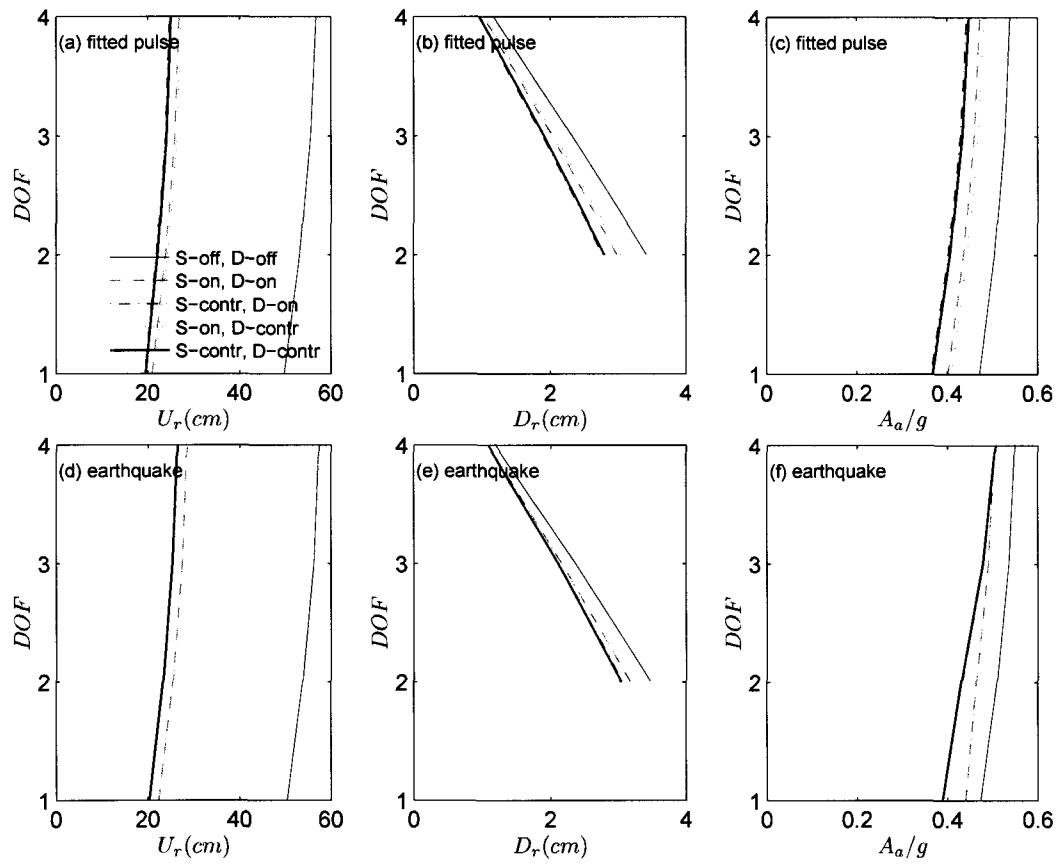


**Figure 5.44** Peak response profiles for 4-DOF system subjected to Erzincan-NS record and fitted pulse type  $C_1$  ( $T_p = 2.00$  s)

## Chapter 6

### Semi-active Single/Multiple Tuned Mass Dampers (sTMD/sMTMD) under Deterministic Excitations

In this chapter application of single and multiple semi-active variable stiffness tuned mass dampers (sTMD/ sMTMD) to reduce the the response of the main structure under several type of excitations is proposed. A new semi-active control algorithm is developed based on real-time frequency tracking of excitation signal by short time Fourier transform (STFT). It is shown that frequencies of simple harmonic signals can be tracked accurately using STFT. Based on this result, a parametric study is performed in the frequency domain to investigate the dynamic characteristics and effectiveness of sTMDs. Time history responses of single-degree-of-freedom (SDOF) and five-degree-of-freedom (5-DOF) main structures equipped with sTMDs at the roof level, subjected to harmonic, stationary, and non-stationary excitations are presented. sTMD/ sMTMD are most effective when they have low damping ratios and the excitation frequency can be tracked accurately. They are superior to their passive counterparts in reducing the response of the main structure both under force and base excitations.

#### 6.1 Modelling of MDOF System with MTMD

The main structure is modelled as a regular multistory shear building in which the structural properties (stiffness and damping) of each story are uniform. The model of  $N$ -story building with  $n$ -TMD at the roof is presented in Figure 6.1. The frequencies of the  $n$ -TMD are distributed around the natural frequency of the main structure, as shown in Figure 6.2. Several definitions and assumptions made in this study are listed below:

1. The main structure is symmetric and has uniform mass ( $M_1 = \dots = M_N = M_0$ ), stiffness ( $K_1 = \dots = K_N = K_0$ ) and stiffness-proportional damping ( $C_1 = \dots = C_N = C_0$ ) properties throughout its height.  $\omega_0 = \sqrt{K_0/M_0}$  and  $\zeta_0 = C_0/(2M_0\omega_0)$  are the parameters chosen such that the first mode frequency and damping ratio of the main structure have the desired values. First modal damping ratio of the main structure is 1 percent ( $\zeta_{n1} = 0.01$ ). Only SDOF ( $N = 1$ ) and 5-DOF ( $N = 5$ ) models of main structure are considered for simulations, without loss of generality.
2. TMDs are modelled as SDOF systems with same mass ( $m_1 = \dots = m_n = m_0$ ), damping ratio ( $\xi_1 = \dots = \xi_n = \xi_0$ ) but different stiffness ( $k_j : j = 1, 2, \dots, n$ ) properties.
3.  $\gamma_j$  is defined as the frequency of  $j^{th}$  TMD ( $\omega_j = \sqrt{k_j/m_j}$ ) normalized by first natural frequency of the main structure ( $\omega_{n1}$ ).  $\gamma_c = \omega_c/\omega_{n1}$  is the normalized frequency of the central TMD ( $\omega_c$  is the frequency of central TMD) and  $\gamma_0 (= \gamma_c - 1)$  is the offset of the central frequency of the MTMD from the natural frequency of the main structure.  $\Delta\gamma$  is the normalized frequency range of the MTMD.
4. Each TMD has a slightly different damping coefficient depending on  $\omega_j$  (i.e.  $c_j = 2m_0\omega_j\xi_j$ ).
5. Total mass ratio ( $\mu = \sum_1^n m_0 / \sum_1^N M_0$ ) is fixed to 1 percent such that  $j^{th}$  TMD mass ratio,  $\mu_j$  is equal to  $0.01/n$  in an n-TMD system.
6. The optimum frequency ratio  $\gamma_{opt}$  and damping ratio  $\xi_{opt}$  for TMD in a SDOF structure is obtained numerically using frequency response functions. The central frequency of MTMD is set to the same frequency of the single TMD; then optimum



frequency range and individual TMD damping ratio are computed numerically. In 5-DOF structure, TMD and MTMD are designed with respect to first mode properties of the 5-DOF structure ( $\mu = 0.0159$ ).

## 6.2 Modelling of MDOF System with SMTMD

There are several semi-active variable stiffness devices that are proposed and studied in the literature. As described earlier the SAIVS device has been developed by Nagarajiah (2000) with capability to continuously and independently vary stiffness. The SAIVS device, shown in Figure 6.3, consists of four spring elements arranged in a plane rhombus configuration with pivot joints at the vertices. A linear electromechanical actuator configures the aspect ratio of the rhombus configuration of SAIVS device. The aspect ratio changes between the fully closed (joint 1 and 2 are in closest position) and open configurations (joint 3 and 4 are in closest position) leading to maximum and minimum stiffness, respectively. A control algorithm and controller are used to regulate the linear electromechanical actuator. The power required by the actuator to change the aspect ratio of the device is nominal. The variable stiffness of the SAIVS device is described by:

$$k(t) = k_e \cos^2 (\theta(t)) \quad (6.1)$$

where  $k(t)$  = time varying stiffness of the device,  $k_e$  = the constant spring stiffness of each spring element, and  $\theta(t)$  = time varying angle of the spring elements with the horizontal in any position of the device. The SAIVS device has maximum stiffness in its fully closed ( $\theta(t) = 0$ ) and minimum stiffness in its fully open position ( $\theta(t) \sim \pi/2$ ). The device can be positioned in any configuration, changing its stiffness continuously, independently and smoothly between maximum and minimum stiffness.

The previous assumptions and definitions made for TMD and MTMD are also same

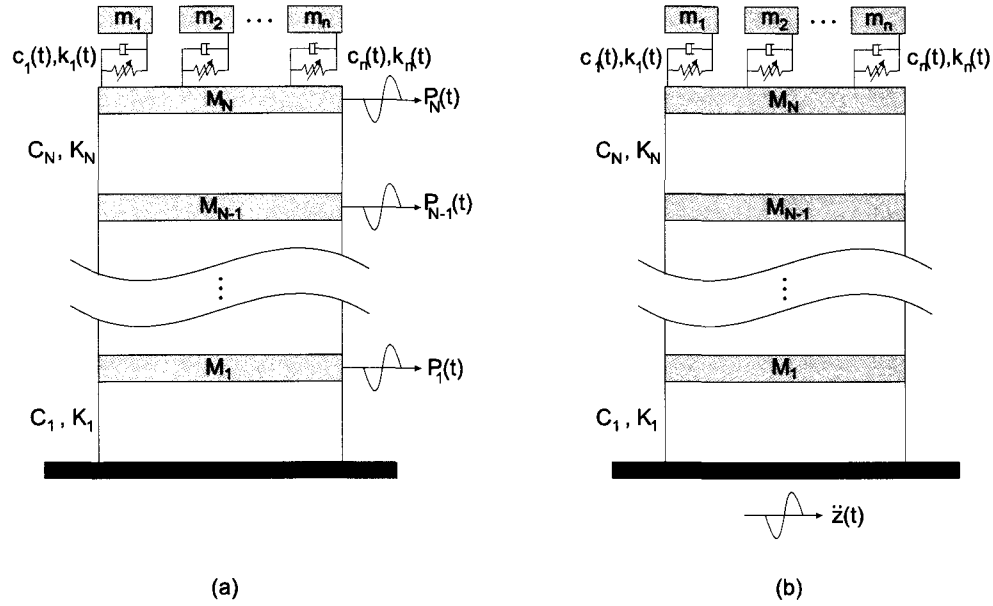


**Figure 6.1** MDOF Structural Model with sMTMD (varying  $k_1, \dots, k_n$ ) at the roof level: (a) Force Excited; (b) Base Excited

for sTMD and sMTMD except that in the semi-active case central TMD is tuned to excitation frequency ( $\omega(t)$ ) such that  $\gamma_c(t) = \omega(t)/\omega_{n1}$ . In each sTMD, damping coefficient is constant and damping ratio varies with time due to varying tuning frequency ( $c_j = 2\xi_j(t)\omega_j(t)m_0$ ). For convenience damping coefficient is defined with respect to selected reference damping ratio ( $\xi_j^{ref} = \xi^{ref}$ ) and corresponding passive TMD frequency ( $\omega_j^p$ ) such that  $c_j = 2\xi_j^{ref}\omega_j^p m_0 = 2\xi_j(t)\omega_j(t)m_0$ . Time dependent damping ratio can be obtained as  $\xi_j(t) = c_j/(2\omega_j(t)m_0)$  or  $\xi_j(t) = \xi_j^{ref}\omega_j^p/\omega_j(t)$ . For ease of presenting and interpreting the results, sTMDs are parameterized with respect to reference damping ratio, which corresponds to the damping ratio when sTMD is tuned to the same frequency of corresponding passive TMD.

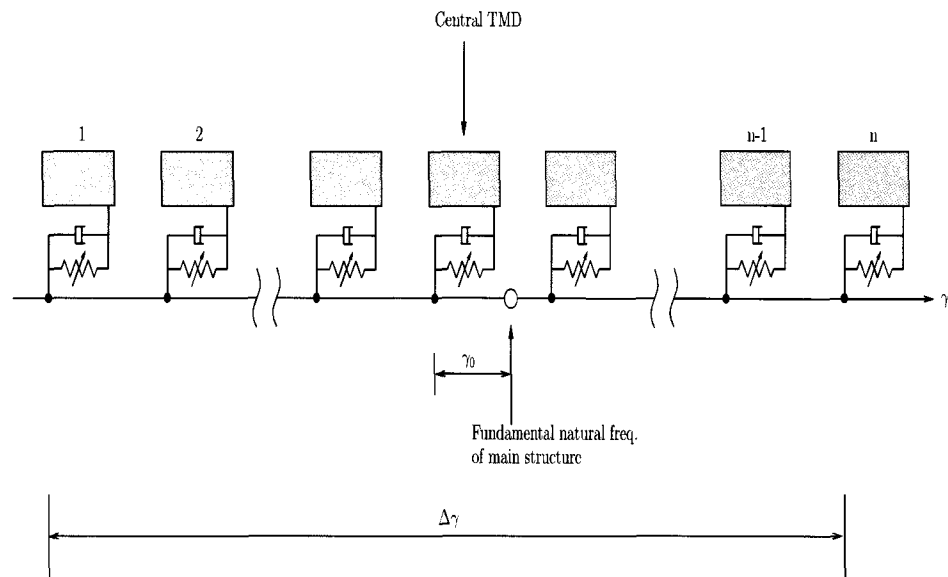


**Figure 6.2** Frequency Distribution of sMTMD

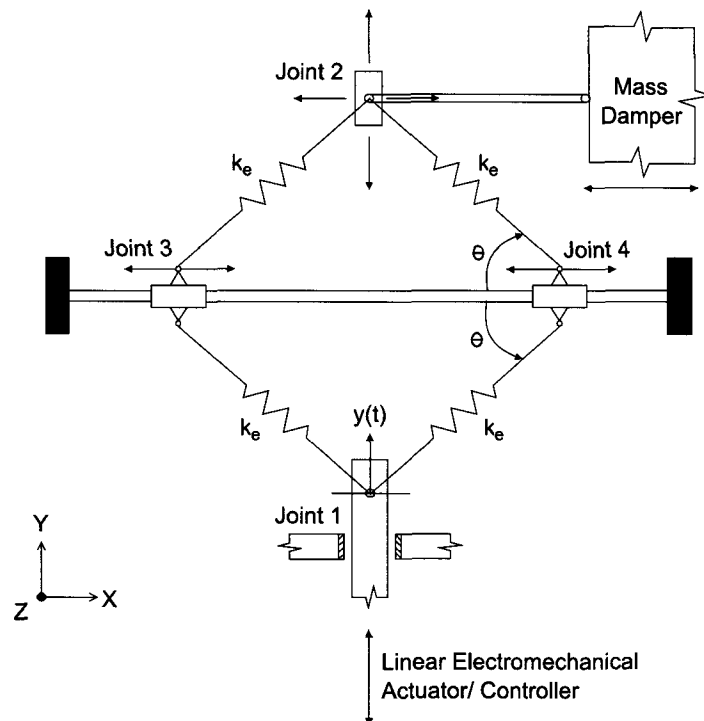


**Figure 6.3** Semiactive Independently Variable Stiffness (SAIVS) Device

### 6.3 Formulation

The equations of motion for the structural model given in Figure 6.1 can be written as follows

$$\mathbf{M}\ddot{\mathbf{X}} + \mathbf{C}\dot{\mathbf{X}} + \mathbf{K}\mathbf{X} = \mathbf{P}(t) \quad (6.2)$$

where  $\mathbf{X} = \{X_1 \ X_2 \ \dots \ X_N \ x_1 \ x_2 \ \dots \ x_n\}^T$  is the displacement vector in which  $X_i$  is the displacement of  $i^{th}$  story and  $x_j$  is the displacement of  $j^{th}$  TMD.  $\mathbf{P}(t)$  is the force vector. The coefficient matrices in Equation (6.2) are the mass, damping and stiffness matrices, defined as

$$\begin{aligned} \mathbf{M} &= \begin{bmatrix} M_1 & 0 & \dots & & \\ 0 & M_2 & 0 & \dots & \\ \vdots & 0 & \ddots & \ddots & \\ & \vdots & \ddots & M_N & \\ & & & & m_1 & 0 & \dots \\ & & & & 0 & m_2 & \ddots \\ & & & & \vdots & \ddots & \ddots \\ & & & & & & & m_n \end{bmatrix} \\ &= M_0 \begin{bmatrix} \mathbf{I} & \mathbf{0} \\ \mathbf{0} & \mu_0 \mathbf{I} \end{bmatrix} \\ &= M_0 \overline{\mathbf{M}} \end{aligned} \quad (6.3)$$

$$\begin{aligned}
\mathbf{C} &= \begin{bmatrix} \lceil C_1 + C_2 & -C_2 & 0 & \cdots & \rceil \\ -C_2 & C_2 + C_3 & -C_3 & \ddots & \\ 0 & -C_3 & C_3 + C_4 & \ddots & \\ \vdots & \ddots & \ddots & \ddots & -C_{N-1} \\ \lfloor & & -C_{N-1} & C_N + \lceil \sum_{j=1}^n c_j & -c_1 & -c_2 & \cdots & -c_n \rceil \\ & & & -c_1 & c_1 & 0 & \cdots & 0 \\ & & & -c_2 & 0 & c_2 & \ddots & \vdots \\ & & & \vdots & \vdots & \ddots & \ddots & \\ & & & \lfloor -c_n & & & & c_n \rfloor \end{bmatrix} \\
&= C_0 \overline{\mathbf{C}}
\end{aligned} \tag{6.4}$$

$$\begin{aligned}
\mathbf{K} &= \begin{bmatrix} \lceil K_1 + K_2 & -K_2 & 0 & \cdots & \rceil \\ -K_2 & K_2 + K_3 & -K_3 & \ddots & \\ 0 & -K_3 & K_3 + K_4 & \ddots & \\ \vdots & \ddots & \ddots & \ddots & -K_{N-1} \\ \lfloor & & -K_{N-1} & K_N + \lceil \sum_{j=1}^n k_j & -k_1 & -k_2 & \cdots & -k_n \rceil \\ & & & -k_1 & k_1 & 0 & \cdots & 0 \\ & & & -k_2 & 0 & k_2 & \ddots & \vdots \\ & & & \vdots & \vdots & \ddots & \ddots & \\ & & & \lfloor -k_n & & & & k_n \rfloor \end{bmatrix} \\
&= K_0 \overline{\mathbf{K}}
\end{aligned} \tag{6.5}$$

where  $\bar{\mathbf{M}}$ ,  $\bar{\mathbf{C}}$ ,  $\bar{\mathbf{K}}$  are the normalized mass, damping, stiffness matrices and  $\mu_0 = m_0/M_0$ .

The force vector is defined for force and base excitations as

$$\mathbf{P}(\mathbf{t}) = \begin{cases} \bar{\mathbf{P}}p(t) = \bar{\mathbf{P}}p_0 \bar{p}(t) & \text{(force excited)} \\ -\mathbf{M}\mathbf{1}\ddot{z}(t) = -M_0\bar{\mathbf{M}}\mathbf{1}\ddot{z}_0\bar{\ddot{z}}(t) & \text{(base excited)} \end{cases} \quad (6.6)$$

A reference response value,  $X_{0,st}$  is defined as  $X_{0,st} = p_0/K_0$  for force excitation and  $X_{0,st} = M_0\ddot{z}_0/K_0$  for base excitation. Substituting  $X_{0,st}$  in Equation (6.2) gives

$$\bar{\mathbf{M}}\ddot{\mathbf{X}} + 2\zeta_0\omega_0\bar{\mathbf{C}}\dot{\mathbf{X}} + \omega_0^2\bar{\mathbf{K}}\mathbf{X} = \begin{cases} \omega_0^2 X_{0,st} \bar{\mathbf{P}} \bar{p}(t) & \text{(force excited)} \\ -\omega_0^2 X_{0,st} \bar{\mathbf{M}}\mathbf{1} \bar{\ddot{z}}(t) & \text{(base excited)} \end{cases} \quad (6.7)$$

Dividing  $\mathbf{X}$ ,  $\dot{\mathbf{X}}$ ,  $\ddot{\mathbf{X}}$  by  $X_{0,st}$  leads to the normalized equations of motion as

$$\bar{\mathbf{M}} \bar{\ddot{\mathbf{X}}} + 2\zeta_0\omega_0\bar{\mathbf{C}} \bar{\dot{\mathbf{X}}} + \omega_0^2\bar{\mathbf{K}} \bar{\mathbf{X}} = \begin{cases} \omega_0^2 \bar{\mathbf{P}} \bar{p}(t) \\ -\omega_0^2 \bar{\mathbf{M}}\mathbf{1} \bar{\ddot{z}}(t) \end{cases} \quad (6.8)$$

Equations (6.7-8) can be solved by Newmark's method to obtain the actual or normalized response, respectively.

The aforementioned formulation can also be specified in state space in the form

$$\dot{\mathcal{X}} = \mathbf{A}\mathcal{X} + \mathbf{A}_s(t)\mathcal{X} + \mathbf{B}\mathbf{F} \quad (6.9)$$

where  $\mathcal{X} = [\mathbf{X} \quad \dot{\mathbf{X}}]^T$  is the state vector,  $\mathbf{A}$  is the time independent state matrix (corresponding to passive properties),  $\mathbf{A}_s(t)$  is the time dependent state matrix (corresponding to semi-active properties),  $\mathbf{B}$  is the input coupling matrix and  $\mathbf{F}$  is the input force vector.

## 6.4 Results

### 6.4.1 Excitation Frequency Tracking by STFT

In this chapter, the tracking of instantaneous frequency of the excitation is obtained by short-time Fourier transform (STFT). The details of STFT and frequency tracking algo-

rithm are given in Chapters 3 and 4. Mathematical expression of the short-time Fourier transform given in Equation (3.31) is repeated below:

$$STFT(t, \omega) = S(t, \omega) = \frac{1}{2\pi} \int s(\tau) w(\tau - t) e^{-j\omega\tau} d\tau \quad (6.10)$$

where  $s(t)$  is the signal and  $w(\tau - t)$  is the window function which is chosen to leave the signal more or less unaltered around the time  $t$  but to suppress the signal for times distant from the time of interest. The instantaneous (or dominant) frequency of the excitation signal at discrete time  $t_i$  is computed by

$$f_{inst.}(t_i) = \frac{\sum_{k=\max(1, i-m+1)}^i f_{inst.}(t_k) \max [|S(t_k, f)|^2]}{\sum_{k=\max(1, i-m+1)}^i \max [|S(t_k, f)|^2]} \quad (6.11)$$

where  $m$  is the number of points used for averaging, and  $f$  is the cyclic frequency in  $Hz$ .

The block diagram for control algorithm is given in Figure 6.4. Note that the feedback shown in Figure 6.4 is only for adjusting the proper positioning of semi-active device. Further details in implementation of frequency tracking and tuning of sTMD are shown in Figure 6.5. The procedure starts by selecting an STFT window and a window length ( $WL$ ) of  $n\Delta t$  ( $n + 1$  is the number of points in the window). Time lapse ( $TL$ ) of  $L\Delta t$  is the time period between successive windows. The signal is convolved with window function,  $w(\tau)$  and then zero padded for the desired frequency resolution. FFT power spectrum of each window is calculated and dominant excitation frequency is determined using Equation (6.11) by weighting the dominant frequency by its maximum FFT power at the corresponding time. Averaging length,  $AL = m\Delta t$  is the time length considered in weighted averaging of dominant frequency.  $t_0$  is the time required before starting to tune sTMDs to ensure sufficient number of signal points are collected for FFT calculation.

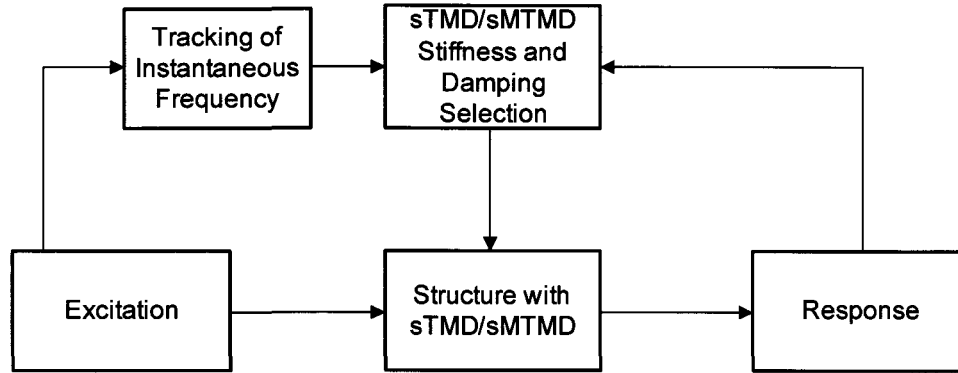


**Figure 6.4** Control Algorithm

Once  $t > t_0$ , dominant frequency is checked if it is satisfying the lower and upper frequency limits ( $f_{lim1}$  and  $f_{lim2}$ ). If it is within lower and upper bounds, sTMD is tuned to dominant frequency; if it is not within the bounds or  $t < t_0$ , sTMD is tuned to optimum passive TMD frequency.

Three kinds of harmonic signals and their frequency tracking are shown in Figure 6.6. The first signal is harmonic sinusoidal with 2 Hz frequency, the second signal is discrete sinusoidal sweep with consecutive 10 cycles of five frequencies (1.6 Hz, 1.8 Hz, 2.0 Hz, 2.2 Hz, 2.4 Hz) and the third signal is a linear chirp with frequencies varying from 1.6 Hz to 2.4 Hz continuously. A rectangular window with a length of  $WL = 2$  sec,  $TL = \Delta t = 0.02$  sec,  $AL = 1$  sec and  $t_0 = 1.5$  sec are used to track the harmonic sinusoidal signal; for the discrete sinusoidal sweep and linear chirp signal the parameters are selected as  $WL = 1$  sec,  $TL = \Delta t = 0.02$  sec,  $AL = 0.5$  sec and  $t_0 = 1.5$  sec. It is clear from the figure that such signals can be tracked satisfactorily.

#### 6.4.2 Parametric Study

In order to study the parameters governing sTMD/sMTMD systems, the main structure is considered as a SDOF system (representing the fundamental mode of a MDOF system).



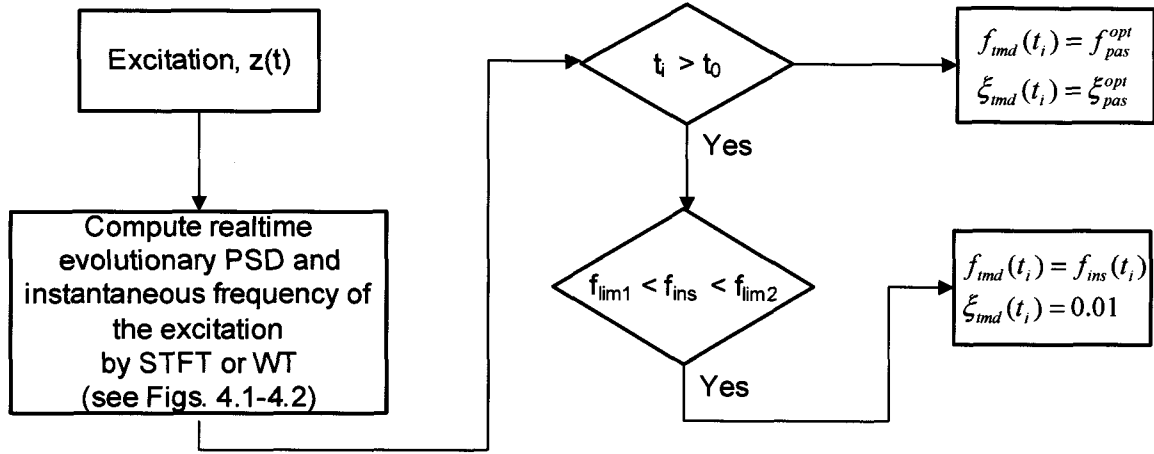


**Figure 6.5** Frequency Tracking by STFT and sTMD/sMTMD Tuning

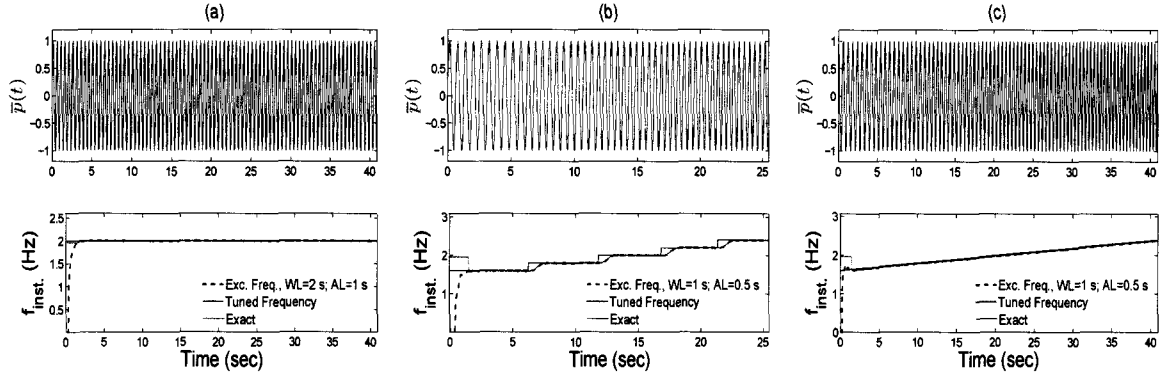


**Figure 6.6** Frequency Tracking for (a) Harmonic Sinusoidal; (b) Discrete Sinusoidal Sweep; (c) Linear Chirp

Thus, parameters  $\omega_0$ ,  $\zeta_0$  become natural frequency,  $\omega_n$  and damping ratio,  $\zeta_n$  of the main structure. The excitation is limited to harmonic loading and it is assumed that the exact excitation frequency is known or can be tracked as in Figure 6.6. Defining the excitation as a complex harmonic function such that  $\bar{p}(t) = e^{i\omega t}$ ,  $\bar{z}(t) = e^{i\omega t}$ , Equation (6.8) becomes

$$\bar{\mathbf{M}} \ddot{\bar{\mathbf{X}}} + 2\zeta_n \omega_n \bar{\mathbf{C}} \dot{\bar{\mathbf{X}}} + \omega_n^2 \bar{\mathbf{K}} \bar{\mathbf{X}} = \begin{cases} \omega_n^2 \bar{\mathbf{P}} e^{i\omega t} \\ -\omega_n^2 \bar{\mathbf{M}} \mathbf{1} e^{i\omega t} \end{cases} \quad (6.12)$$

Assuming a harmonic solution as

$$\bar{\mathbf{X}} = \Phi e^{i\omega t} \quad (6.13)$$

Substituting force and solution expressions above into equations of motion leads to

$$(-\omega^2 \bar{\mathbf{M}} + 2\zeta_n \omega_n i \omega \bar{\mathbf{C}} + \omega_n^2 \bar{\mathbf{K}}) \Phi = \begin{cases} \omega_n^2 \bar{\mathbf{P}} \\ -\omega_n^2 \bar{\mathbf{M}} \mathbf{1} \end{cases} \quad (6.14)$$

The frequency response functions can be obtained by

$$\left| \Phi \left( \frac{\omega}{\omega_n} \right) \right| = \begin{cases} \left| \left[ -\left( \frac{\omega}{\omega_n} \right)^2 \bar{\mathbf{M}} + 2\zeta_n \left( \frac{\omega}{\omega_n} \right) i \bar{\mathbf{C}} + \bar{\mathbf{K}} \right]^{-1} \bar{\mathbf{P}} \right| \\ \left| -\left[ -\left( \frac{\omega}{\omega_n} \right)^2 \bar{\mathbf{M}} + 2\zeta_n \left( \frac{\omega}{\omega_n} \right) i \bar{\mathbf{C}} + \bar{\mathbf{K}} \right]^{-1} \bar{\mathbf{M}} \mathbf{1} \right| \end{cases} \quad (6.15)$$

The frequency response functions of force excited and base excited SDOF are presented in Figure 6.7a,b for several passive and semi-active cases. The optimum frequency, damping ratio, and frequency range of passive TMDs are slightly different for force excited and base excited SDOF; however, they have very similar frequency response characteristics. In both figures, semi-active TMDs reduce the response more than their passive counterparts. The passive TMDs lose their efficiency beyond resonance frequency; they have even higher response than “No TMD” case for  $\omega/\omega_n < \sim 0.95$  and  $\omega/\omega_n > \sim 1.05$ .

The optimum frequency, damping ratio, and frequency range of passive TMDs in a forced-excited SDOF are computed numerically from the minimum value of curves shown in Figures 6.8 and 6.9. The corresponding figures for base excited SDOF are essentially the same; therefore are not presented here to avoid duplicity. As seen in both Figures 6.8 and 6.9, passive TMDs have specific optimum damping ratio and frequency range whereas sTMD decreases the response further as frequency range,  $\Delta\gamma$  and reference damping ratio,  $\xi_{stmd}^{ref}$  decrease. Also sMTMD can behave as a single sTMD by decreasing the frequency range to zero. Another interesting observation in Figure 6.9 is the convergence of maximum frequency response in both passive and semi-active TMDs as damping ratio of TMDs increases.

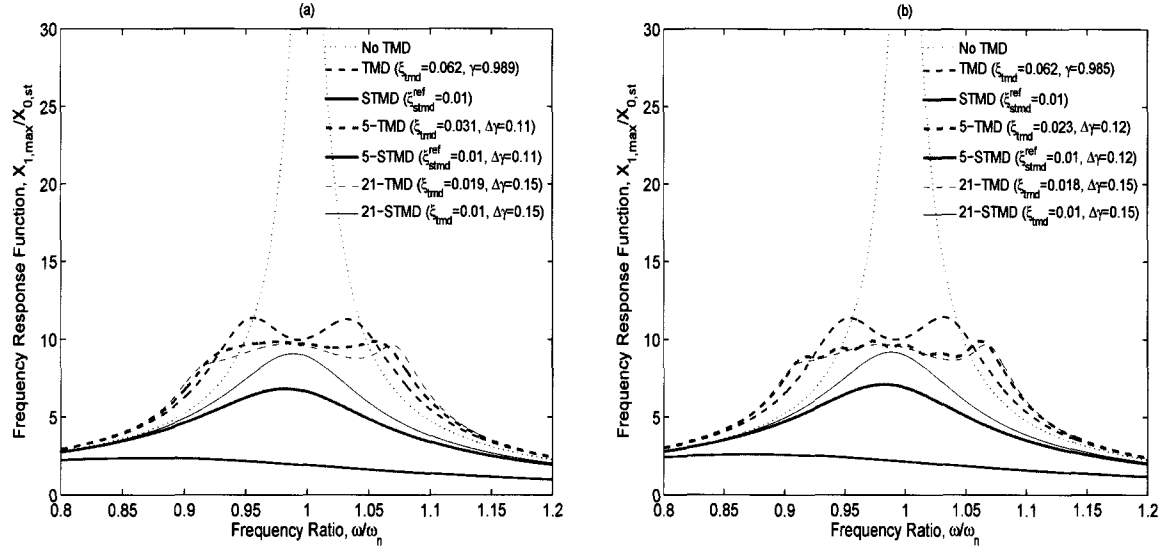


**Figure 6.7** Frequency Response Functions of SDOF Main Structure ( $\zeta_n = 0.01$ ) for No TMD, TMD, MTMD, sTMD, and sMTMD ( $\mu = 0.01$ ): (a) Force Excitation; (b) Base Excitation

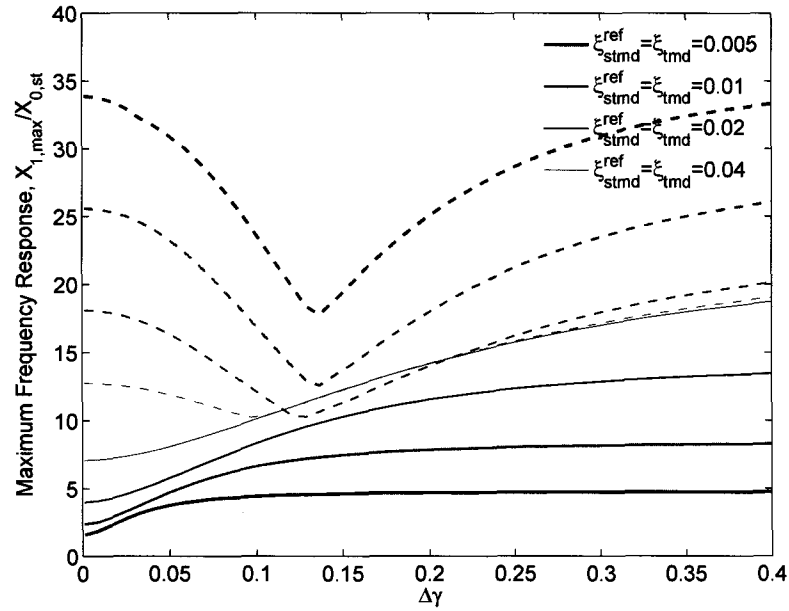


**Figure 6.8** Maximum Frequency Response versus MTMD Frequency Range for Force Excited SDOF with 5-TMD (---) / 5-sTMD (—)

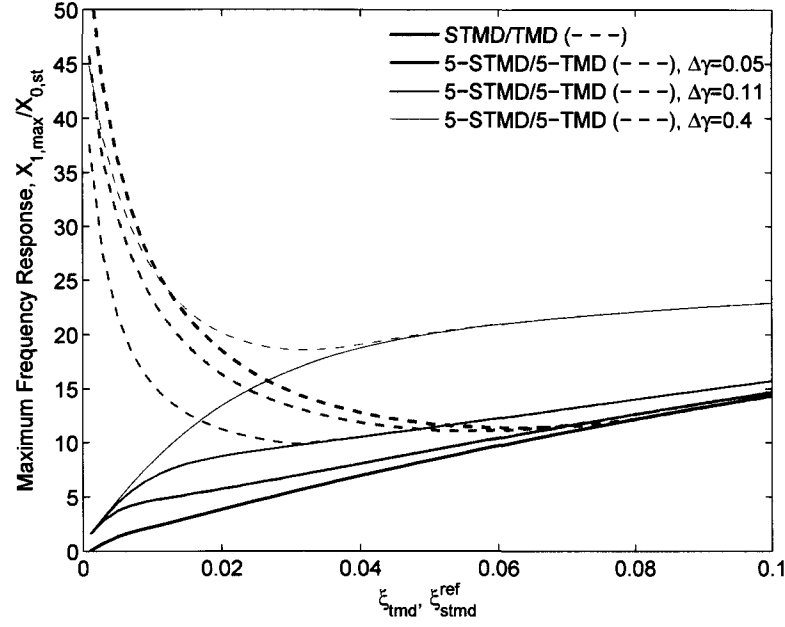


**Figure 6.9** Maximum Frequency Response versus TMD Damping Ratio for Force Excited SDOF with TMD/sTMD and 5-TMD(- - -) / 5-sTMD (—)

### 6.4.3 Time Histories

In order to verify the results in the previous section, SDOF and 5-DOF main structures equipped with real-time tuned sTMDs are subjected to several force and base excitations; time history responses are computed and compared with passive TMDs. Optimum parameters of passive TMD and 5-TMD used in the following simulations are listed in Table 6.1. For 5-DOF primary structure, mass ratio  $\mu$  is calculated with respect to first modal mass and optimum parameters are computed numerically for an equivalent SDOF primary structure.

First, time histories of force excited SDOF and 5-DOF structures are studied for harmonic type signals shown in Figure 6.6. The fundamental frequency is 2 Hz and fundamental damping ratio is 1% for both SDOF and 5-DOF system. Both structures equipped with sTMD and 5-sTMD are compared with their passive counterparts in Figures 6.10-15.

**Table 6.1**  $H_\infty$  Optimized Parameters of Passive TMD and 5-TMD

		Force Excitation		Base Excitation	
		SDOF	5-DOF	SDOF	5-DOF
TMD	$\mu$	0.01	0.0159	0.01	0.0159
	$\gamma$	0.989	0.982	0.985	0.978
	$\xi_{tmd}$	0.062	0.079	0.062	0.080
5-TMD	$\mu$	0.01	0.0159	0.01	0.0159
	$\gamma_c$	0.989	0.982	0.985	0.978
	$\Delta\gamma$	0.11	0.15	0.12	0.14
	$\xi_{tmd}$	0.031	0.031	0.023	0.035

For 2 Hz harmonic sinusoidal force excitation the dynamic response of SDOF is shown in Figure 6.10. Semiactive systems reduce the steady state response significantly. Similar performance is observed in 5-DOF structure in Figure 6.11, which shows the normalized maximum steady state story displacements (normalized with respect to maximum steady state response of top floor displacement of the original structure without any passive or semi-active TMDs). For harmonic sinusoidal excitation, sTMD leads to least response, which is in agreement with results in frequency domain (see Figure 6.9). However, it was found that if the excitation frequency is not tracked very accurately, 5-sTMD becomes more effective since 5-sTMD tuned within a small frequency range compensates for tracking errors.

Figures 6.12-13 show the responses of SDOF and 5-DOF structure under discrete sinusoidal sweep load with consecutive 10 cycles of five frequencies (1.6 Hz, 1.8 Hz, 2.0 Hz, 2.2 Hz, 2.4 Hz). Figure 6.12 presents the normalized maximum transient story displace-

ments (normalized with respect to maximum transient response of top floor displacement of the original structure without any passive or semi-active TMDs). In Figure 6.13, 5-sTMD leads to smaller response than others. 5-sTMD distributed within a small frequency range is more effective due to the capability to compensate the small errors/delays in frequency tracking in the excitation signal (Figure 6.6b). The third harmonic signal is a linear chirp with frequencies varying from  $1.6 \text{ Hz}$  to  $2.4 \text{ Hz}$  continuously. The responses shown in Figures 6.14 and 6.15 are similar to discrete sinusoidal sweep case. In linear chirp signal, the excitation frequency changes gradually with time and delay is small. The advantage of whole TMD mass tuned to single frequency in sTMD balances with benefit of covering a frequency range in 5-sTMD. Therefore, in both cases (Figures 6.14-15) sTMD and 5-sTMD perform almost same.

Time histories clearly prove that excitation frequency of simple harmonic signals can be tracked accurately and semi-active TMDs tuned to excitation frequency with low damping ratios outperforms their passive counterparts. Next, response to narrow band stationary excitation is evaluated. Therefore, dynamic responses of SDOF and 5-DOF structures (with  $0.5 \text{ Hz}$  fundamental frequency) under a narrow-band force excitation are studied. Figure 6.16 shows the excitation signal and its frequency tracking. STFT parameters are selected as: a rectangular window of length,  $WL = 4 \text{ sec}$ ,  $TL = \Delta t = 0.02 \text{ sec}$ ,  $AL = 1 \text{ sec}$  and  $t_0 = 3 \text{ sec}$ . As observed from Figures 6.17-18, sTMDs are superior than passive systems in reducing the response of the force excited SDOF and 5-DOF main structures. To investigate the potential of sTMDs in non-stationary signals, time history responses of SDOF and 5-DOF structures (with  $2 \text{ Hz}$  fundamental frequency) subjected to first 10 seconds of 1940 El Centro Earthquake are computed. The ground acceleration and frequency tracking are shown in Figure 6.19. Time step for the acceleration record is  $0.01 \text{ sec}$ . STFT parameters are selected as: a rectangular window of length,  $WL = 1 \text{ sec}$ ,  $TL = \Delta t = 0.01 \text{ sec}$ ,

$AL = 1 \text{ sec}$  and  $t_0 = 1.5 \text{ sec}$ . The main structure response is reduced most by sTMD and 5-sTMD as seen in Figures 6.20-21, whereas passive TMD and 5-TMD increase the response of the main structure.

It is also interesting to study the performance of sTMDs when some damage occurs in the main structure. 5-DOF main structure subjected to stationary and non-stationary excitations (shown in Figures 6.16a and 6.19a, respectively) is considered. The damage is modelled such that  $K_0$  reduces to  $0.8 K_0$  at the first story. Figures 6.22-23 show the top floor displacement and normalized maximum response of 5-DOF structure ( $f_{n1} = 0.5 \text{ Hz}$ ) subjected to stationary excitation presented in Figure 6.16a. The damage is a step function at  $t = 20 \text{ sec}$ . Similarly, Figures 6.24-25 show the top floor displacement and normalized maximum response of 5-DOF structure ( $f_{n1} = 2 \text{ Hz}$ ) subjected to first 10 seconds of 1940 El Centro Earthquake presented in Figure 6.16a. The damage is a step function at  $t = 2.5 \text{ sec}$ . In both cases semi-active TMDs have superior performance compared to passive ones. sTMDs have significant potential against stationary and non-stationary signals as evident from preliminary simulations presented here. A more extensive study is needed to generalize the results of this study for random excitations.

## 6.5 Concluding Remarks

For harmonic signals, if the excitation frequency is known or tracked very accurately, single sTMD leads to the least response of the main structure compared to multiple sTMDs, since sTMD has the advantage of greater mass tuned to exact excitation frequency. But in practice, the excitation frequency is either not known or can be tracked with some error and/or delay. Therefore, multiple sTMDs distributed within a small frequency range may be more effective due to the capability to compensate the small errors/delays in frequency

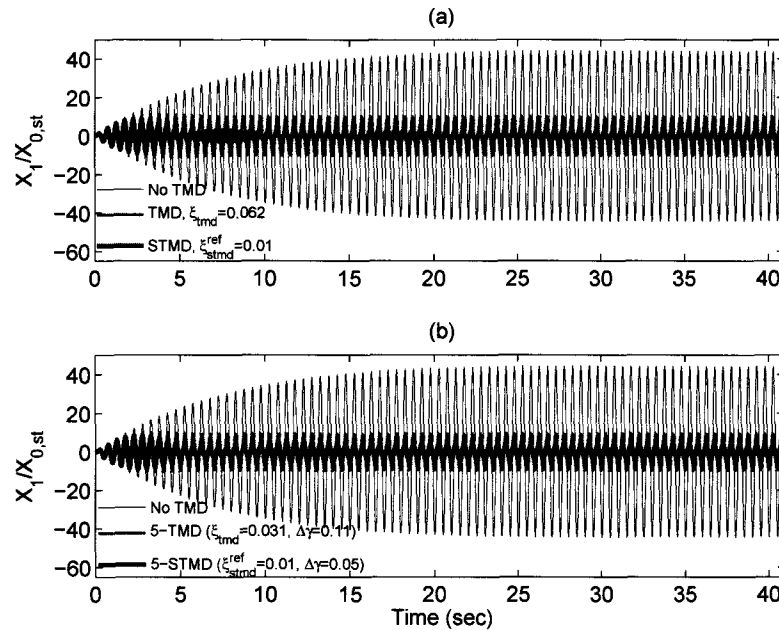


**Figure 6.10** Dynamic Response of Force Excited SDOF Main Structure ( $f_n = 2 \text{ Hz}$ ) under Harmonic Sinusoidal Load ( $f = 2 \text{ Hz}$ ): (a) No TMD, TMD, sTMD; (b) No TMD, MTMD, sMTMD

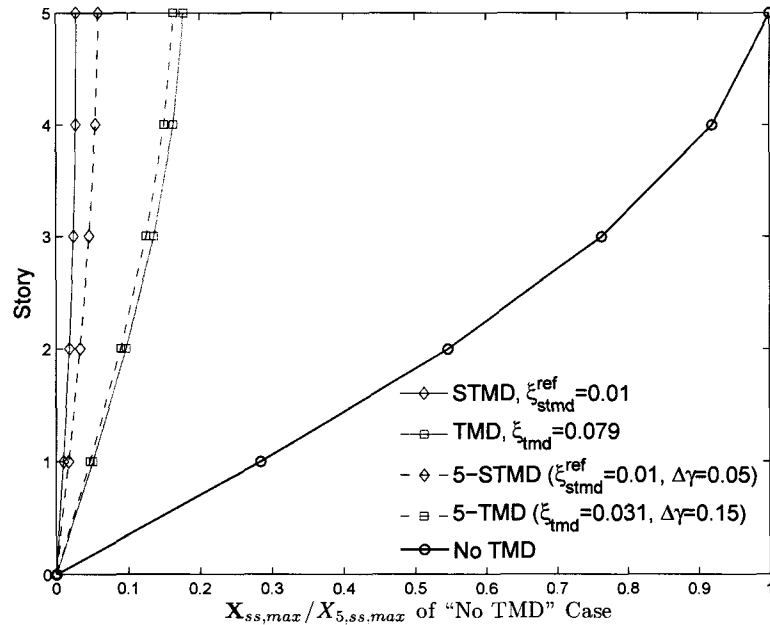


**Figure 6.11** Maximum Steady-State Response of Force Excited 5-DOF Main Structure ( $f_{n1} = 2 \text{ Hz}$ ) under Harmonic Sinusoidal Loading ( $f = 2 \text{ Hz}$ ) for No TMD, TMD, MTMD, sTMD, sMTMD



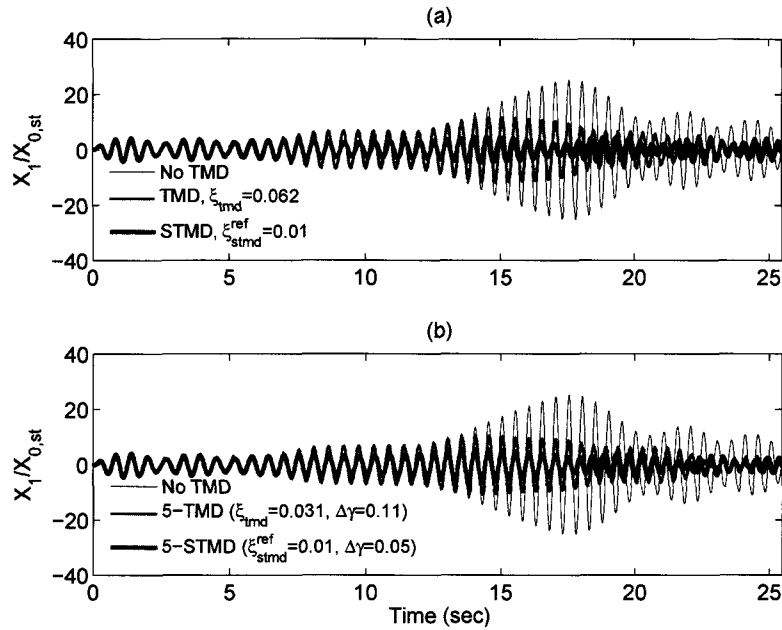


**Figure 6.12** Dynamic Response of Force Excited SDOF Main Structure ( $f_n = 0.5 \text{ Hz}$ ) under Discrete Sinusoidal Sweep Load ( $1.6 \text{ Hz} < f < 2.4 \text{ Hz}$ ): (a) No TMD, TMD, sTMD; (b) No TMD, MTMD, sMTMD

tracking and/or randomness in the excitation signal. If the sMTMD frequency range is increased further, its effectiveness would decrease because of distributing the mass away from the resonance frequency and sTMD would be superior again in agreement with results of parametric study.

MTMD has an optimum frequency range and an optimum damping ratio for a given number of TMDs similar to optimum frequency and damping ratio of a single TMD. Once the number of TMDs is decided, optimum values of the frequency range and damping ratio can be found for the design of MTMD. In case of sMTMD, there are no specific optimum values. The lower the damping ratio and the frequency range, the better performance sMTMD will have for the mono-component harmonic signals or random signals with significant energy at a specific instantaneous (dominant) frequency.

sMTMD can also behave as a single sTMD in real-time by reducing the frequency

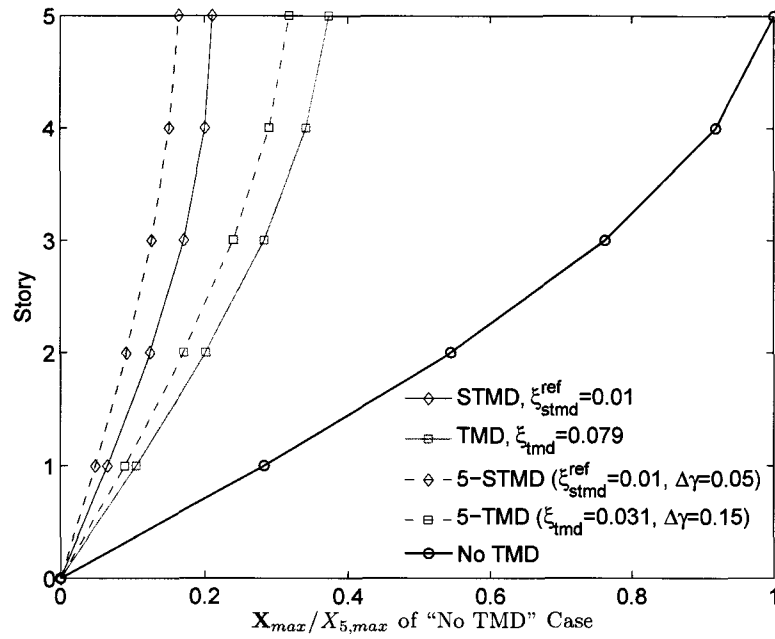


**Figure 6.13** Maximum Transient Response of Force Excited 5-DOF Main Structure ( $f_{n1} = 2 \text{ Hz}$ ) under Discrete Sinusoidal Sweep Loading ( $1.6 \text{ Hz} < f < 2.4 \text{ Hz}$ ) for No TMD, TMD, MTMD, sTMD, sMTMD

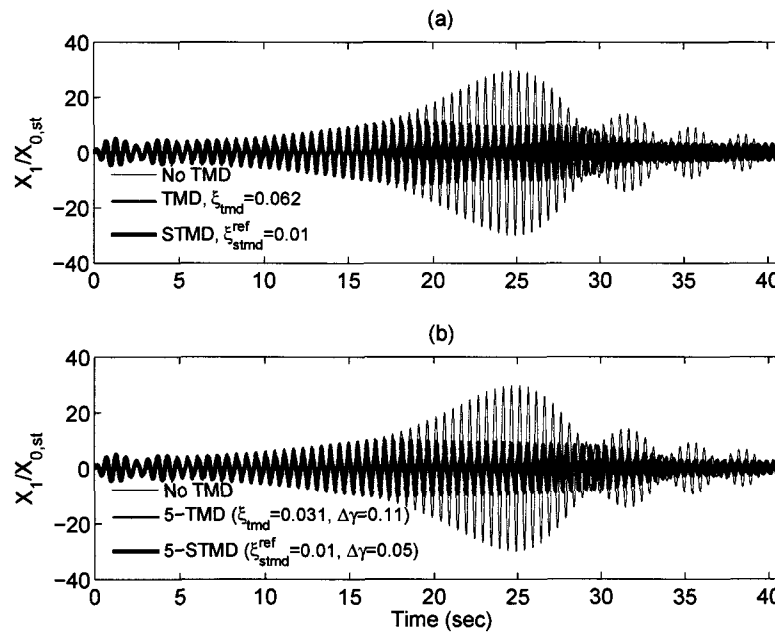


**Figure 6.14** Dynamic Response of Force Excited SDOF Main Structure ( $f_n = 2 \text{ Hz}$ ) under Linear Chirp Load ( $1.6 \text{ Hz} < f < 2.4 \text{ Hz}$ ): (a) No TMD, TMD, sTMD; (b) No TMD, MTMD, sMTMD

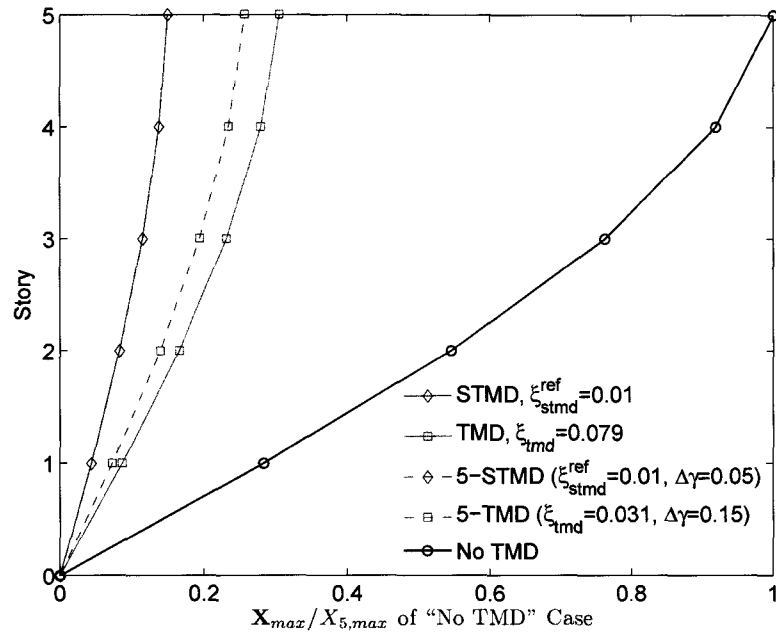


**Figure 6.15** Maximum Transient Response of Force Excited 5-DOF Main Structure ( $f_{n1} = 2 \text{ Hz}$ ) under Linear Chirp Loading ( $1.6 \text{ Hz} < f < 2.4 \text{ Hz}$ ) for No TMD, TMD, MTMD, sTMD, sMTMD

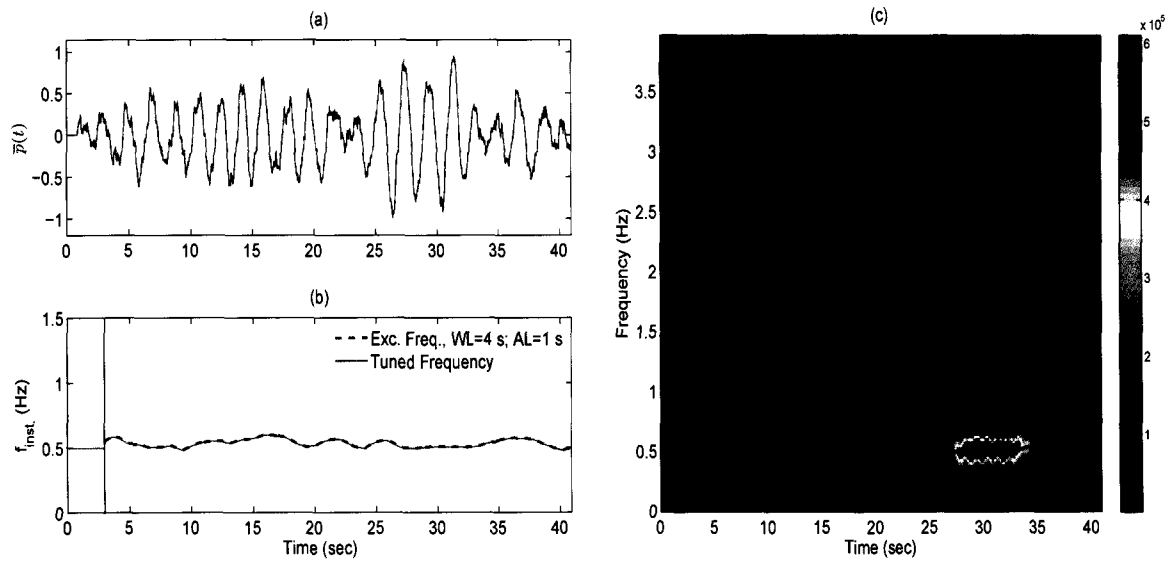


**Figure 6.16** (a) Narrow Band Stationary Excitation; (b) Frequency Tracking; (c) STFT Spectrum

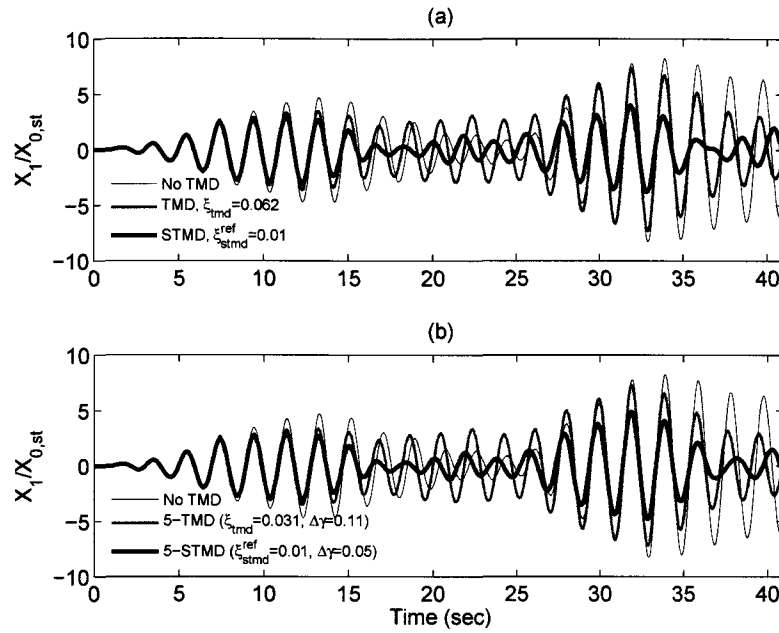


**Figure 6.17** Dynamic Response of Force Excited SDOF Main Structure ( $f_n = 0.5 \text{ Hz}$ ) under Stationary Excitation: (a) No TMD, TMD, sTMD; (b) No TMD, MTMD, sMTMD

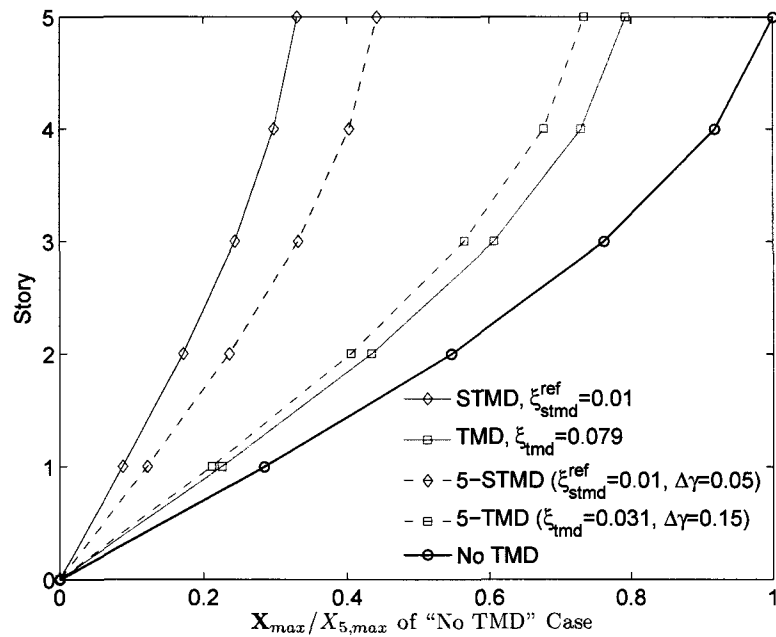


**Figure 6.18** Maximum Transient Response of Force Excited 5-DOF Main Structure ( $f_{n1} = 0.5 \text{ Hz}$ ) under Stationary Excitation for No TMD, TMD, MTMD, sTMD, sMTMD

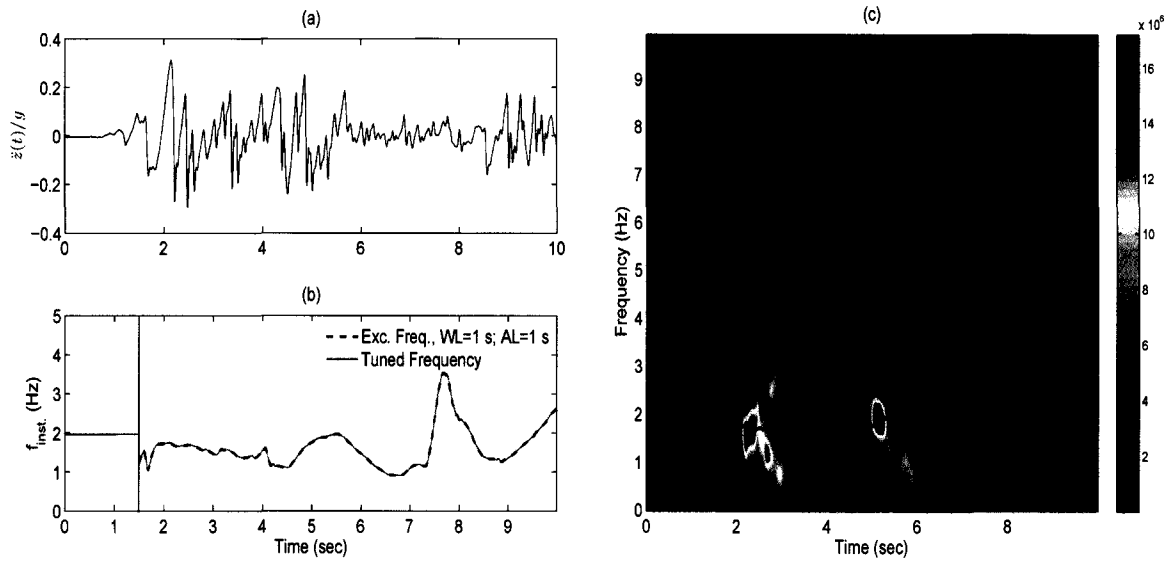


**Figure 6.19** (a) 1940 El Centro Earthquake ; (b) Frequency Tracking; (c) STFT Spectrum

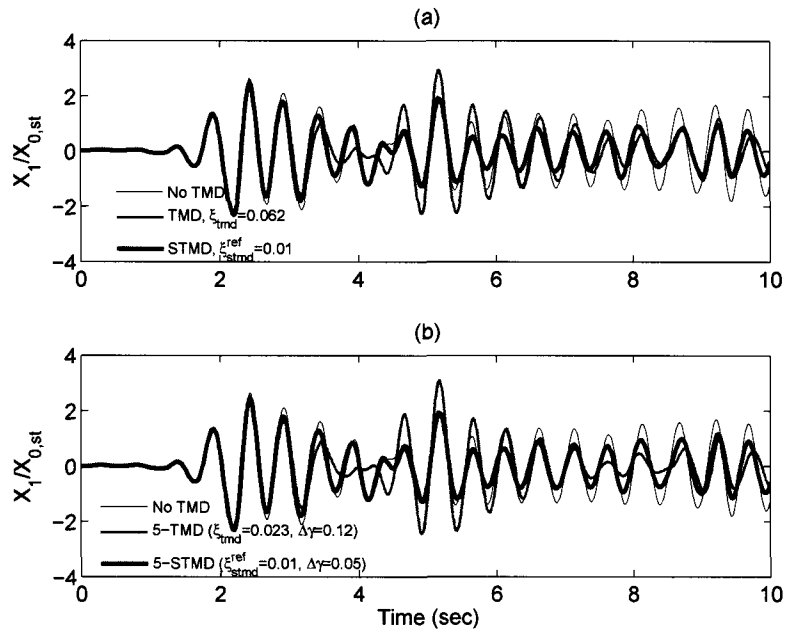


**Figure 6.20** Dynamic Response of Base Excited SDOF Main Structure ( $f_n = 2 Hz$ ) under 1940 El Centro Earthquake: (a) No TMD, TMD, sTMD; (b) No TMD, MTMD, sMTMD

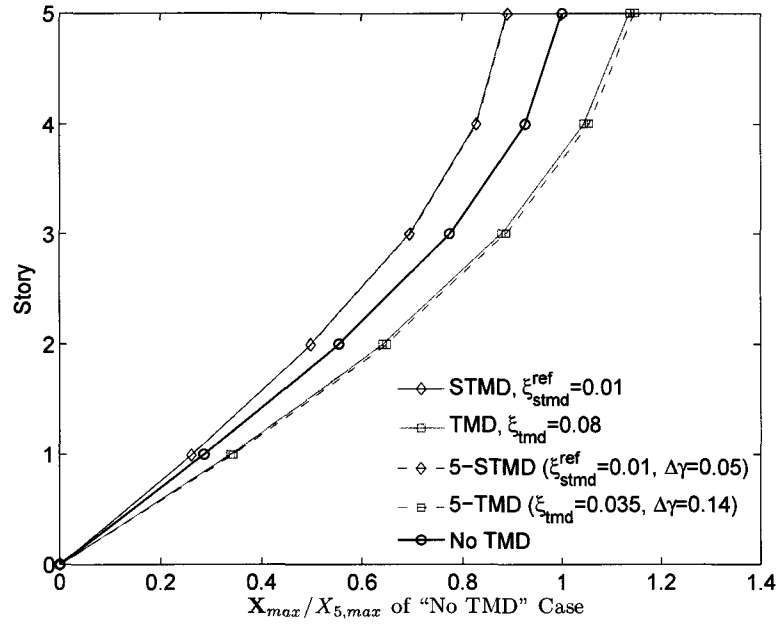


**Figure 6.21** Maximum Transient Response of Base Excited 5-DOF Main Structure ( $f_{n1} = 2 \text{ Hz}$ ) under 1940 El Centro Earthquake for No TMD, TMD, MTMD, sTMD, sMTMD

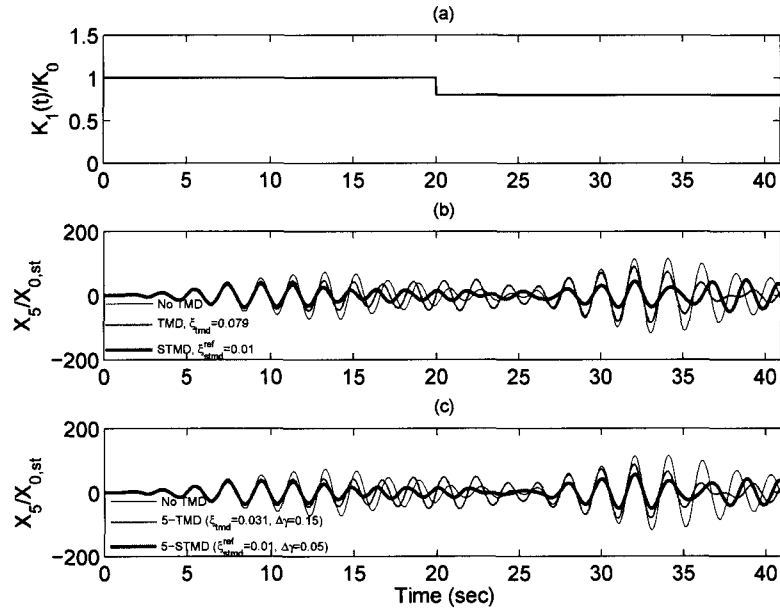


**Figure 6.22** Top Floor Displacement of Force Excited 5-DOF Main Structure ( $f_{n1} = 0.5 \text{ Hz}$ ) under under Stationary Excitation: (a) Step Stiffness Change (b) No TMD, TMD, sTMD; (c) No TMD, MTMD, sMTMD

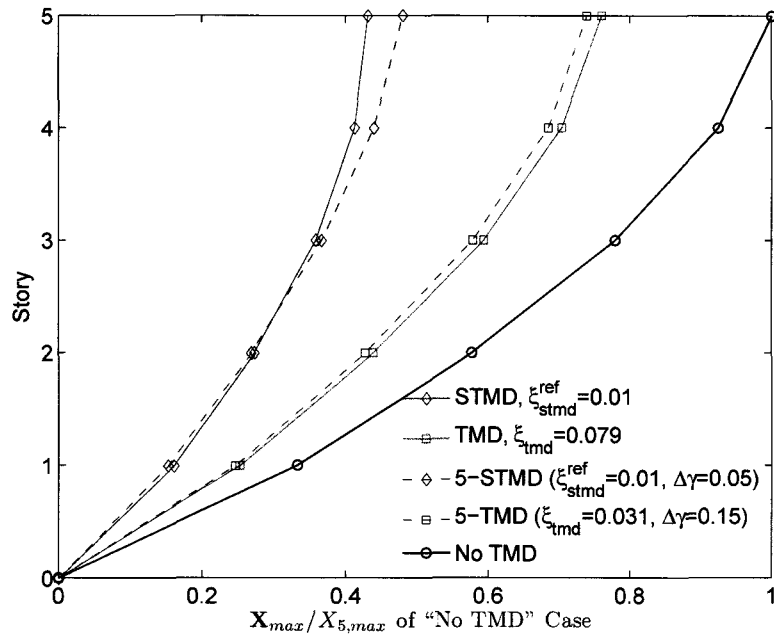


**Figure 6.23** Maximum Transient Response of Force Excited 5-DOF Main Structure ( $f_{n1} = 0.5 \text{ Hz}$ ) with a Step Stiffness Change under Stationary Excitation for No TMD, TMD, MTMD, sTMD, sMTMD

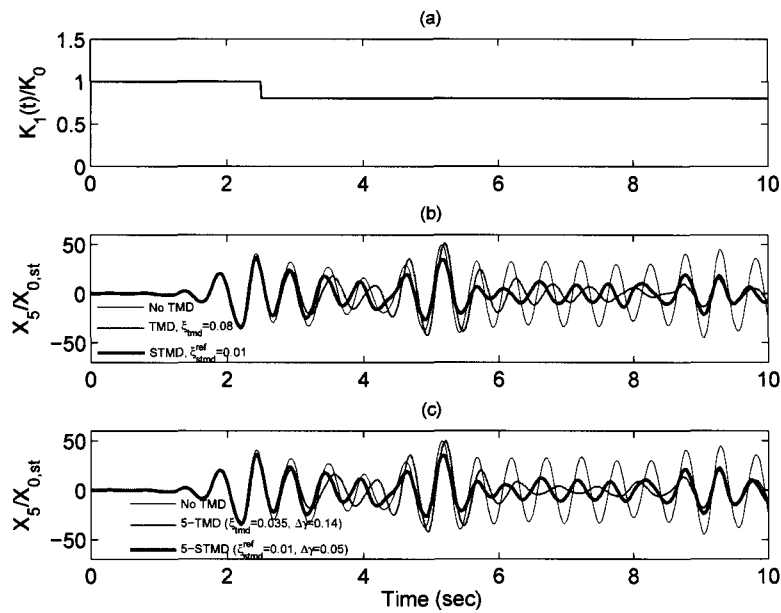


**Figure 6.24** Top Floor Displacement of Base Excited 5-DOF Main Structure ( $f_{n1} = 2 \text{ Hz}$ ) under 1940 El Centro Earthquake: (a) Step Stiffness Change (b) No TMD, TMD, sTMD; (c) No TMD, MTMD, sMTMD

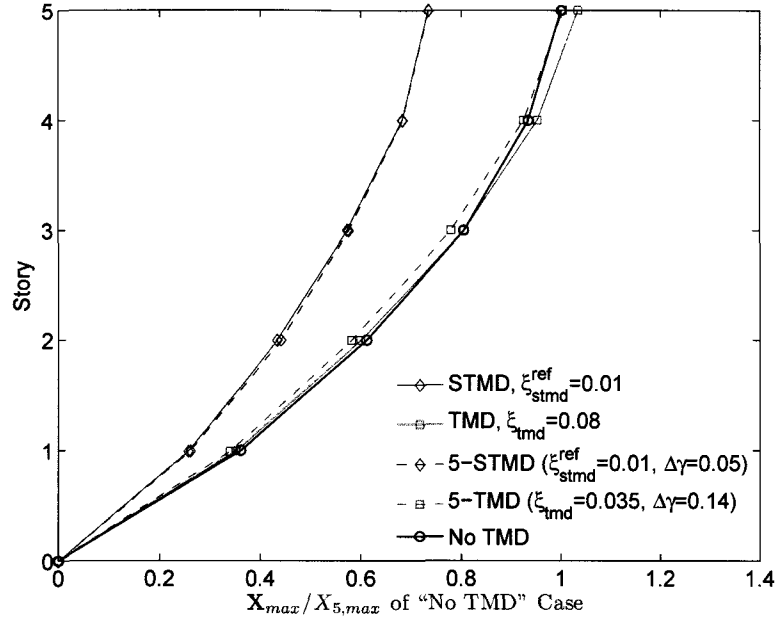


**Figure 6.25** Maximum Transient Response of Base Excited 5-DOF Main Structure ( $f_{n1} = 2 \text{ Hz}$ ) with a Step Stiffness Change under 1940 El Centro Earthquake for No TMD, TMD, MTMD, sTMD, sMTMD

range to zero. They can be tuned as a single sTMD depending on the time-frequency characteristics of the excitation signal. The redundancy in sMTMD makes it more reliable in the sense that if one sTMD fails, the rest can be readjusted instantaneously.

Feedforward sTMD and sMTMD are more robust against changes in individual TMD damping ratio and changes in main structure natural frequency compared to passive TMD and MTMD.



## Chapter 7

### Semi-active Single/Multi-Degree-Of-Freedom Systems (sSDOF/sMDOF) under Stochastic Excitations

Two control algorithms - one for variable stiffness (variable structure control) and one for variable damping (Lyapunov control) - have been presented in Chapter 5 for semi-active single/multi-degree-of-freedom (sSDOF/sMDOF) systems under near-fault earthquakes and fitted cycloidal pulses. This chapter presents another novel control algorithm developed for semi-active SDOF/MDOF systems based on adaptive  $H_2$  control. The algorithm involves obtaining the real-time time-frequency characteristics of the excitation and then applying instantaneous  $H_2$  control by an independently variable stiffness device. The proposed control basically keeps the fundamental frequency of the system away from the dominant frequencies of the excitation by minimizing the  $H_2$  norm of the instantaneous response spectrum. For MDOF systems, the scope is limited to application of variable damping and stiffness between the base and first DOF, which can be considered as a semi-active base-isolation system. The proposed control is formulated for a combined independently variable stiffness and independently variable damping. However, unless the excitation is a narrow band signal, the algorithm always picks the maximum damping in a given range making the use of a semi-active damping system unnecessary or limited. Therefore, systems which can independently vary stiffness only are primarily investigated herein. The performance of the control algorithm is evaluated for several random ground motion processes and 1940 El Centro Earthquake. Stochastic responses are computed from Monte Carlo simulations of the target evolutionary spectra describing the ground motion processes.

## 7.1 SDOF Structural Model and Formulation

The single-degree-of-freedom structural model equipped with both variable damping and stiffness devices (sSDOF) is shown in Figure 7.1. The equation of motion is given by

$$m\ddot{u}(t) + c(t)\dot{u}(t) + k(t)u(t) = P(t) = -m\ddot{z}(t) \quad (7.1)$$

where  $m$  is the mass,  $c(t)$  is the time-varying damping coefficient,  $k(t)$  is the time-varying stiffness coefficient.  $u$ ,  $\dot{u}$ ,  $\ddot{u}$  are the relative displacement, velocity and acceleration with respect to ground.  $P(t)$  is the external force which is equal to  $-m\ddot{z}(t)$  for base excited systems where  $\ddot{z}(t)$  is the ground acceleration. The time-varying coefficients of damping and stiffness are defined as

$$c(t) = c_{min} + c_s(t) = c_{min} + \beta(t)\Delta c \quad (7.2)$$

and

$$k(t) = k_{max} - k_s(t) = k_{max} - \alpha(t)\Delta k \quad (7.3)$$

where  $c_{min}$  is the damping coefficient corresponding to conventional damping mechanisms within the structures itself,  $\Delta c$  is the maximum additional damping due to variable damping device,  $k_{min}$  is the original stiffness of the structure, and  $\Delta k$  is the maximum additional stiffness due to variable stiffness device. The time-varying stiffness and damping coefficients  $k_s(t)$  and  $c_s(t)$  varies such that  $-\Delta k < k_s(t) < 0$  and  $0 < c_s(t) < \Delta c$ .  $\alpha(t)$  and  $\beta(t)$  are the normalized values of the variable stiffness and damping such that  $-\Delta k/k_{max} < \alpha(t) < 0$  and  $0 < \beta(t) < \Delta c/c_{min}$ .

Rewriting Equation (7.1)

$$m\ddot{u} + 2\zeta_n(t)\omega_n(t)m\dot{u} + \omega_n(t)^2 mu = -m\ddot{z}(t) \quad (7.4)$$

Dividing by  $m$ ,

$$\ddot{u} + 2\zeta_n(t)\omega_n(t)\dot{u} + \omega_n(t)^2 u = -\ddot{z}(t) \quad (7.5)$$

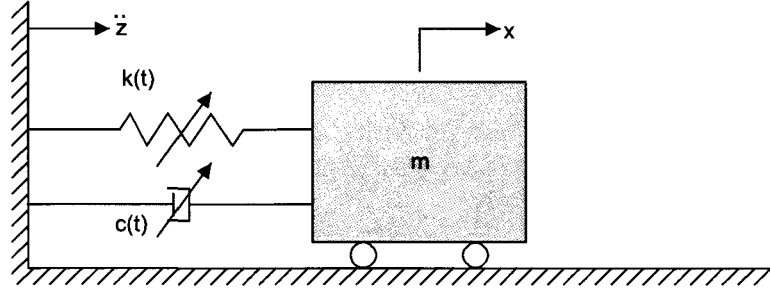


**Figure 7.1** Analytical model of the SDOF system equipped with variable stiffness and variable damping device

Time-varying damping is implemented in the formulation through the damping ratio. The damping ratio ( $\zeta_n(t)$ ) can be varied such that damping coefficient ( $c(t) = 2\zeta_n(t)\omega_n(t)m$ ) has the target value determined by the control algorithm independent from the time-varying stiffness. Since the largest values of damping is always the most optimum for wide-band excitations, there is no need for independently variable damping. However, for better comparison of passive and semi-active systems, the damping ratio is kept same for all systems, leading to a variable damping coefficient depending on the time-varying stiffness in the semi-active system.

For a slowly time-varying sSDOF system, instantaneous complex frequency response function can be written approximately as

$$H(t, \omega) \approx \frac{1}{-\omega^2 - 2\zeta_n(t)\omega_n(t)\omega i + \omega_n(t)^2} \quad (7.6)$$

As shown in Chapter 4, evolutionary spectrum of an excitation can be obtained by time-frequency methods. Following the evolutionary spectrum approach in Section 1.2.10, the instantaneous power spectral density (PSD) of the responses (relative displacement, velocity, and acceleration) of the sSDOF system can be written approximately as

$$G_u(t = t_i, \omega) \approx |H(t = t_i, \omega)|^2 G_z(t = t_i, \omega) \quad (7.7)$$

$$G_{\ddot{u}}(t = t_i, \omega) \approx \omega^2 |H(t = t_i, \omega)|^2 G_z(t = t_i, \omega) \quad (7.8)$$

$$G_{\ddot{u}}(t = t_i, \omega) \approx \omega^4 |H(t = t_i, \omega)|^2 G_z(t = t_i, \omega) \quad (7.9)$$

where  $G_z(t_i, \omega)$  is the instantaneous PSD of  $z(t)$ . The root-mean-square (RMS) responses can be approximated by

$$\sigma_u(t) \approx \int_0^\infty G_u(t, \omega) d\omega \quad (7.10)$$

$$\sigma_{\dot{u}}(t) \approx \int_0^\infty G_{\dot{u}}(t, \omega) d\omega \quad (7.11)$$

$$\sigma_{\ddot{u}}(t) \approx \int_0^\infty G_{\ddot{u}}(t, \omega) d\omega \quad (7.12)$$

The proposed control algorithm determines the optimum natural frequency that minimizes the  $H_2$  norm of the instantaneous PSD of the responses (Equations (7.10-7.12)) depending on the position of instantaneous fundamental frequency with respect to dominant excitation frequency. The flowcharts of the control algorithm are given in Figures 7.3 and 7.4.

## 7.2 MDOF Structural Model and Formulation

The formulation for the SDOF model can be extended straightforward to the multi-degree-of-freedom (MDOF) system. The structural model equipped with both variable damping and stiffness devices between the base and first DOF (sMDOF) is shown in Figure 7.2. The equations of motion can be written as

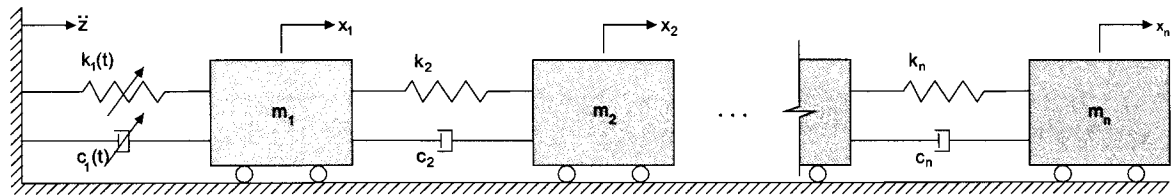


**Figure 7.2** Analytical model of the MDOF system equipped with variable stiffness and variable damping device

$$\mathbf{M}\ddot{\mathbf{U}} + \mathbf{C}\dot{\mathbf{U}} + \mathbf{K}\mathbf{U} = \mathbf{P}(t) \quad (7.13)$$

where  $\mathbf{U} = \{u_1 \ u_2 \ \dots \ u_n\}^T$  is the displacement vector in which  $u_i$  is the displacement of  $i^{th}$  dof.  $\mathbf{P}(t)$  is the force vector, which is  $-\mathbf{M}\mathbf{1}\ddot{z}$  for a base excited system. The coefficient matrices in Equation (7.13) are the mass, damping and stiffness matrices defined as

$$\mathbf{M} = \begin{bmatrix} m_1 & 0 & 0 & \dots & 0 \\ 0 & m_2 & 0 & \dots & 0 \\ 0 & 0 & m_3 & \ddots & 0 \\ \vdots & \vdots & \ddots & \ddots & \vdots \\ 0 & 0 & 0 & \dots & m_n \end{bmatrix} = m_0 \overline{\mathbf{M}} \quad (7.14)$$

$$\mathbf{C} = \begin{bmatrix} c_1(t) + c_2 & -c_2 & 0 & \dots & 0 \\ -c_2 & c_2 + c_3 & -c_3 & \dots & 0 \\ 0 & -c_3 & c_3 + c_4 & \ddots & \vdots \\ \vdots & \vdots & \ddots & \ddots & -c_{n-1} \\ 0 & 0 & \dots & -c_{n-1} & c_n \end{bmatrix} = c_0 \overline{\mathbf{C}} \quad (7.15)$$

$$\mathbf{K} = \begin{bmatrix} k_1(t) + k_2 & -k_2 & 0 & \dots & 0 \\ -k_2 & k_2 + k_3 & -k_3 & \dots & 0 \\ 0 & -k_3 & k_3 + k_4 & \ddots & \vdots \\ \vdots & \vdots & \ddots & \ddots & -k_{n-1} \\ 0 & 0 & \dots & -k_{n-1} & k_n \end{bmatrix} = k_0 \overline{\mathbf{K}} \quad (7.16)$$

where  $\overline{\mathbf{M}}$ ,  $\overline{\mathbf{C}}$ ,  $\overline{\mathbf{K}}$  are the normalized mass, damping, stiffness matrices and  $\mu_0 = m_0/M_0$ .

The force vector is defined as

$$\mathbf{P}(t) = -\mathbf{M}\mathbf{1}\ddot{z}(t) = -m_0 \overline{\mathbf{M}}\mathbf{1}\ddot{z}_0(t) \quad (7.17)$$

where  $\ddot{z}_0$  is a reference normalization factor for the ground acceleration. For simulated random motions it is selected as  $\sqrt{f_{Nyq}G_0}$  in which  $f_{Nyq}$  is the Nyquist frequency of the simulated history and  $G_0$  the spectral intensity. For actual recorded motions,  $\ddot{z}_0$  is the maximum ground acceleration.

The structure is assumed to have uniform distribution of mass, damping and stiffness except the first DOF, such that  $m_1 = m_2 = \dots = m_n = m_0$ ,  $c_2 = \dots = c_n = c_0$ , and  $k_2 = \dots = k_n = k_0$ . The variable damping and stiffness are formulated similar to SDOF system as

$$c_1(t) = c_{min} + c_s(t) = c_{min} + \beta(t)\Delta c \quad (7.18)$$

and

$$k_1(t) = k_{max} - k_s(t) = k_{max} - \alpha(t)\Delta k \quad (7.19)$$

where  $\alpha$  and  $\beta$  are the normalized values of the variable stiffness and damping as described in Section 7.1.

Using modal analysis technique, the equations of motion can be uncoupled. Substituting the modal transformation  $\mathbf{U} = \Phi\mathbf{Q}$  and multiplying the equations of motion by  $\Phi^T$

$$\Phi^T \overline{\mathbf{M}} \Phi \ddot{\mathbf{Q}} + \Phi^T \overline{\mathbf{C}} \Phi \dot{\mathbf{Q}} + \Phi^T \overline{\mathbf{K}} \Phi \mathbf{Q} = -\Phi^T \overline{\mathbf{M}} \mathbf{1} \ddot{z}(t) \quad (7.20)$$

The uncoupled equation of motion for the 1<sup>st</sup> mode is

$$m_{n1} \ddot{q}_1(t) + c_{n1}(t) \dot{q}_1(t) + k_{n1}(t) q_1(t) = -\phi_1^T \overline{\mathbf{M}} \mathbf{1} \ddot{z}(t) \quad (7.21)$$

For a slowly time-varying sMDOF system, instantaneous complex frequency response function of the first mode can be written approximately as

$$H_1(t, w) \approx \frac{\phi_1^T \overline{\mathbf{M}} \mathbf{1} / m_{n1}}{-\omega^2 - 2\zeta_{n1}(t)\omega_{n1}(t)\omega + \omega_{n1}(t)^2} \quad (7.22)$$

Similar to previous section for sSDOF, the instantaneous PSD of the first modal responses (relative displacement, velocity, and acceleration) of the sMDOF system can be written approximately as

$$G_u^{(1)}(t = t_i, \omega) \approx |H_1(t = t_i, \omega)|^2 G_z(t = t_i, \omega) \quad (7.23)$$

$$G_{\dot{u}}^{(1)}(t = t_i, \omega) \approx \omega^2 |H_1(t = t_i, \omega)|^2 G_z(t = t_i, \omega) \quad (7.24)$$

$$G_{\ddot{u}}^{(1)}(t = t_i, \omega) \approx \omega^4 |H_1(t = t_i, \omega)|^2 G_z(t = t_i, \omega) \quad (7.25)$$

where  $G_z(t_i, \omega)$  is the instantaneous PSD of  $z(t)$ . The root-mean-square (RMS) responses contributed from the 1<sup>st</sup> mode can be approximated by

$$\sigma_u^{(1)}(t) \approx \int_0^\infty G_u^{(1)}(t, \omega) d\omega \quad (7.26)$$

$$\sigma_{\dot{u}}^{(1)}(t) \approx \int_0^\infty G_{\dot{u}}^{(1)}(t, \omega) d\omega \quad (7.27)$$

$$\sigma_{\ddot{u}}^{(1)}(t) \approx \int_0^\infty G_{\ddot{u}}^{(1)}(t, \omega) d\omega \quad (7.28)$$

The proposed control algorithm determines the optimum natural frequency that minimizes the  $H_2$  norm of the instantaneous PSD of the first modal responses (Equations (7.26-7.28)) depending on the position of instantaneous fundamental frequency with respect to dominant excitation frequency. The flowcharts of the control algorithm are given in Figures 7.3 and 7.4.

### 7.3 Control Algorithm

The block diagram for the control algorithm is given in Figure 7.3. Further details in implementation of evolutionary spectrum estimation and tuning the semi-active stiffness and damping devices are shown in Figure 7.4. The control algorithm operates as follows:

1. At time  $t = 0$ , variable stiffness and damping devices are set to their maximum value.
2. A moving window of  $n$  time steps of signal is chosen at certain time instants  $t_i$ .  $WL$  is the window length of  $n\Delta t$  and  $t_i = 0 : L\Delta t : t(end)$  is the new time array for the time-frequency spectra incremented with  $L\Delta t$  between successive windows.
3. Stiffness and damping variation starts after  $t = t_0$  to allow sufficient amount of data to be collected for accurate estimation.
4. If the excitation amplitude is less than a pre-defined level  $z_{lim}$ , stiffness and damping values from previous time step do not change.  $z_{lim}$  is set to 15% of the reference acceleration value  $\ddot{z}_0$  in this study.
5. Instantaneous power spectral density of the excitation is estimated by STFT or WT. Instantaneous (dominant) frequency of the excitation is tracked by averaging the highest energy frequencies detected over an averaging time length  $AL$ .
6. Assuming a slowly time-varying system, instantaneous power spectral densities of the responses (displacement, velocity and acceleration) for a range of variable stiffness and damping are estimated. For MDOF system, only fundamental modal response is considered since the scope is limited to semi-active base isolation systems.
7. Depending on the location of instantaneous (dominant) excitation frequency, an optimum stiffness (and damping value) is selected minimizing the  $H_2$  norm of the instantaneous PSD of the selected response (displacement, velocity, or acceleration). If  $f_{n1}(t_i) > 1.1f_{ins}(t_i)$  (where the structure is stiffer compared to excitation frequency) the variable parameters are selected to minimize the displacement RMS response (in which the displacement response instantaneous (dominant) frequency is



closer and more sensitive to the higher frequency components of the excitation). If  $f_{n1}(t_i) < 0.9f_{ins}(t_i)$  (where the structure is softer compared to excitation frequency) the variable parameters are selected to minimize the acceleration RMS response (in which the acceleration response instantaneous (dominant) frequency is closer and more sensitive to the lower frequency components of the excitation). In between region where  $0.9f_{ins}(t_i) < f_{n1}(t_i) < 1.1f_{ins}(t_i)$ , the variable parameters are selected to minimize the RMS velocity response.

8. Based on the optimum values of the parameters  $\alpha$  and  $\beta$ , the time-varying damping and the target stiffness are computed. If the target stiffness is different than the current stiffness, a local time parameter  $\tau$  is defined for smooth stiffness variation as  $\tau = t_i + \tau_0$  in which  $\tau_0 = 0.06 \text{ sec}$ .
9. A smoothing function  $\lambda = 1 / (1 + e^{c\rho*(t-\tau)})$  is applied to the selected stiffness parameter to ensure a slowly varying system and avoiding jumps in acceleration response.  $c$  is the smoothing constant set to 50 in this study.
10. In order to ensure the stiffness change is dissipative, a constraint is defined as follows: if the target stiffness is higher than the current stiffness and any of the product  $u\dot{u}$  for the last  $m = 10$  time steps is less than zero, the stiffness is kept same as the previous time step.

## 7.4 Results for sSDOF

Several random ground motion processes and 1940 El Centro earthquake are used to evaluate the the proposed control algorithm. For random ground motion processes, a target evolutionary spectrum is specified and 500 sample functions have been simulated for

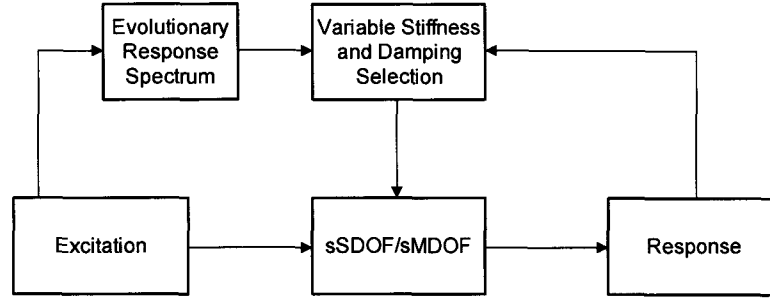


**Figure 7.3** Control Algorithm

excitation acceleration history. Each simulation has 1024 data points with a time step of  $\Delta t = 0.02 \text{ sec}$ . The time history responses of different sSDOF systems have been computed for each sample excitation and the response statistics have been obtained. Semiactive stiffness coefficient,  $k_s(t)$  varies between 0 and  $-\Delta k = -0.5k_{max}$  (or  $-0.5 < \alpha(t) < 0$ ). The damping ratio of both passive and semi-active systems is set to be constant such that  $\zeta_n(t) = \zeta_0 = 0.05$ . The damping coefficient in the semi-active system varies in time due to the time varying stiffness. In the following sections, response time histories are presented for sample responses, instantaneous RMS responses are presented for ensemble responses, and response spectra are presented for sSDOF systems with different reference fundamental frequencies. sSDOF responses (referred as ‘controlled’) are compared with two reference passive systems: one with highest stiffness (‘pass. on’) and one with lowest stiffness of the sSDOF system (‘pass. off’).

Since the responses are normalized and fundamental frequency of the sSDOF system is changing with time, an equivalent fundamental frequency is obtained from the response of every simulation. This equivalent fundamental frequency is used to present the response spectra results in a consistent manner and is obtained by

$$\omega_{eq}^2 = \frac{E[u^2 \omega_n^2(t)]}{\sigma_u^2} \quad (7.29)$$

The displacement responses are normalized to present the dynamic amplification factor for

the considered passive and semi-active systems such that

$$\frac{u}{u_{st}^*} = \begin{cases} \frac{\omega_{n,off}^2 u}{\ddot{z}_0} & \text{(passive-off)} \\ \frac{\omega_{n,on}^2 u}{\ddot{z}_0} & \text{(passive-on)} \\ \frac{\omega_{eq}^2 u}{\ddot{z}_0} & \text{(controlled)} \end{cases} \quad (7.30)$$

in which

$$u_{st}^* = \begin{cases} \frac{\ddot{z}_0}{\omega_{n,off}^2} & \text{(passive-off)} \\ \frac{\ddot{z}_0}{\omega_{n,on}^2} & \text{(passive-on)} \\ \frac{\ddot{z}_0}{\omega_{eq}^2} & \text{(controlled)} \end{cases} \quad (7.31)$$

The RMS values of the normalized responses are

$$\sigma_{u/u_{st}^*} = \begin{cases} \sqrt{E \left[ \left( \frac{\omega_{n,off}^2 u}{\ddot{z}_0} \right)^2 \right]} & \text{(passive-off)} \\ \sqrt{E \left[ \left( \frac{\omega_{n,on}^2 u}{\ddot{z}_0} \right)^2 \right]} & \text{(passive-on)} \\ \sqrt{E \left[ \left( \frac{\omega_{eq}^2 u}{\ddot{z}_0} \right)^2 \right]} & \text{(controlled)} \end{cases} \quad (7.32)$$

where  $\ddot{z}_0$  is a reference normalization factor for the ground acceleration. For simulated random motions, it is selected as  $\sqrt{f_{Nyq} G_0}$  in which  $f_{Nyq}$  is the Nyquist frequency of the simulated ground acceleration and  $G_0$  the spectral intensity. For actual recorded motions,  $\ddot{z}_0$  is the maximum ground acceleration.

#### 7.4.1 Wide-band Stationary Excitations

500 wide-band stationary excitations are simulated using the near-fault earthquake spectrum given by Equation (1.110). The soil parameters are selected as  $\omega_g = 2\pi \text{ rad/sec}$  ( $f_g = \omega_g/(2\pi) = 1 \text{ Hz}$ ) and  $\xi_g = 0.3$ . The estimated evolutionary excitation spectrum

(by STFT), a sample excitation are shown in Figure 7.5 along with the RMS responses and the response spectra. The response spectra points correspond to the reference fundamental frequency, which is the fundamental frequency of the 'pass. on' system. Time history responses and variable stiffness corresponding to two different reference fundamental frequencies are presented in Figures 7.6. Response spectra in Figure 7.5 clearly show that sSDOF successfully adapts to the optimum passive system for a given excitation. Same observation can be made for specific cases shown in the ensemble RMS response histories in Figure 7.5 and sample response histories in Figure 7.6 for specific reference frequencies (i.e.  $f_n^{on} = 1Hz$  and  $2Hz$  (pass. on)).

#### 7.4.2 Locally Stationary Excitations

500 locally stationary excitations are simulated using the near-fault earthquake spectrum given by Equation (1.110). The soil parameters are selected as  $\omega_g = 2\pi \text{ rad/sec}$  ( $f_g = \omega_g/(2\pi) = 1 \text{ Hz}$ ) and  $\xi_g = 0.3$ . A time envelope is applied in the form of

$$g = \frac{e^{-at} - e^{-bt}}{\max[e^{-at} - e^{-bt}]} \quad (7.33)$$

in which  $a = 0.20$  and  $b = 0.25$ .

The estimated evolutionary excitation spectrum (by STFT), a sample excitation are shown in Figure 7.7 along with the RMS responses and the response spectra. Time history responses and variable stiffness corresponding to two different reference fundamental frequencies are presented in Figures 7.8. Response spectra in Figure 7.7 clearly show that sSDOF successfully adapts to the optimum passive system for a given excitation. Same observation can be made for specific cases shown in the ensemble RMS response histories in Figure 7.7 and sample response histories in Figure 7.8 for specific reference frequencies (i.e.  $f_n^{on} = 1Hz$  and  $2Hz$  (pass. on)).

### 7.4.3 Non-stationary Excitations

500 non-stationary excitations are simulated using the near-fault earthquake spectrum given by Equation (1.110). The soil parameters are selected as  $f_g = 0.5 - 2.5 \text{ Hz}$  and  $\xi_g = 0.3$ . A time envelope as given in Equation (7.33) and a linear shift in the dominant frequency are applied to model non-stationarity in amplitude and frequency. The estimated evolutionary excitation spectrum (by STFT), a sample excitation are shown in Figure 7.9 along with the RMS responses and the response spectra. Time history responses and variable stiffness corresponding to two different reference fundamental frequencies are presented in Figures 7.10. Response spectra in Figure 7.10 clearly show that sSDOF successfully adapts to the optimum passive system for a given excitation. Same observation can be made for specific cases shown in the ensemble RMS response histories in Figure 7.9 and sample response histories in Figure 7.10 for specific reference frequencies (i.e.  $f_n^{on} = 1 \text{ Hz}$  and  $3 \text{ Hz}$  (pass. on)).

### 7.4.4 Recorded Earthquake

The performance of the sSDOF is further examined under 1940 El Centro Earthquake. The estimated evolutionary excitation spectrum (by WT), the acceleration record are shown in Figure 7.11 along with the RMS responses and the response spectra. Time history responses and variable stiffness corresponding to two different reference fundamental frequencies are presented in Figures 7.12. Response spectra in Figure 7.11 clearly show that sSDOF successfully adapts to the optimum passive system. Same observation can be made for specific cases shown in the ensemble RMS response histories in Figure 7.11 and sample response histories in Figure 7.12 for specific reference frequencies (i.e.  $f_n^{on} = 1 \text{ Hz}$  and  $2 \text{ Hz}$  (pass. on)).

## 7.5 Results for sMDOF

One 4-DOF example is studied next to study the effectiveness of sMDOF. 500 locally-stationary excitations are simulated using the near-fault earthquake spectrum given by Equation (1.124). The soil parameters are selected as  $f_g = 0.5 - 2.5 \text{ Hz}$  and  $\xi_g = 0.3$ . A linear shift in the dominant frequency is applied to model non-stationarity in frequency. The time history responses of a specific s4DOF system ( $0.95\text{Hz} < f_{n1} < 1.53\text{Hz}$ ) have been computed for each sample excitation and the response statistics have been obtained. In the following section, instantaneous and peak RMS responses are presented for ensemble responses. sMDOF responses are compared with two reference passive MDOF systems: one with highest stiffness ('pass. on') and one with lowest stiffness ('pass. off') between the first and second DOFs. Semiactive stiffness coefficient ( $k_1(t)$ ) varies between  $0.13k_0$  and  $0.42k_0$ . The modal damping ratio of both passive and semi-active systems are set to be same such that  $\zeta_{n1} = 0.09$ ,  $\zeta_{n2} = 0.12$ ,  $\zeta_{n3} = 0.17$ , and  $\zeta_{n4} = 0.21$ . The damping coefficient in the semi-active system varies in time due to the time varying stiffness.

### 7.5.1 Locally Stationary Excitations

The evolutionary excitation spectrum (obtained by STFT) and a sample excitation are shown in Figure 7.13 along with the RMS responses. Maximum RMS responses for each DOF are presented in Figure 7.14. The target EPSD for the excitation is constructed with a linear shift in the dominant frequency in order to create a spectrum that can excite both passive systems that sMDOF varies in between. The RMS histories shown in Figure 7.13 show the sMDOF can successfully adapt to the optimum passive system as the frequency characteristics of the excitation changes. Significant reduction in the peak RMS responses are also observed in Figure 7.14.

## 7.6 Approximate Response of sSDOF Systems through Time-Varying Complex Frequency Response Function

Using the evolutionary spectrum approach (described in Section 1.2.10), a non-stationary input process  $x(t)$  can be written as

$$x(t) = \int_{-\infty}^{\infty} A(t, \omega) e^{i\omega t} dX(\omega) \quad (7.34)$$

whereas  $dX(\omega)$  is a zero-mean random orthogonal process and  $A(t, \omega)$  is a deterministic modulation function.

The evolutionary power spectral density (EPSD) function of the non-stationary process  $x(t)$  can be written as

$$S_x(t, \omega) = |A(t, \omega)|^2 S_x(\omega) \quad (7.35)$$

where  $S_x(\omega)$  is the power spectral density function of the stationary process  $x(t)$ .

For a linear time invariant (LTI) SDOF system that is initially rest, the response can be obtained from the impulse response function  $h(t)$  as

$$y(t) = \int_0^t h(t - \tau) x(\tau) d\tau \quad (7.36)$$

Substituting Equation (7.34) into Equation (7.36)

$$y(t) = \int_{\tau=0}^t \left[ \int_{-\infty}^{\infty} A(\tau, \omega) e^{i\omega\tau} dX(\omega) \right] h(t - \tau) d\tau \quad (7.37)$$

Substituting  $t - \tau = \theta$  and changing the order of integration leads to

$$y(t) = \int_{\omega=-\infty}^{\infty} e^{i\omega t} \left[ \int_{\theta=0}^t A(t - \theta, \omega) e^{-i\omega\theta} h(\theta) d\theta \right] dX(\omega) \quad (7.38)$$

Defining the stationary output process  $dY(\omega)$  for the stationary input process  $dX(\omega)$  as

$$dY(\omega) = H_1(\omega) dX(\omega) \quad (7.39)$$

and substituting it into Equation (7.38) gives

$$y(t) = \int_{\omega=-\infty}^{\infty} e^{i\omega t} \left[ \int_{\theta=0}^t A(t-\theta, \omega) e^{-i\omega\theta} h(\theta) d\theta \right] \frac{1}{H_1(\omega)} dY(\omega) \quad (7.40)$$

Employing a similar definition of Equation (7.34) for the non-stationary output process  $y(t)$  as

$$y(t) = \int_{-\infty}^{\infty} B(t, \omega) e^{i\omega t} dY(\omega) \quad (7.41)$$

the output power spectral density function can be written as

$$S_y(t, \omega) = |B(t, \omega)|^2 S_y(\omega) = |B(t, \omega)|^2 |H_1(\omega)|^2 S_x(\omega) \quad (7.42)$$

where

$$B(t, \omega) = \frac{1}{H_1(\omega)} \int_{\tau=0}^t A(t-\tau, \omega) e^{-i\omega\tau} h(\tau) d\tau \quad (7.43)$$

The corresponding time-varying transfer function is approximately given by

$$H(t, \omega) = \int_{\tau=0}^t A(t-\tau, \omega) e^{-i\omega\tau} h(\tau) d\tau \approx A(t, \omega) H_1(\omega) \quad (7.44)$$

Equations (7.42) and (7.44) are valid approximations as long as  $A(t, \omega)$  varies slowly with respect to the impulse response function  $h(t)$ .

The above formulation can be extended to linear time varying (LTV) systems by replacing  $H_1(\omega)$  with  $H_1(t, \omega)$ . The time-varying transfer function and evolutionary power spectral density function of the response of an LTV system can be approximately written as

$$H(t, \omega) \approx A(t, \omega) H_1(t, \omega) \quad (7.45)$$

and

$$S_y(t, \omega) \approx |H(t, \omega)|^2 S_x(\omega) \quad (7.46)$$



Equations (7.45) and (7.46) are valid approximations as long as  $A(t, \omega)$  varies slowly with respect to the time varying impulse response function  $h(t, \tau)$  where  $h(t, \tau)$  is the response to the impulse  $\delta(t - \tau)$  applied at time  $\tau$  with no initial energy.

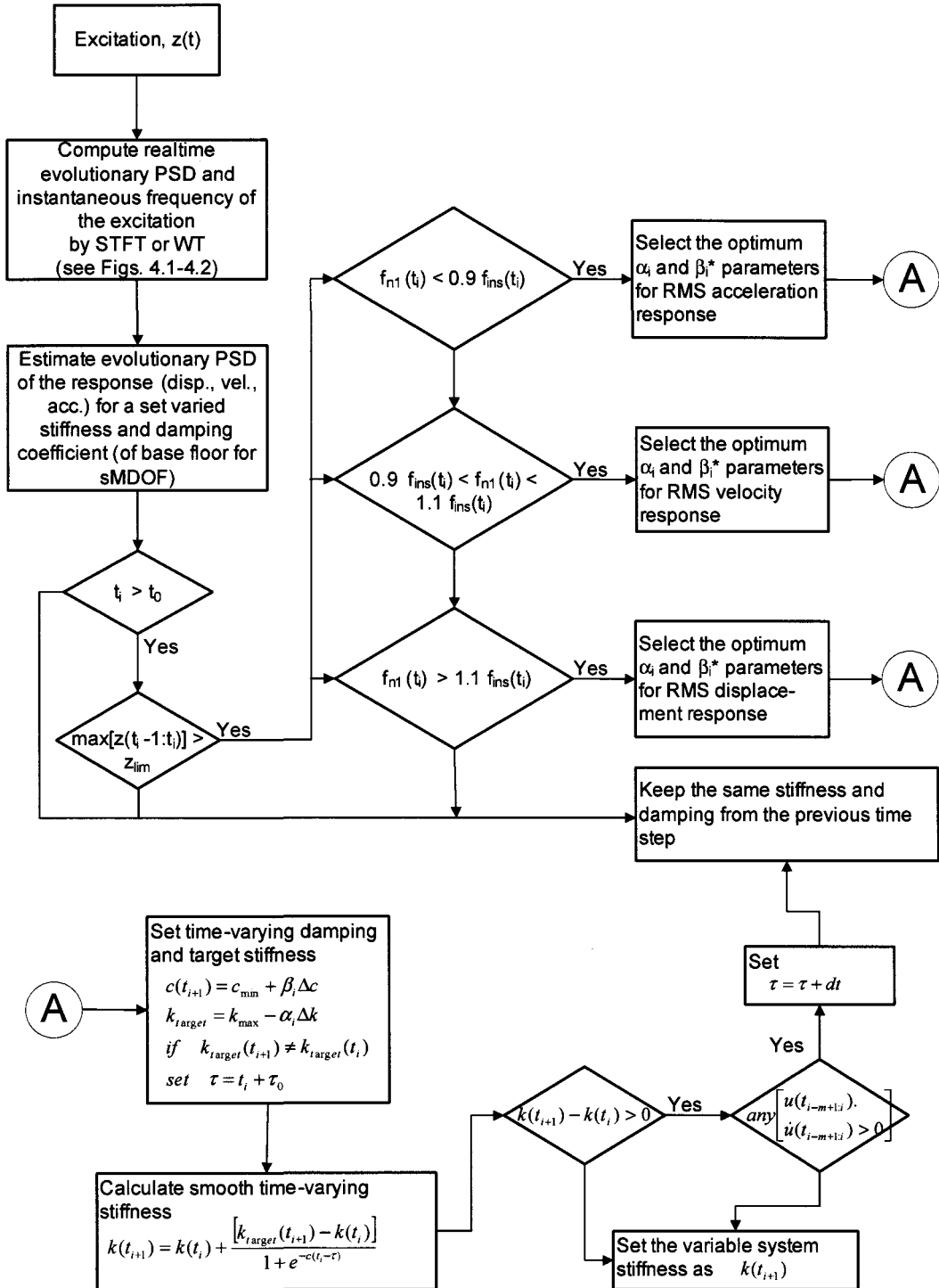
The developed control algorithm for the semi-active systems in this chapter uses the evolutionary PSD estimate for each sample excitation to determine the instantaneous optimum stiffness (and damping) resulting in a time-varying linear system with a time-varying complex frequency response function. Using the above formulation, the response of the semi-active SDOF system can be estimated directly from the time-varying complex frequency response function determined for a given ensemble evolutionary PSD of a slowly varying excitation process. In this section time-varying complex frequency response function for the sSDOF subjected to a non-stationary excitation process defined by an ensemble (500 sample) evolutionary PSD is determined and used to obtain the evolutionary PSD of the displacement response. The evolutionary PSD for the excitation, the corresponding displacement response spectra are presented in Figure 7.15 along with the stiffness variation and the RMS displacement responses for one specific sSDOF system with fundamental frequency ranging from  $1.41Hz$  (pass. off) and  $2.0Hz$  (pass. on). The approximate results obtained by the time-varying complex frequency response function are compared with results of Monte Carlo simulation. For the given example, it is shown that the mean stiffness variation in the Monte Carlo simulation is similar to the stiffness variation determined directly based on the ensemble evolutionary PSD of the excitation. RMS displacement response history obtained from time-varying complex frequency response function also follows the Monte Carlo simulation result closely. This example shows the potential of using time-varying complex frequency response function determined from an ensemble excitation EPD for approximate results of a sSDOF system, with the limitation of a slowly varying linear system subjected to a slowly varying excitation process.

## 7.7 Concluding Remarks

Semi-active SDOF system with variable stiffness based on adaptive  $H_2$  control can successfully adapt to the optimum passive system as the excitation evolves.

Semi-active MDOF systems, which can be described accurately by their first mode, can similarly adapt the optimum passive system with minimum  $H_2$  norm of the first modal response determined for the instantaneous PSD of the excitation.

The time-varying RMS response of the sSDOF/sMDOF can be approximated from the evolutionary PSD and the time-varying complex frequency response function.



\* For the scope of this study, independently variable damping is not considered; therefore,  $\beta_i$  is actually varying depending on  $\alpha_i$  value.

**Figure 7.4** Variable Stiffness and Damping Parameter Selection

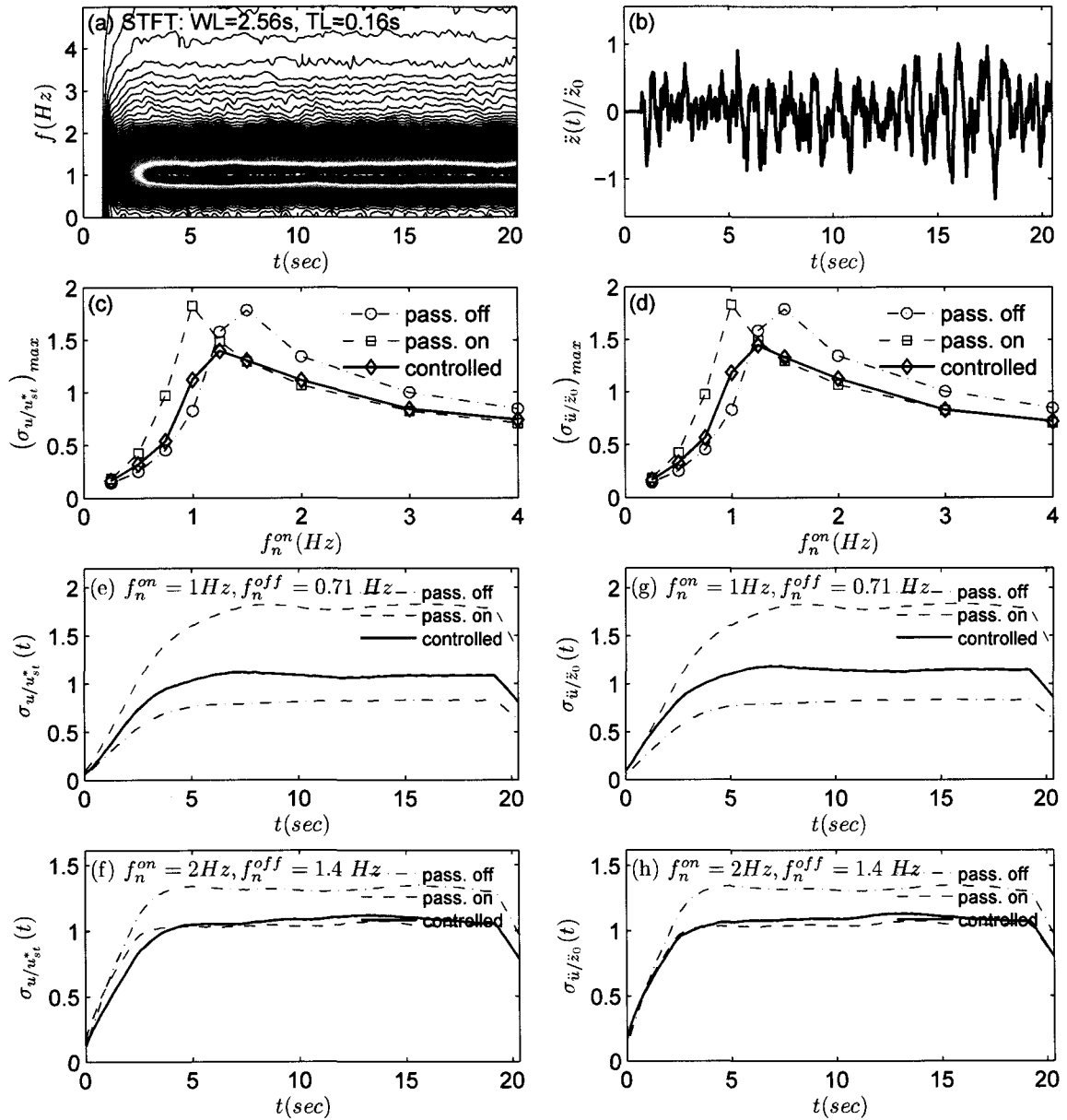


**Figure 7.5** Wide-band stationary base excitation of SDOF: (a) EPSD for 500 sample, (b) Sample ground acceleration, (c) Displacement response spectra, (d) Acceleration response spectra, (e) RMS displacement response ( $f_n^{on} = 1.0$  - pass. on), (e) RMS acceleration response ( $f_n^{on} = 1.0$  - pass. on), (g) RMS displacement response ( $f_n^{on} = 2.0$  - pass. on), (h) RMS acceleration response ( $f_n^{on} = 2.0$  - pass. on)

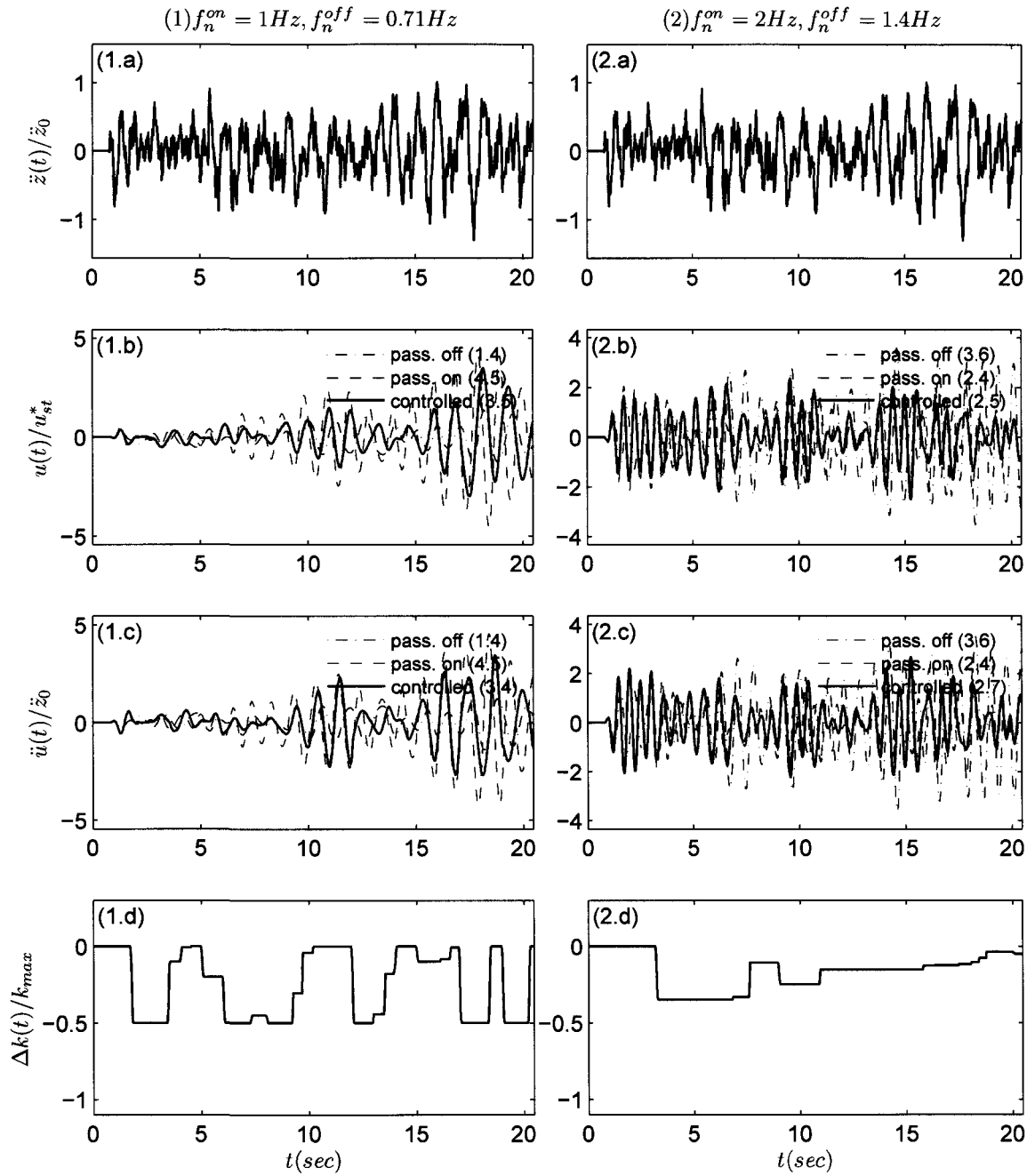


**Figure 7.6** Wide-band stationary base excitation of SDOF: Sample ground acceleration, time history responses and variable stiffness: (1)  $f_n = 1.0Hz$  (pass. on); (2)  $f_n = 2.0Hz$  (pass. on)

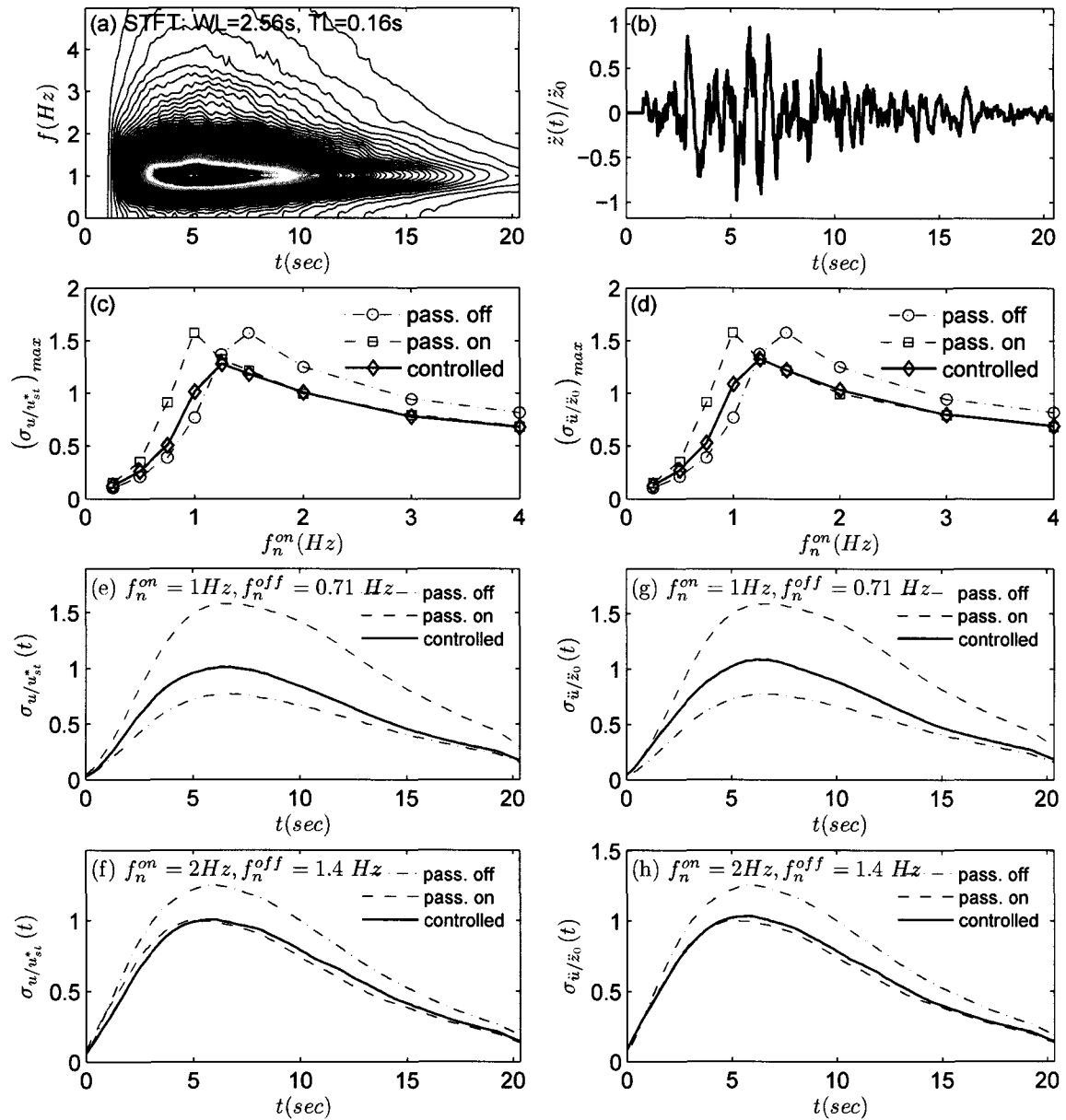


**Figure 7.7** Locally stationary base excitation of SDOF: (a) EPSD for 500 sample, (b) Sample ground acceleration, (c) Displacement response spectra, (d) Acceleration response spectra, (e) RMS displacement response ( $f_n^{on} = 1.0$  - pass. on), (f) RMS acceleration response ( $f_n^{on} = 1.0$  - pass. on), (g) RMS displacement response ( $f_n^{on} = 2.0$  - pass. on), (h) RMS acceleration response ( $f_n^{on} = 2.0$  - pass. on)

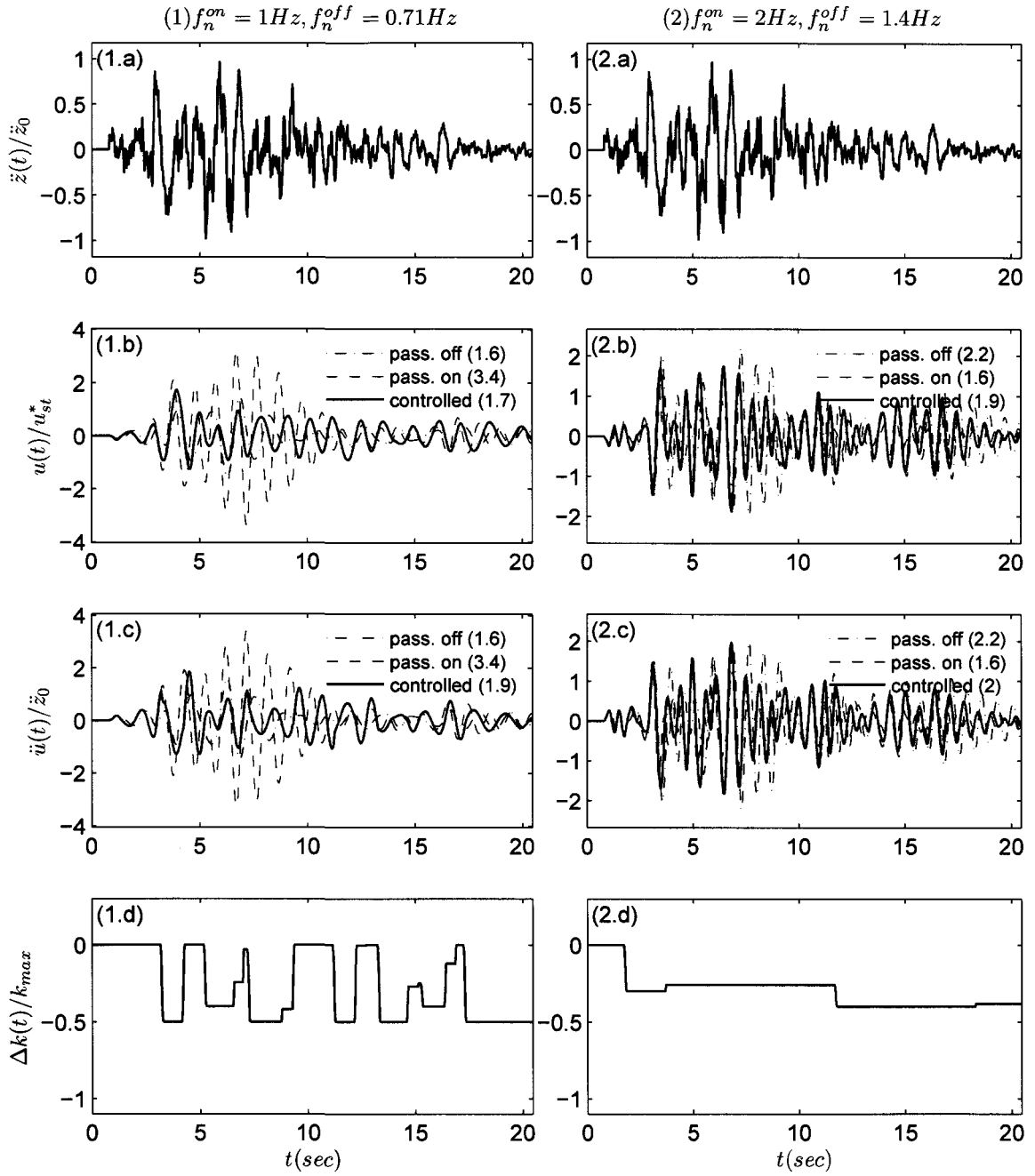


**Figure 7.8** Locally stationary base excitation of SDOF: Sample ground acceleration, time history responses and variable stiffness: (1)  $f_n^{on} = 1.0Hz$  (pass. on); (2)  $f_n^{on} = 2.0Hz$  (pass. on)

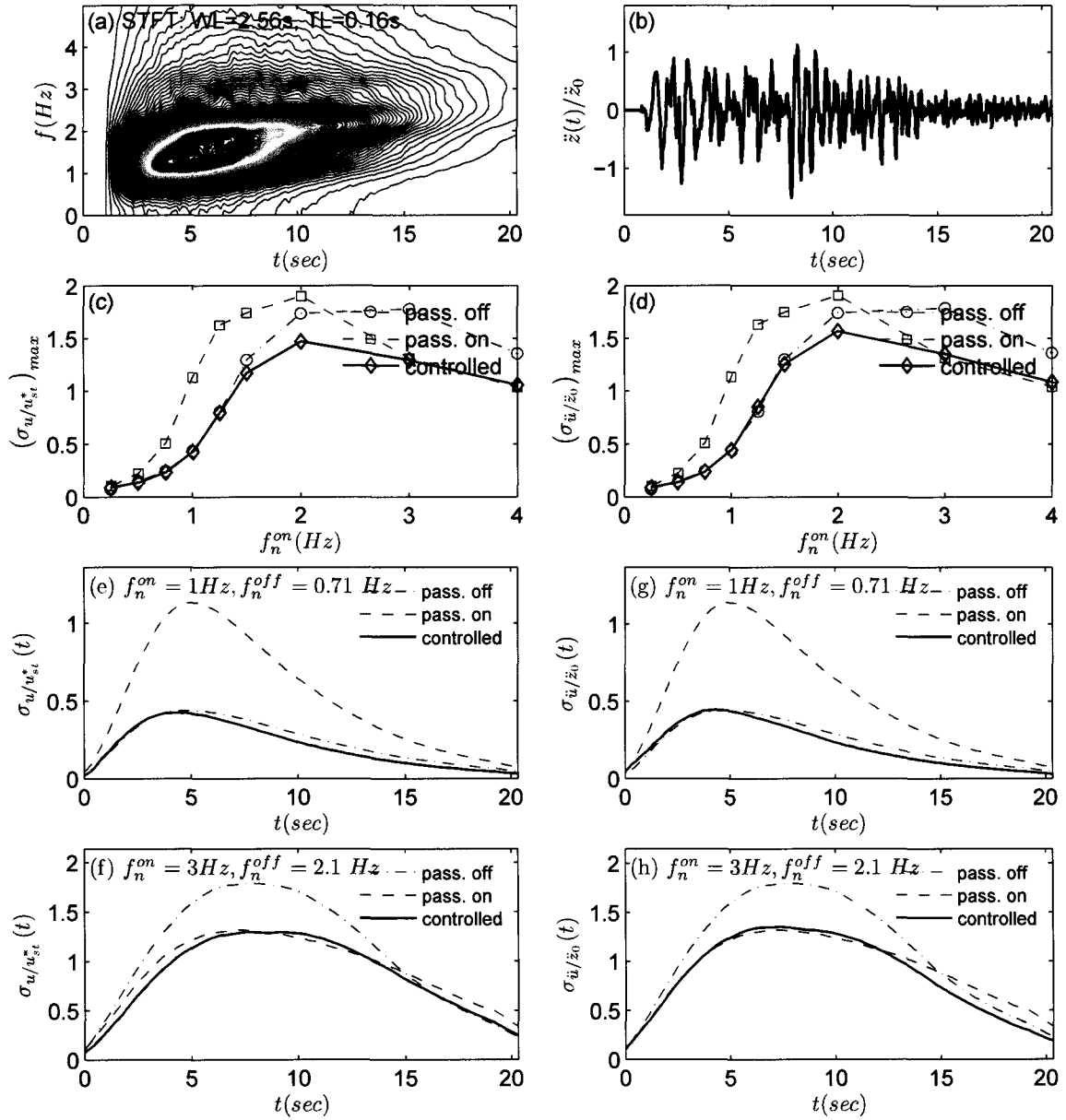


**Figure 7.9** Non-stationary base excitation of SDOF: (a) EPSD for 500 sample, (b) Sample ground acceleration, (c) Displacement response spectra, (d) Acceleration response spectra, (e) RMS displacement response ( $f_n^{on} = 1.0$  - pass. on), (e) RMS acceleration response ( $f_n^{on} = 1.0$  - pass. on), (g) RMS displacement response ( $f_n^{on} = 3.0$  - pass. on), (h) RMS acceleration response ( $f_n^{on} = 3.0$  - pass. on)



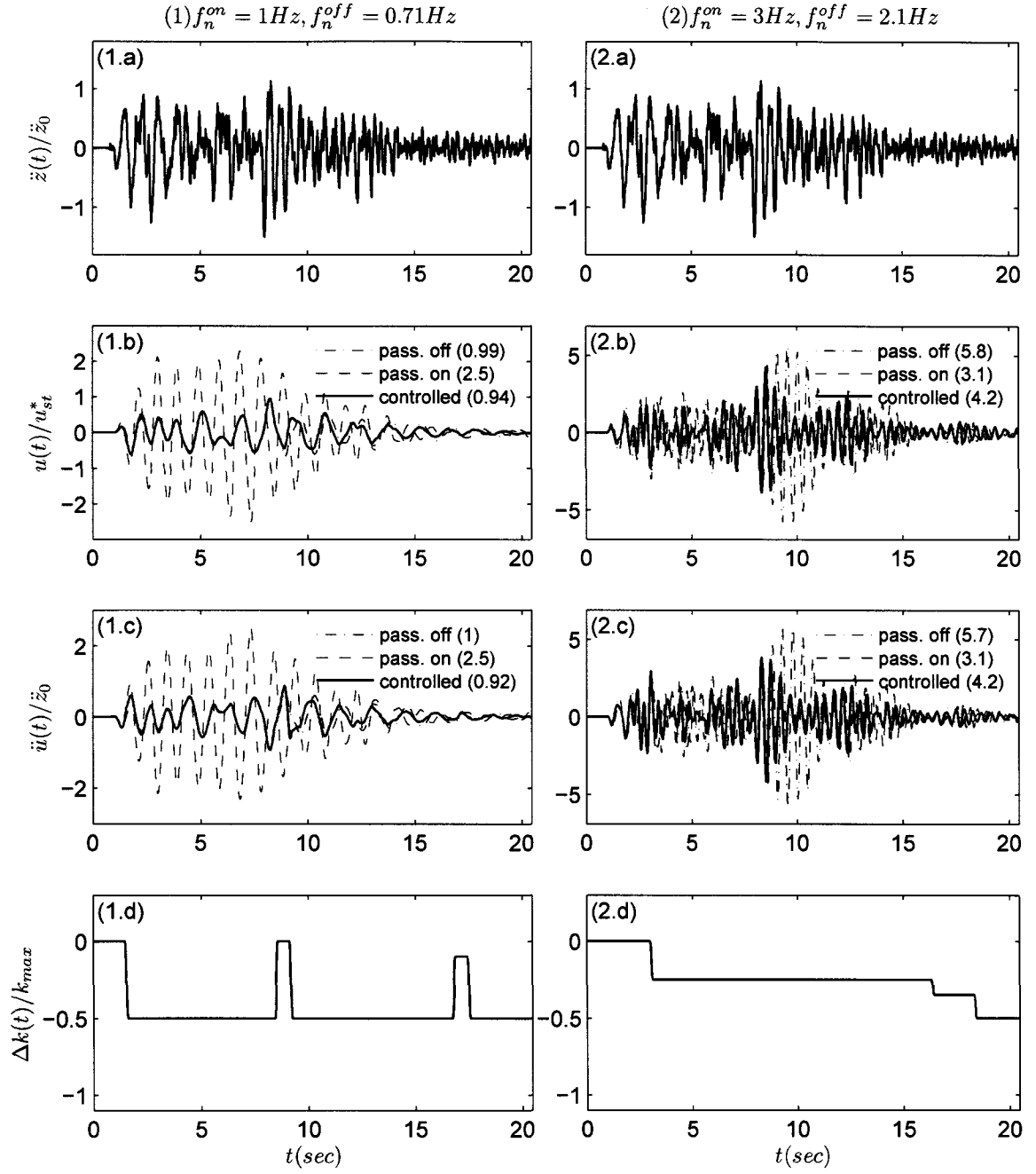


**Figure 7.10** Non-stationary base excitation of SDOF: Sample ground acceleration, time history responses and variable stiffness: (1)  $f_n^{on} = 1.0Hz$  (pass. on); (2)  $f_n^{on} = 3.0Hz$  (pass. on)

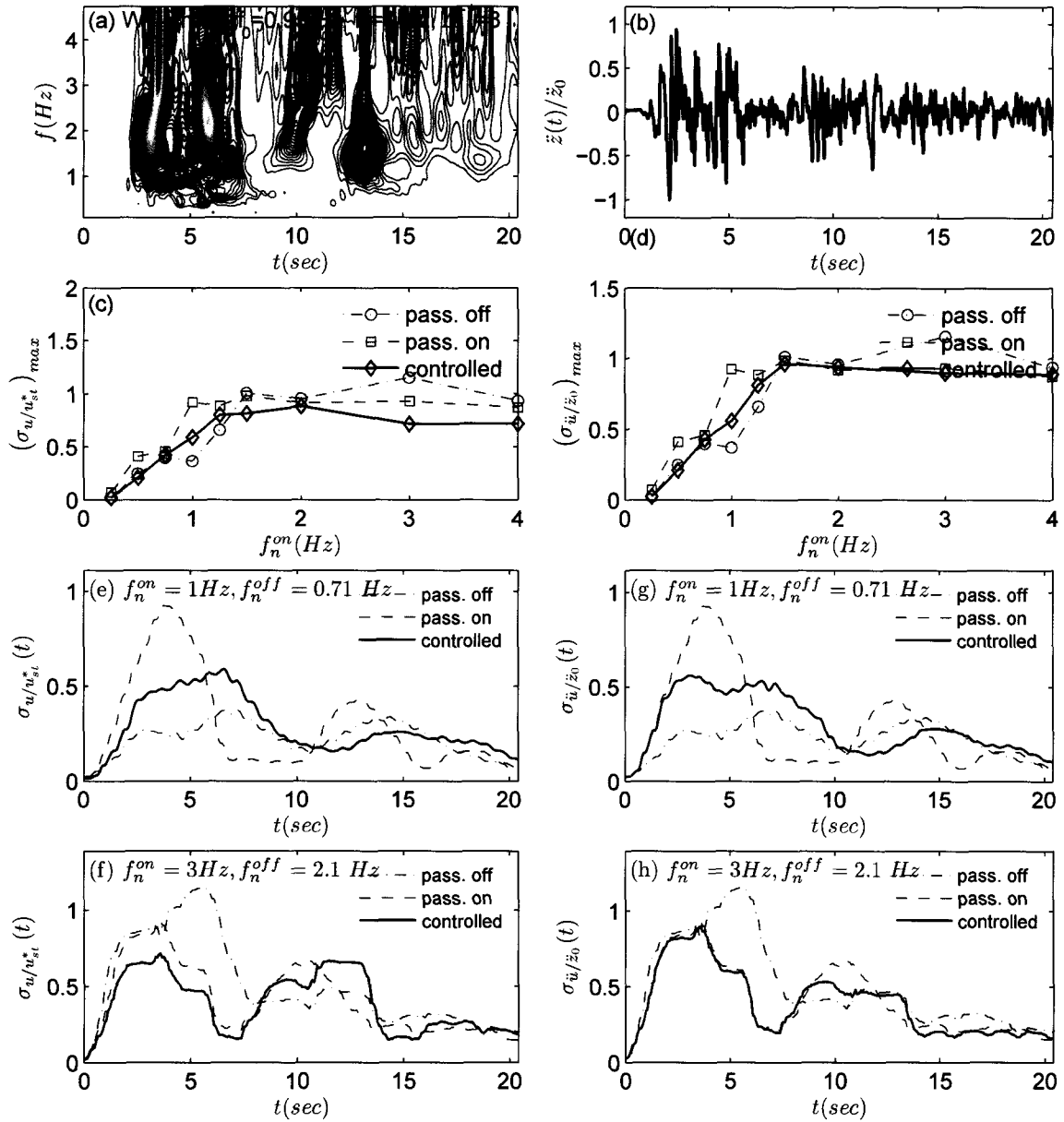


**Figure 7.11** 1940 El Centro Earthquake excitation of SDOF: (a) EPSD, (b) Ground acceleration, (c) Displacement response spectra, (d) Acceleration response spectra, (e) RMS displacement response ( $f_n^{on} = 1.0$  - pass. on), (f) RMS acceleration response ( $f_n^{on} = 1.0$  - pass. on), (g) RMS displacement response spectra ( $f_n^{on} = 3.0$  - pass. on), (h) RMS acceleration response ( $f_n^{on} = 3.0$  - pass. on)

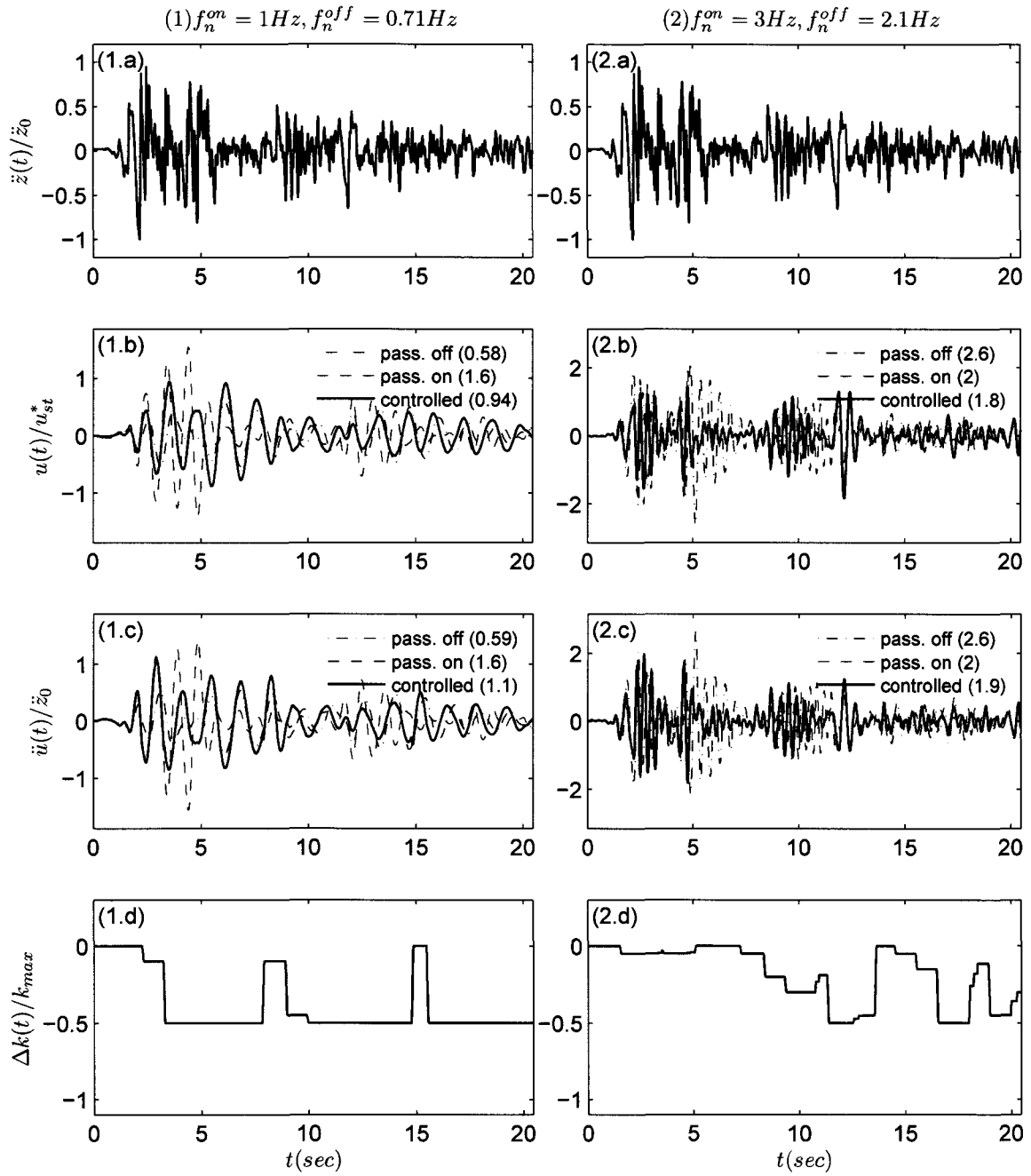


**Figure 7.12** 1940 El Centro Earthquake excitation of SDOF: Ground acceleration, time history responses and variable stiffness: (1)  $f_n^{on} = 1.0Hz$  (pass. on); (2)  $f_n^{on} = 3.0Hz$  (pass. on)

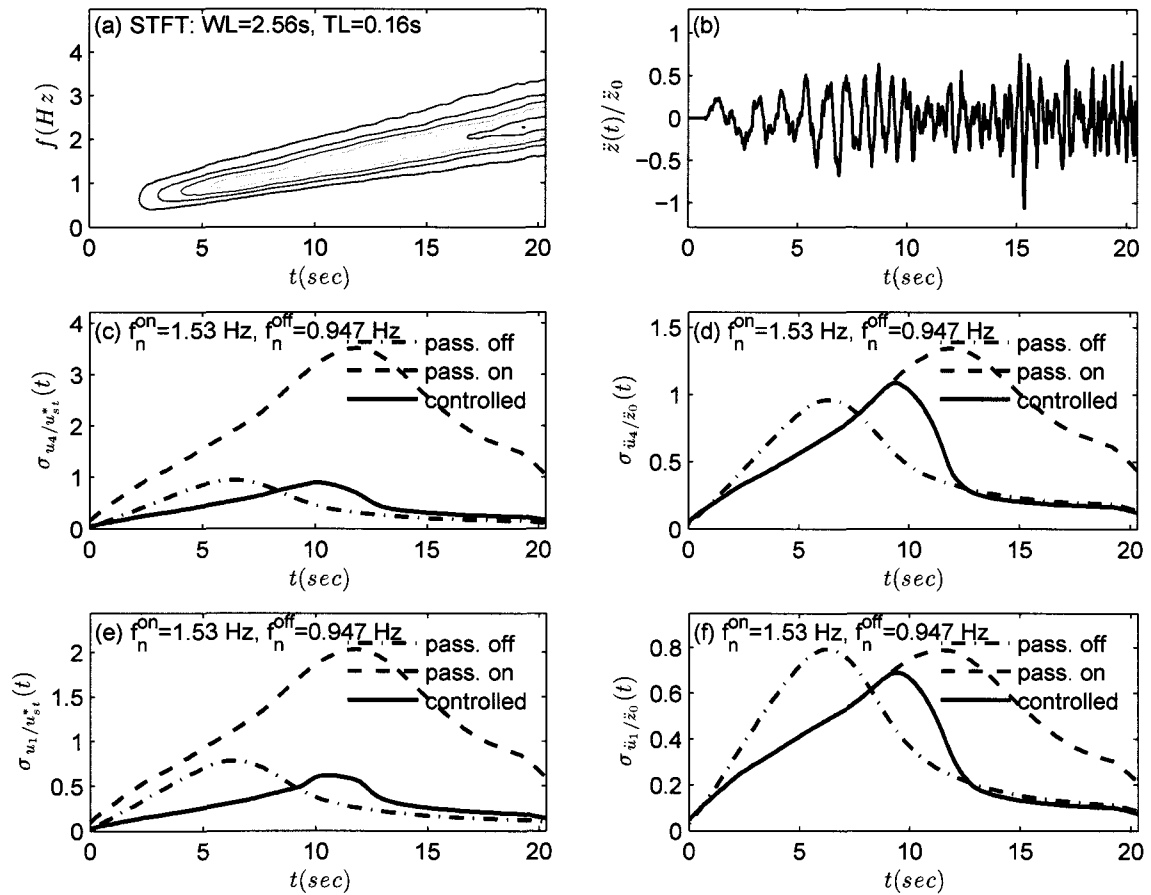


**Figure 7.13** Locally stationary base excitation of s4DOF ( $f_n^{on} = 1.53Hz$  - pass. on) (a) EPSD for 500 sample ( $0.5Hz < f_g < 2.5Hz$ ), (b) Sample ground acceleration, (c) RMS displacement response - top floor, (d) RMS acceleration response - top floor, (e) RMS displacement response - 1st floor, and (f) RMS acceleration response - 1st floor

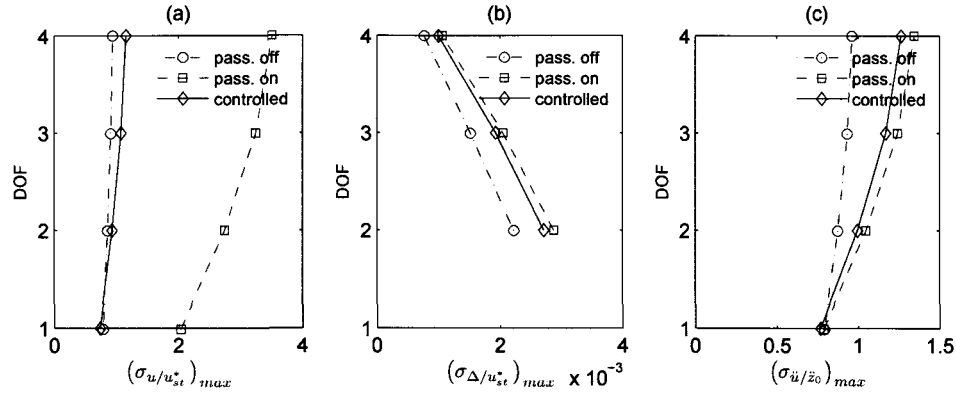


**Figure 7.14** Peak RMS responses of s4DOF ( $f_n^{on} = 1.53Hz$  - pass. on,  $0.5Hz < f_g < 2.5Hz$ )  
(a) Displacements, (b) Drifts and (c) Accelerations

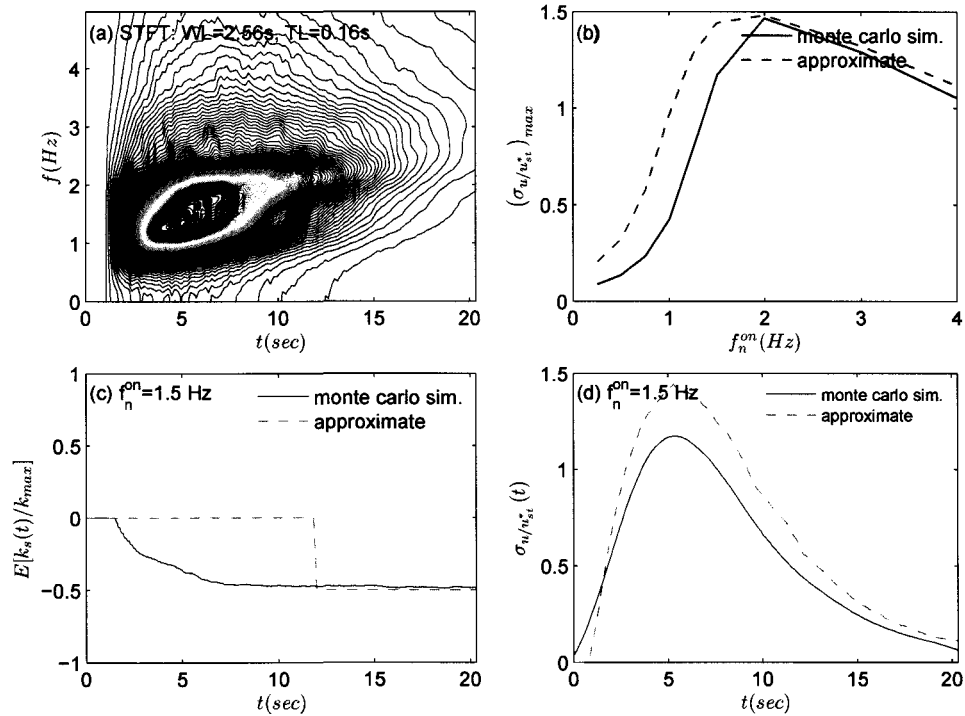


**Figure 7.15** Approximate solution via evolutionary complex frequency response function (a) EPD for 500 sample ( $1Hz < f_g < 3Hz$ ), (b) Displacement response spectrum, (c) Mean stiffness variation ( $f_n^{on} = 1.5$  - pass. on), and (d) RMS displacement response ( $f_n^{on} = 1.5$  - pass. on)

## Chapter 8

### Semi-active Single/Multiple Tuned Mass Dampers (sTMD/sMTMD) under Stochastic Excitations

Single and multiple semi-active variable stiffness tuned mass dampers (sTMD/ sMTMD) are studied under a broader range of random excitations in this chapter. Two semi-active control algorithms - one based on feedforward control by tracking excitation frequency (similar to the one proposed in Chapter 6) and the other based on feedback control by tracking the displacement response frequency - are examined under ensembles of different random excitation processes. SDOF and MDOF systems equipped with sTMD and sMTMD subjected to narrow-band stationary force excitations, wide-band locally stationary base excitations, and 1940 El Centro earthquake are investigated. Stochastic responses are computed from Monte Carlo simulations of the target evolutionary spectra describing the ground motion processes. It is shown that both feedforward and feedback control provide similar performance to passive TMD and MTMD when the structure's natural frequency is accurately identified and passive TMDs are tuned with optimum stiffness and damping. However, when a stiffness change is imposed to the primary structure and the passive TMDs becomes off-tuned, they lose their efficiency in vibration control whereas the sTMD and sMTMD successfully reduces the response. Although the proposed feedforward control has a significant potential, it is important to note certain limitations. Its efficiency depends on the presence of a distinct dominant frequency range and sufficient intensity of the excitation. As the excitation intensity decreases, the response will be controlled more by its natural frequency and less by the excitation's instantaneous (dominant) frequency, leading to a decrease in the efficiency of the feedforward control.

## 8.1 Structural Model and Formulation

The detailed information on modelling of sMTMD systems are presented in Chapter 6. Figure 6.1 is re-plotted in Figure 8.1, showing the MDOF structural model with sMTMD for force and base excitations. The normalized equations of motion given in Equation (6.7) is re-written in Equation (8.1), which is slightly modified for a more convenient presentation for random excitation processes.

$$\bar{\mathbf{M}}\ddot{\mathbf{X}} + 2\zeta_0\omega_0\bar{\mathbf{C}}\dot{\mathbf{X}} + \omega_0^2\bar{\mathbf{K}}\mathbf{X} = \begin{cases} \frac{p_0}{m_0}\bar{\mathbf{P}} f(t) & \text{(force excited)} \\ -\bar{\mathbf{M}}\mathbf{1}\ddot{z}_0(t) & \text{(base excited)} \end{cases} \quad (8.1)$$

where  $p_0 = \rho C v_0^2(z_{ref})A$  and  $\bar{\mathbf{P}} = ([1 \ 2 \ 3 \ \dots \ N]^T * h/z_{ref})^{2\alpha}$  for wind excitations.  $\rho$  is the density of the air,  $C$  is the drag coefficient,  $v_0$  is the mean wind velocity at the reference height ( $z_{ref} = 10 \text{ m}$ ),  $A$  is the effective cross-section area at each floor,  $h = 0.3 z_{ref}$  is the story height and  $\alpha = 0.4$  (for urban areas).  $\ddot{z}_0$  is selected as  $\sqrt{f_{Nyq}G_0}$  for simulated random ground motions or maximum ground acceleration for real earthquake records.

## 8.2 Control Algorithm

The control algorithm developed in Chapter 6 is slightly modified for stochastic excitations. The block diagrams for the control algorithms are given in Figure 8.2. It should be noted that the feedback shown in Figure 8.2(a) is only for adjusting the proper positioning of semi-active device. Further details in implementation of evolutionary spectrum estimation and tuning the semi-active stiffness and damping devices are shown in Figure 8.3. The control algorithms operate as follows:

1. At time  $t = 0$ , variable stiffness and damping of the sTMDs are set to the optimum values for passive TMDs.

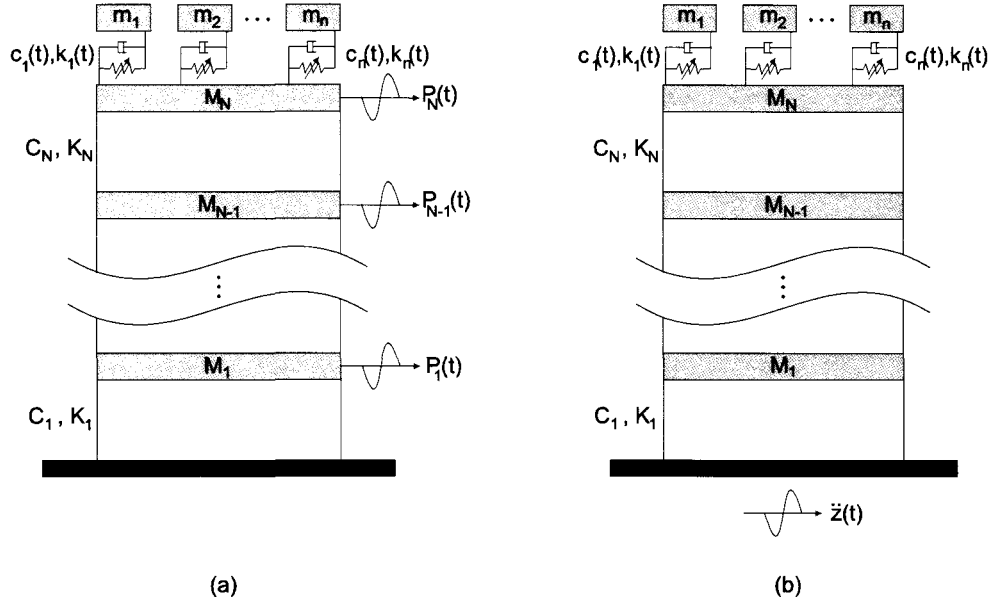
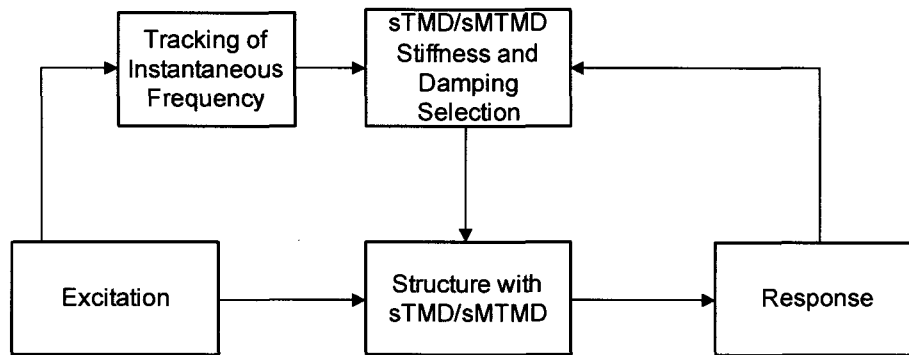


**Figure 8.1** MDOF Structural Model with sMTMD (varying  $k_1, \dots, k_n$ ) at the roof level: (a) Force Excited; (b) Base Excited

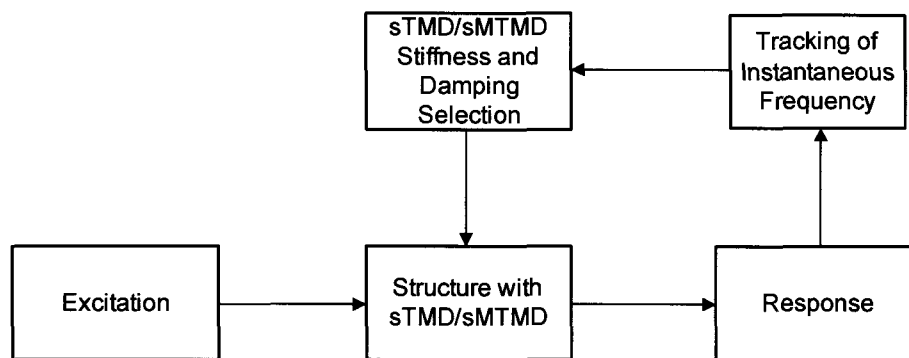
2. A moving window of  $n$  time steps of signal is chosen at certain time instants  $t_i$ .  $WL$  is the window length of  $n\Delta t$  and  $t_i = 0 : L\Delta t : t(end)$  is the new time array for the time-frequency spectra incremented with  $L\Delta t$  between successive windows.
3. Instantaneous power spectral density of the excitation (in feedforward control) and the response (in feedback control) is estimated by STFT or WT. Instantaneous (dominant) frequency is tracked by averaging the highest energy frequencies detected over an averaging time length ( $AL$ ).
4. Stiffness and damping variation starts after  $t = t_0$  to allow sufficient amount of data to be collected for accurate estimation.
5. For feedforward control, several checks are performed as follows: (i) if the excitation amplitude is less than a pre-defined level  $z_{lim}$ , sTMD stiffness and damping values from the previous time step are not changed; (ii) if the normalized energy ( $E_{band}$ )



in the region of instantaneous frequency is higher than the threshold value ( $E_{lim} = 0.9$ ) and the instantaneous frequency is within the pre-defined limits (i.e.  $f_{lim1} < f_{ins}(t_i) < f_{lim2}$ ), sTMD is tuned to the instantaneous frequency and a minimal value of damping ratio (0.01); otherwise sTMD is tuned to the instantaneous frequency and optimum damping ratio for passive TMD. The limit frequencies are set as  $f_{lim1} = 0.5f_{n1}$  and  $f_{lim2} = 2f_{n1}$  in this study. The threshold intensity level is selected as 15% of maximum intensity occurred before any given instant of the excitation. It should be noted that  $E_{lim} = 0.9$  for the wide-band processes considered in this chapter is too high, therefore, sTMD damping ratio is practically constant and is equal to the optimum damping ratio for passive TMD.

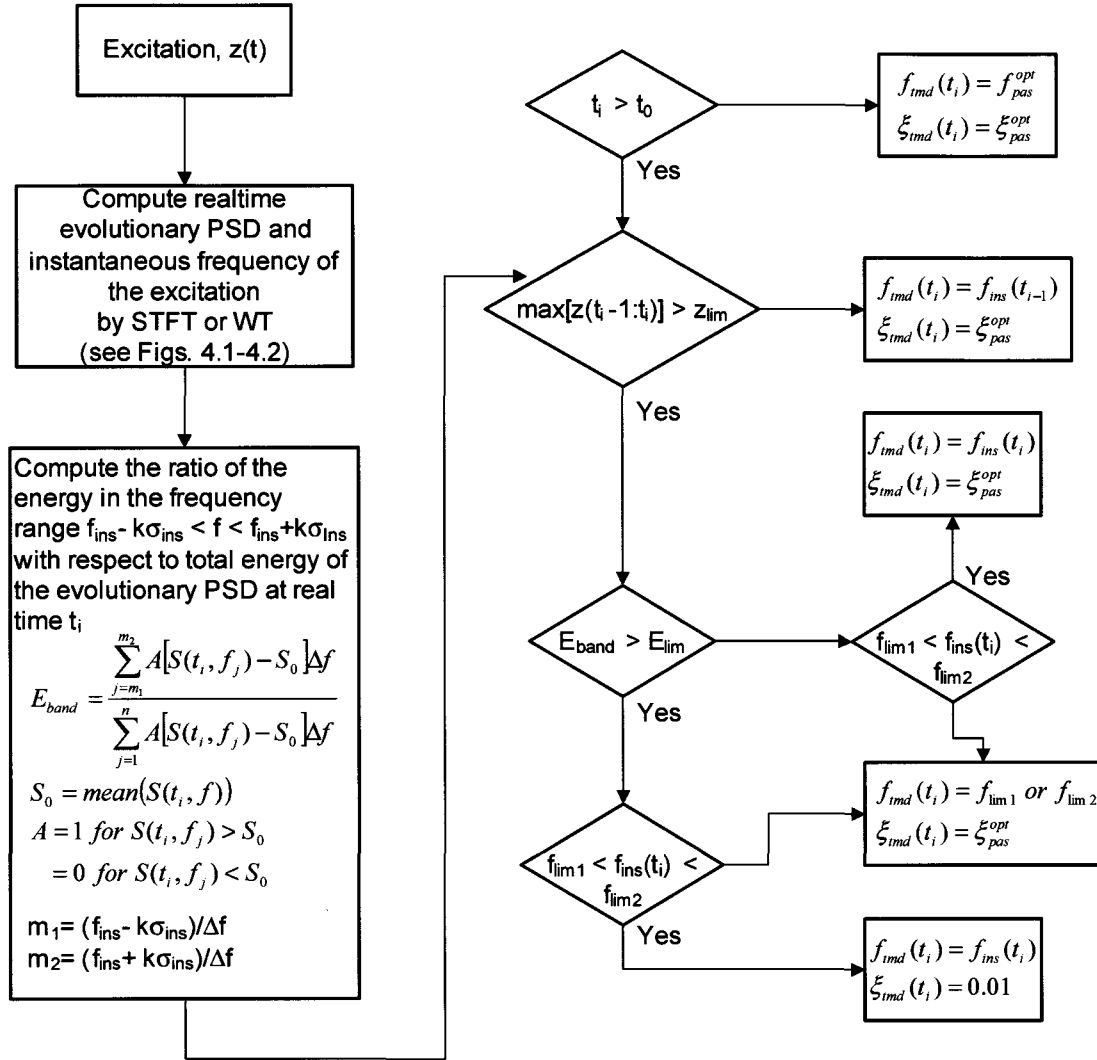


(a) Feedforward control based on tracking of instantaneous frequency of the excitation

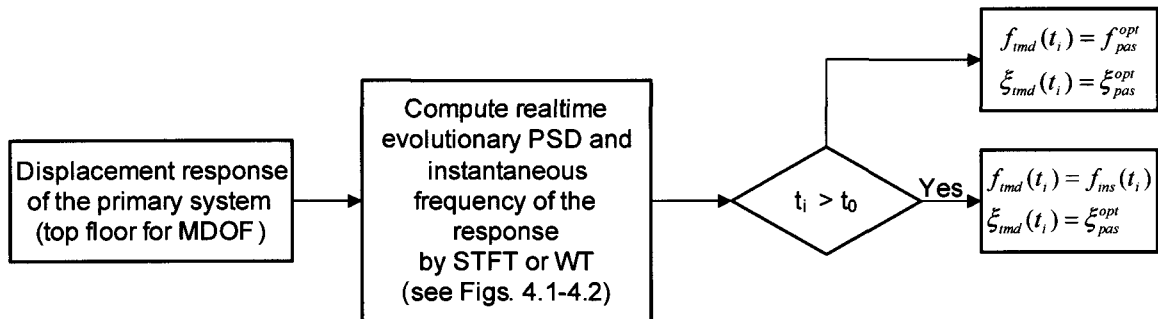


(b) Feedback control based on tracking of instantaneous frequency of the response

**Figure 8.2** Control Algorithm



(a) Feedforward control based on tracking of instantaneous frequency of the excitation



(b) Feedback control based on tracking of instantaneous frequency of the response

**Figure 8.3** Variable Stiffness and Damping Parameter Selection

### 8.3 Results for sTMD/sMTMD Systems under Stochastic Excitations

One stationary narrowband force excitation process, one stationary along-wind excitation process and one locally stationary ground motion process are used to examine the proposed control algorithms under stochastic excitations. For the excitation processes, a target evolutionary spectrum is specified and 500 sample functions have been simulated. Each simulation for the narrowband excitation has 1024 data points with a time step of  $\Delta t = 0.02 \text{ sec}$  and each simulation for the along-wind velocity has 1024 data points with a time step of  $\Delta t = 0.1 \text{ sec}$ . Ground motion simulations have 1024 data points with a time step of  $\Delta t = 0.02 \text{ sec}$ . The time history responses of different sTMD/sMTMD systems have been computed for each sample excitation and the response statistics have been obtained. In the following sections, response time histories are presented for sample responses, instantaneous RMS responses are presented for ensemble responses, and response spectra are presented for different fundamental frequencies of the main structure. sTMD/sMTMD responses are compared with passive TMD and MTMD systems. Further, 1940 El Centro Earthquake is used to study the performance of the sTMD/sMTMD under a real, highly non-stationary ground motion record. The displacement responses are normalized to present the dynamic amplification factor as follows.

$$\frac{u}{u_{st}^*} = \frac{\omega_0^2 u}{\ddot{z}_0} \quad (8.2)$$

in which

$$u_{st}^* = \frac{\ddot{z}_0}{\omega_n^2} \quad (8.3)$$

The RMS values of the normalized responses are

$$\sigma_{u/u_{st}^*} = \sqrt{E \left[ \left( \frac{\omega_0^2 u}{\ddot{z}_0} \right)^2 \right]} \quad (8.4)$$

**Table 8.1**  $H_2$  Optimized Parameters of Passive TMD and 5-TMD

		Force Excitation		Base Excitation	
		SDOF	5-DOF	SDOF	5-DOF
TMD	$\mu$	0.01	0.0159	0.01	0.0159
	$\gamma$	0.992	0.988	0.985	0.977
	$\xi_{tmd}$	0.05	0.06	0.05	0.06
5-TMD	$\mu$	0.01	0.0159	0.01	0.0159
	$\gamma_c$	0.996	0.995	0.987	0.981
	$\Delta\gamma$	0.12	0.16	0.12	0.16
	$\xi_{tmd}$	0.02	0.02	0.02	0.02

where  $\ddot{z}_0$  is the reference acceleration value.  $\ddot{z}_0$  is selected as  $\sqrt{f_{Nyq}G_0}$  for simulated random ground motions and random force excitations or maximum ground acceleration for real earthquake records. For force excitations,  $\ddot{z}_0 = p_0/m_0$  in which  $p_0 = \rho C v_0^2(z_{ref})A$  if the force excitation is obtained from wind velocity spectrum.

Optimum parameters for the passive TMD and 5-TMD, which are studied in the following sections, are numerically calculated based on minimum  $H_2$  norm and are shown in Table 8.1. For 5-DOF primary structure, mass ratio  $\mu$  is calculated with respect to first modal mass and optimum parameters are computed for an equivalent SDOF primary structure. The number of the tuned mass dampers in the multiple tuned mass damper case are set to 5, therefore MTMD and sMTMD abbreviations in the text or figures correspond to 5-TMD and 5-sTMD, respectively.

### 8.3.1 Narrow-band Stationary Excitations

To study the feedforward sTMD/sMTMD performance, 500 narrow-band stationary force excitations are simulated using the same filter for the near-fault earthquake spectrum with parameters  $f_g = 1 \text{ Hz}$  and  $\xi_g = 0.05$ . Another 500 narrow-band stationary excitations are simulated using Davenport along-wind spectrum given by Equation (1.116) to study the feedback sTMD/sMTMD performance. The wind parameters are selected as  $u_* = 1.76 \text{ m/sec}$  and  $v_0 = 45 \text{ m/sec}$ . The mean velocity profile is defined by the power law [Eq. (1.112)] with  $\alpha = 0.4$  and story heights are assumed to be uniform as  $h/z_{ref} = 0.3$  where  $z_{ref} = 10 \text{ m}$ .

The results for sTMD/sMTMD with feedforward control are presented in Figures 8.4 through 8.7. The estimated evolutionary excitation spectrum (by STFT), a sample excitation are shown in Figure 8.4 along with the RMS responses and the response spectra. Figure 8.4 (c, d) correspond to the SDOF primary structure without any damage whereas Figure 8.4 (e,f) correspond to the damaged SDOF primary structure after  $t = 4.1 \text{ sec}$ . sTMD/sMTMD with feedforward control provides similar response reduction with respect to passive TMD/MTMD in no damage case. For damaged case, both passive TMDs become off-tuned and inefficient while sTMDs continue to provide significant response reduction at the resonance region. Sample time history responses of the SDOF primary structure (damaged at  $t = 4.1 \text{ sec}$  and  $f_n = 1.5 \text{ Hz} \rightarrow 1.1 \text{ Hz}$ ) along with variable stiffness and damping of sTMDs are presented in Figure 8.5. The response of a 5-DOF primary structure is studied next for further investigation of the sTMD/sMTMD performance. The peak floor displacements of a 5-DOF uniform primary structure are presented in Figures 8.6 for undamaged case ((a)  $f_n = 1 \text{ Hz}$ ) and for damaged case ((b)  $f_n = 1.2 \text{ Hz} \rightarrow 1.0 \text{ Hz}$ ). The damage is induced by decreasing the stiffness of the first DOF by half. The top floor

displacement response history for the damaged case is presented in Figure 8.7. Similar observations can be made for these specific cases as in the ensemble RMS response histories and spectra presented in Figure 8.4.

The results for sTMD/sMTMD with feedback control are presented in Figures 8.8 through 8.11. The estimated evolutionary excitation spectrum (by STFT), a sample excitation are shown in Figure 8.8 along with the RMS responses and the response spectra. Figure 8.8 (c, d) correspond to the SDOF primary structure without any damage whereas Figure 8.8 (e, f) correspond to the damaged SDOF primary structure after  $t = 20 \text{ sec}$ . Response spectra in Figure 8.8 clearly show that sTMD/sMTMD with feedback control have similar efficiencies compared to passive ones for undamaged structures. For damaged case, passive TMDs become off-tuned and inefficient while sTMD/sMTMD leads to significant response reduction. Sample time history responses of the SDOF primary structure (damaged at  $t = 20 \text{ sec}$  and  $f_n = 0.3 \text{ Hz} \rightarrow 0.21 \text{ Hz}$ ) along with variable stiffness and damping of sTMDs are presented in Figure 8.9. The response of a 5-DOF primary structure is studied next for further investigation of the sTMD/sMTMD performance. The peak floor displacements of a 5-DOF uniform primary structure are presented in Figures 8.10 for undamaged case ((a)  $f_n = 0.3 \text{ Hz}$ ) and for damaged case ((b)  $f_n = 0.3 \text{ Hz} \rightarrow 0.21 \text{ Hz}$ ). The damage is induced by decreasing the stiffness of the first DOF by half. The top floor displacement response history for the damaged case is presented in Figure 8.11. Similar observations can be made for these specific cases as in the ensemble RMS response histories and spectra presented in Figure 8.8.

### 8.3.2 Locally Stationary Excitations

500 locally stationary excitations are simulated using the near-fault earthquake spectrum given by Equation (1.124). The soil parameters are selected as  $\omega_g = 2\pi \text{ rad/sec}$  and

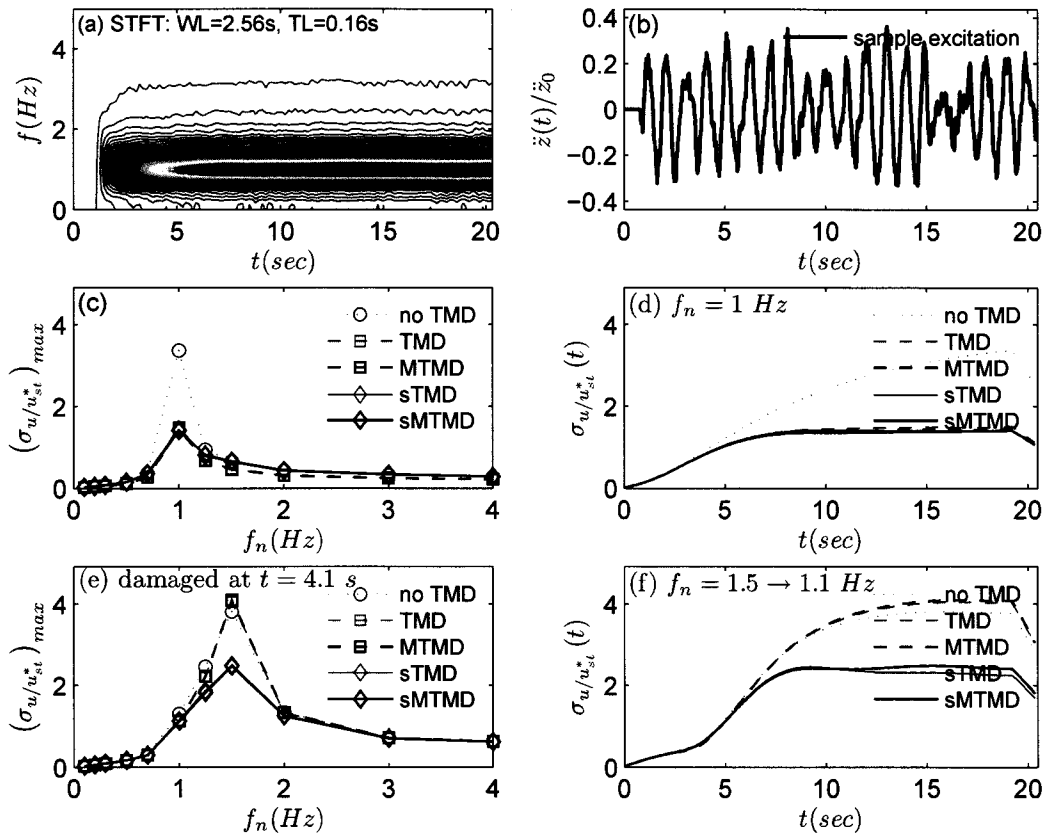


**Figure 8.4** Narrow-band stationary force excitation of SDOF (feedforward): (a) EPSD for 500 sample, (b) Sample acceleration, (c) Displacement response spectra, (d) RMS displacement response ( $f_n = 1.0$  Hz), (e) Displacement response spectra - damaged, (f) RMS displacement response - damaged ( $f_n = 1.5 \rightarrow 1.1$  Hz for  $t > 4.1$  sec)

$\xi_g = 0.3$ . A time envelope is applied in the form of Equation (7.32).

The results for sTMD/sMTMD with feedforward control are presented in Figures 8.12 through 8.15. The estimated evolutionary excitation spectrum (by STFT), a sample excitation are shown in Figure 8.12 along with the RMS responses and the response spectra. Figure 8.12 (c, d) correspond to the SDOF primary structure at 1.0 Hz without any damage whereas Figure 8.12 (e, f) correspond to the damaged SDOF primary structure after  $t = 4.1$  sec. sTMD/sMTMD with feedforward control provides response reduction



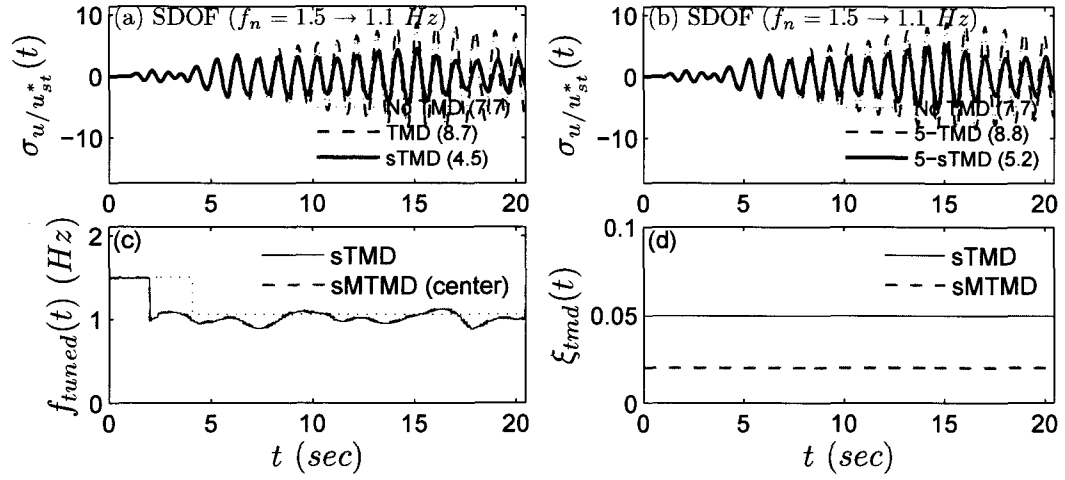


**Figure 8.5** Narrow-band stationary force excitation of SDOF (feedforward): (a,b) Time history response, (c,d) variable stiffness and damping

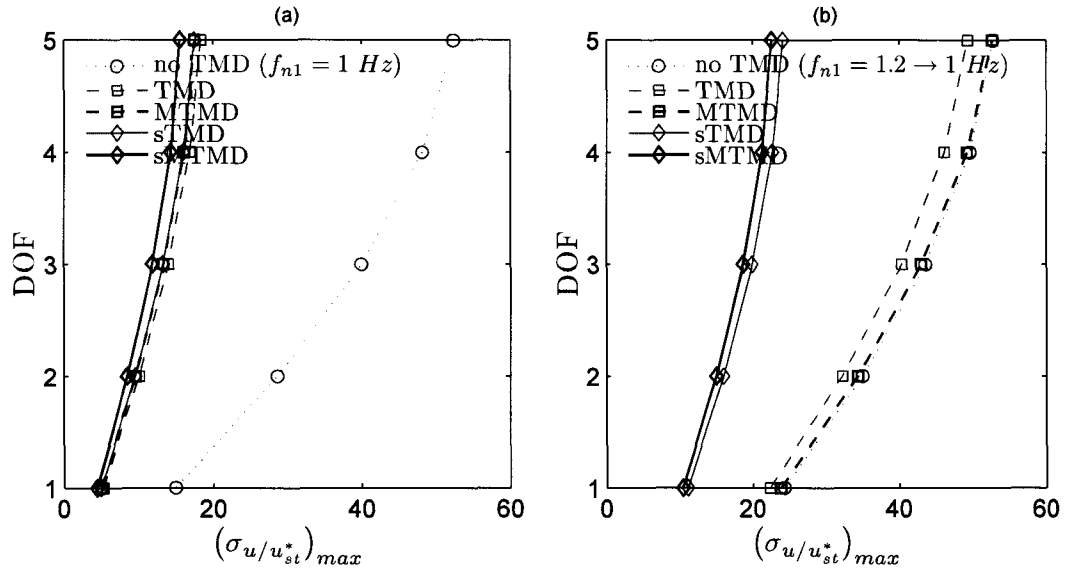


**Figure 8.6** Narrow-band stationary force excitation of 5-DOF (feedforward): (a) Peak RMS displacements ( $f_n = 1.0$  Hz), (b) Peak RMS displacements - damaged ( $f_n = 1.2 \rightarrow 1.0$  Hz for  $t \geq 4.1$  sec)

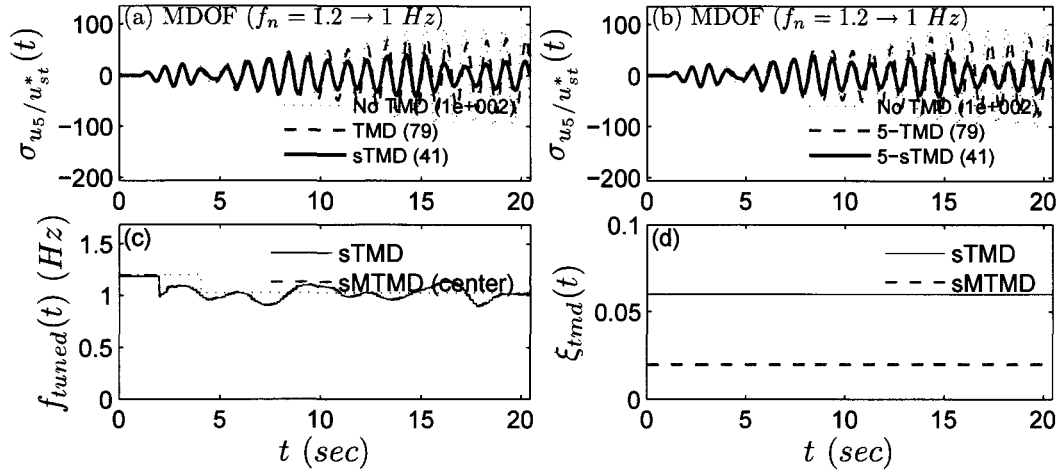


**Figure 8.7** Narrow-band stationary force excitation of 5-DOF (feedforward): (a,b) Top floor displacement response history, (c,d) variable stiffness and damping

close to passive TMD/MTMD in no damage case. For damaged case, passive TMDs become off-tuned and inefficient while sTMD/sMTMD lead to significant response reduction. Sample time history responses of the SDOF primary structure (damaged at  $t = 4.1$  sec and  $f_n = 1.5$  Hz  $\rightarrow$  1.1 Hz) along with variable stiffness and damping of sTMDs are presented in Figure 8.13. The response of a 5-DOF primary structure is studied next for further investigation of the sTMD/sMTMD performance. The peak floor displacements of a 5-DOF uniform primary structure are presented in Figure 8.14 for undamaged case ((a)  $f_n = 1.0$  Hz) and for damaged case ((b)  $f_n = 1.3$  Hz  $\rightarrow$  1.1 Hz). The damage is induced by decreasing the stiffness of the first DOF by half. The top floor displacement response history for the damaged case is presented in Figure 8.15. Similar observations can be made for these specific cases as in the ensemble RMS response histories and spectra presented in Figure 8.12.

The results for sTMD/sMTMD with feedback control are presented in Figures 8.16 through 8.19. The estimated evolutionary excitation spectrum (by STFT), a sample excitation are shown in Figure 8.16 along with the RMS responses and the response spectra.

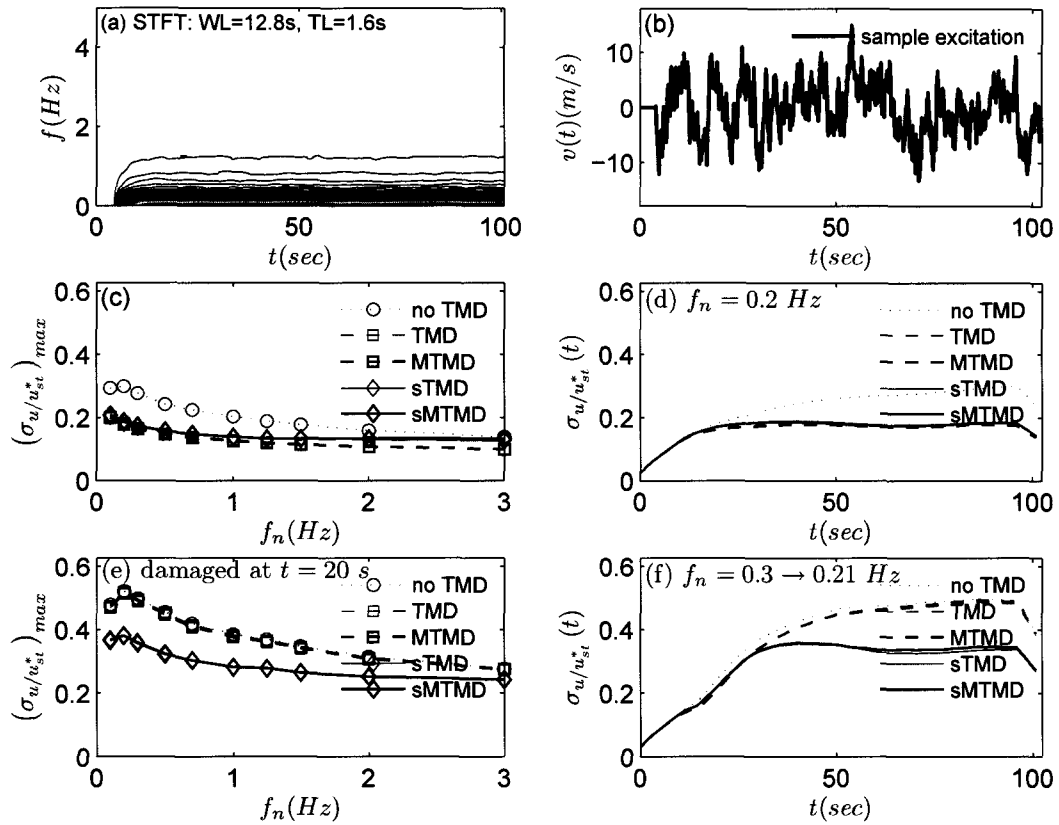


**Figure 8.8** Narrow-band stationary wind excitation of SDOF (feedback): (a) EPSP for 500 sample, (b) Sample wind velocity, (c) Displacement response spectra, (d) RMS displacement response ( $f_n = 0.2$  Hz), (e) Displacement response spectra - damaged, (f) RMS displacement response - damaged ( $f_n = 0.3 \rightarrow 0.21$  Hz for  $t > 20$  sec)

Figure 8.16 (c, d) correspond to the SDOF primary structure without any damage whereas Figure 8.16 (e, f) correspond to the damaged SDOF primary structure after  $t = 4.1$  sec. Response spectra in Figure 8.16 clearly show that sTMD/sMTMD with feedback control have similar efficiencies compared to passive ones for undamaged structures. For damaged case, passive TMDs become off-tuned and inefficient while sTMD/sMTMD leads to significant response reduction. Sample time history responses of the SDOF primary structure (damaged at  $t = 4.1$  sec and  $f_n = 1.5$  Hz  $\rightarrow$  1.1 Hz) along with variable stiffness and damping of sTMDs are presented in Figure 8.17. The response of a 5-DOF primary structure is

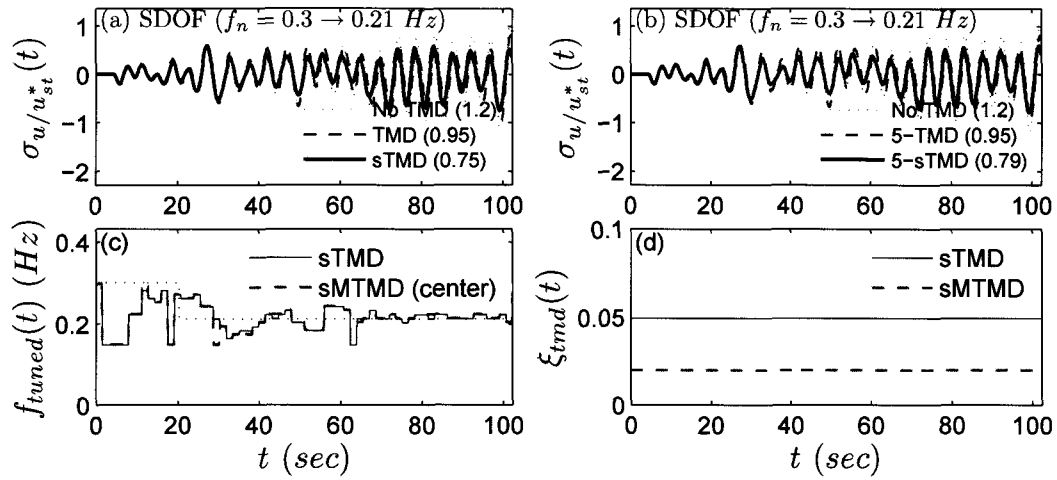


**Figure 8.9** Narrow-band stationary wind excitation of SDOF (feedback): (a,b) Time history response, (c,d) variable stiffness and damping

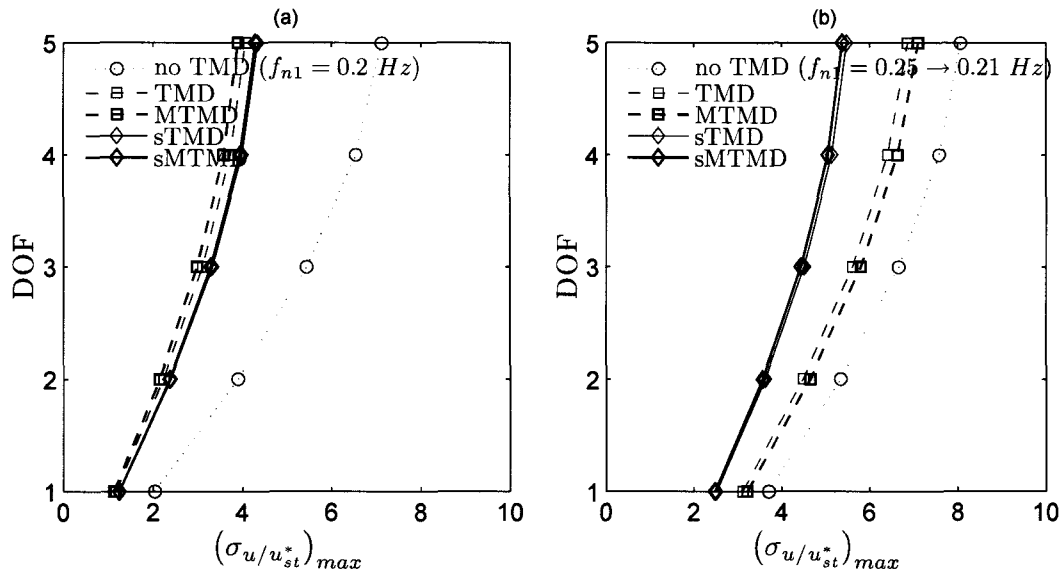


**Figure 8.10** Narrow-band stationary wind excitation of 5-DOF (feedback): (a) Peak RMS displacements ( $f_n = 0.2$  Hz), (b) Peak RMS displacements - damaged ( $f_n = 0.25 \rightarrow 0.21$  Hz for  $t \geq 20$  sec)

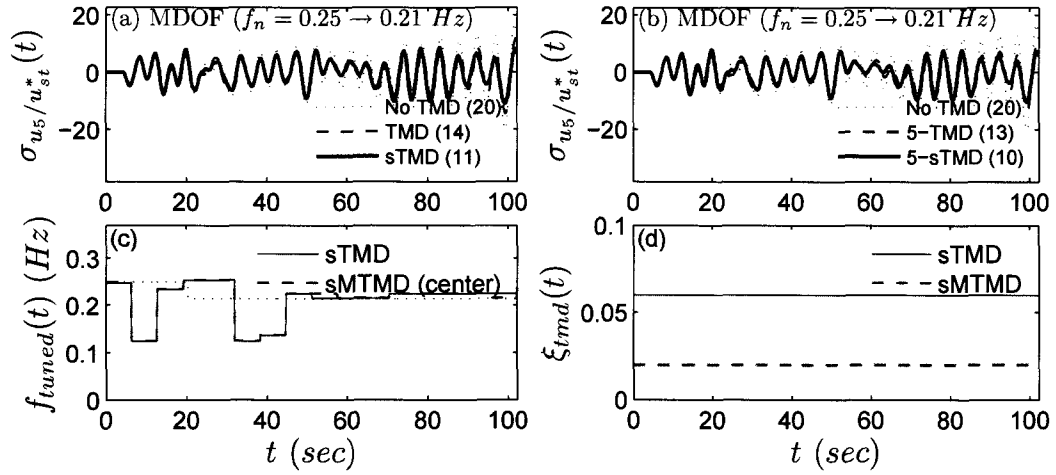


**Figure 8.11** Narrow-band stationary wind excitation of 5-DOF (feedback): (a,b) Top floor displacement response history, (c,d) variable stiffness and damping

studied next for further investigation of the sTMD/sMTMD performance. The peak floor displacements of a 5-DOF uniform primary structure are presented in Figure 8.18 for undamaged case ((a)  $f_n = 1.0$  Hz) and for damaged case ((b)  $f_n = 1.2$  Hz  $\rightarrow$  1.0 Hz). The damage is induced by decreasing the stiffness of the first DOF. The top floor displacement response history for the damaged case is presented in Figure 8.19. Similar observations can be made for these specific cases as in the ensemble RMS response histories and spectra presented in Figure 8.16.

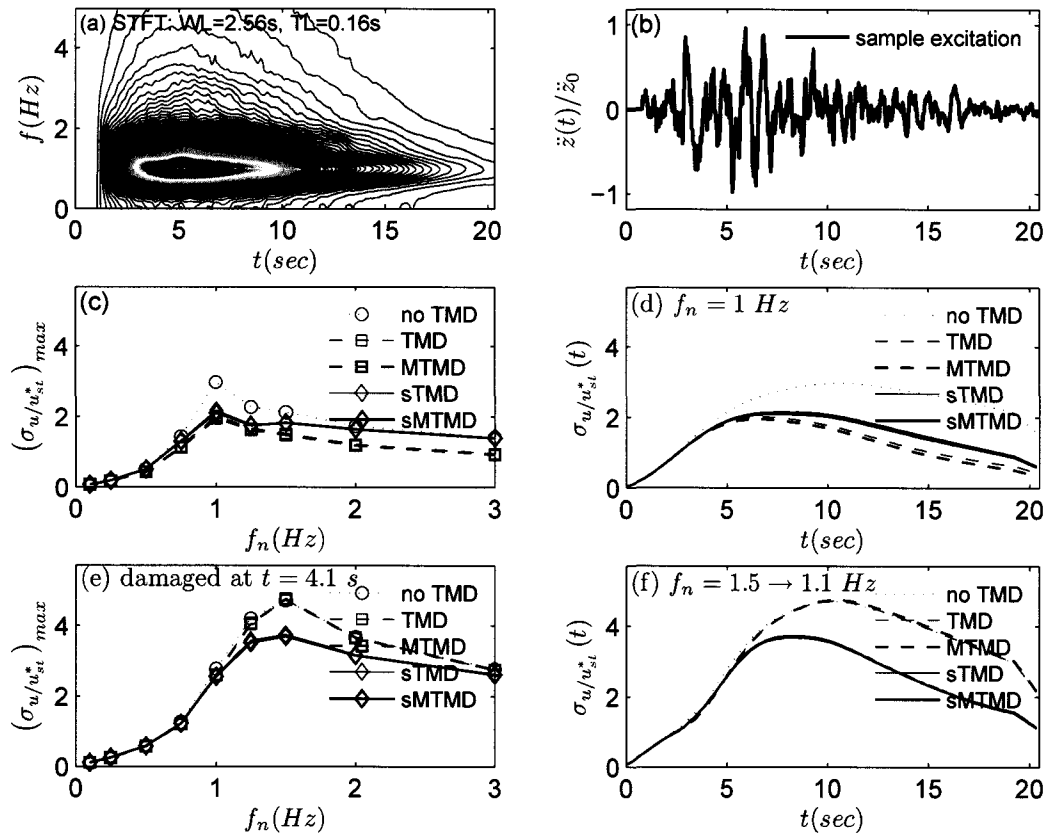


**Figure 8.12** Locally stationary base excitation of SDOF (feedforward): (a) EPSD for 500 sample, (b) Sample ground acceleration, (c) Displacement response spectra, (d) RMS displacement response ( $f_n = 1.0$  Hz), (e) Displacement response spectra - damaged, (f) RMS displacement response - damaged ( $f_n = 1.5 \rightarrow 1.1$  Hz for  $t > 4.1$  sec)

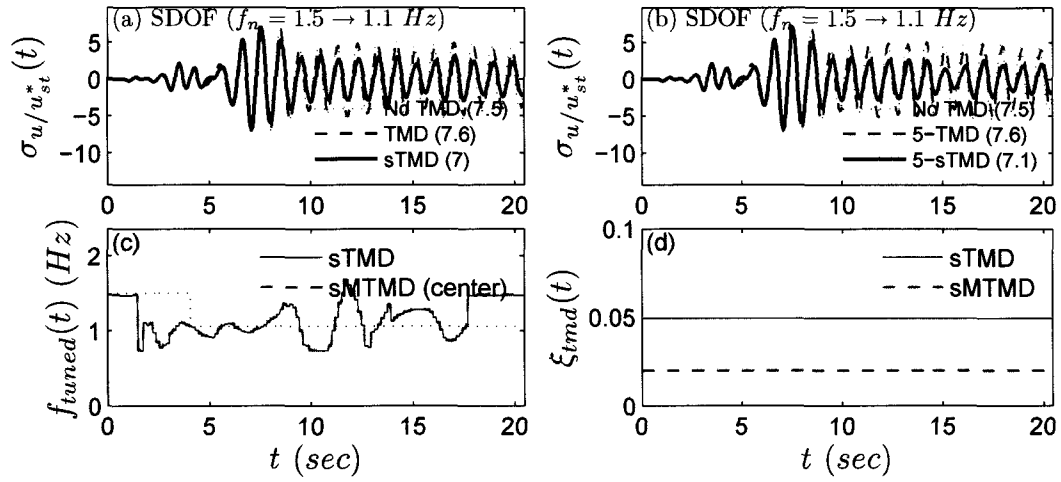


**Figure 8.13** Locally stationary base excitation of SDOF (feedforward): (a,b) Time history response, (c,d) variable stiffness and damping

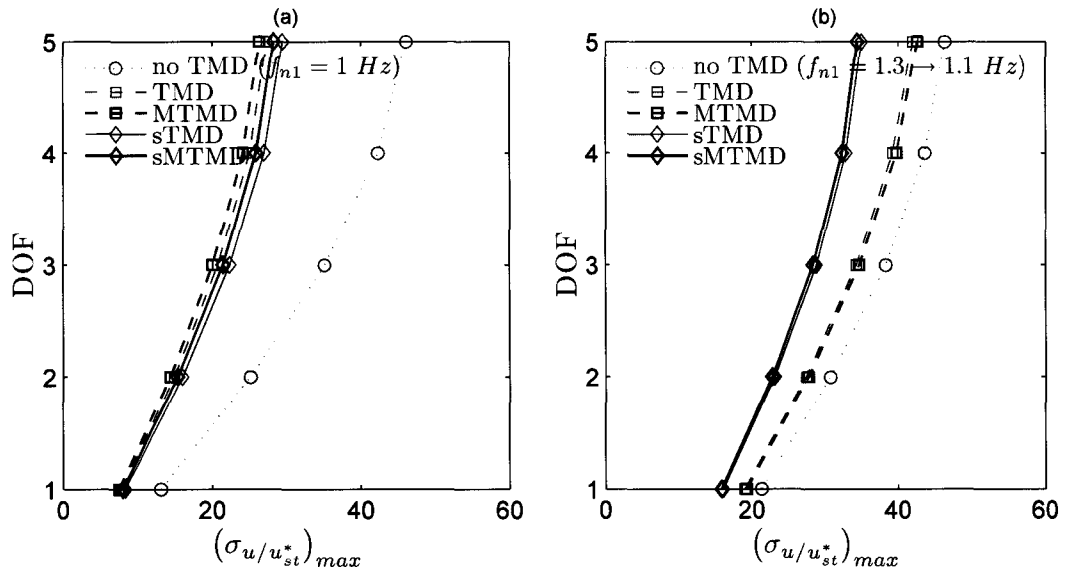


**Figure 8.14** Locally stationary base excitation of 5-DOF (feedforward): (a) Peak RMS displacements ( $f_n = 1.0 \text{ Hz}$ ), (b) Peak RMS displacements - damaged ( $f_n = 1.3 \rightarrow 1.1 \text{ Hz}$  for  $t \geq 4.1 \text{ sec}$ )

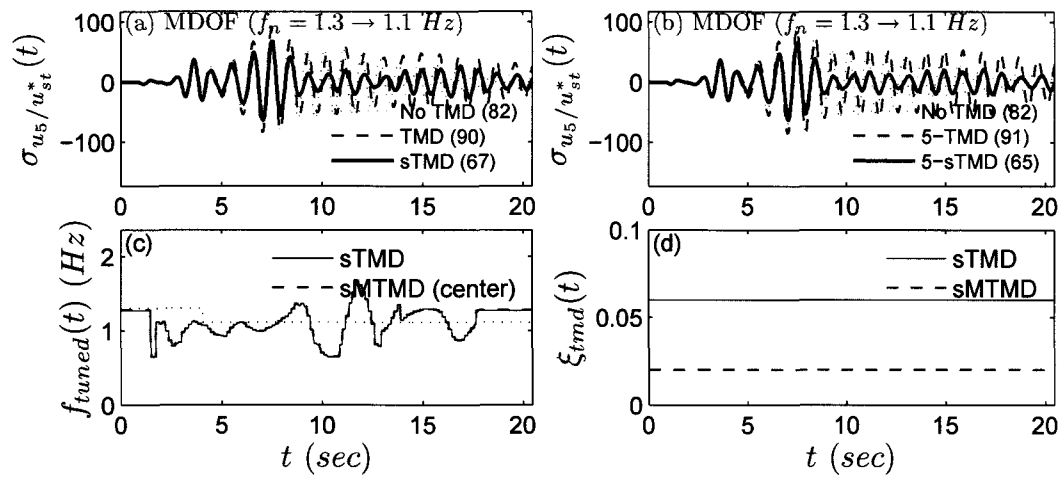


**Figure 8.15** Locally stationary base excitation of 5-DOF (feedforward): (a,b) Top floor displacement response history, (c,d) variable stiffness and damping



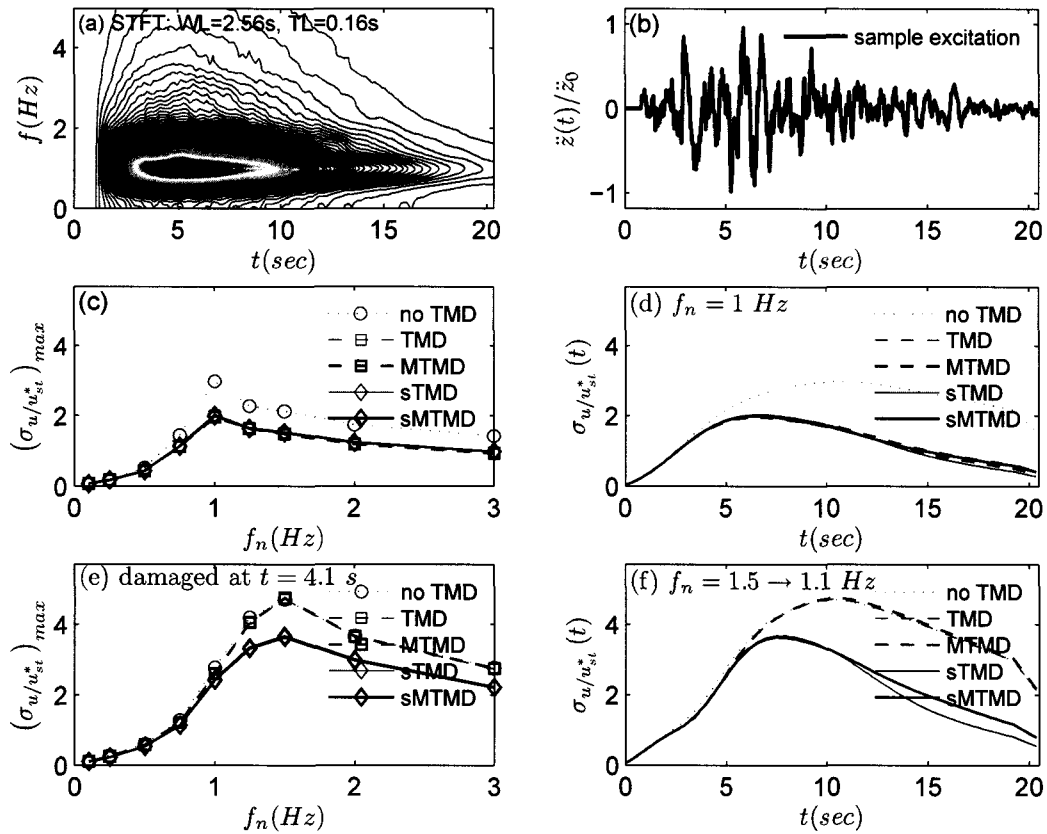


**Figure 8.16** Locally stationary base excitation of SDOF (feedback): (a) EPSD for 500 sample, (b) Sample ground acceleration, (c) Displacement response spectra, (d) RMS displacement response ( $f_n = 1.0 Hz$ ), (e) Displacement response spectra - damaged, (f) RMS displacement response - damaged ( $f_n = 1.5 \rightarrow 1.1 Hz$  for  $t > 4.1 sec$ )

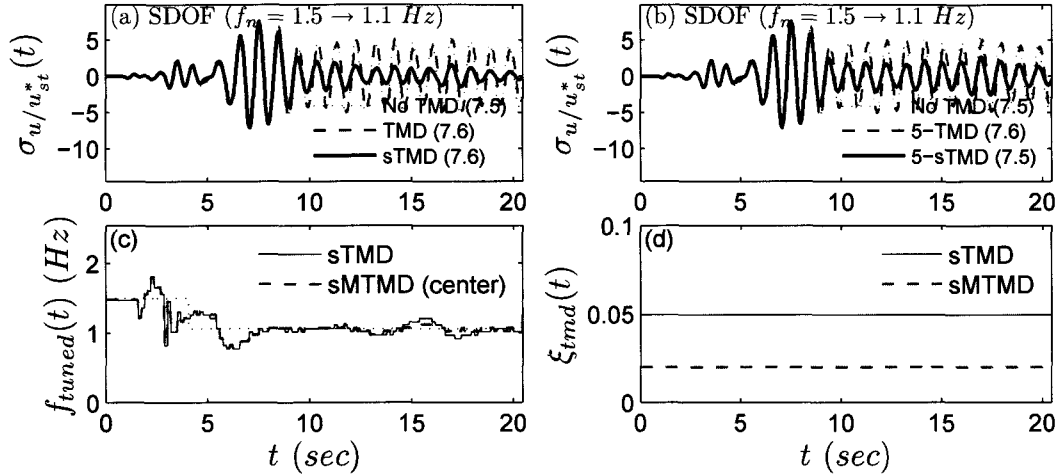


**Figure 8.17** Locally stationary base excitation of SDOF (feedback): (a,b) Time history response, (c,d) variable stiffness and damping

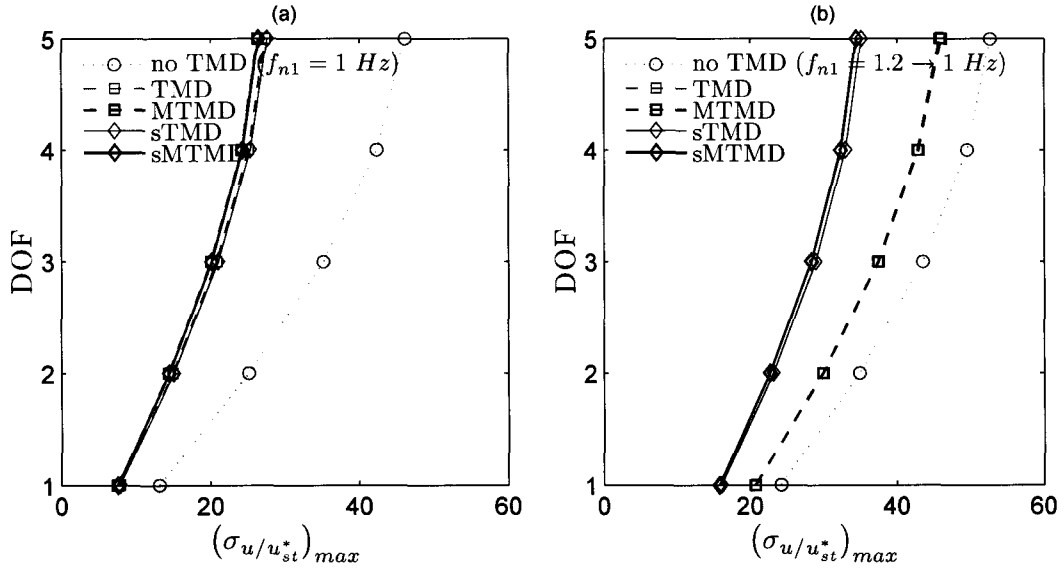


**Figure 8.18** Locally stationary base excitation of 5-DOF (feedback): (a) Peak RMS displacements ( $f_n = 1.0$  Hz), (b) Peak RMS displacements - damaged ( $f_n = 1.2 \rightarrow 1.0$  Hz for  $t \geq 4.1$  sec)

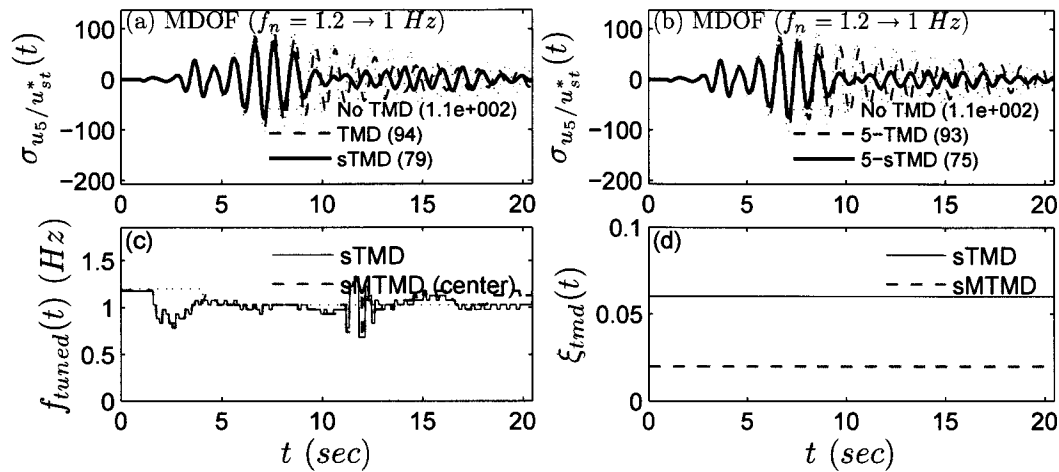


**Figure 8.19** Locally stationary base excitation of 5-DOF (feedback): (a,b) Top floor displacement response history, (c,d) variable stiffness and damping

### 8.3.3 Recorded Earthquake

1940 El Centro Earthquake is used to study the performance of the sTMD/sMTMD under a real, highly non-stationary ground motion record.

The results for sTMD/sMTMD with feedforward control are presented in Figures 8.20 through 8.23. The estimated evolutionary excitation spectrum (by STFT), the acceleration record are shown in Figure 8.20 along with the RMS responses and the response spectra. Figure 8.20 (c, d) correspond to the SDOF primary structure without any damage whereas Figure 8.20 (e,f) correspond to the damaged SDOF primary structure after  $t = 2.6 \text{ sec}$ . sTMD/sMTMD with feedforward control provides response reduction close to passive TMD/MTMD in no damage case. For damaged case, passive TMDs become off-tuned and inefficient while sTMD/sMTMD lead to significant response reduction. Sample time history responses of the SDOF primary structure (damaged at  $t = 2.6 \text{ sec}$  and  $f_n = 2.0 \text{ Hz} \rightarrow 1.4 \text{ Hz}$ ) along with variable stiffness and damping of sTMDs are presented in Figure 8.21. The response of a 5-DOF primary structure is studied next for

further investigation of the sTMD/sMTMD performance. The peak floor displacements of a 5-DOF uniform primary structure are presented in Figure 8.22 for undamaged case ((a)  $f_n = 1.7 \text{ Hz}$ ) and for damaged case ((b)  $f_n = 1.7 \text{ Hz} \rightarrow 1.5 \text{ Hz}$ ). The damage is induced by decreasing the stiffness of the first DOF by half. The top floor displacement response history for the damaged case is presented in Figure 8.23. Similar observations can be made for these specific cases as in the ensemble RMS response histories and spectra presented in Figure 8.20.

The results for sTMD/sMTMD with feedback control are presented in Figures 8.24 through 8.27. The estimated evolutionary excitation spectrum (by STFT), a sample excitation are shown in Figure 8.24 along with the RMS responses and the response spectra. Figure 8.24 (c, d) correspond to the SDOF primary structure without any damage whereas Figure 8.24 (e, f) correspond to the damaged SDOF primary structure after  $t = 2.6 \text{ sec}$ . Response spectra in Figure 8.24 clearly show that sTMD/sMTMD with feedback control have similar efficiencies compared to passive ones for undamaged structures. For damaged case, passive TMDs become off-tuned and inefficient while sTMD/sMTMD leads to significant response reduction. Sample time history responses of the SDOF primary structure (damaged at  $t = 2.6 \text{ sec}$  and  $f_n = 3.0 \text{ Hz} \rightarrow 2.1 \text{ Hz}$ ) along with variable stiffness and damping of sTMDs are presented in Figure 8.25. The response of a 5-DOF primary structure is studied next for further investigation of the sTMD/sMTMD performance. The peak floor displacements of a 5-DOF uniform primary structure are presented in Figures 8.26 for undamaged case ((a)  $f_n = 2.5 \text{ Hz}$ ) and for damaged case ((b)  $f_n = 2.5 \text{ Hz} \rightarrow 2.0 \text{ Hz}$ ). The damage is induced by decreasing the stiffness of the first DOF. The top floor displacement response history for the damaged case is presented in Figure 8.27. Similar observations can be made for these specific cases as in the ensemble RMS response histories and spectra presented in Figure 8.24.

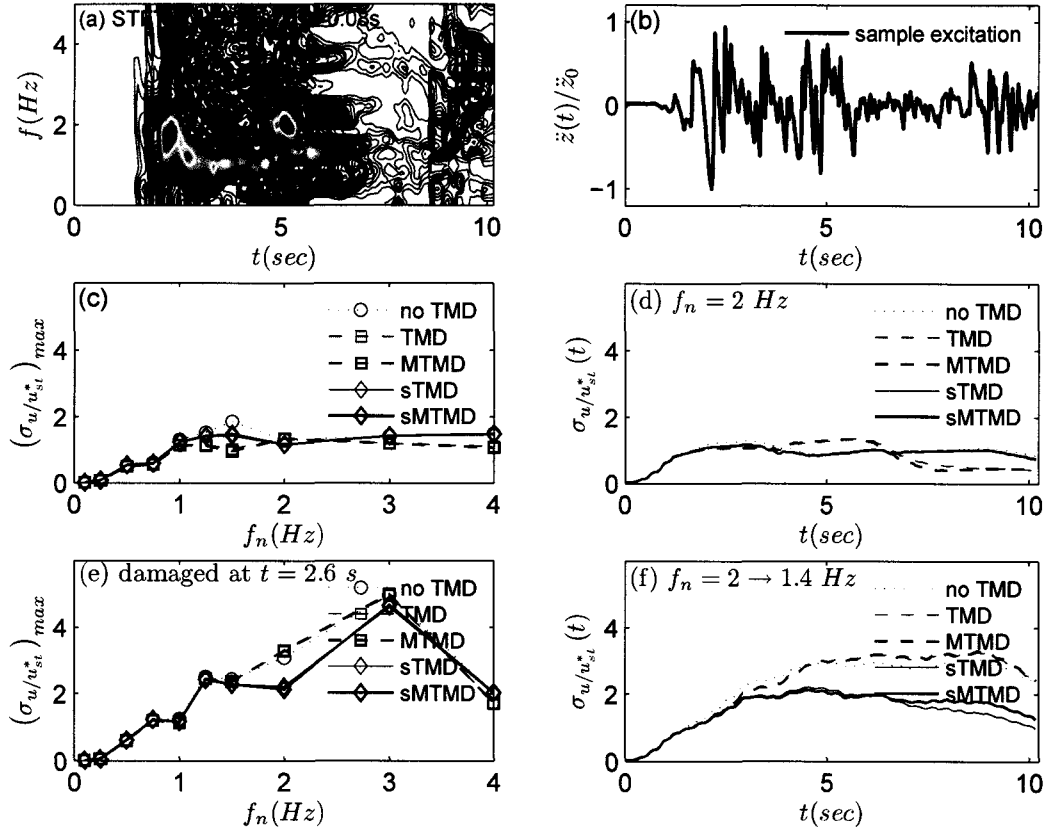


**Figure 8.20** 1940 El Centro Earthquake excitation of SDOF (feedforward): (a) EPSD, (b) Ground acceleration, (c) Displacement response spectra, (d) RMS displacement response ( $f_n = 2.0$  Hz), (e) Displacement response spectra - damaged, (f) RMS displacement response - damaged ( $f_n = 2.0 \rightarrow 1.4$  Hz for  $t > 2.6$  sec)

## 8.4 Concluding Remarks

For random signals, feedforward sTMD/ sMTMD have similar RMS responses compared to the passive counterparts. However, if the primary structure's natural frequency changes, passive TMDs become off-tuned and ineffective, whereas sTMD and sMTMD continues to suppress the vibration robustly.

Feedback sTMD/ sMTMD are slightly more effective and robust than feedforward sTMD/ sMTMD since the response signal is smoother and slowly varying due to filter-

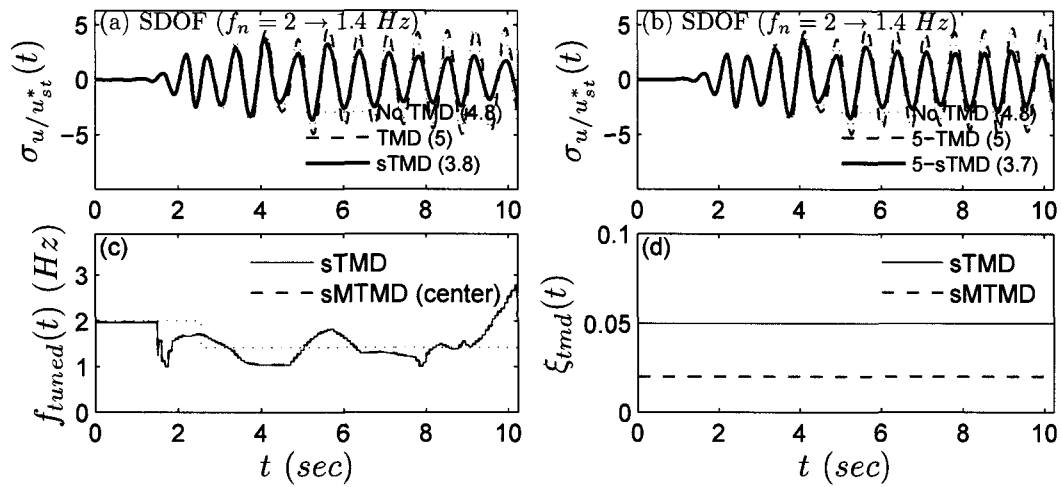


**Figure 8.21** 1940 El Centro Earthquake excitation of SDOF (feedforward): (a,b) Time history response, (c,d) variable stiffness and damping

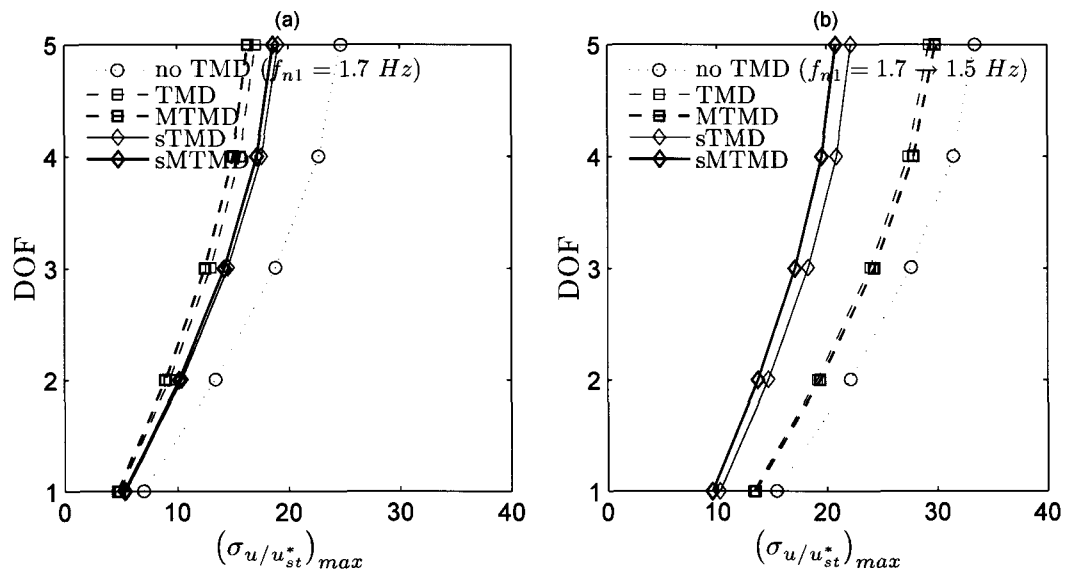


**Figure 8.22** 1940 El Centro Earthquake excitation of 5-DOF (feedforward): (a) Peak RMS displacements ( $f_n = 1.7$  Hz), (b) Peak RMS displacements - damaged ( $f_n = 1.7 \rightarrow 1.5$  Hz for  $t \geq 2.6$  sec)

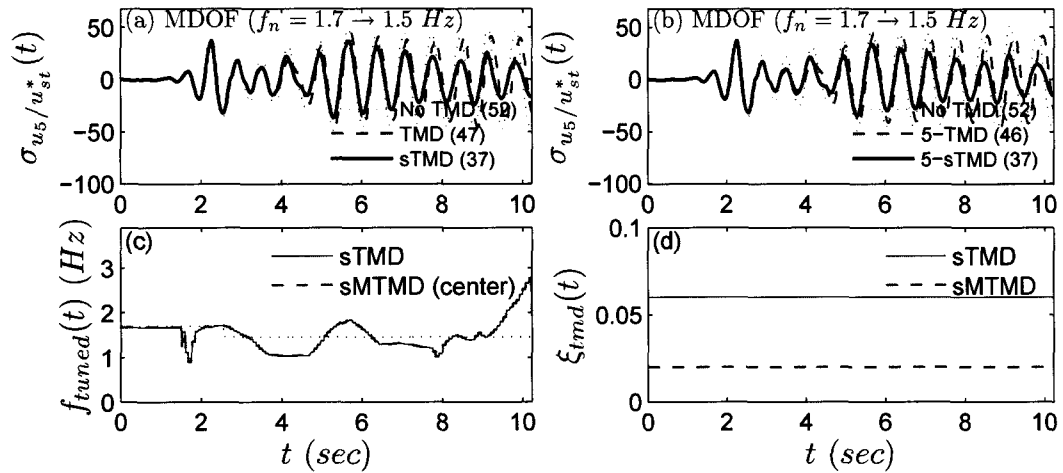


**Figure 8.23** 1940 El Centro Earthquake excitation of 5-DOF (feedforward): (a,b) Top floor displacement response history, (c,d) variable stiffness and damping

ing effect of the structure with respect to the random excitation process.

Feedback sTMD/sMTMD have again similar RMS responses compared to the passive counterparts and their advantage becomes apparent when the primary structure's natural frequency changes and passive TMDs become off-tuned and ineffective.

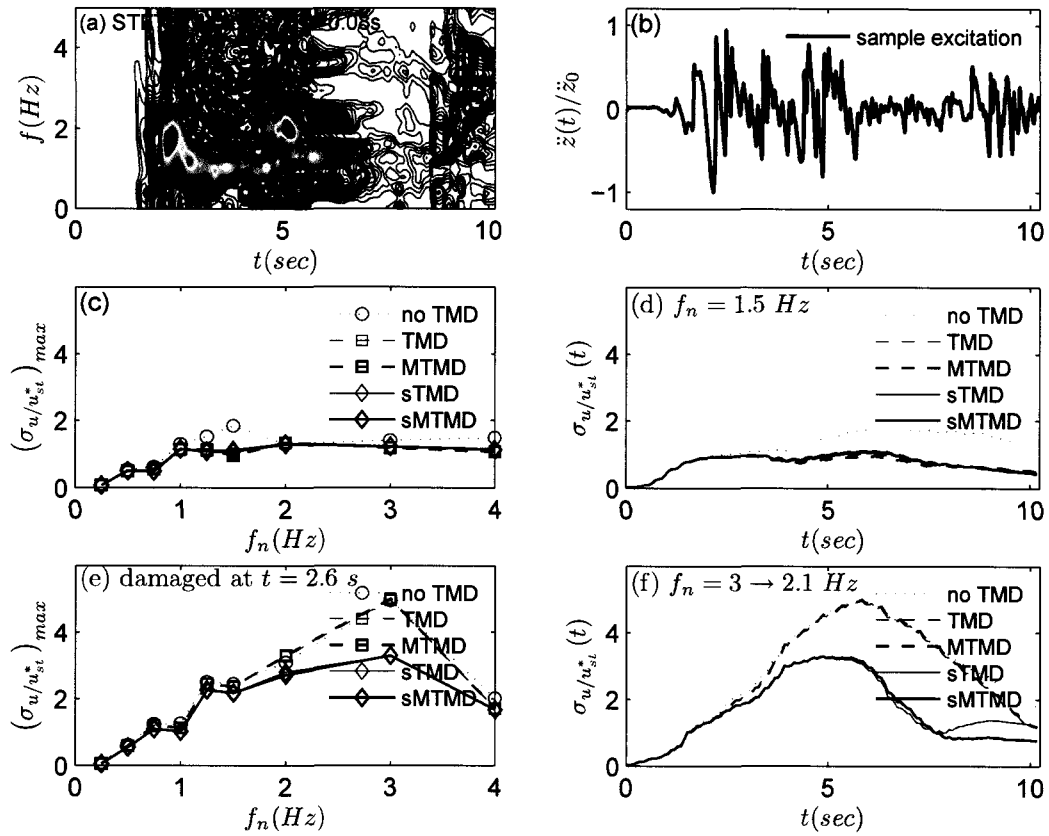


**Figure 8.24** 1940 El Centro Earthquake excitation of SDOF (feedback): (a) EPSD, (b) Ground acceleration, (c) Displacement response spectra, (d) RMS displacement response ( $f_n = 1.5$  Hz), (e) Displacement response spectra - damaged, (f) RMS displacement response - damaged ( $f_n = 3.0 \rightarrow 2.1$  Hz for  $t > 2.6$  sec)



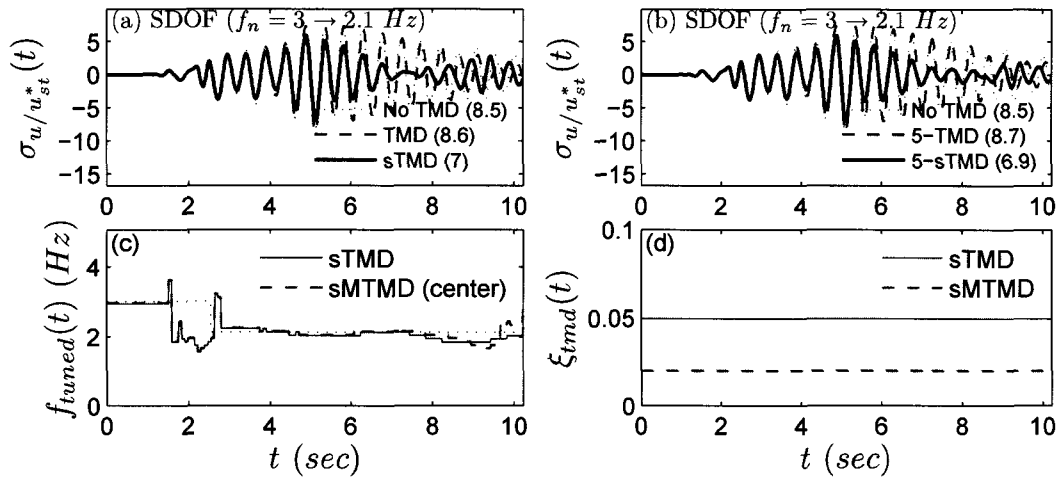


**Figure 8.25** 1940 El Centro Earthquake excitation of SDOF (feedback): (a,b) Time history response, (c,d) variable stiffness and damping

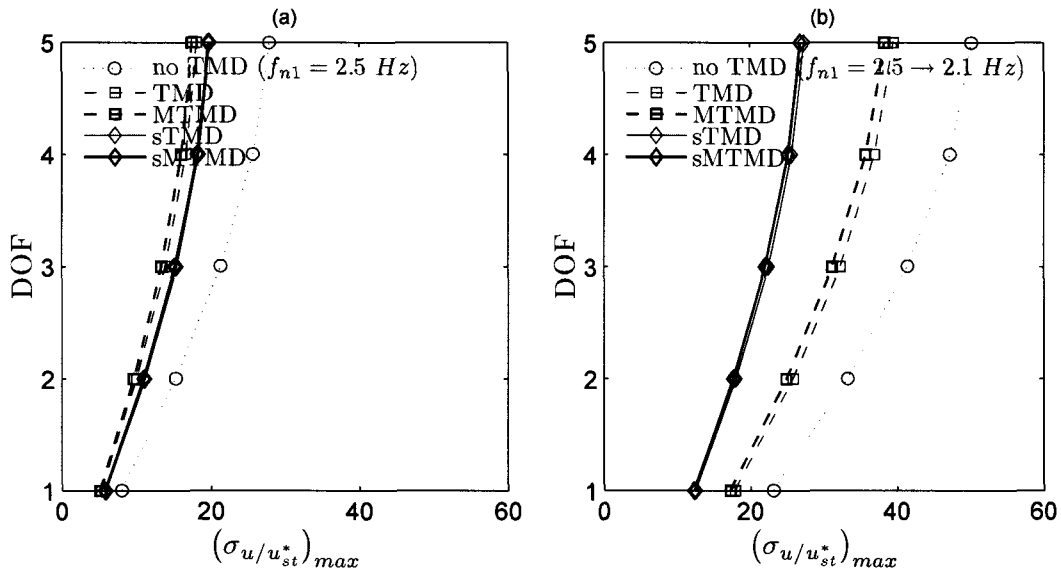


**Figure 8.26** 1940 El Centro Earthquake excitation of 5-DOF (feedback): (a) Peak RMS displacements ( $f_n = 2.5$  Hz), (b) Peak RMS displacements - damaged ( $f_n = 2.5 \rightarrow 2.0$  Hz for  $t \geq 2.6$  sec)

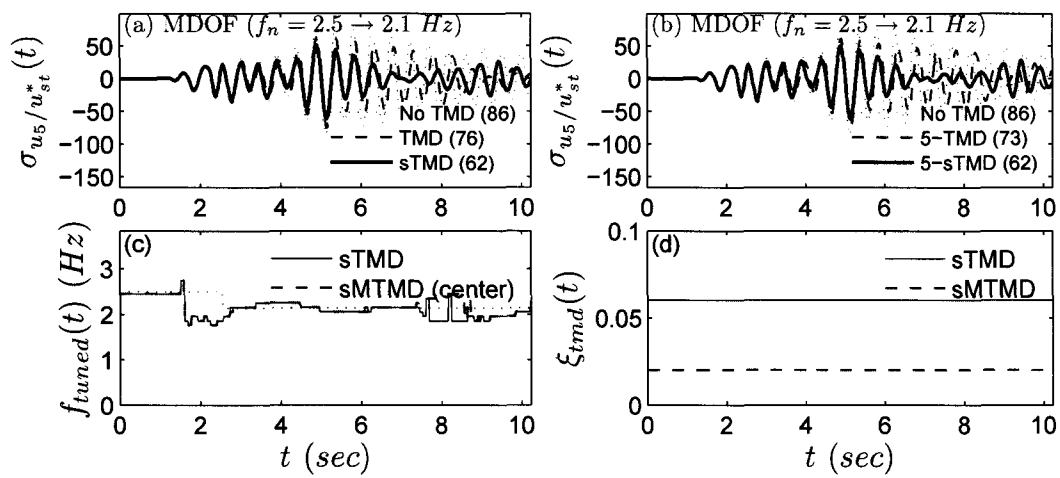


**Figure 8.27** 1940 El Centro Earthquake excitation of 5-DOF (feedback): (a,b) Top floor displacement response history, (c,d) variable stiffness and damping

## Chapter 9

### Semi-active Tuned Liquid Column Dampers (sTLCD)

Tuned liquid column dampers (TLCDs) are a class of mechanical dampers similar to tuned mass dampers (TMDs) and are typically used for flexible structures since the damper has long period. In this chapter, a semi-active spring-connected TLCD (sTLCD) is proposed to overcome the restriction on the applicability of TLCD to stiff structures subjected to earthquake excitation, and to make it adaptive against frequency variations in the excitation or the primary structure response. The semi-active control algorithms (feedforward and feedback) developed in the previous chapter for sTMD are extended to sTLCD and their performances are evaluated for a broad range of random excitations. SDOF and MDOF systems equipped with sTLCD subjected to narrow-band stationary force excitations, wide-band locally stationary base excitations, and 1940 El Centro earthquake are investigated. Stochastic responses are computed from Monte Carlo simulations of the target evolutionary spectra describing the wind or ground excitation processes. It is shown that both feedforward and feedback control provide similar performance to passive spring-connected TLCD (pTLCD) when the structure's natural frequency is accurately identified and passive TLCD is tuned with optimum stiffness. However, when a stiffness change is imposed to the primary structure and the passive TLCD becomes off-tuned, it loses its efficiency in vibration control whereas the sTLCD successfully reduces the response. Although the proposed feedforward control has a significant potential, it is important to note certain limitations. Its efficiency depends on the presence of a distinct dominant frequency range and sufficient intensity of the excitation. As the excitation intensity decreases, the response will be controlled more by its natural frequency and less by the excitation's in-

stantaneous (dominant) frequency, leading to a decrease in the efficiency of the feedforward control.

## 9.1 Structural Model and Formulation

The model of the MDOF structure equipped with sTLCD is shown in Figure 9.1. The formulation is developed for a SDOF primary structure first, and then is extended to MDOF primary structure. The LCD is composed of a U-shaped tube-like container of arbitrary configuration with orifice(s) installed in it. The mass, damping, and stiffness parameters of the SDOF primary structure are denoted by  $M_1$ ,  $C_1$  and  $K_1$ , respectively. The damping and stiffness coefficients of the spring connecting the LCD to the primary system are denoted by  $c_2$  and  $k_2$ . The following parameters are used in the formulation: cross-sectional area of the tube,  $A$ , cross-sectional area of the orifice,  $A_1$ , total length of the liquid column in the tube,  $L$ , horizontal dimension,  $B$ , density of the liquid,  $\rho$ . The coefficient of head loss, controlled by the opening ratio of the orifice ( $A/A_1$ ), is denoted by  $\xi$ . The mass of the container of the LCD, excluding the liquid mass, is denoted by  $M_c$ . Thus, the total mass of the structure and damper system is  $(M_1 + M_c + \rho AL)$ .

The SDOF version of the primary structure (shown as MDOF in Figure 9.1) equipped with pTLCD or sTLCD has three degrees-of-freedom (DOF). The DOFs, which are the motions of the primary mass, the LCD container and the liquid column elevation, are denoted by  $x(t)$ ,  $y(t)$ ,  $z(t)$ , respectively. The relative acceleration of the LCD container to the primary system is denoted by  $\ddot{y}(t)$ . The structure is subjected to a base acceleration,  $\ddot{z}(t)$ . The equation of motion of the liquid column may be written as (Saoka et al. 1988)

$$\rho AL\ddot{u}(t) + \frac{1}{2}\rho A\zeta_d|\dot{u}(t)|\dot{u}(t) + 2\rho Ag u(t) = -\rho AB\{\ddot{y} + \ddot{x} + \ddot{z}(t)\} \quad (9.1)$$

where  $\zeta_d$  is the damping ratio of the LCD.

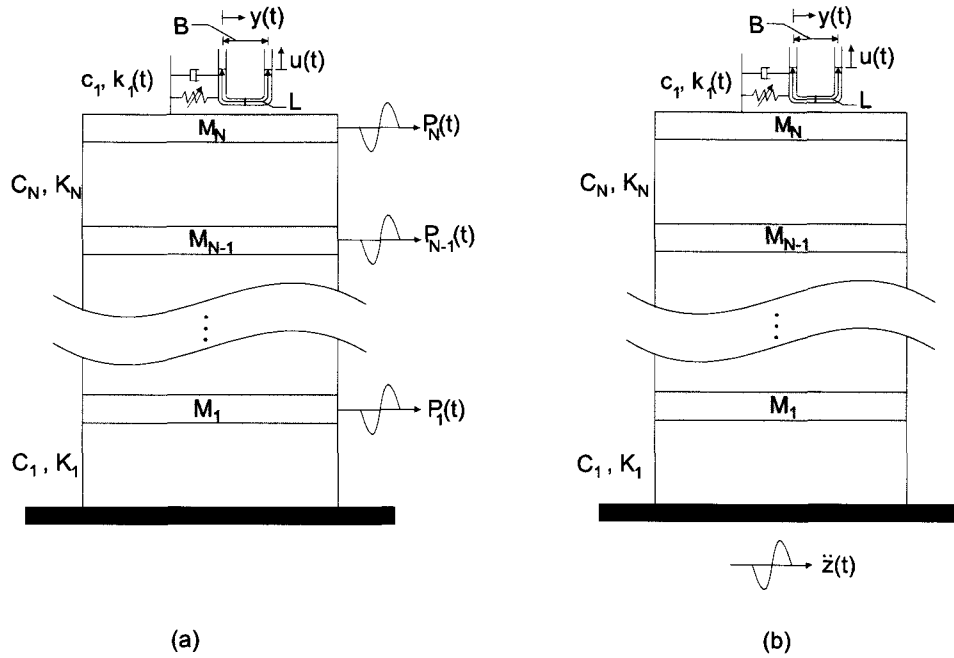


**Figure 9.1** MDOF Structural Model with sTLCD: (a) Force excited, (b) Base excited

The detailed formulation of the passive spring connected TLCD (pTLCD) is given in Ghosh and Basu (2004). By adopting an equivalent linearization procedure and normalizing with respect to mass, the equivalent linear equation of motion of the liquid column may be written as

$$\ddot{u}(t) + 2\frac{C_p}{L}\dot{u}(t) + \omega_L^2 u(t) = -\alpha \{\ddot{y} + \ddot{x} + \ddot{z}(t)\} \quad (9.2)$$

where  $\omega_L = \sqrt{2g/L}$ , natural frequency of the LCD and  $\alpha = B/L$ , the ratio of the horizontal length to the total length.  $C_p$  represents the equivalent linearized damping coefficient expressed as

$$C_p = \frac{\sigma_{\dot{u}} \xi}{\sqrt{2\pi}} \quad (9.3)$$

in which  $\sigma_{\dot{u}}$  is the standard deviation of the liquid velocity,  $\dot{u}(t)$ .

The normalized equation of the motion for the damper system may be written as

$$\{\ddot{y} + \ddot{x} + \ddot{z}(t)\} + \frac{\alpha}{1 + \tau} \ddot{u}(t) + 2\xi_2 \omega_2 \dot{y}(t) + \omega^2 y(t) = 0 \quad (9.4)$$

where  $\omega_2 = \sqrt{k_2/(\rho AL + M_c)}$  and  $\xi_2 = c_2/[2\omega_2(\rho AL + M_c)]$  represent the natural frequency and damping ratio of the damper system.  $\tau = M_c/\rho AL$  is the ratio of the container mass to liquid mass.

The normalized equation of motion for the primary system

$$\{\ddot{x} + \ddot{z}(t)\} + \frac{\alpha}{1 + \tau} \ddot{u}(t) + 2\xi_2 \omega_2 \dot{y}(t) + \omega^2 y(t) = 0 \quad (9.5)$$

where  $\mu = (M_c + \rho AL)/M_1$  is the ratio of total mass of damper to the primary system.

Re-writing Equations (9.5), (9.4) and (9.2) in matrix form and modifying the right hand side of the equations to include force excitations in the formulation

$$\begin{aligned} & \begin{bmatrix} M_1 & 0 & 0 \\ (\rho AL + M_c) & (\rho AL + M_c) & \rho AB \\ \rho AB & \rho AB & \rho AL \end{bmatrix} \begin{Bmatrix} \ddot{x} \\ \ddot{y} \\ \ddot{u} \end{Bmatrix} + \begin{bmatrix} C_1 & -c_2 & 0 \\ 0 & c_2 & 0 \\ 0 & 0 & 2\rho AC_p \end{bmatrix} \begin{Bmatrix} \dot{x} \\ \dot{y} \\ \dot{u} \end{Bmatrix} \\ & + \begin{bmatrix} K_1 & -k_2 & 0 \\ 0 & k_2 & 0 \\ 0 & 0 & 2\rho Ag \end{bmatrix} \begin{Bmatrix} x \\ y \\ u \end{Bmatrix} = \begin{Bmatrix} -M_1 \\ -(\rho AL + M_c) \\ -\rho AB \end{Bmatrix} \ddot{z}(t) + \begin{Bmatrix} 1 \\ 0 \\ 0 \end{Bmatrix} p_0 f(t) \end{aligned} \quad (9.6)$$

Normalizing the each equation of motion by  $M_1$ ,  $(\rho AL + M_c)$ , and  $\rho AL$ , respectively

$$\begin{aligned} \begin{bmatrix} 1 & 0 & 0 \\ 1 & 1 & \frac{\alpha}{1+\tau} \\ \alpha & \alpha & 1 \end{bmatrix} \begin{Bmatrix} \ddot{x} \\ \ddot{y} \\ \ddot{u} \end{Bmatrix} + \begin{bmatrix} 2\zeta_1\omega_1 & -\mu 2\zeta_2\omega_2 & 0 \\ 0 & 2\zeta_2\omega_2 & 0 \\ 0 & 0 & \frac{2C_p}{L} \end{bmatrix} \begin{Bmatrix} \dot{x} \\ \dot{y} \\ \dot{u} \end{Bmatrix} \\ + \begin{bmatrix} \omega_1^2 & -\mu\omega_2^2 & 0 \\ 0 & \omega_2^2 & 0 \\ 0 & 0 & \omega_L^2 \end{bmatrix} \begin{Bmatrix} x \\ y \\ u \end{Bmatrix} = \begin{Bmatrix} (-1)^b \\ -b \\ -b\alpha \end{Bmatrix} \ddot{z}(t) \end{aligned} \quad (9.7)$$

in which

$$\mu = \frac{\rho AL + M_c}{M_1} \quad (9.8)$$

$$\omega_L = \sqrt{\frac{2g}{L}} \quad (9.9)$$

$$\alpha = \frac{B}{L} \quad (9.10)$$

$$\tau = \frac{M_c}{\rho AL} \quad (9.11)$$

$$\zeta_1 = \frac{C_1}{2\omega_1 M_1} \quad (9.12)$$

$$\zeta_2 = \frac{c_2}{2\omega_2(\rho AL + M_c)} = \frac{c_2}{2\omega_2 \mu M_1} \quad (9.13)$$

$$\omega_1 = \sqrt{\frac{K_1}{M_1}} \quad (9.14)$$

$$\omega_2 = \sqrt{\frac{k_2}{\mu M_1}} \quad (9.15)$$

$$b = \begin{cases} 0 & \text{force excitation} \\ 1 & \text{base excitation} \end{cases} \quad (9.16)$$

Assuming a complex harmonic excitation and a corresponding solution, Equation (9.7) can be written in the frequency domain as follows.

$$\begin{aligned} & \left( -\omega^2 \begin{bmatrix} 1 & 0 & 0 \\ 1 & 1 & \frac{\alpha}{1+\tau} \\ \alpha & \alpha & 1 \end{bmatrix} + i\omega \begin{bmatrix} 2\zeta_1\omega_1 & -\mu 2\zeta_2\omega_2 & 0 \\ 0 & 2\zeta_2\omega_2 & 0 \\ 0 & 0 & \frac{2C_p}{L} \end{bmatrix} \right. \\ & \left. + \begin{bmatrix} \omega_1^2 & -\mu\omega_2^2 & 0 \\ 0 & \omega_2^2 & 0 \\ 0 & 0 & \omega_L^2 \end{bmatrix} \right) \begin{Bmatrix} H_x(\omega) \\ H_y(\omega) \\ H_u(\omega) \end{Bmatrix} = \begin{Bmatrix} (-1)^b \\ -b \\ -b\alpha \end{Bmatrix} \ddot{z}(t) \end{aligned} \quad (9.17)$$

Multiplying the third equation with  $(1+\tau)/(\alpha^2\omega^2)$  and adding the matrices on the left side

$$\begin{bmatrix} \frac{1}{H_1(\omega)} & -\mu(2\zeta_2\omega_2\omega i + \omega_2^2) & 0 \\ -\omega^2 & \frac{1}{H_2(\omega)} & -\frac{\alpha\omega^2}{1+\tau} \\ -\frac{1+\tau}{\alpha} & -\frac{1+\tau}{\alpha} & \frac{1}{\beta(\omega)} \end{bmatrix} \begin{Bmatrix} H_x(\omega) \\ H_y(\omega) \\ H_u(\omega) \end{Bmatrix} = \begin{Bmatrix} (-1)^b \\ -b \\ -b\left(\frac{1+\tau}{\alpha\omega^2}\right) \end{Bmatrix} \quad (9.18)$$

where

$$\beta(\omega) = \frac{\alpha^2\omega^2}{(1+\tau)(\omega_L^2 - \omega^2 + i2\frac{C_p}{L}\omega)} \quad (9.19)$$

$$H_1(\omega) = \frac{1}{-\omega^2 + i2\zeta_1\omega_1\omega + \omega_1^2} \quad (9.20)$$

$$H_2(\omega) = \frac{1}{-\omega^2 + i2\zeta_2\omega_2\omega + \omega_2^2} \quad (9.21)$$

$H_1(\omega)$  and  $H_2(\omega)$  are the transfer functions of the primary system and the LCD, respectively as if they were individual SDOF systems excited by the input  $\ddot{z}(t)$ .

Re-arranging Equation 9.18 leads to

$$\begin{bmatrix} \frac{1}{\beta(\omega)} & -\frac{1+\tau}{\alpha} & -\frac{1+\tau}{\alpha} \\ 0 & \frac{1}{H_1(\omega)} & -\mu(2\zeta_2\omega_2\omega i + \omega_2^2) \\ -\frac{\alpha\omega^2}{1+\tau} & -\omega^2 & \frac{1}{H_2(\omega)} \end{bmatrix} \begin{Bmatrix} H_x(\omega) \\ H_y(\omega) \\ H_u(\omega) \end{Bmatrix} = \begin{Bmatrix} -b\left(\frac{1+\tau}{\alpha\omega^2}\right) \\ (-1)^b \\ -b \end{Bmatrix} \quad (9.22)$$



Multiplying the first row by  $\beta(\omega)\alpha^2\omega^2/(1+\tau)$  and adding it to the third row

$$\begin{bmatrix} \frac{1}{\beta(\omega)} & -\frac{1+\tau}{\alpha} & -\frac{1+\tau}{\alpha} \\ 0 & \frac{1}{H_1(\omega)} & -\mu(2\zeta_2\omega_2\omega i + \omega_2^2) \\ 0 & -\omega^2(1+\beta\omega) & \frac{1}{H_2(\omega)} - \omega^2\beta(\omega) \end{bmatrix} \begin{Bmatrix} H_x(\omega) \\ H_y(\omega) \\ H_u(\omega) \end{Bmatrix} = \begin{Bmatrix} -b\left(\frac{1+\tau}{\alpha\omega^2}\right) \\ (-1)^b \\ -b(1+\beta(\omega)) \end{Bmatrix} \quad (9.23)$$

Multiplying the second row by  $H_1(\omega)[\omega^2 + \omega^2\beta(\omega)]$  and adding it to the third row

$$\begin{bmatrix} \frac{1}{\beta(\omega)} & -\frac{1+\tau}{\alpha} & -\frac{1+\tau}{\alpha} \\ 0 & \frac{1}{H_1(\omega)} & -\mu(2\zeta_2\omega_2\omega i + \omega_2^2) \\ 0 & 0 & \frac{1}{H_2(\omega)} - \omega^2\beta(\omega) - \omega^2 H_1(\omega)(1+\beta(\omega)) \end{bmatrix} \begin{Bmatrix} H_x(\omega) \\ H_y(\omega) \\ H_u(\omega) \end{Bmatrix} = \begin{Bmatrix} -b\left(\frac{1+\tau}{\alpha\omega^2}\right) \\ (-1)^b \\ -b(1+\beta(\omega))(\omega^2 H_1(\omega) - b) \end{Bmatrix} \quad (9.24)$$

The system transfer functions can be written as follows.

$$H_y(\omega) = \frac{-H_2(\omega)\{1+\beta(\omega)\}(b - (-1)^b\omega^2 H_1(\omega))}{1 - \omega^2\beta(\omega)H_2(\omega) - \omega^2 H_1(\omega)H_2(\omega)\mu(2\zeta_2\omega_2\omega i + \omega_2^2)(1+\beta(\omega))} \quad (9.25)$$

$$H_x(\omega) = \frac{H_1(\omega)[(-1)^b[1 - \omega^2\beta(\omega)H_2(\omega)] - b\mu H_2(\omega)(2\zeta_2\omega_2\omega i + \omega_2^2)\{1+\beta(\omega)\}]}{1 - \omega^2\beta(\omega)H_2(\omega) - \omega^2 H_1(\omega)H_2(\omega)\mu(2\zeta_2\omega_2\omega i + \omega_2^2)(1+\beta(\omega))} \quad (9.26)$$

$$H_u(\omega) = \frac{(1+\tau)\beta(\omega)}{(\alpha\omega^2)} \left[ \frac{\omega^2 H_2(\omega)\{1+\beta(\omega)\}\{\omega^2 H_x(\omega) - 1\}}{\{1 - \omega^2\beta(\omega)H_2(\omega)\}} + \omega^2 H_x(\omega) - b \right] \quad (9.27)$$

For a SDOF primary structure equipped with sTLCD, the frequency and damping ratio of the sTLCD in the above formulation become time-varying. The SDOF system formulation can be extended to a MDOF system equipped with sTLCD by the following equations

of motion:

$$\begin{aligned}
 & \begin{bmatrix} \mathbf{M} & \mathbf{0} & \mathbf{0} \\ (\rho AL + M_c) & (\rho AL + M_c) & \rho AB \\ \rho AB & \rho AB & \rho AL \end{bmatrix} \begin{Bmatrix} \ddot{\mathbf{x}} \\ \ddot{y} \\ \ddot{u} \end{Bmatrix} + \begin{bmatrix} \mathbf{C} \begin{Bmatrix} 0 \\ 0 \\ -c_2(t) \end{Bmatrix} & \mathbf{0} \\ 0 & c_2(t) & 0 \\ 0 & 0 & 2\rho AC_p(t) \end{bmatrix} \begin{Bmatrix} \dot{\mathbf{x}} \\ \dot{y} \\ \dot{u} \end{Bmatrix} \\
 & + \begin{bmatrix} \mathbf{K} \begin{Bmatrix} 0 \\ 0 \\ -k_2(t) \end{Bmatrix} & \mathbf{0} \\ 0 & k_2(t) & 0 \\ 0 & 0 & 2\rho Ag \end{bmatrix} \begin{Bmatrix} \mathbf{x} \\ y \\ u \end{Bmatrix} = \begin{Bmatrix} (-1)^b \mathbf{M1} \\ -b(\rho AL + M_c) \\ -b\alpha AL \end{Bmatrix} \ddot{\mathbf{z}}(t)
 \end{aligned} \tag{9.28}$$

where

$$\mathbf{M} = m_0 \begin{bmatrix} 1 & 0 & 0 \\ 0 & 1 & 0 \\ 0 & 0 & 1 \end{bmatrix} \tag{9.29}$$

$$\mathbf{C} = c_0 \begin{bmatrix} 2 & -1 & 0 \\ -1 & 2 & -1 \\ 0 & -1 & 1 \end{bmatrix} \tag{9.30}$$

$$\mathbf{K} = k_0 \begin{bmatrix} 2 & -1 & 0 \\ -1 & 2 & -1 \\ 0 & -1 & 1 \end{bmatrix} \tag{9.31}$$

The corresponding frequency and damping ratio for the uniform building floors are defined as  $\omega_0 = \sqrt{k_0/m_0}$  and  $\zeta_0 = c_0/(2\omega_0 m_0)$ .

The value of linear equivalent damping coefficient  $C_p$  needs to be estimated for both pTLCD and sTLCD. One approach is estimating a constant  $C_p$  iteratively using the transfer function of liquid velocity  $H_u(\omega)$  and a white noise excitation with a target spectral intensity as given in Ghosh and Basu (2004). The orifice head loss coefficient ( $\xi$ ) can be optimized for the design spectral intensity and kept constant. However, the value of the  $C_p$  is closely related to the intensity of the excitation as it is apparent from Equation (9.3). Therefore, it is more appropriate to use a time-varying  $C_p$  for evolutionary excitation processes. Varying the orifice opening ratio (and therefore the head loss coefficient) is beyond the scope of this study, but it is worth noting that a gain scheduled control strategy (Yalla et al. 2001) to vary the orifice opening ratio can be included for further improvement of the sTLCD.

The PSD of liquid velocity in pTLCD or sTLCD can be estimated as

$$S_u(t, \omega) \approx \omega^2 |H_u(t, \omega)|^2 S(t, \omega) \quad (9.32)$$

Similarly, the PSD of the primary structure displacement response can be estimated as,

$$S_x(t, \omega) \approx |H_x(\omega, t_i)|^2 S(t, \omega) \quad (9.33)$$

The root-mean-square (RMS) of the liquid velocity and primary structure displacement response can be obtained by

$$\sigma_u \approx \sqrt{\int_{-\infty}^{\infty} S_u(t, \omega) d\omega} \quad (9.34)$$

and

$$\sigma_x \approx \sqrt{\int_{-\infty}^{\infty} S_x(t, \omega) d\omega} \quad (9.35)$$

Once the head loss coefficient is optimized using a iterative solution of Equations (9.34) and (9.3) for a design spectral intensity, which can be selected as mean spectral intensity

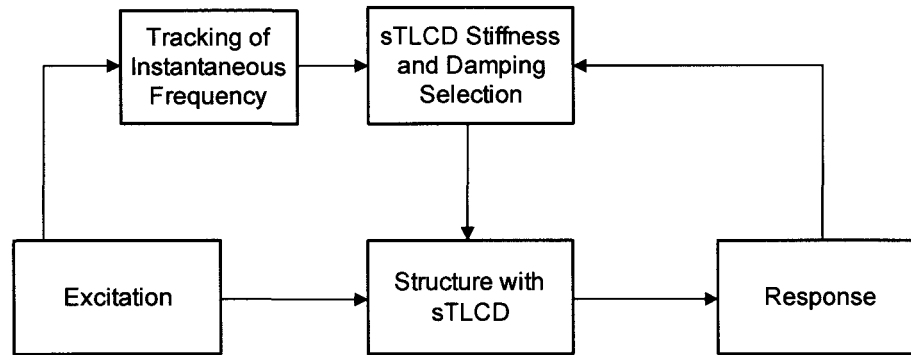
of a design evolutionary PSD, time-varying  $C_p$  can be obtained iteratively for each slice of an evolutionary PSD at a given time  $t_i$ .

## 9.2 Control Algorithm

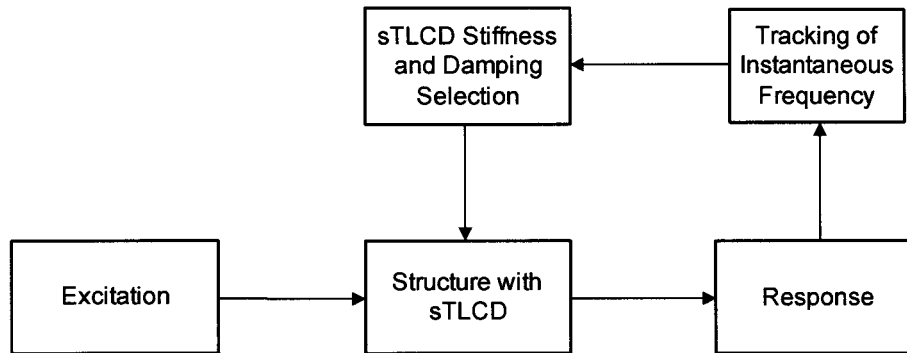
The control algorithms developed in Chapter 8 are extended to sTLCD. The block diagrams for the control algorithms are given in Figure 9.2. Note that the feedback shown in Figure 9.2(a) is only for adjusting the proper positioning of semi-active device. Further details in implementation of evolutionary spectrum estimation and tuning the semi-active stiffness device are shown in Figure 9.3. The control algorithms operate as follows:

1. At time  $t = 0$ , variable stiffness of the sTLCD is set to the optimum value for passive TLCD. Since the main source for damping is provided by the fluid motion in the TLCD,  $\zeta_2$  is set to a minimal value of 0.01 for both pTLCD and sTLCD.
2. A moving window of  $n$  time steps of signal is chosen at certain time instants  $t_i$ .  $WL$  is the window length of  $n\Delta t$  and  $t_i = 0 : L\Delta t : t(end)$  is the new time array for the time-frequency spectra incremented with  $L\Delta t$  between successive windows.
3. Instantaneous power spectral density of the excitation (in feedforward control) and the response (in feedback control) is estimated by STFT or WT. Instantaneous (dominant) frequency is tracked by averaging the highest energy frequencies detected over an averaging time length ( $AL$ ).
4. Stiffness and damping variation starts after  $t = t_0$  to allow sufficient amount of data to be collected for accurate estimation.
5. For feedforward control, if the instantaneous frequency is within the pre-defined limits (i.e.  $f_{lim1} < f_{ins}(t_i) < f_{lim2}$ ), sTLCD is tuned to the instantaneous frequency;

otherwise sTLCD is tuned to the nearest frequency limit for the sTLCD. The limit frequencies are set as  $f_{lim1} = 0.5f_{n1}$  and  $f_{lim2} = 2f_{n1}$  in this study.

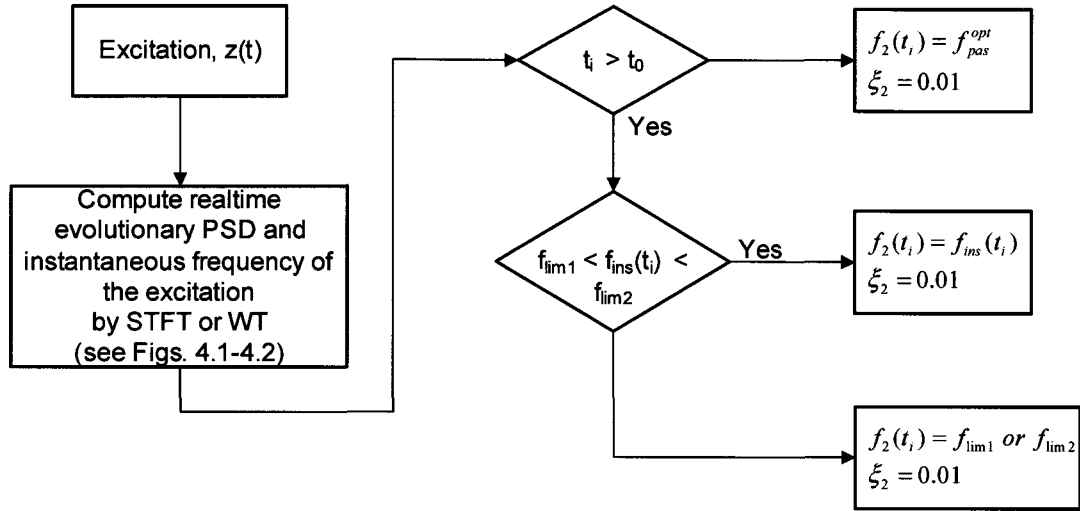


(a) Feedforward control based on tracking of instantaneous frequency of the excitation

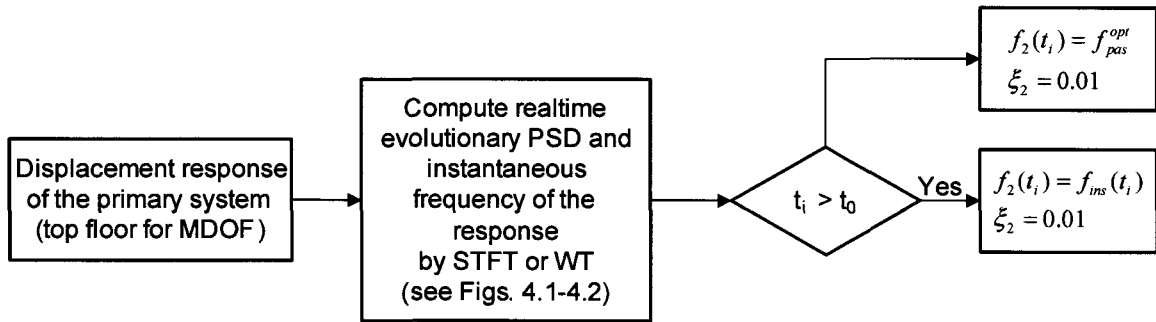


(b) Feedback control based on tracking of instantaneous frequency of the response

**Figure 9.2** Control Algorithm



(a) Feedforward control based on tracking of instantaneous frequency of the excitation



(b) Feedback control based on tracking of instantaneous frequency of the response

**Figure 9.3** Variable Stiffness Parameter Selection

## 9.3 Results for sTLCD Systems

### 9.3.1 Parametric Study

A parametric study similar to the one in Chapter 6 is conducted to demonstrate the potential of sTLCD with feedforward control and to understand the parameters governing the effectiveness of pTLCD and sTLCD. sTLCD with feedback control will have a similar performance of an optimum pTLCD without off-tuning and therefore it is not considered

within this section. The primary structure is considered as a SDOF system (representing the fundamental mode of a MDOF system). Assuming a slowly varying mono-component excitation, the transfer function for the damper system (sTLCD with feedforward control) can be approximated by substituting  $\omega_2 = \omega$  into Equation (9.21),

$$H_{2s}(\omega) \approx \frac{1}{2i\xi_2\omega^2} \quad (9.36)$$

After substituting  $H_{2s}(\omega)$  into Equations (9.26) and (9.27),  $H_x(\omega)$  and  $H_u(\omega)$  for the sTLCD system may be expressed as

$$H_{xs}(\omega) = \frac{H_1(\omega) [(-1)^b [1 - \omega^2\beta(\omega)H_{2s}(\omega)] - b\mu H_{2s}(\omega) (2\xi_2\omega_2\omega i + \omega_2^2) \{1 + \beta(\omega)\}]}{1 - \omega^2\beta(\omega)H_{2s}(\omega) - \omega^2 H_1(\omega)H_{2s}(\omega)\mu(2\xi_2\omega_2\omega i + \omega_2^2)(1 + \beta(\omega))} \quad (9.37)$$

$$H_{us}(\omega) = \frac{(1 + \tau)\beta(\omega)}{(\alpha\omega^2)} \left[ \frac{\omega^2 H_{2s}(\omega) \{1 + \beta(\omega)\} \{\omega^2 H_{xs}(\omega) - 1\}}{\{1 - \omega^2\beta(\omega)H_{2s}(\omega)\}} + \omega^2 H_{xs}(\omega) - b \right] \quad (9.38)$$

It is important to note that Equation (9.36) is exact only for the single harmonic excitation. However, it will still be a good approximation for a broad class of excitations where the input processes are slowly varying and have significant energy about a particular dominant frequency at a given instant.

The RMS values of the primary structure displacement response with respect to head loss coefficient (normalized by  $L$ ) are given in Figure 9.4 for both pTLCD and feedforward sTLCD for two different primary structures (one with  $f_n = 0.3$  Hz under force excitation, and the other with  $f_n = 1.5$  Hz). The results are obtained by iterative solution of  $C_p$  using Equation (9.34). The excitation is assumed to be a white noise process with  $S_0 = 0.2$   $m^2/s^3$ . The damping ratio of the primary structure is taken as 1%. The ratio of total mass of damper to the primary system,  $\mu$ , is 0.05. The ratio of the horizontal length to the total length of the liquid column tube ( $\alpha = B/L$ ) is set to 0.9. The tuning ratio of the damper system is selected as  $1/(1 + \mu)$  for pTLCD (for the parametric study). The

liquid column mass is assumed to be same as the LCD container mass ( $\tau = M_c/(\rho AL) = 1$ ). The optimal values of  $\xi$  for the two systems are listed in Table 9.1 along with the corresponding RMS displacement responses of the primary structure with no damper, with pTLCD and with sTLCD. Figure 9.4 indicates that the RMS displacement response of the primary structure can be more effectively reduced using an sTLCD. For pTLCD, there exists an optimal value for  $\xi$  corresponding to a minimum response, whereas in feedforward sTLCD the larger the coefficient  $\xi$  is, the better vibration reduction it is. Despite this observation,  $\xi$  is set to the value that is optimum for pTLCD and kept same for sTLCD within the scope of this study.

The transfer functions for the two SDOF primary structures studied in Figure 9.4 are shown in Figure 9.5. Five cases are considered: (i) primary structure with no damper, (ii) primary structure with pTLCD, (iii) primary structure equipped with sTLCD, (iv) damaged primary structure with off-tuned pTLCD, and (iv) damaged primary structure equipped with sTLCD. sTLCD - with the assumption of perfect frequency tracking of the mono-component excitation - leads to a much smaller transfer function for the primary structure compared to the fixed and pTLCD cases. Since the feedforward sTLCD tunes itself to excitation frequency, the transfer function of the primary structure has only a single peak as opposed to the optimized two peaks in the pTLCD case. More importantly, pTLCD loses its efficiency when it becomes off-tuned due to a change in the natural period of the primary structure whereas sTLCD is robust to the change in the primary structure.

For the random excitations in the following sections, tuning ratio for the passive spring in pTLCD is set to the  $H_2$  optimum tuning ratio ( $\gamma_{opt}$ ) of TMD with the same mass ratio ( $\mu$ ), which is selected as 5% for the examples studied in the following sections. For force-excited SDOF primary structure  $\gamma_{opt} = 0.963$  and for base-excited SDOF primary structure  $\gamma_{opt} = 0.935$ . For 5-DOF primary structure, mass ratio  $\mu$  (=7.94%) is calculated with



**Table 9.1** Comparison of pTLCD and sTLCD

Case	Force excitation	Base excitation
Natural Frequency (Hz)	0.3	1.5
$S_0 [m^2/s^3]$	0.2	0.2
Optimal $\xi$ (pTLCD)	25	212
RMS Disp. (Fixed) [ $10^{-3}m$ ]	484.3	43.3
RMS Disp. (pTLCD) [ $10^{-3}m$ ]	274.5	24.1
RMS Disp. (sTLCD) [ $10^{-3}m$ ]	113.3	15.3

respect to first modal mass and optimum tuning ratio is 0.943 for force-excited system and 0.901 for base-excited system.

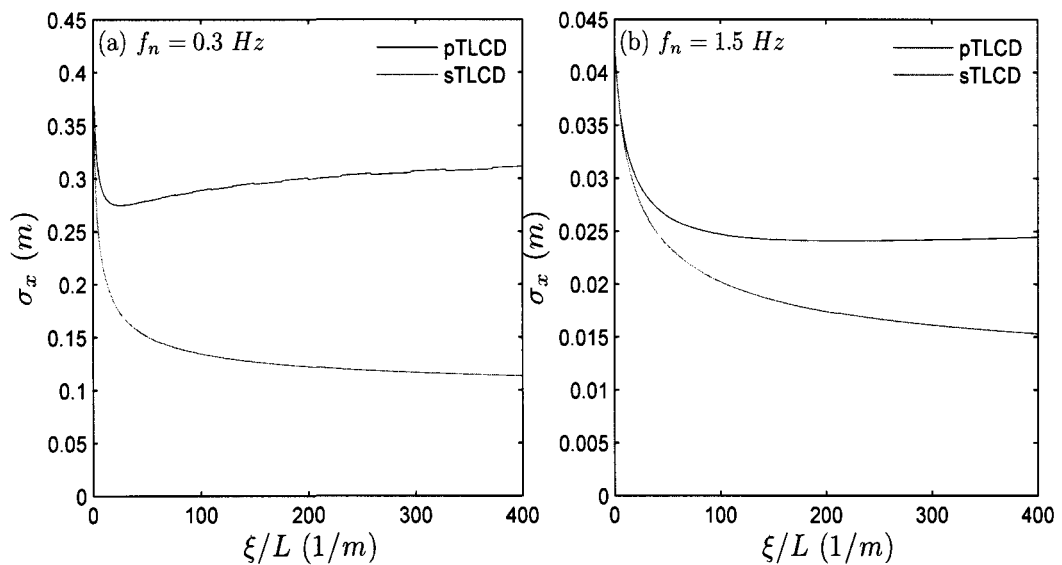


**Figure 9.4** RMS value of SDOF system with sTLCD: (a)  $f_n = 0.3 \text{ Hz}$  (force excited), (b)  $f_n = 1.5 \text{ Hz}$  (base excited)

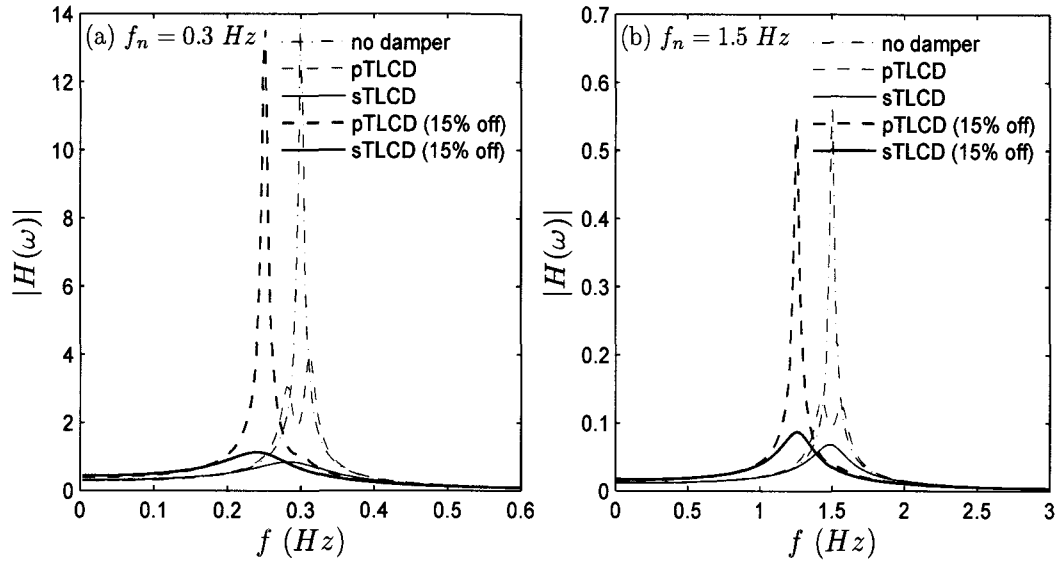


**Figure 9.5** Transfer functions for SDOF system with sTLCD: (a)  $f_n = 0.3$  Hz (force excited), (b)  $f_n = 1.5$  Hz (base excited)

### 9.3.2 Narrow-band Stationary Excitations

To study the feedforward sTLCD performance, 500 narrow-band stationary force excitations are simulated using the same filter for the near-fault earthquake spectrum with parameters  $f_g = 1$  Hz and  $\xi_g = 0.05$ . Another 500 narrow-band stationary excitations are simulated using Davenport along-wind spectrum given by Equation (1.116) to study the feedback sTLCD performance. The wind parameters are selected as  $u_* = 1.76$  m/sec and  $v_0 = 45$  m/sec. The mean velocity profile is defined by the power law [Eq. (1.112)] with  $\alpha = 0.4$  and story heights are assumed to be uniform as  $h/z_{ref} = 0.3$  where  $z_{ref} = 10$  m.

The results for sTLCD with feedforward control are presented in Figures 9.6 through 9.9. The estimated evolutionary excitation spectrum (by STFT), a sample excitation are shown in Figure 9.6 along with the RMS responses and the response spectra. Figure 9.6 (c, d) correspond to the SDOF primary structure without any damage whereas Figure 9.6 (e, f) correspond to the damaged SDOF primary structure after  $t = 4.1$  sec. sTLCD with

feedforward control provides similar response reduction with respect to passive TLCD in no damage case. For damaged case, passive TLCD becomes off-tuned and inefficient while sTLCD continues to provide significant response reduction. Sample time history responses of the SDOF primary structure (damaged at  $t = 4.1 \text{ sec}$  and  $f_n = 1.5 \text{ Hz} \rightarrow 1.1 \text{ Hz}$ ) along with variable spring frequency of sTLCD are presented in Figure 9.7. The response of a 5-DOF primary structure is studied next for further investigation of the sTLCD performance. The peak floor displacements of a 5-DOF uniform primary structure are presented in Figures 9.8 for undamaged case ((a)  $f_n = 1.0 \text{ Hz}$ ) and for damaged case ((b)  $f_n = 1.2 \text{ Hz} \rightarrow 1.0 \text{ Hz}$ ). The damage is induced by decreasing the stiffness of the first DOF by half. The top floor displacement response history for the damaged case is presented in Figure 9.9. Similar observations can be made for these specific cases as in the ensemble RMS response histories and spectra presented in Figure 9.6.

The results for sTLCD with feedback control are presented in Figures 9.10 through 9.13. The estimated evolutionary excitation spectrum (by STFT), a sample excitation are shown in Figure 9.10 along with the RMS responses and the response spectra. Figure 9.10 (c, d) correspond to the SDOF primary structure without any damage whereas Figure 9.10 (e,f) correspond to the damaged SDOF primary structure after  $t = 20 \text{ sec}$ . Response spectra in Figure 8.8 clearly show that sTLCD with feedback control have similar efficiencies compared to passive ones for undamaged structures. For damaged case, passive TLCD become off-tuned and less efficient while sTLCD continues to provide significant response reduction. Sample time history responses of the SDOF primary structure (damaged at  $t = 20 \text{ sec}$  and  $f_n = 0.2 \text{ Hz} \rightarrow 0.14 \text{ Hz}$ ) along with variable spring frequency of sTLCD are presented in Figure 9.11. The response of a 5-DOF primary structure is studied next for further investigation of the sTLCD performance. The peak floor displacements of a 5-DOF uniform primary structure are presented in Figures 9.12 for undamaged case ((a)

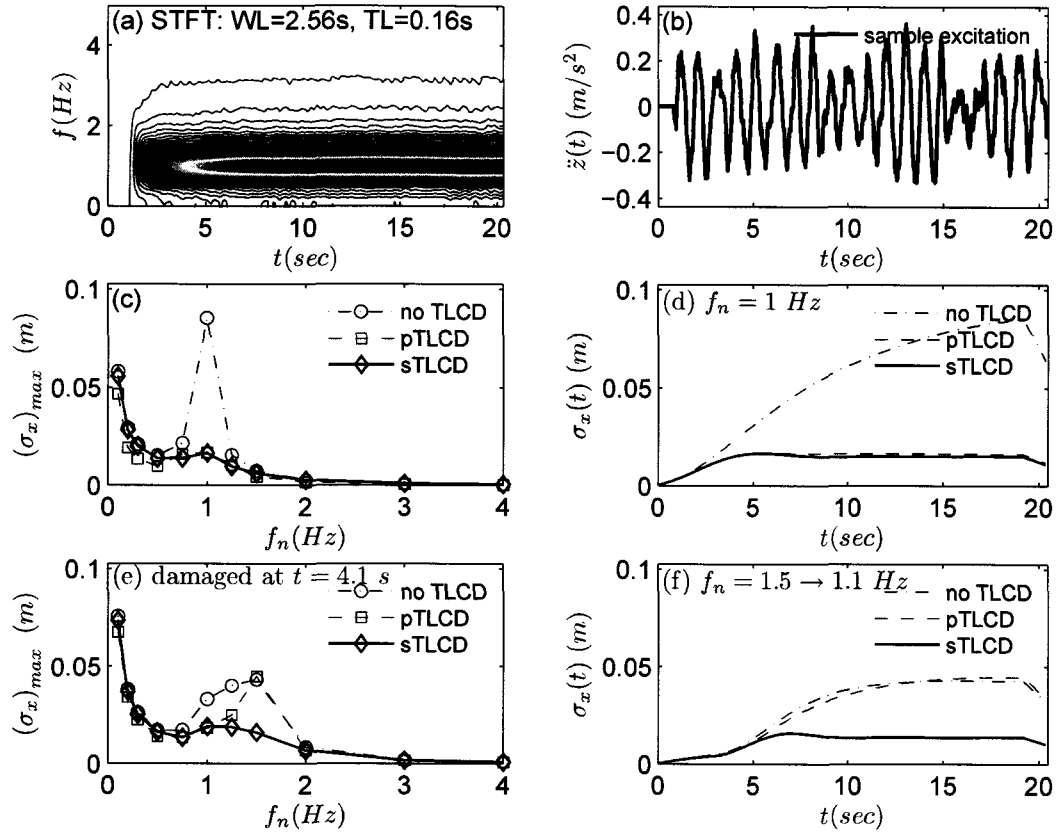


**Figure 9.6** Narrow-band stationary force excitation of SDOF (feedforward): (a) EPSD for 500 sample, (b) Sample acceleration, (c) Displacement response spectra, (d) RMS displacement response ( $f_n = 1.0 \text{ Hz}$ ), (e) Displacement response spectra - damaged, (f) RMS displacement response - damaged ( $f_n = 1.5 \rightarrow 1.1 \text{ Hz}$  for  $t > 4.1 \text{ sec}$ )

$f_n = 0.2 \text{ Hz}$ ) and for damaged case ((b)  $f_n = 0.2 \text{ Hz} \rightarrow 0.17 \text{ Hz}$ ). The damage is induced by decreasing the stiffness of the first DOF by half. The top floor displacement response history for the damaged case is presented in Figure 9.13. Similar observations can be made for these specific cases as in the ensemble RMS response histories and spectra presented in Figure 9.10.

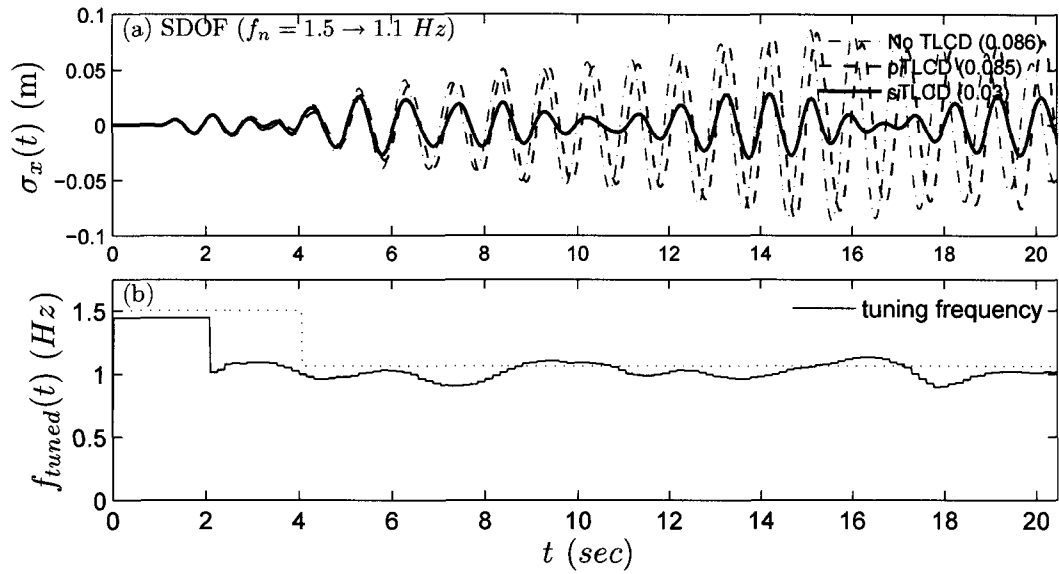


**Figure 9.7** Narrow-band stationary force excitation of SDOF (feedforward): (a) Time history response, (b) Variable spring frequency

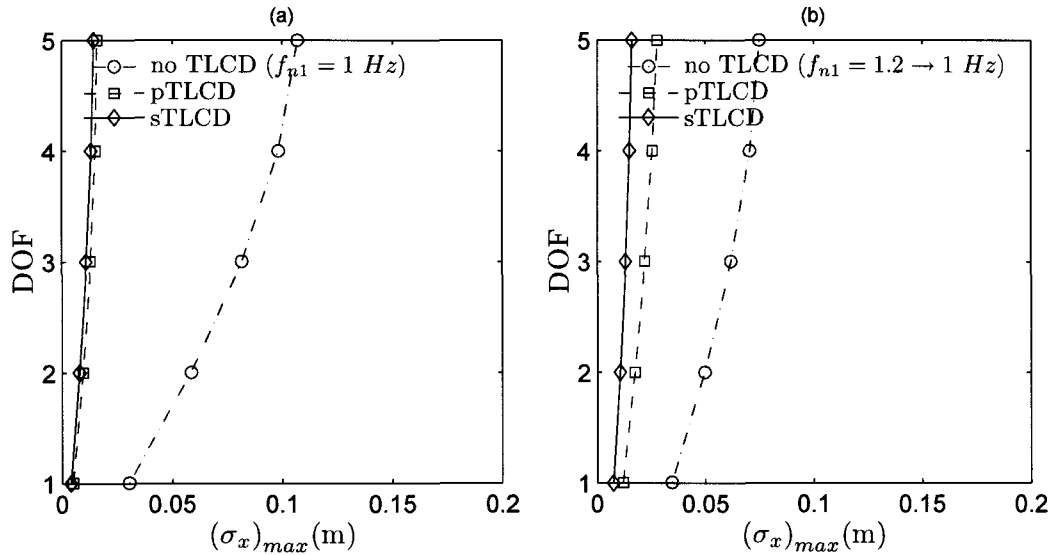


**Figure 9.8** Narrow-band stationary force excitation of 5-DOF (feedforward): (a) Peak RMS displacements ( $f_n = 1.0$  Hz), (b) Peak RMS displacements - damaged ( $f_n = 1.2 \rightarrow 1.0$  Hz for  $t \geq 4.1$  sec)

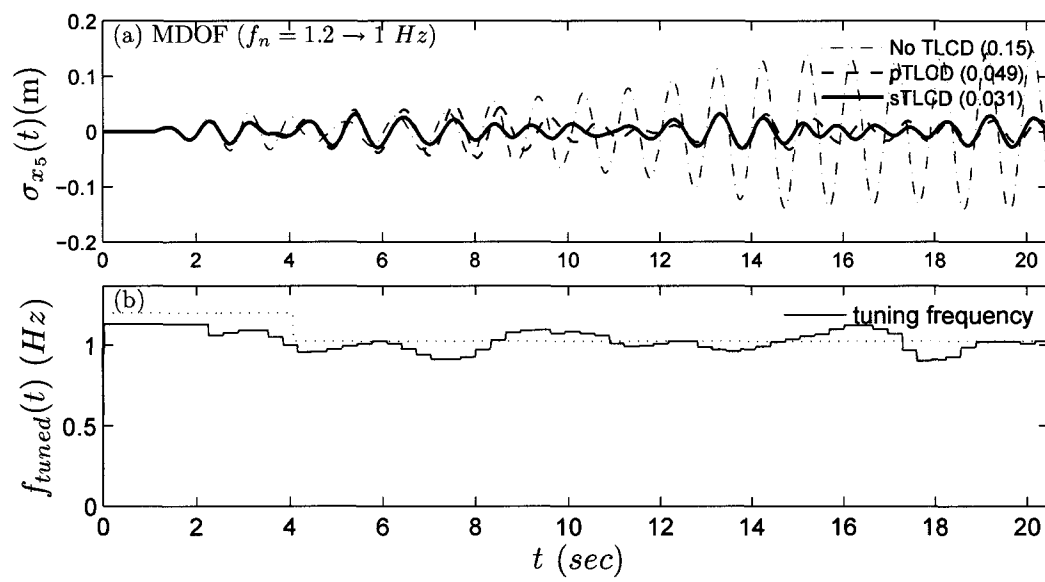


**Figure 9.9** Narrow-band stationary force excitation of 5-DOF (feedforward): (a) Top floor displacement response history, (b) variable spring frequency

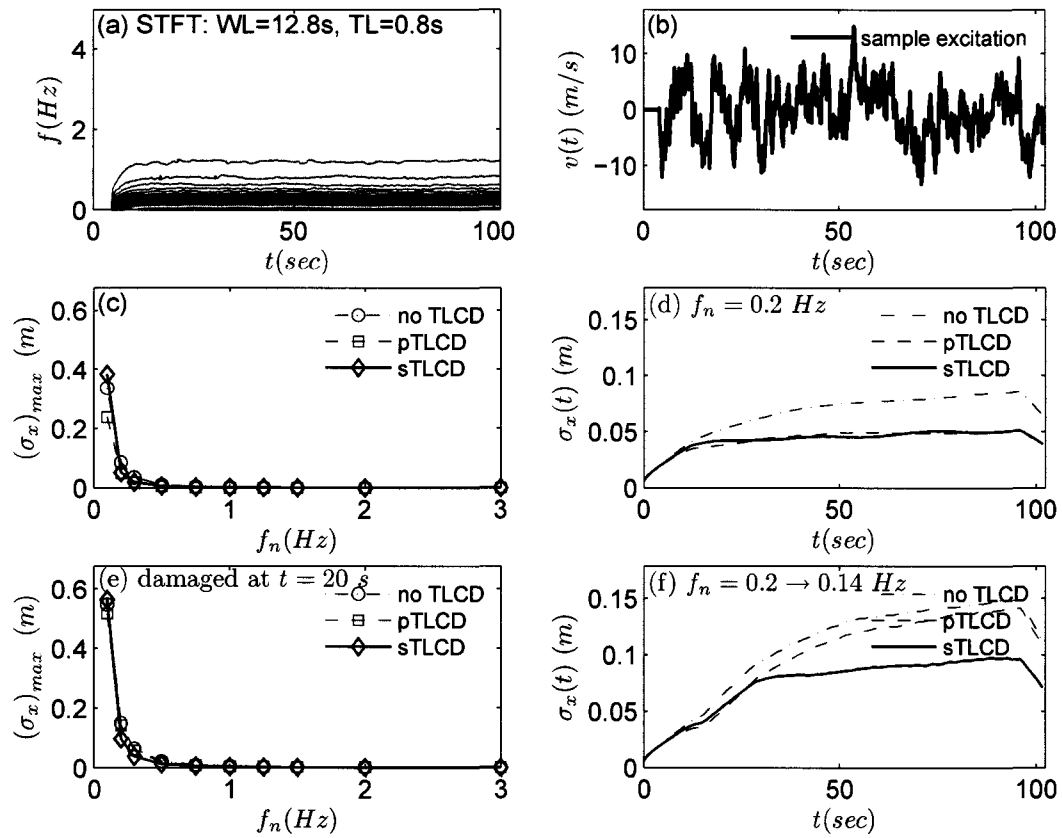


**Figure 9.10** Narrow-band stationary wind excitation of SDOF (feedback): (a) EPSP for 500 sample, (b) Sample wind velocity, (c) Displacement response spectra, (d) RMS displacement response ( $f_n = 0.2$  Hz), (e) Displacement response spectra - damaged, (f) RMS displacement response - damaged ( $f_n = 0.2 \rightarrow 0.14$  Hz for  $t > 20$  sec)

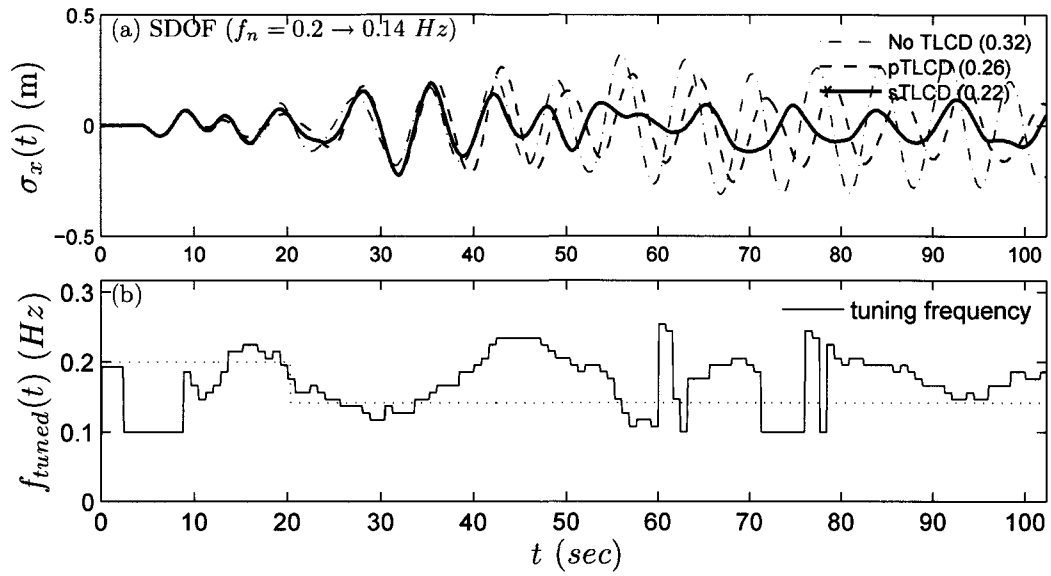


**Figure 9.11** Narrow-band stationary wind excitation of SDOF (feedback): (a) Time history response, (b) Variable spring frequency

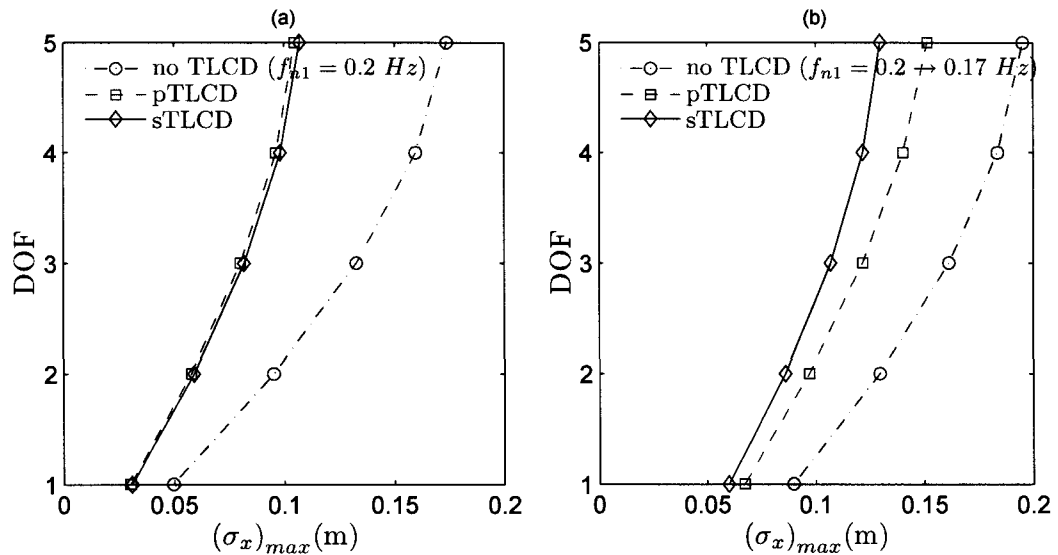


**Figure 9.12** Narrow-band stationary wind excitation of 5-DOF (feedback): (a) Peak RMS displacements ( $f_n = 0.2$  Hz), (b) Peak RMS displacements - damaged ( $f_n = 0.2 \rightarrow 0.17$  Hz for  $t \geq 20$  sec)



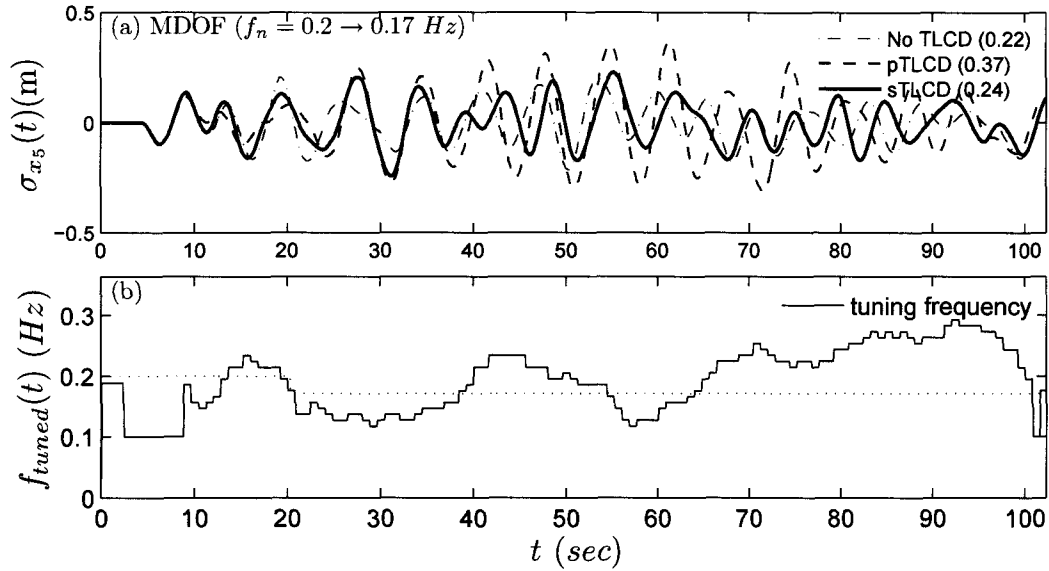


**Figure 9.13** Narrow-band stationary wind excitation of 5-DOF (feedback): (a) Top floor displacement response history, (b) Variable spring frequency

### 9.3.3 Locally Stationary Excitations

500 locally stationary excitations are simulated using the near-fault earthquake spectrum given by Equation (1.124). The soil parameters are selected as  $\omega_g = 2\pi$  rad/sec and  $\xi_g = 0.3$ . A time envelope is applied in the form of Equation (7.32).

The results for sTLCD with feedforward control are presented in Figures 9.14 through 9.17. The estimated evolutionary excitation spectrum (by STFT), a sample excitation are shown in Figure 9.14 along with the RMS responses and the response spectra. Figure 9.14 (c, d) correspond to the SDOF primary structure without any damage whereas Figure 9.14 (e, f) correspond to the damaged SDOF primary structure after  $t = 4.1$  sec. sTLCD with feedforward control provides response reduction close to passive TLCD in no damage case. For damaged case, passive TLCD becomes off-tuned and inefficient while sTLCD leads to significant response reduction. Sample time history responses of the SDOF primary structure (damaged at  $t = 4.1$  sec and  $f_n = 1.5$  Hz  $\rightarrow$  1.1 Hz) along with variable spring

frequency of sTLCD are presented in Figure 9.15. The response of a 5-DOF primary structure is studied next for further investigation of the sTLCD performance. The peak floor displacements of a 5-DOF uniform primary structure are presented in Figure 9.16 for undamaged case ((a)  $f_n = 1.0 \text{ Hz}$ ) and for damaged case ((b)  $f_n = 1.3 \text{ Hz} \rightarrow 1.1 \text{ Hz}$ ). The damage is induced by decreasing the stiffness of the first DOF by half. The top floor displacement response history for the damaged case is presented in Figure 9.17. Similar observations can be made for these specific cases as in the ensemble RMS response histories and spectra presented in Figure 9.14.

The results for sTLCD with feedback control are presented in Figures 9.18 through 9.20. The estimated evolutionary excitation spectrum (by STFT), a sample excitation are shown in Figure 9.18 along with the RMS responses and the response spectra. Figure 9.18 (c, d) correspond to the SDOF primary structure without any damage whereas Figure 9.18 (e, f) correspond to the damaged SDOF primary structure after  $t = 4.1 \text{ sec}$ . Response spectra in Figure 9.18 clearly show that sTLCD with feedback control have similar efficiencies compared to passive ones for undamaged structures. For damaged case, passive TLCD becomes off-tuned and inefficient while sTLCD leads to significant response reduction. Sample time history responses of the SDOF primary structure (damaged at  $t = 4.1 \text{ sec}$  and  $f_n = 1.5 \text{ Hz} \rightarrow 1.1 \text{ Hz}$ ) along with variable spring frequency of sTLCD are presented in Figure 9.19. The response of a 5-DOF primary structure is studied next for further investigation of the sTLCD performance. The peak floor displacements of a 5-DOF uniform primary structure are presented in Figures 9.20 for undamaged case ((a)  $f_n = 1.0 \text{ Hz}$ ) and for damaged case ((b)  $f_n = 1.2 \text{ Hz} \rightarrow 1.0 \text{ Hz}$ ). The damage is induced by decreasing the stiffness of the first DOF by half. The top floor displacement response history for the damaged case is presented in Figure 9.21. Similar observations can be made for these specific cases as in the ensemble RMS response histories and spectra presented in Figure

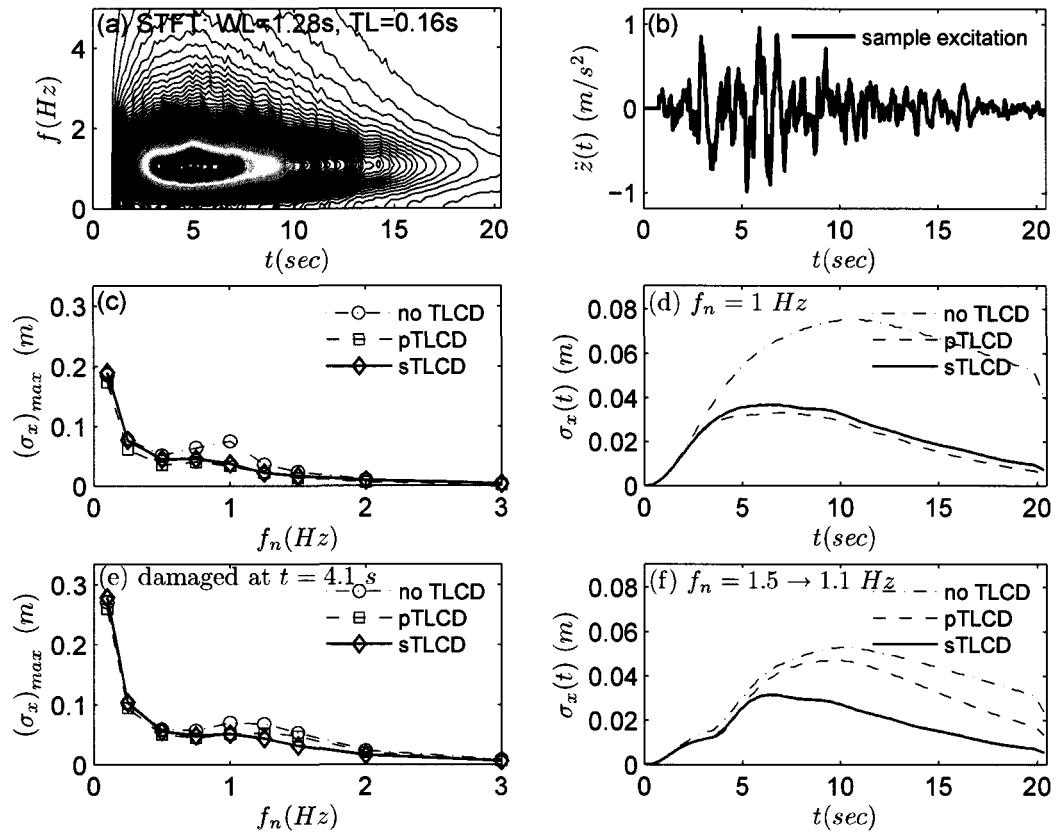


**Figure 9.14** Locally stationary base excitation of SDOF (feedforward): (a) EPSP for 500 sample, (b) Sample ground acceleration, (c) Displacement response spectra, (d) RMS displacement response ( $f_n = 1.0$  Hz), (e) Displacement response spectra - damaged, (f) RMS displacement response - damaged ( $f_n = 1.5 \rightarrow 1.1$  Hz for  $t > 4.1$  sec)

9.18.

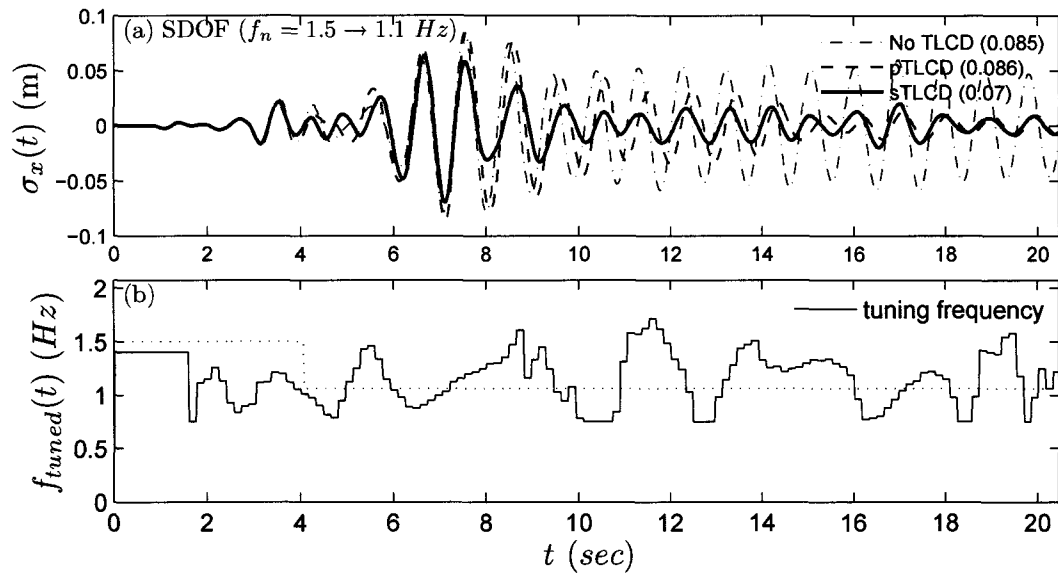


**Figure 9.15** Locally stationary base excitation of SDOF (feedforward): (a) Time history response, (b) Variable spring frequency

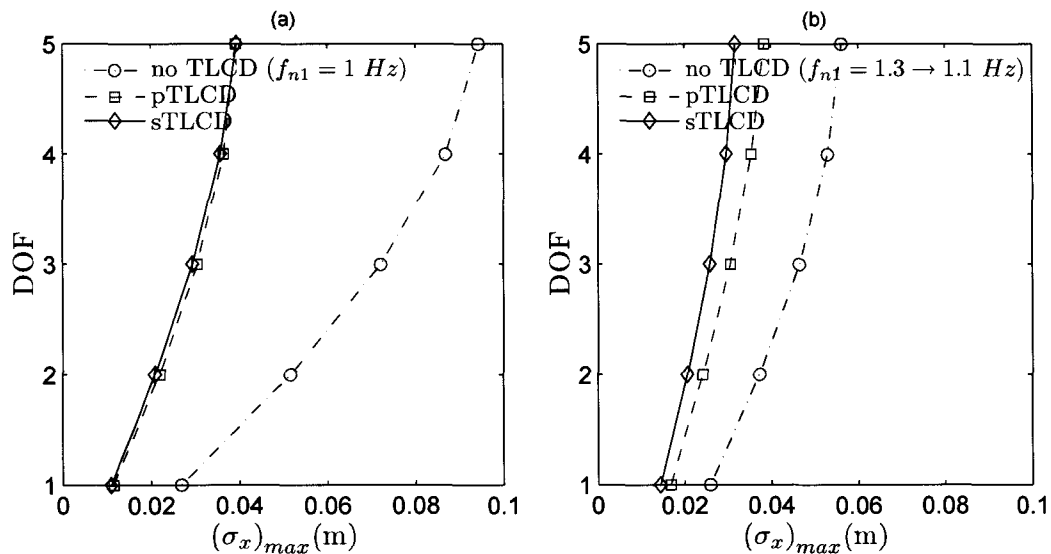


**Figure 9.16** Locally stationary base excitation of 5-DOF (feedforward): (a) Peak RMS displacements ( $f_n = 1.0$  Hz), (b) Peak RMS displacements - damaged ( $f_n = 1.3 \rightarrow 1.1$  Hz for  $t \geq 4.1$  sec)

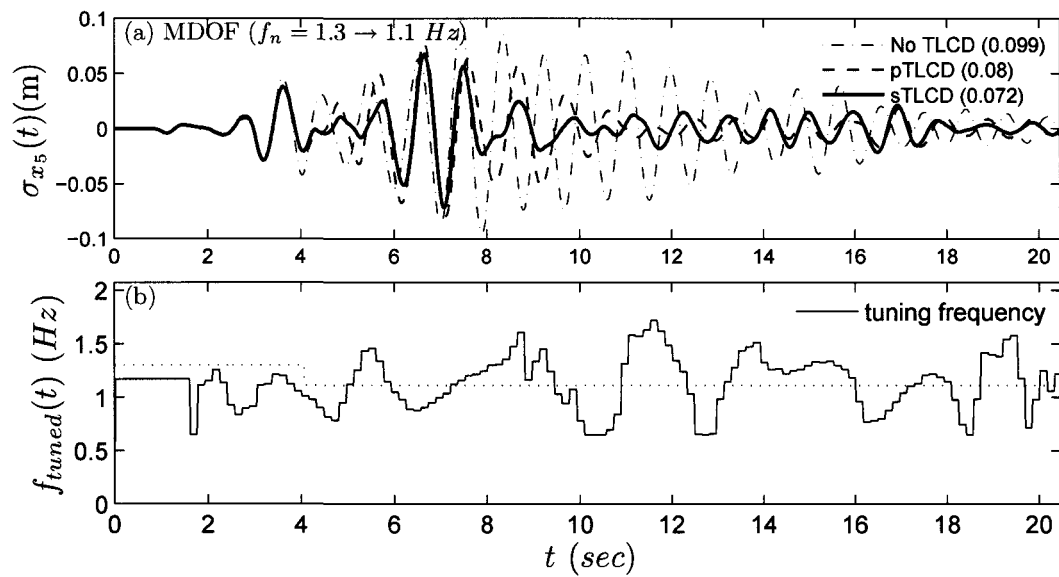


**Figure 9.17** Locally stationary base excitation of 5-DOF (feedforward): (a) Top floor displacement response history, (b) Variable spring frequency

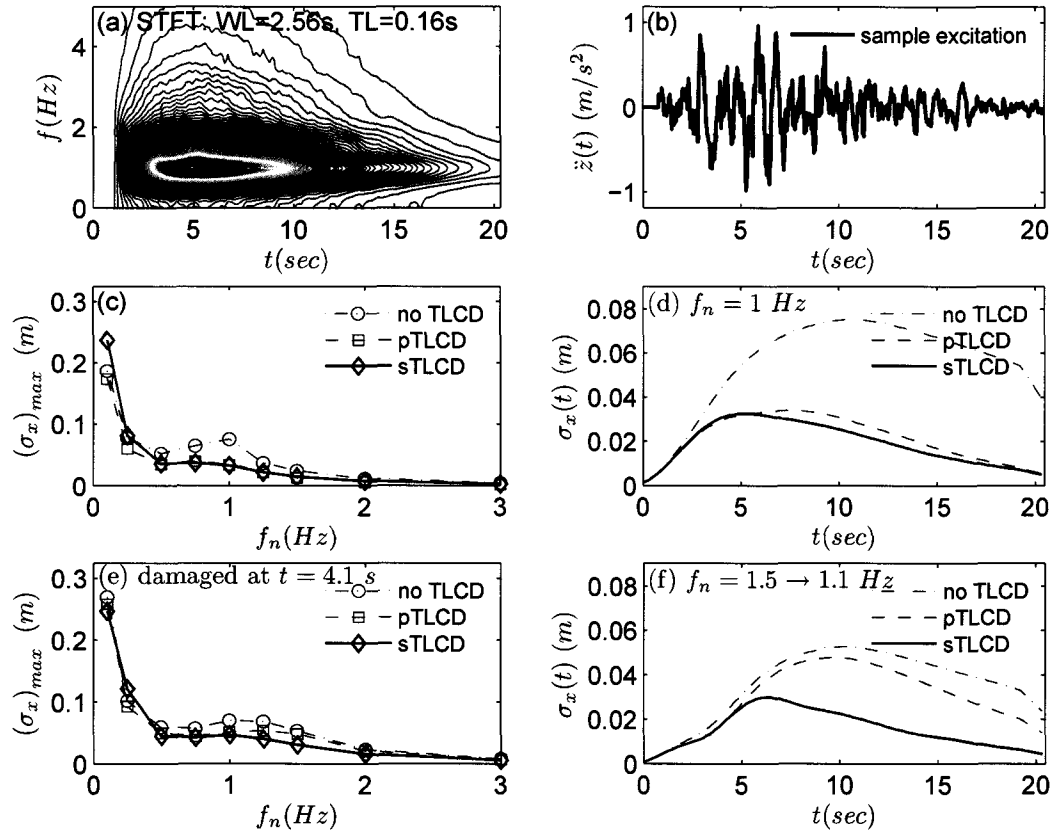


**Figure 9.18** Locally stationary base excitation of SDOF (feedback): (a) EPSD for 500 sample, (b) Sample ground acceleration, (c) Displacement response spectra, (d) RMS displacement response ( $f_n = 1.0$  Hz), (e) Displacement response spectra - damaged, (f) RMS displacement response - damaged ( $f_n = 1.5 \rightarrow 1.1$  Hz for  $t > 4.1$  sec)

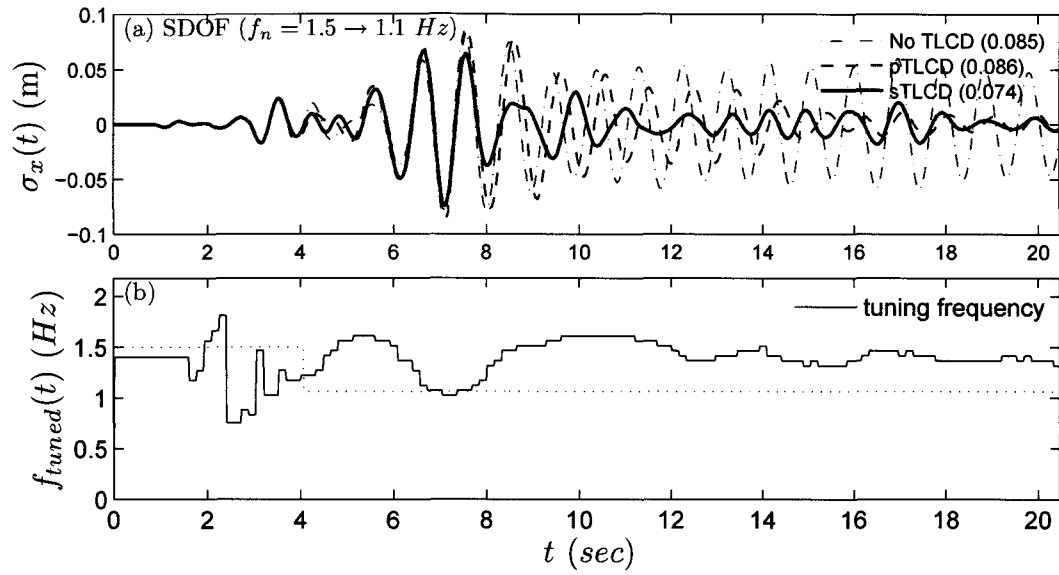


**Figure 9.19** Locally stationary base excitation of SDOF (feedback): (a) Time history response, (b) variable spring frequency

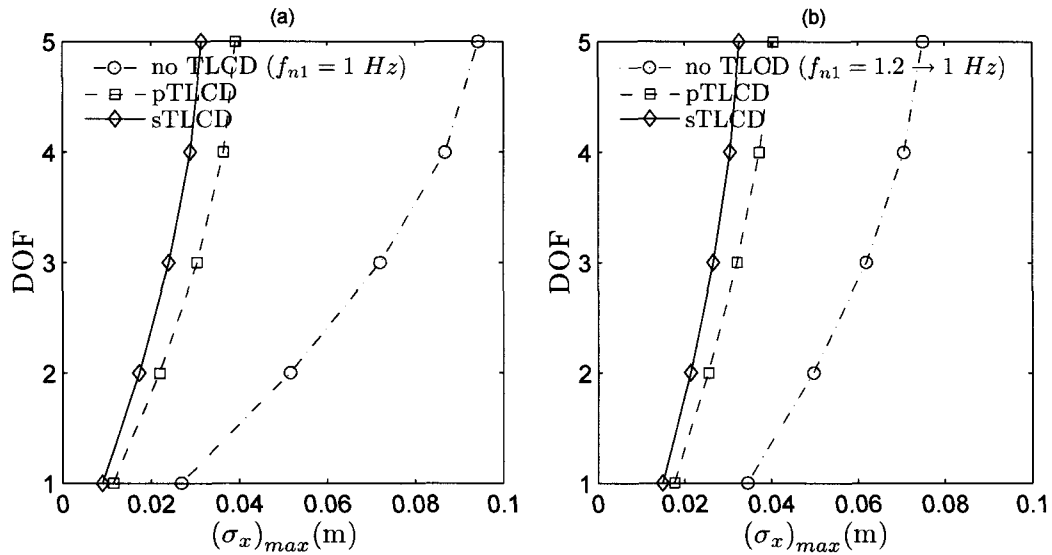


**Figure 9.20** Locally stationary base excitation of 5-DOF (feedback): (a) Peak RMS displacements ( $f_n = 1.0$  Hz), (b) Peak RMS displacements - damaged ( $f_n = 1.2 \rightarrow 1.0$  Hz for  $t \geq 4.1$  sec)

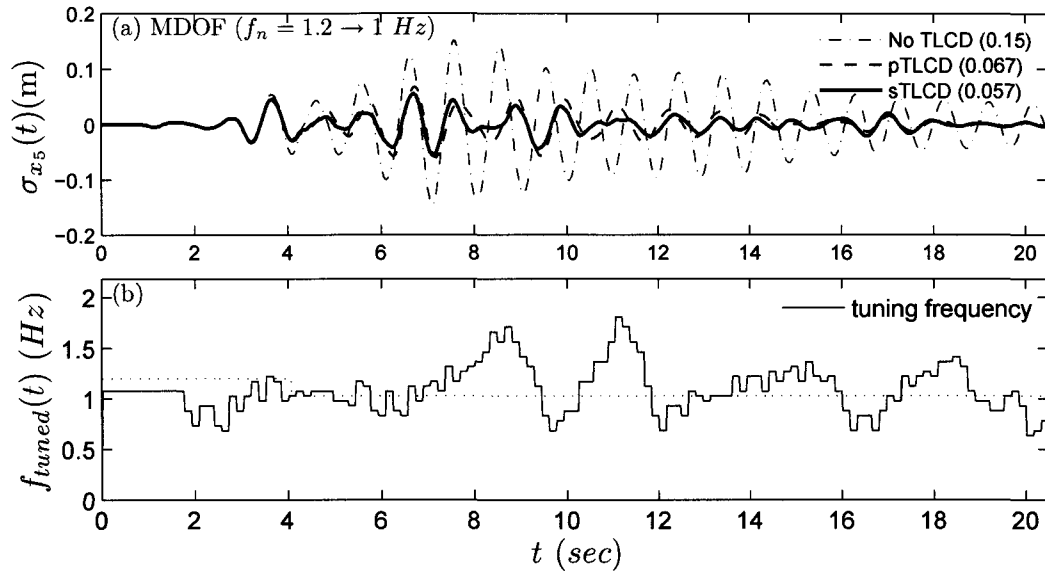


**Figure 9.21** Locally stationary base excitation of 5-DOF (feedback): (a) Top floor displacement response history, (b) Variable spring frequency

### 9.3.4 Recorded Earthquake

1940 El Centro Earthquake is used to study the performance of the sTLCD under a real, highly non-stationary ground motion record.

The results for sTLCD with feedforward control are presented in Figures 9.22 through 9.25. The estimated evolutionary excitation spectrum (by STFT), the acceleration record are shown in Figure 9.22 along with the RMS responses and the response spectra. Figure 9.22 (c, d) correspond to the SDOF primary structure without any damage whereas Figure 9.22 (e, f) correspond to the damaged SDOF primary structure after  $t = 2.6$  sec. sTLCD with feedforward control provides response reduction close to passive TLCD in no damage case. For damaged case, passive TLCD becomes off-tuned and inefficient while sTLCD lead to significant response reduction. Time history response of the SDOF primary structure (damaged at  $t = 2.6$  sec and  $f_n = 2.0$  Hz  $\rightarrow$  1.4 Hz) along with variable spring frequency of sTLCD are presented in Figure 9.23. The response of a 5-DOF primary struc-



ture is studied next for further investigation of the sTLCD performance. The peak floor displacements of a 5-DOF uniform primary structure are presented in Figure 9.24 for undamaged case ((a)  $f_n = 1.6 \text{ Hz}$ ) and for damaged case ((b)  $f_n = 1.6 \text{ Hz} \rightarrow 1.4 \text{ Hz}$ ). The damage is induced by decreasing the stiffness of the first DOF by half. The top floor displacement response history for the damaged case is presented in Figure 9.25. Similar observations can be made for these specific cases as in the ensemble RMS response histories and spectra presented in Figure 9.22.

The results for sTLCD with feedback control are presented in Figures 9.26 through 9.29. The estimated evolutionary excitation spectrum (by STFT), a sample excitation are shown in Figure 9.26 along with the RMS responses and the response spectra. Figure 9.26 (c, d) correspond to the SDOF primary structure without any damage whereas Figure 9.26 (e, f) correspond to the damaged SDOF primary structure after  $t = 2.6 \text{ sec}$ . Response spectra in Figure 9.26 clearly show that sTLCD with feedback control have similar efficiencies compared to passive ones for undamaged structures. For damaged case, passive TLCD becomes off-tuned and inefficient while sTLCD leads to significant response reduction. Time history response of the SDOF primary structure (damaged at  $t = 2.6 \text{ sec}$  and  $f_n = 2.0 \text{ Hz} \rightarrow 1.4 \text{ Hz}$ ) along with variable spring frequency of sTLCD are presented in Figure 9.27. The response of a 5-DOF primary structure is studied next for further investigation of the sTLCD performance. The peak floor displacements of a 5-DOF uniform primary structure are presented in Figures 9.28 for undamaged case ((a)  $f_n = 2.6 \text{ Hz}$ ) and for damaged case ((b)  $f_n = 1.6 \text{ Hz} \rightarrow 1.4 \text{ Hz}$ ). The damage is induced by decreasing the stiffness of the first DOF by half. The top floor displacement response history for the damaged case is presented in Figure 9.29. Similar observations can be made for these specific cases as in the ensemble RMS response histories and spectra presented in Figure 9.26.

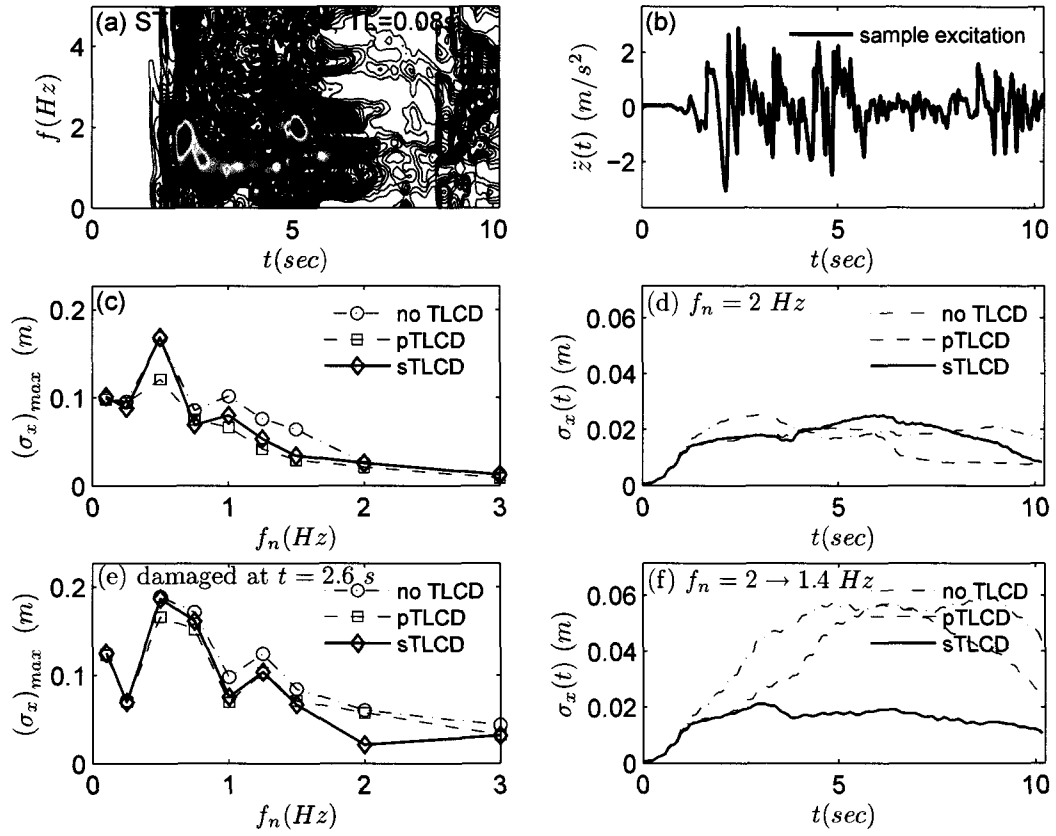


**Figure 9.22** 1940 El Centro Earthquake excitation of SDOF (feedforward): (a) EPSD, (b) Ground acceleration, (c) Displacement response spectra, (d) RMS displacement response ( $f_n = 1.5 Hz$ ), (e) Displacement response spectra - damaged, (f) RMS displacement response - damaged ( $f_n = 2.0 \rightarrow 1.4 Hz$  for  $t > 2.6 sec$ )

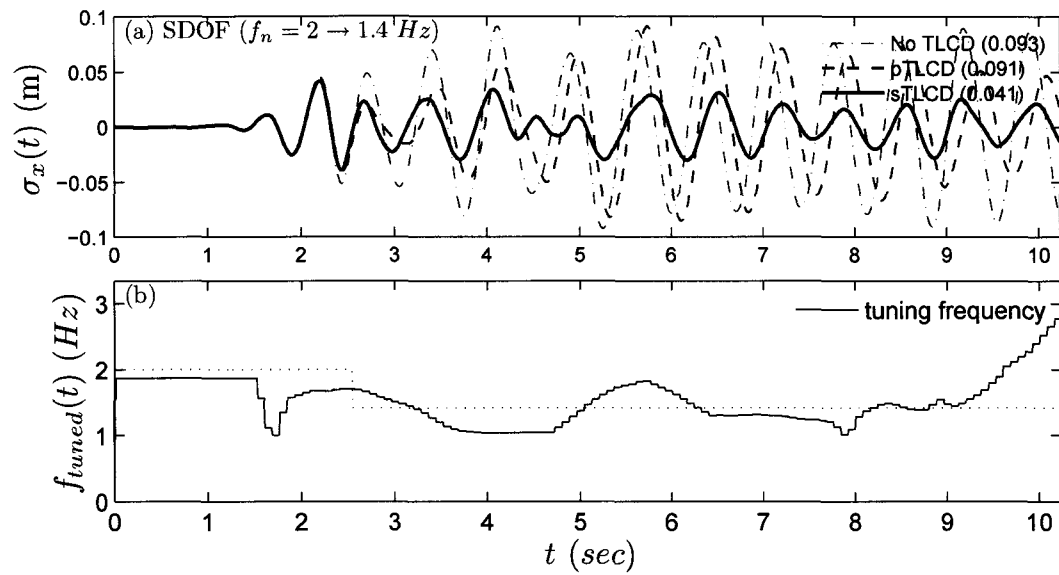


**Figure 9.23** 1940 El Centro Earthquake excitation of SDOF (feedforward): (a) Time history response, (b) Variable spring frequency

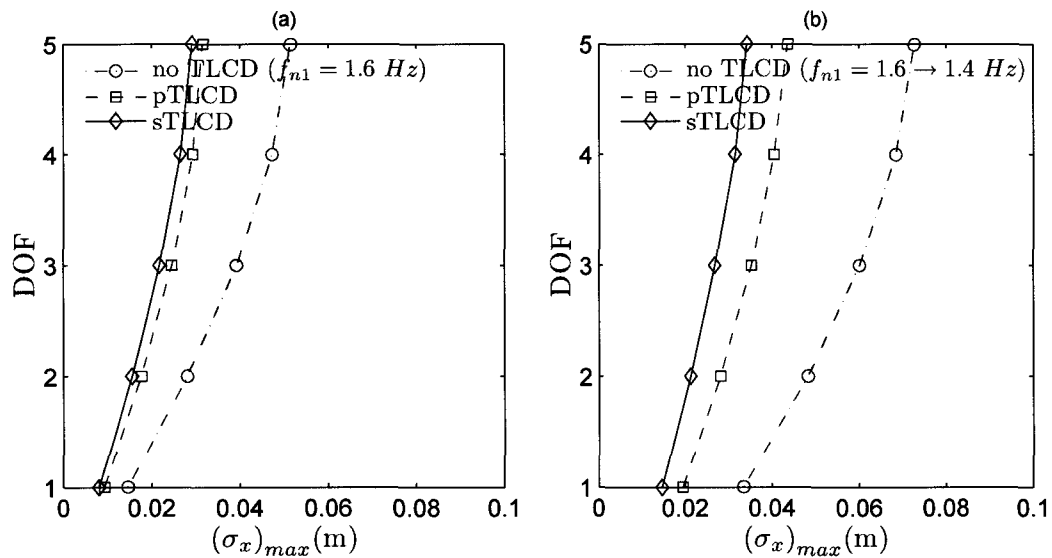


**Figure 9.24** 1940 El Centro Earthquake excitation of 5-DOF (feedforward): (a) Peak RMS displacements ( $f_n = 1.6$  Hz), (b) Peak RMS displacements - damaged ( $f_n = 1.6 \rightarrow 1.4$  Hz for  $t \geq 2.6$  sec)

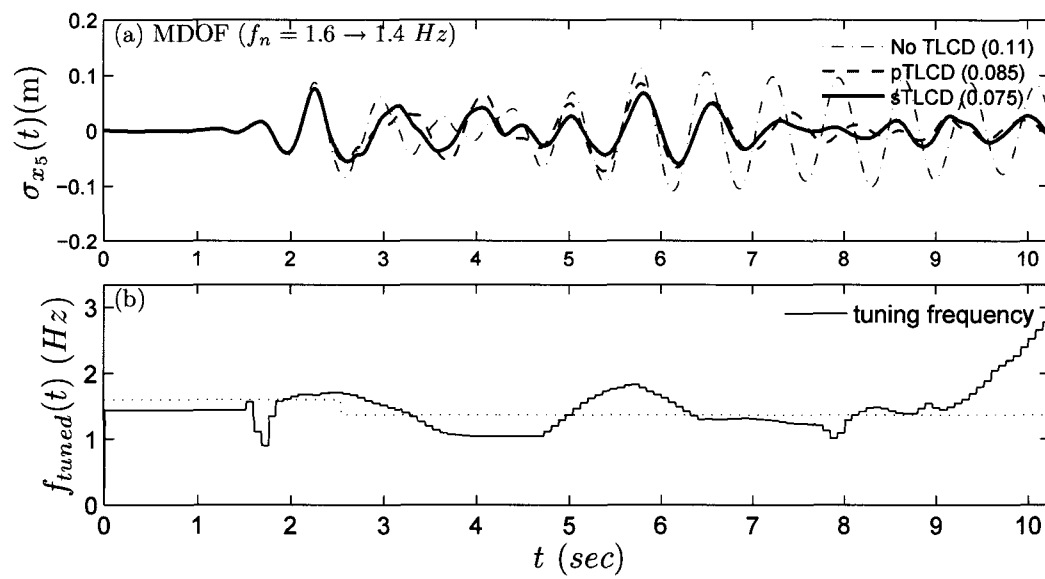


**Figure 9.25** 1940 El Centro Earthquake excitation of 5-DOF (feedforward): (a) Top floor displacement response history, (b) Variable spring frequency

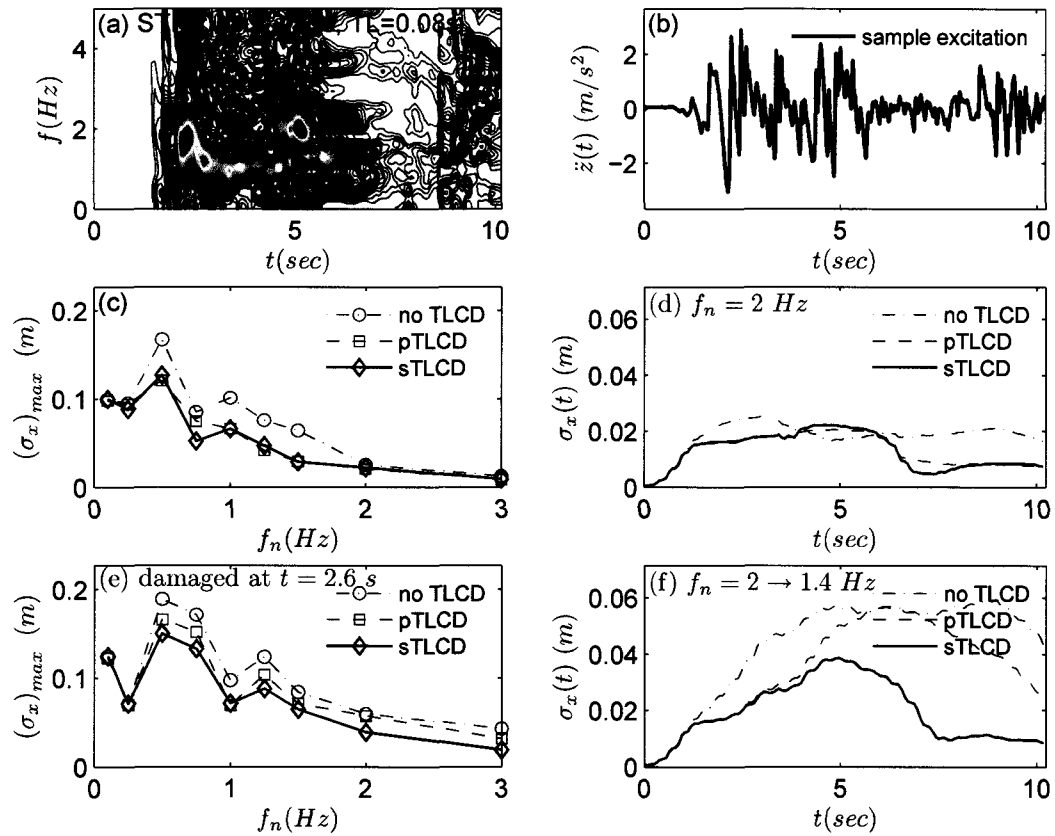


**Figure 9.26** 1940 El Centro Earthquake excitation of SDOF (feedback): (a) EPSD, (b) Ground acceleration, (c) Displacement response spectra, (d) RMS displacement response ( $f_n = 2.0 Hz$ ), (e) Displacement response spectra - damaged, (f) RMS displacement response - damaged ( $f_n = 2.0 \rightarrow 1.4 Hz$  for  $t > 2.6 sec$ )

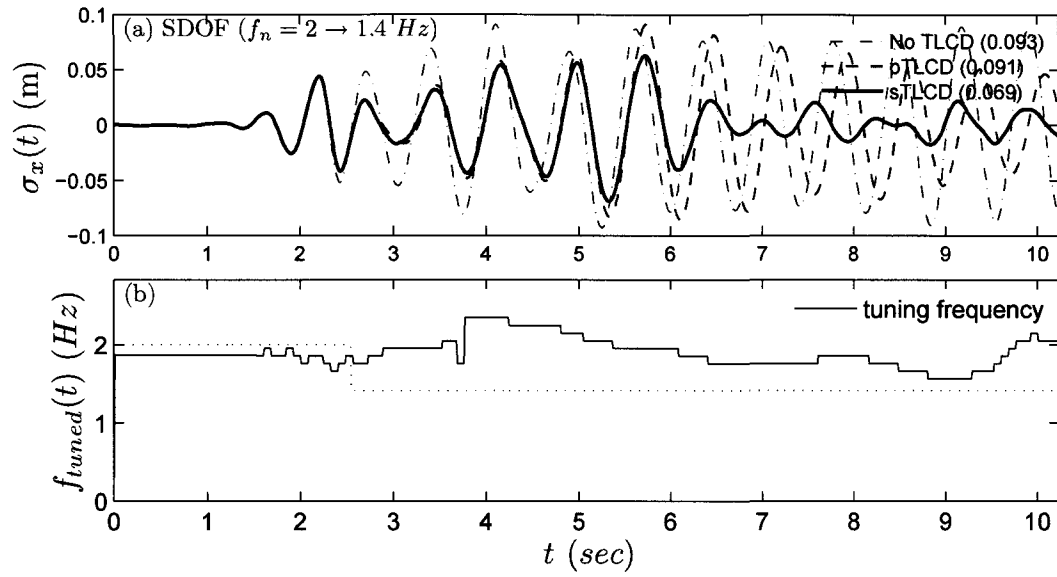


**Figure 9.27** 1940 El Centro Earthquake excitation of SDOF (feedback): (a) Time history response, (b) Variable spring frequency

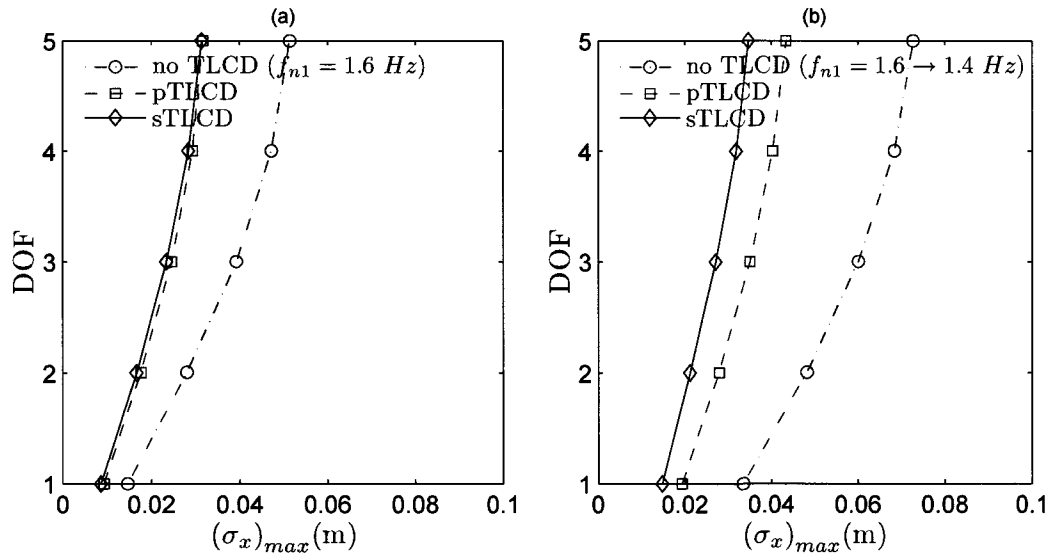


**Figure 9.28** 1940 El Centro Earthquake excitation of 5-DOF (feedback): (a) Peak RMS displacements ( $f_n = 1.6$  Hz), (b) Peak RMS displacements - damaged ( $f_n = 1.6 \rightarrow 1.4$  Hz for  $t \geq 2.6$  sec)

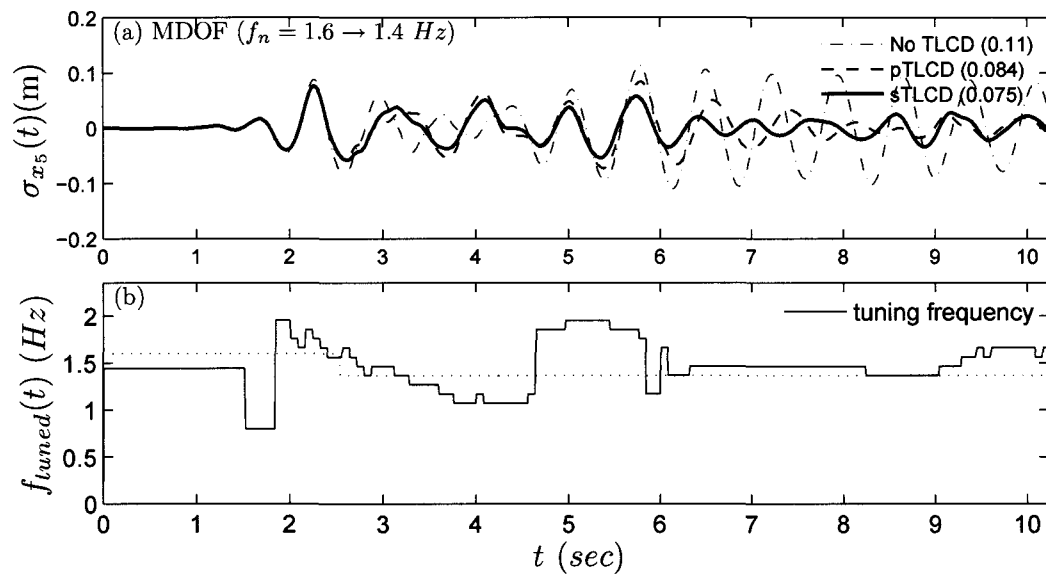


**Figure 9.29** 1940 El Centro Earthquake excitation of 5-DOF (feedback): (a) Top floor displacement response history, (b) Variable spring frequency

## 9.4 Concluding Remarks

Passive TLCD has an optimum head loss coefficient affecting the equivalent linear damping coefficient  $C_p$ , whereas in feedforward sTLCD, the primary structure response decreases as the head loss coefficient increases.

Similar to sTMD, feedforward sTLCD has superior performance than the passive counterpart for mono-component harmonic signals or random signals with significant energy at a specific instantaneous (dominant) frequency.

For random signals, feedforward sTLCD has similar RMS responses compared to the passive counterpart. However, if the primary structure's natural frequency changes, passive TLCD becomes off-tuned and ineffective, whereas sTLCD continues to suppress the vibration robustly.

Feedback sTLCD is slightly more effective than feedforward sTLCD since the response signal is smoother and slowly varying due to filtering effect of the structure with respect to the random excitation process.

Feedback sTLCD has again similar RMS responses compared to the passive counterpart and its advantage becomes apparent when the primary structure's natural frequency changes and passive TLCD becomes off-tuned and ineffective.



## **Chapter 10**

### **Conclusions and Future Work**

#### **10.1 Conclusions**

Semi-active control has been successfully applied on many civil structures in the past and it has been proved to be an effective solution for vibration control. Its main advantage is making the structure smart and adaptive to varying structural and environmental conditions while keeping the inherent stability characteristic of passive systems. In this thesis, semi-active control algorithms are developed and examined for a variety of civil engineering applications subjected to a wide range of excitations. Except two control algorithms based on continuous variable stiffness and Lyapunov method, the developed semi-active controllers are based on real-time estimation of instantaneous (dominant) frequency and the evolutionary power spectral density by time-frequency analysis of either the excitation or the response of the structure. Time-frequency analyses are performed by either short-time Fourier transform (STFT) or wavelet transform (WT) method. While STFT is more suited for harmonic and stationary signals, WT is more successful in identifying sudden changes in non-stationary signals. The performance of the control algorithms are evaluated by studying the deterministic and stochastic responses of the examined semi-active structures. Stochastic responses are computed from Monte Carlo simulations of various target evolutionary spectra. The semi-active applications considered in this study can be grouped in three main categories: (1) semi-active single/multiple degree-of-freedom systems (sSDOF/sMDOF) subjected to pulse-type excitations and random ground excitations, (2) semi-active tuned mass dampers (sTMD/sMTMD) subjected to random wind and ground excitations, and (3) semi-active tuned liquid column dampers (sTLCD) subjected

to random wind and ground excitations.

For semi-active SDOF/MDOF systems, nonlinear control algorithms developed to independently vary stiffness and damping in structures are examined against near-fault earthquakes and pulse type of excitations fitted to them. Studies of the recorded near source ground motions in the literature have shown that such motions resemble to long period pulses (especially in ground displacement and velocity) in many occasions and the response of structures also resemble to that of long period pulses. Although such simple cycloidal pulses can capture many of the kinematic characteristics of near-fault ground displacement and velocity, they do not capture the high-frequency components of the acceleration record and sometimes local, distinguishable acceleration pulses can override the long period velocity (and displacement) pulses. Despite their limitations, these cycloidal pulses are worth considering for longer period structures, such as base isolated buildings. Using nonlinear least squares technique, five different types of cycloidal pulses ( $A$ ,  $B$ ,  $C_1$ ,  $C_2$ ,  $C_1 + C_1 + C_1$ ) are fitted to several near-fault ground motion records and used to evaluate the performance of two nonlinear control algorithms: continuous variable structure control and Lyapunov control. The algorithms are examined individually and combined as (i) independently variable stiffness control, (ii) independently variable damping control, and (iii) combined variable stiffness and damping control. The nonlinear control law for variable stiffness systems is designed to produce a variable structure without sliding mode. Semi-active damping control algorithm has been derived based on Lyapunov method, such that the derivative of a Lyapunov function (representing total energy) is always negative.

A novel semi-active (time-frequency) controller for semi-active SDOF/MDOF systems is developed based on minimizing the instantaneous  $H_2$  norm of the response of the structure. The proposed control basically keeps the fundamental frequency of the system away from the dominant frequencies of the excitation by minimizing the  $H_2$  norm of the instan-

taneous response spectrum.

Two novel time-frequency controllers (feedforward and feedback) are developed for single and multiple tuned mass dampers (sTMD/sMTMD) subjected to either force or base excitation. In the feedforward control, the tuned mass damper stiffness and damping are varied based on the instantaneous (dominant) frequency of the excitation, whereas in the feedback control the tuned mass damper stiffness is varied based on the instantaneous (dominant) frequency of the response. The developed algorithms are also extended to tuned liquid column dampers (sTLCD) subjected to force or base excitation.

The presented results verify that semi-active control strategies have great potential for a wide range of applications. The main conclusions of this study are as follows:

*Approximation of near-fault earthquakes by cycloidal pulses:*

1. Responses of a SDOF system subjected to fitted single cycloidal pulses provide good approximation for those of the actual near-fault earthquake records, especially in the region of fitted pulse period. Beyond that region, the quality of the approximation reduces based on the kinematic characteristics of the actual record.
2. The difference in the absolute acceleration response between the actual record and the fitted pulse is significant in the low period (high frequency) region of the spectra since the fitted pulse acceleration is usually smaller in value and unable to match the local high-frequency fluctuations. Therefore, use of long period velocity pulses is best suited for flexible structures such as base-isolated buildings.
3. Using multiple pulses improves the resemblance between the responses to actual records and its fitted pulse.

*Semi-active single/multi degree-of-freedom (sSDOF/sMDOF) systems - continuous variable structure control and Lyapunov control:*

1. Similar to passive systems, responses of sSDOF/sMDOF subjected to fitted cycloidal pulses provide good approximation for those of the actual records. The approximation is especially good for the higher period systems as commented above.
2. The variable structure control is very effective in reducing the response in the neighborhood of the resonant peaks of the passive systems for all types of pulses.
3. The Lyapunov control for semi-active damping is effective in reducing the response for pulse type excitations, however its performance is about same as 'pass. on' system (with higher damping). For Type-*A* pulse, the control leads to higher response in the high period region (higher  $T/T_p$  range, typically greater than  $T/T_p = 1.5 - 2.0$ ) of the response spectra. For other pulses (*B*,  $C_1$ ,  $C_2$ ), Lyapunov control leads to slightly lower response than 'pass. on' system and its performance improves for higher damped systems.
4. When the two controls are executed simultaneously the benefits of both the controls are superimposed. Significant reduction in all the response quantities is observed for a wider range of  $T/T_p$  from spectra. This is because of the fact that the two control algorithms are effective in almost complementary  $T = T_p$  ranges.
5. The control strategies, namely, variable structure control for stiffness and Lyapunov control for damping can be effectively implemented in long period structures such as base-isolated structures either separately or together to reduce vibrations.

*Frequency tracking and evolutionary power spectrum:*

1. Wavelet transform (WT) has two major advantages over short-time Fourier transform (STFT): (i) it is more accurate due to variable window lengths (scales) instead of fixed window length (as in STFT), which causes inaccuracy by aliasing of low and high frequency components outside the frequency range of the window; and (ii) it is more efficient due to variable frequency (or scale) resolution with high resolution in high frequency (small scales) region and low resolution in low frequency (large scales) region, which allows identifying low and high frequency components of the signal efficiently. These advantages favor wavelet transform in time-frequency analysis of non-stationary signals, where sudden changes occur.
2. Real-time estimation of instantaneous frequency and evolutionary power spectrum requires use of a window with only priori data at any given time instant. This imposes the same limitation of STFT to wavelet transform limiting its accuracy.
3. Both STFT and WT accurately track the instantaneous frequency of harmonic and sine sweep signals.
4. For the target evolutionary spectra of random processes studied, the real-time instantaneous frequency and root mean square (RMS) values obtained from Monte Carlo simulations indicate similar performances by STFT and WT. However, this is also partly due to averaging of the sample simulations. For individual sample simulations, it is likely that WT would detect the non-stationarity characteristics more accurately.

*Semi-active single/multi degree-of-freedom (sSDOF/sMDOF) systems - adaptive  $H_2$  control:*

1. sSDOF with variable stiffness based on adaptive  $H_2$  control can successfully adapt to the optimum passive system as the excitation evolves.
2. sMDOF systems, which can be described accurately by their first mode, can similarly adapt the optimum passive system with minimum  $H_2$  norm of the first modal response determined for the instantaneous PSD of the excitation.
3. The time-varying RMS response of the sSDOF/sMDOF can be approximated from the evolutionary PSD and the time-varying complex frequency response function.

*Feedforward semi-active tuned mass dampers (Feedforward sTMD/sMTMD):*

1. For harmonic signals, if the excitation frequency is known or tracked very accurately, single sTMD leads to the least response of the main structure compared to multiple sTMDs, since sTMD has the advantage of greater mass tuned to exact excitation frequency. But in practice, the excitation frequency is either not known or can be tracked with some error and/or delay. Therefore, multiple sTMDs distributed within a small frequency range may be more effective due to the capability to compensate the small errors/delays in frequency tracking and/or randomness in the excitation signal. If the sMTMD frequency range is increased further, its effectiveness would decrease because of distributing the mass away from the resonance frequency and sTMD would be superior again in agreement with results of parametric study in Chapter 6.
2. MTMD has an optimum frequency range and an optimum damping ratio for a given number of TMDs similar to optimum frequency and damping ratio of a single TMD.

Once the number of TMDs is decided, optimum values of the frequency range and damping ratio can be found for the design of MTMD. In case of sMTMD, there are no specific optimum values. The lower the damping ratio and the frequency range, the better performance sMTMD will have for the mono-component harmonic signals or random signals with significant energy at a specific instantaneous (dominant) frequency.

3. sMTMD can also behave as a single sTMD in real-time by reducing the frequency range to zero. They can be tuned as a single sTMD depending on the time-frequency characteristics of the excitation signal. The redundancy in sMTMD makes it more reliable in the sense that if one sTMD fails, the rest can be readjusted instantaneously.
4. Feedforward sTMD and sMTMD are more robust against changes in individual TMD damping ratio and changes in main structure natural frequency compared to passive TMD and MTMD. This is observed both in frequency domain and time domain responses for harmonic and stationary excitations.
5. For random signals, feedforward sTMD/sMTMD have similar RMS responses compared to the passive counterparts. However, if the primary structure's natural frequency changes, passive TMDs become off-tuned and ineffective, whereas sTMD and sMTMD continues to suppress the vibration robustly.

*Feedback semi-active tuned mass dampers (Feedback sTMD/sMTMD):*

1. Feedback sTMD/sMTMD are slightly more effective than feedforward sTMD/sMTMD since the response signal is smoother and slowly varying due to filtering effect of the structure with respect to the random excitation process.

2. Feedback sTMD/sMTMD have again similar RMS responses compared to the passive counterparts and their advantage becomes apparent when the primary structure's natural frequency changes and passive TMDs become off-tuned and ineffective.

*Feedforward semi-active tuned liquid column dampers (Feedforward sTLCD):*

1. Passive TLCD has an optimum head loss coefficient affecting the equivalent linear damping coefficient  $C_p$ , whereas in feedforward sTLCD, the primary structure response decreases as the head loss coefficient increases. It is important to note the variable head loss coefficient (that can be obtained by varying the orifice opening ratio) can be employed for a complementary variable damping; however, it was beyond the scope of this study, and therefore optimum head loss coefficient selected for the passive TLCD is also used in sTLCD.
2. Similar to sTMD, feedforward sTLCD has superior performance than the passive counterpart for mono-component harmonic signals or random signals with significant energy at a specific instantaneous (dominant) frequency.
3. For random signals, feedforward sTLCD has similar RMS responses compared to the passive counterpart. However, if the primary structure's natural frequency changes, passive TLCD becomes off-tuned and ineffective, whereas sTLCD continues to suppress the vibration robustly.

*Feedback semi-active tuned liquid column dampers (Feedback sTLCD):*

1. Feedback sTLCD is slightly more effective than feedforward sTLCD since the response signal is smoother and slowly varying due to filtering effect of the structure with respect to the random excitation process.



2. Feedback sTLCD has again similar RMS responses compared to the passive counterpart and its advantage becomes apparent when the primary structure's natural frequency changes and passive TLCD becomes off-tuned and ineffective.

## 10.2 Future Work

The presented research in this study can be further improved and extended on several areas. The recommended areas for future research are as follows:

1. The possible benefits of variable damping in the adaptive  $H_2$  control can be further investigated.
2. The feedforward and feedback control strategies for the semi-active TMD/MTMD and semi-active TLCD can be implemented together to increase the efficiency and robustness of the semi-active tuned mass/liquid dampers.
3. Considering the proposed semi-active (time-frequency) control concepts are mostly based on the evolutionary power spectrum estimation, approximate stochastic solution for the semi-active linear time varying systems can be further investigated.
4. More realistic target evolutionary spectra and synthetic accelerograms compatible to aseismic design response spectra or sets of actual accelerogram records can be considered.
5. Semi-active damping strategy can be further investigated in semi-active TLCD (by varying the orifice opening ratio) and in semi-active feedback TMD/MTMD.

## Bibliography

- Abe, M. (1996). "Semi-active tuned mass dampers for seismic protection of civil structures." *Earthquake Engineering and Structural Dynamics*, 25, 743–749.
- Abe, M. and Fujino, Y. (1994). "Dynamic characterization of multiple tuned mass dampers and some design formulas." *Earthquake Engineering and Structural Dynamics*, 23, 813–835.
- Abe, M. and Igusa, T. (1995). "Tuned mass dampers for structures with closely spaced natural frequencies." *Earthquake Engineering and Structural Dynamics*, 24, 247–261.
- Abe, M. and Igusa, T. (1996). "Semi-active dynamic vibration absorbers for controlling transient response." *Journal of Sound and Vibration*, 198(25), 547–569.
- Addison, P. S. (2002). *The Illustrated Wavelet Transform Handbook*. Institute of Physics Publishing, London.
- Agrawal, A. (2004). *Response of semi-active variable stiffness and damping systems to pulse type excitations : analytical and experimental study*. Rice University, Houston, Texas.
- Asami, T., Nishihara, O., and Baz, A. M. (2002). "Analytical solutions to  $h_{\infty}$  and  $h_2$  optimization of dynamic vibration absorbers attached to damped linear systems." *Transactions of the ASME*, 124, 284–295.
- Balendra, T., Wang, C., and Rakesh, G. (1999). "Vibration control of various types of buildings using tlcd." *Journal of Wind Engineering and Industrial Aerodynamics*, 83, 197–208.
- Basu, B. and Nagarajaiah, S. (2008). "A wavelet-based time-varying adaptive lqr algorithm for structural control." *Engineering Structures*, 30(9), 2470–2477.
- Basu, B., Nagarajaiah, S., and Chakraborty, A. (2008). "Online identification of linear time-varying stiffness of structural systems by wavelet analysis." *International Journal of Structural Health Monitoring*, 7(1), 21–36.
- Burrus, C. S., Gopinath, R. A., and Guo, H. (1998). *Introduction to Wavelets and Wavelet*

*Transforms: A primer.* Prentice Hall, New Jersey.

Chapra, S. C. and Canale, R. P. (2002). *Numerical Methods for Engineers*. McGraw-Hill, New York, 4th edition.

Cohen, L. (1995). *Time-Frequency Analysis*. Prentice Hall, New Jersey.

Conte, J. P. and Peng, B. F. (1997). "Fully nonstationary analytical earthquake ground-motion model." *Journal of Engineering Mechanics, ASCE*, 123(1), 15–24.

Daubechies, I. (1992). *Ten Lectures on Wavelets*. SIAM, Philadelphia.

Davenport, A. G. (1961). "The spectrum of horizontal gustiness near the ground in high winds." *Journal of Royal Meteorological Society*, 87, 194–211.

Den Hartog, J. P. (1956). *Mechanical Vibrations*. McGraw-Hill, New York, 4th edition.

Deodatis, G. and Shinozuka, M. (1988). "Auto-regressive model for nonstationary stochastic processes." *Journal of Engineering Mechanics, ASCE*, 114(11), 1995–2012.

Dyke, S. J., Spencer, B. F. J., Sair, M. K., and Carlson, J. D. (1998). "An experimental study of mr dampers for seismic protection." *Smart Materials and Structures*, 7, 693–703.

Farge, M. (1992). "Wavelet transforms and their applications to turbulence." *Annu. Rev. Fluid Mech.*, 24, 395–457.

Gao, H., Kwok, K. C. S., and Samali, B. (1997). "Optimization of tuned liquid column dampers." *Engineering Structures*, 19(6), 476–486.

Gavin, H. P. (2001). "Control of seismically excited vibration using electrorheological materials and lyapunov methods." *IEEE Trans. Automatic Control*, 9(1), 27–36.

Ghosh, A. and Basu, B. (2004). "Seismic vibration control of short period structures using the liquid column damper." *Engineering Structures*, 26(13), 1905–1913.

Giaralis, A. and Spanos, P. D. (2009). "Wavelet-based response spectrum compatible synthesis of accelerograms - eurocode application (ec8)." *Soil Dynamics and Earthquake Engineering*, 29, 219–235.

- Housner, G. W., Bergman, L. A., Caughey, T. K., Chassiakos, A. G., Claus, R. O., Masri, S. F., Skelton, R. E., Soong, T. T., Spencer, B. F., and Yao, J. T. P. (1997). "Structural control: past, present, and future." *Journal of Structural Engineering, ASCE*, 123(9), 897–971.
- Hrovat, D., Barak, P., and Rabins, M. (1983). "Semi-active versus passive or active tuned mass dampers for structural control." *Journal of Engineering Mechanics*, 109(3), 691–705.
- Igusa, T. and Xu, K. (1994). "Vibration control using multiple tuned mass dampers." *Journal of Sound and Vibration*, 175(4), 491–503.
- Ivers, D. E. and Miller, L. R. (1991). "Semi-active suspension technology: An evolutionary view." *Advanced Automotive Technologies, ASME*, 40, 327–346.
- Jangid, R. S. (2004). "Response of sdof system to non-stationary earthquake excitation." *Earthquake Engineering and Structural Dynamics*, 33, 1417–1428.
- Kaimal, J. C. and and (1972). "Spectral characteristics of surface-layer turbulence." *Journal of Royal Meteorological Society*, 98, 563–589.
- Kaiser, G. (1992). *A friendly guide to wavelets*, Vol. 24.
- Kamen, E. W. (1995). *Fundamentals of linear time-varying systems*. In: Levine, W. S., editor. *The Control Handbook*. CRC Press/IEEE Press.
- Kareem, A. (1984). "A model for prediction of the acrosswind response of buildings." *Engineering Structures*, 26(2), 136–141.
- Kareem, A. (1985). "Lateral-torsional motion of tall buildings to wind loads." *Journal of Structural Engineering, ASCE*, 111(11), 2479–2496.
- Kareem, A. (1987). "Wind effects on structures: a probabilistic viewpoint." *Probabilistic Engineering Mechanics*, 2(4), 166–200.
- Kareem, A. (1992). "Dynamic response of high-rise buildings to stochastic wind loads." *Journal of Wind Engineering and Industrial Aerodynamics*, 42, 1101–1112.
- Kareem, A. and Kline, S. (1995). "Performance of multiple mass dampers under random loading." *Journal of Structural Engineering, ASCE*, 121(2), 348–361.

- Karnopp, D., Crosby, M. J., and Harwood, R. A. (1974). "Vibration control using semi-active force generators." *Journal of Engineering for Industry*, 619–626.
- Kavand, A. and Zahrai, S. M. (2006). "Impact of seismic excitation characteristics on the efficiency of tuned liquid column dampers." *Earthquake Engineering and Engineering Vibration*, 5(2), 235–243.
- Kaynia, A. M., Veneziano, D., and Biggs, J. M. (1981). "Seismic effectiveness of tuned mass dampers." *Journal of the Structural Division, ASCE*, 107(8), 1465–1484.
- Kelly, J. M. (1993). *Earthquake-resistant design with rubber*. Springer-Verlag, London.
- Kijewski, T. and Kareem, A. (2002). "On the presence of end effects and their melioration in wavelet-based analysis." *Journal of Sound and Vibration*, 256(5), 980–988.
- Kijewski, T. and Kareem, A. (2003). "Wavelet transforms for system identification in civil engineering." *Computer-Aided Civil and Infrastructure Engineering*, 18, 339–355.
- Kobori, T., Takahashi, M., Nasu, T., Niwa, N., and Ogasawara, K. (1993). "Seismic response controlled structure with active variable stiffness system." *Earthquake Engineering and Structural Dynamics*, 22(12), 925–941.
- Liang, S., Liu, S., Li, Q. S., Zhang, L., and Gu, M. (2002). "Mathematical model of acrosswind dynamic loads on rectangular tall buildings." *Journal of Wind Engineering and Industrial Aerodynamics*, 90, 1757–1770.
- Lin, Y. K. and Cai, G. Q. (1981). *Probabilistic structural dynamics : advanced theory and applications*. McGraw-Hill, New York.
- Madden, G. J., Symans, M. D., and Wongprasert, N. (2002). "Experimental verification of seismic response of building frame with adaptive sliding base-isolation system." *Journal of Structural Engineering, ASCE*, 128(8), 1037–1045.
- Makris, N. (1997). "Rigidity-plasticity-viscosity: can electrorheological dampers protect base isolated structures from near-source ground motions?." *Earthquake Engineering and Structural Dynamics*, 26, 571–591.
- Makris, N. and Chang, S. (2000a). "Response of damped oscillators to cycloidal pulses." *Journal of Engineering Mechanics*, 126(2), 123–131.

- Makris, N. and Chang, S. P. (2000b). "Effect of viscous, viscoplastic, and friction damping in response of seismically isolated structures." *Earthquake Engineering and Structural Dynamics*, 29, 85–107.
- Mao, Y. (2002). *Sliding mode control and nonlinear spectra of smart base isolated structures*. Rice University, Houston, Texas.
- McNamara, R. J. (1977). "Tuned mass dampers for buildings." *Journal of the Structural Division, ASCE*, 103(9), 1785–1798.
- Meyers, S. D., Kelly, B. G., and O'Brien, J. J. (1993). "An introduction to wavelet analysis in oceanography and meteorology: with application to the dispersion of yanai waves." *Mon. Wea. Rev.*, 121, 2858–2866.
- Mukherjee, S. and Gupta, V. K. (2002). "Wavelet-based characterization of design ground motions." *Earthquake Engineering and Structural Dynamics*, 31, 1173–1190.
- Nagarajaiah, S. (2000). "Structural vibration damper with continuously variable stiffness." *US Patent No. 6,098,969*, August 8.
- Nagarajaiah, S. (Aug 28 (2009)). "Adaptive passive, semiactive, smart tuned mass dampers: identification and control using empirical mode decomposition, hilbert transform, and short-term fourier transform." *Structural Control and Health Monitoring*, DOI: 10.1002/stc.349, published online.
- Nagarajaiah, S., Mao, Y. Q., and Sahasrabudhe, S. (2006). "Nonlinear, seismic response spectra of smart sliding isolated structures with independently variable mr dampers and variable stiffness saivs system." *J. of Struct. Eng. and Mech.*, 24(3), 375–393.
- Nagarajaiah, S. and Mate, D. (1998). "Semiactive control of continuously variable stiffness system." *Proc., 2nd World Conf. Struct. Control*, Vol. 1, Kyoto, Japan. 397–405.
- Nagarajaiah, S. and Narasimhan, S. (2005). "Smart base isolated benchmark building part ii: Phase i sample controllers for linear isolation system." *Journal of Structural Control and Health Monitoring*, 13(2-3), 589–604.
- Nagarajaiah, S., Sahasrabudhe, S., and Iyer, R. (2000). "Seismic response of sliding isolated bridges with mr dampers." *Proc. American Control Conference*, Chicago. CD-ROM.

- Nagarajaiah, S. and Sonmez, E. (2007). "Structures with semiactive variable stiffness single/multiple tuned mass dampers." *Journal of Structural Engineering, ASCE*, 133(1), 67–77.
- Nagarajaiah, S. and Varadarajan, N. (2000). "Novel semiactive variable stiffness tuned mass damper with real time tuning capacity." *Proc., 13th Engineering Mechanics Conf.*, (CDROM), ASCE, Reston, Va.
- Nagarajaiah, S. and Varadarajan, N. (2005). "Short time fourier transform algorithm for wind response control of buildings with variable stiffness tmd." *Engineering Structures*, 27(3), 431–441.
- Nagarajaiah, S., Varadarajan, N., and Sahasrabudhe, S. (1999). "Variable stiffness and instantaneous frequency." *Proc., World Structures Congress*, ASCE, Reston, Va. 858–861.
- Narasimhan, S. (2004). *Control of smart base isolated buildings with new semiactive devices and novel  $H^*/LQG$ ,  $H$  [infinity] and time-frequency controllers*. Rice University, Houston, Texas.
- Narasimhan, S. and Nagarajaiah, S. (2005). "A stft semiactive controller for base isolated buildings with variable stiffness isolation systems." *Journal of Engineering Mechanics, ASCE*, 27(4), 514–523.
- Newland, D. E. (1993). *An introduction to Random Vibrations, Spectral & Wavelet Analysis*. Wiley, New York, 3rd edition.
- Nigam, N. C. and Narayanan, S. (1994). *Applications of Random Vibrations*. Springer-Verlag, New York.
- Priestley, M. B. (1965). "Evolutionary spectra and non-stationary processes." *Journal of the Royal Statistical Society, Series B*, 27(2), 204–237.
- Priestley, M. B. (1981). *Spectral analysis and time series*. Academic Press, London.
- Priestley, M. B. (1988). *Non-linear and non-stationary time series analysis*. Academic Press, London.
- Qian, S. (2002). *Introduction to Time-Frequency and Wavelet Transforms*. Prentice Hall, New Jersey.

- Rana, R. and Soong, T. T. (1998). "Parametric study and simplified design of tuned mass dampers." *Engineering Structures*, 20(3), 193–204.
- Roberts, J. B. and Spanos, P. D. (2003). *Random Vibration and Statistical Linearization*. Dover, New York.
- Saharabudhe, S. and Nagarajaiah (2005). "Seismic response control of sliding isolated bridges with mr dampers: Experimental and numerical study." *Earthquake Engineering and Structural Dynamics Journal*, 34(7), 965–983.
- Sahasrabudhe, S., Nagarajaiah, S., and Hard, C. (2000). "Experimental study of sliding isolated buildings with smart dampers subjected to near source ground motions." *Proc., Eng. Mech. Conf., EM 2000*, UT Austin. (CDROM).
- Sakai, F., Takeda, S., and Tamaki, T. (1991). "Tuned liquid column dampers (tlcd) for cable-stayed bridges." *Proceedings of the Specialty Conference Innovation in Cable-Stayed Bridges*, Fukuoka, JSCE, Japan. 197–205.
- Saoka, Y., Sakai, F., Takaeda, S., and Tamaki, T. (1988). "On the suppression of vibrations by tuned liquid column dampers." *Annual Meeting of JSCE*, Japan Society of Civil Engineers, Tokyo, Japan.
- Schuëller, G. I. and Shinozuka, M., e. (1987). *Stochastic Methods in Structural Dynamics*. Martinus Nijhoff Publishers, Dordrecht.
- Shinozuka, M. (1970). "Random processes with evolutionary power." *Journal of Engineering Mechanics Division, ASCE*, 96(4), 543–545.
- Shinozuka, M. and Jan, C. M. (1972). "Digital simulation of random processes and its applications." *Journal of Sound and Vibration*, 25(1), 111–128.
- Simiu, E. and Scanlan, R. H. (1986). *Wind effects on structures*. Wiley, New York, 2nd edition.
- Sladek, J. R. and Klingner, R. E. (1983). "Effect of tuned-mass dampers on seismic response." *Journal of Structural Engineering, ASCE*, 109(8), 2004–2009.
- Soong, T. T. and Dargush, G. F. (1997). *Passive energy dissipation systems in structural engineering*. Wiley, Chichester.



- Soong, T. T. and Mircea, G. (1993). *Random Vibration of Mechanical and Structural Systems*. Prentice Hall, New Jersey.
- Spanos, P. D. and Failla, G. (2004). "Evolutionary spectra estimation using wavelets." *Journal of Engineering Mechanics, ASCE*, 130(8), 952–960.
- Spanos, P. D., Giaralis, A., and Jie, L. (2009). "Synthesis of accelerograms compatible with the chinese gb 50011-2001 design spectrum via harmonic wavelets: artificial and historic records." *Earthquake Engineering and Engineering Vibration*, 8(2), 189–206.
- Spanos, P. D., Giaralis, A., and Politis, N. P. (2007). "Numerical treatment of seismic accelerograms and of inelastic seismic structural responses using harmonic wavelets." *Computer-Aided Civil and Infrastructure Engineering*, 22, 254–264.
- Spanos, P. D., Tezcan, J., and Tratskas, P. (2005). "Stochastic processes evolutionary spectrum estimation via harmonic wavelets." *Comput. Methods Appl. Mech. Engrg.*, 194, 1367–1383.
- Spencer, B. F., Dyke, S. J., Sain, M. K., and Carlson, J. D. (1997). "Phenomenological model of a magnetorheological damper." *Journal of Engineering Mechanics*, 123(3), 230–238.
- Spencer, B. F. and Nagarajaiah, S. (2003). "State of the art of structural control." *Journal of Structural Engineering, ASCE*, 129(7), 1–10.
- Sun, J. Q., Jolly, M. R., and Norris, M. A. (1995). "Passive, adaptive and active tuned vibration absorber - a survey." *Transactions of the ASME*, 117, 234–242.
- Torrence, C. and Compo, G. G. (1998). "A practical guide to wavelet analysis." *Bulletin of the American Meteorological Society*, 79(1), 61–78.
- Varadarajan, N. (2005). *Novel smart variable stiffness tuned mass damper and its real time identification and control using time frequency techniques*. Rice University, Houston, Texas.
- Varadarajan, N. and Nagarajaiah, S. (2004). "Wind response control of building with variable stiffness tuned mass damper using empirical mode decomposition/hilbert transform." *Journal of Engineering Mechanics, ASCE*, 130(4), 451–458.

- Čačko, J., Bílý, M., and Bukoveczky, J. (1988). *Random Processes: Measurement, Analysis and Simulation*. Elsevier, New York.
- Vickery, B. J. and Clark, A. W. (1972). "Lift or across-wind response of tapered stacks." *Journal of Structural Division, ASCE*, 98(1), 1–20.
- Warburton, G. B. (1981). "Optimum absorber parameters for minimizing vibration response." *Earthquake Engineering and Structural Dynamics*, 9, 251–262.
- Xu, K. and Igusa, T. (1992). "Dynamic characteristics of multiple substructures with closely spaced frequencies." *Earthquake Engineering and Structural Dynamics*, 21, 1059–1070.
- Xu, Y. L. and Samali, B. (1992). "Control of along-wind response of structures by mass and liquid dampers." *Journal of Engineering Mechanics, ASCE*, 118(1), 20–39.
- Yalla, S. K., Kareem, A., and Kantor, J. C. (2001). "Semi-active tuned liquid column dampers for vibration control of structures." *Engineering Structures*, 23(11), 1469–1479.
- Yamaguchi, H. and Harnpornchai, N. (1993). "Fundamental characteristics of multiple tuned mass dampers for suppressing harmonically forced oscillations." *Earthquake Engineering and Structural Dynamics*, 22, 51–62.
- Yang, C. Y. (1986). *Random Vibration of Structures*. Wiley, New York.
- Yang, J. N., Agrawal, A. K., Samali, B., and Wu, J.-C. (2004). "Benchmark problem for response control of wind-excited tall buildings." *Journal of Engineering Mechanics, ASCE*, 130(4), 437–446.
- Yang, J. N., Kim, J. H., and Agrawal, A. K. (2000). "Resetting semiactive stiffness damper for seismic response control." *Journal of Structural Engineering, ASCE*, 126(12), 1427–1433.